THE UNIVERSITY
of EDINBURGH

Comparative Pulmonary Fibrosis: Imaging fibroproliferation in donkey and man

Amy Miele

Doctor of Philosophy – The University of Edinburgh – 2015

Contents

Table of Figures

Preface

I declare that the research within this thesis is my own work and any assistance received has been duly acknowledged. The work described has not been submitted for any other degree or professional qualification.

Acknowledgements

My studentship was funded by the Medical Research Council, as was the Development Pathway Funding Scheme grant under which the optical molecular imaging aspect of this thesis was carried out.

While the compilation of this thesis has indeed been my own work, I have been fortunate enough to be part of a multi-centre and multi-disciplinary team who have provided significant contributions to my research.

I firstly owe a tremendous amount of gratitude to my supervisors Dr Kev Dhaliwal and Prof Bruce McGorum for granting me the opportunity to undertake my studentship and for all of their guidance, support and encouragement. Kev's endless enthusiasm and ingenuity has been inspirational, while Bruce has kept me grounded with his unwavering patience and wisdom. Without their help the completion of this thesis would not have been possible and I would not have gained such valuable research experience.

I am very grateful to The Donkey Sanctuary, Devon for their collaboration and to Dr Nicole Du Toit, Dr Harriet Brooks and the rest of the veterinary and clinical laboratory teams for their help in the collection of clinical and pathological data. Dr Du Toit and Dr Brooks performed necropsy examinations, including digital photography, collected some of the histopathology samples and prepared lungs for transport to Edinburgh as well as providing me with support regarding the identification and description of pathological features. Dr Sionagh Smith, Royal (Dick) School of Veterinary Studies, was also a great help in this regard, providing interpretation of several of the donkey tissue sections.

Dr William Wallace, Royal Infirmary, Edinburgh, identified the similarity between APF and PPFE and he, together with Dr Catharine Dhaliwal, helped to perform histopathological categorisation of the donkey sections as described in Chapter 2.6. High resolution computed tomography images (HRCT) were obtained and reviewed by Tobias Schwarz, Royal (Dick) School of Veterinary Studies and Dr Saeed

Mirsadraee, Clinical Research Imaging, Centre. Scoring of HRCT images was performed by Dr John Murchison, Royal Infirmary, Edinburgh.

The molecular imaging work formed part of a large multi-disciplinary project, consisting of biologists and chemists working alongside each other. Thus in order to provide a coherent narrative I have included work that was performed by other members of the group.

I am particularly grateful to Dr Chesney Michels, the lead biologist on the project, for his help, guidance and friendship. Dr Michels contributed to many of the biological experiments by assisting with experimental design and providing additional n numbers. I have also included two experiments that were carried out by Dr Michels while I was on maternity leave and I have acknowledged this work in the relevant figure legends.

All in-house probes and inhibitors were synthesised by The Bradley Group, Department of Chemistry, University of Edinburgh, this work was overseen by Prof Mark Bradley. Dr Tashfeen Aslam synthesised TWB-219 and TWB-140. Dr Sunay Chankeshwara synthesised SVC-016, SVC-24, SVC-186 and SVC-196, while Dr Alicia Megia-Fernandez synthesised AMF-25, AMF-106, AMF-59 and AMF-60. All figures containing probe structures were thus designed with the help of the relevant scientist as listed above. All MALDI analysis was performed by Dr Sunay Chankeshwara and Dr Alicia Megia-Fernandez, who also supplied the relevant MALDI figures. Schematic diagrams of probe structures were provided by Dr Alicia Megia-Fernandez and Dr Sunay Chankeshwara.

The majority of fibre confocal fluorescence microscopy (FCFM) experiments were performed with the help of Dr Ahsan Akram and Dr Chesney Michels. Finally I am grateful to all of the members of The Pulmonary Optical Molecular Imaging Group for creating such a supportive (and tolerant!) environment within which to work. On this note I am particularly indebted to Emma Scholefield, who was a very patient teacher and provided me with protocols and technical help in a number of assays (detailed in Chapter 2) as well as with the murine cell lines.

Abbreviations

α-SMA	Alpha smooth muscle actin
AHV	Asinine herpesvirus
APF	Asinine pulmonary fibrosis
APMA	4-aminophenylmercuric acetate
ATS	American Thoracic Society
BAL	Bronchoalveolar lavage
BAPN	β-aminopropionitrile
BSA	Bovine serum albumin
CBA	Cytometric bead array
DAO	Diamine oxidase
DAPI	4',6-diamidino-2-phenylindole
DETCA	Sodium diethyldithiocarbamate trihydrate
DMEM	Dulbecco's Modified Eagle's medium
DMSO	Dimethyl sulfoxide
DNA	Deoxyribonucleic acid
ECM	Extracellular Matrix
EDANS	5-((2-Aminoethyl)amino)naphthalene-1-sulfonic acid
EDTA	Ethylenediaminetetraacetic acid
EHV	Equine herpesvirus
ELISA	Enzyme-linked immunosorbent assay
EMPF	Equine multi-nodular pulmonary fibrosis
EMT	Epithelial mesenchymal transition
EVG	Elastin Van Gieson
FAM	Fluorescein

FBS	Foetal bovine serum
FCFM	Fibred confocal fluorescence microscopy
FRET	Fluorescence resonance energy transfer
H&E	Hematoxylin and eosin
HMDM	Human monocyte derived macrophages
HRCT	High resolution computed tomography
ICC	Immunocytochemistry
IFN-γ	Interferon gamma
IHC	Immunohistochemistry
IL	Interleukin
IMDM	Iscove's Modified Dulbecco's Media
IPF	Idiopathic pulmonary fibrosis
LOX	Lysyl oxidase
LOXF	Lysyl oxidase family
LOXL2	Lysyl oxidase-like-2
LPS	Lipopolysaccharide
LRT	Lower respiratory tract infection
MALDI-TOF	Matrix-assisted laser desorption/ionization time of flight spectrometry
MAO	Monoamine oxidase
MCP-1	Monocyte chemoattractant protein-1
MMPs	Matrix metalloproteinases
MR	Methyl red
MT	Masson’s Trichrome
NIR	Near infrared
OPA	Ovine pulmonary adenocarcinoma
PBS	Phosphate buffered saline

PCR	Polymerase chain reaction
PE	Phycoerythrin
Pen/strep	Penicillin and Streptomycin
PET	Positron emission tomography
PM	Post mortem
PPFE	Pleuroparenchymal fibroelastosis
QMRI	Queen's Medical Research Institute
RAO	Recurrent airway obstruction
RDSVS	Royal (Dick) School of Veterinary Studies
RNA	Ribonucleic acid
SD	Standard deviation
SEM	Standard error of the mean
TGF-β	Tumour growth factor- β
TIMP	Tissue inhibitor of metalloproteinase
TNF	Tumour necrosis factor
TPP	Target product profile
UIP	Usual interstitial pneumonia
UoEDC	University of Edinburgh, Department of Chemistry

Abstract

Pulmonary fibrosis is a chronic and debilitating condition that proposes several challenges to both veterinary and medical clinicians. Despite considerable research, many fibrotic lung diseases remain elusive in terms of aetiology, pathogenesis and treatment. Furthermore, progress is hindered by the lack of a translatable animal model with durable and persistent fibrosis. Asinine Pulmonary Fibrosis (APF) is a spontaneous syndrome of aged donkeys with high prevalence (35%). No previous detailed characterisation of APF has been performed and disease diagnosis remains a challenge.

APF was studied with regard to clinical, pathological and molecular features and the suitability of this condition as a model for a rare fibrotic lung disease in humans known as pleuroparenchymal fibroelastosis (PPFE) was assessed. In addition, target activatable optical imaging reagents for the real time detection of two key molecular markers of fibrosis: matrix metalloproteinases (MMPs) and lysyl oxidases (LOXF) were evaluated in spontaneous *ex vivo* models of fibrosis. Such reagents may be used alongside fibred confocal fluorescence microscopy (FCFM), a relatively non-invasive and cutting edge diagnostic tool, to detect and monitor fibroproliferation in animals and man.

Whole lungs were collected from 32 aged donkeys at routine necropsy. Gross examination revealed pulmonary fibrosis in 19 donkeys (APF cases), while 13 (controls) had grossly normal lungs. HRCT images and histology sections were reviewed independently and blindly for each of the lungs. Ten of 19 APF lungs were categorised as being ‘consistent with’ PPFE according to previously defined histological and imaging criteria. All 10 PPFE-like lungs had marked pleural and subpleural fibrosis, predominantly within the upper lung zone, with accompanying intra-alveolar fibrosis and elastosis.

An activatable Smartprobe for the detection of LOXF, TWB-219, was synthesised by The Bradley Group, Department of Chemistry (UoEDC). The probe was based on a tandem amine oxidation and β-elimination mechanism, resulting in signal

amplification detected at the 488nm wavelength. The probe showed increased fluorescence in the presence of diamine oxidase as well as on incubation with aged human lung tissue cell-free homogenate as determined by a fluorescent plate reader. This signal amplification could be inhibited by β-aminopropionitrile, a recognised LOX inhibitor as well as by an in-house inhibitor specific to LOX.

An evolutionary family of MMP probes with varying cleavage sequences and structures, synthesised by the UoEDC, was evaluated at each stage of progression with regard to signal to noise ratio, sensitivity and specificity. Probes were tested against recombinant enzymes from the MMP family as well as neutrophil elastase and plasmin. Signal amplification was also assessed on incubation with human and ovine *ex vivo* lung tissue. The final 'lead' MMP probe, SVC-186, was cleaved by MMP-2, -9 and -13. Signal amplification was also seen following incubation with both human and ovine tissue with significant inhibition in the presence of the pan-MMP inhibitor, marimastat.

In conclusion, APF is an emerging condition of aged donkeys that shares key pathological and imaging features with human PPFE. Diagnosis of APF and other fibrotic lung conditions across species remains a challenge to veterinary and medical professionals. As such, optical imaging tools may provide dynamic, real time information on the presence and progression of fibroproliferation in the lung. TWB-219 and SVC-186 produce a detectable increase in fluorescent signal at the 488nm wavelength when activated by LOXF and MMPs respectively. These probes have been shown to function in human *ex vivo* tissue as assessed by FCFM.

Lay Summary

Chronic lung scarring or fibrosis is a feature of several debilitating diseases and represents a challenge to both veterinary and medical clinicians. Despite considerable research, much remains to be discovered regarding the cause, development and treatment of fibrotic lung conditions. Furthermore, progress is hindered by the lack of an animal model with durable and persistent fibrosis. Asinine Pulmonary Fibrosis (APF) is a spontaneous syndrome of aged donkeys with high prevalence (35%). Little is known about this debilitating condition and disease diagnosis remains a challenge.

A comprehensive characterisation of APF was performed in order to determine the suitability of this condition as a model for a rare fibrotic lung disease in humans known as pleuroparenchymal fibroelastosis (PPFE). In addition, the expression of two key markers of fibrosis: matrix metalloproteinases (MMPs) and lysyl oxidases (LOXF) was evaluated in human, donkey and sheep lung tissue. This was to aid in the development and evaluation of novel fluorescent imaging reagents that were specifically designed to report on these enzymes within lung tissue. Ultimately these reagents could be used alongside cutting edge optical imaging technology to detect and monitor scar tissue in animals and man.

Chapter 1: Introduction

1.1 Abstract

While the highly regulated process of wound healing has been well characterised, much remains unknown regarding the pathways that lead to the dysregulation of this process and the manifestation of pathological fibrosis. The gradual replacement of tissue architecture with collagenous matrix can be devastating to organ function, particularly in the lung.

Pulmonary fibrosis is a feature of several chronic respiratory diseases with poor prognosis including idiopathic pulmonary fibrosis (IPF). There is a long list of failed anti-fibrotic therapeutics in the treatment of IPF and progress is hindered both by the lack of a translatable animal model for clinical trials and by the current use of crude endpoint targets that fail to inform on the dynamic molecular pathways within the fibrogenic process. With regards to the first of these issues, spontaneous animal models of pulmonary fibrosis in the field of veterinary medicine represent a promising and under-utilised resource. The second issue may be addressed by embracing the emerging field of targeted optical molecular imaging and fibred confocal fluorescence microscopy (FCFM) in particular.

Protease-targeted fluorometric Smartprobes hold the potential to sensitively monitor the dynamic activity of therapeutic targets *in vivo*. These probes are optically quiet in their inactive state but generate signal amplification upon specific enzymatic cleavage. Therapeutically relevant proteases in fibrogenesis include the lysyl oxidases (LOXF) and matrix metalloproteinases (MMPs). Ultimately, the coupling of FCFM with Smartprobes targeting such proteases heralds the potential to challenge traditional methods of therapeutic monitoring of fibrogenic disease within the lung.

1.2 What is fibrosis?

In order to better understand the mechanisms involved in pathological fibrosis, one must first appreciate the process of simple wound healing. Following epithelial/endothelial cell injury, inflammatory mediators are released, triggering platelet aggregation, clot formation and the laying down of an initial extracellular

matrix (ECM). Growth factors, cytokines and chemokines stimulate the proliferation and recruitment of leukocytes and macrophages which in turn promote new blood vessel formation (Keeley et al., 2010). Platelets and macrophages among other cells, secrete platelet-derived growth factor and transforming growth factor β (TGFβ), which play key roles in regulating the activation, proliferation and migration of fibroblasts and myofibroblasts (Razzaque and Taguchi, 2003, Khalil et al., 1989, Nagaoka et al., 1990).

Fibroblasts are ubiquitous mesenchymal cells that are present in most tissues of the body. In the normal adult human lung, they are present in the adventitia of vascular structures and airways (Phan, 2008). Activated fibroblasts replace the provisional matrix with a more mature form containing collagen. As the formation of granulation tissue progresses, the fibroblasts develop characteristics of myofibroblasts, which express alpha-smooth muscle actin (α-SMA) and promote wound contraction. In addition, fibroblasts and other cells produce matrix metalloproteinases (MMPs) and their inhibitors, tissue inhibitors of metalloproteinase (TIMP), which regulate the degradation of ECM. Finally, epithelial/endothelial cells divide and migrate to regenerate the damaged tissue (Keeley et al., 2010, McAnulty, 2007)

Uncontrolled proliferation and/or activation of fibroblasts and myofibroblasts results in an excessive accumulation of ECM components and the laying down of new collagen at a greater rate than it is degraded. Over time, this leads to fibrosis and permanent scarring with the disruption of normal tissue architecture (Keeley et al., 2010, Ogawa et al., 2006). This pathological process is seen in many organ systems and potential initial triggers include infectious agents, autoimmune reactions, toxins, radiation and mechanical injury (Wynn, 2008), although often the inciting cause is unknown.

1.2.1 What is the origin of myofibroblasts?

Historically, myofibroblasts were thought to be derived from local tissue fibroblasts that proliferate and express constituents of the ECM in response to tissue injury. Although recent research has shown that this theory is still very much valid

(Rinkevich et al., 2015), three additional sources of myofibroblasts have also been described (Keeley et al., 2010).

The first of these is from bone-marrow derived circulating progenitor cells known as fibrocytes (Bucala et al., 1994). Fibrocytes express a variety of cell-surface markers including CD34, CD45 and collagen type 1 relating to haematopoietic progenitor cells, leukocytes and mesenchymal cells respectively, as well as the chemokine receptor CXCR4 (Andersson-Sjöland et al., 2008, Choi et al., 2010, Bucala et al., 1994).

Fibrocytes are capable of differentiating into fibroblasts and myofibroblasts (Hong et al., 2007, Abe et al., 2001), as well as adipocytes (Hong et al., 2005) *in vitro*. They also contribute to tissue remodelling by producing collagen I and collagen III and by secreting MMPs (Chesney et al., 1998). Fibrocytes were demonstrated in the lungs of IPF patients using immunofluorescence but were absent from control lungs (Andersson-Sjöland et al., 2008). Increased numbers of fibrocytes were also reported in the circulation of patients with IPF, with a further increase in those patients undergoing acute exacerbation of disease (Moeller et al., 2009).

Fibrocyte differentiation is influenced by a complex profile of local cytokines, chemokines and plasma proteins. TGFβ has been shown to accelerate the differentiation of fibrocytes into myofibroblasts (Abe et al., 2001) and the fibrocyte itself can secrete TGFβ along with other fibrogenic mediators, to promote the differentiation of locally derived tissue fibroblasts into myofibroblasts (Wang et al., 2007).

The second potential source of myofibroblasts involves the dedifferentiation of epithelial cells in a process known as epithelial-mesenchymal transition (EMT) (Keeley et al., 2010). EMT is seen in embryogenesis and tumour proliferation, but its role in fibrosis remains controversial (Morbini et al., 2011). EMT has been implicated in the pathogenesis of pulmonary fibrosis in the bleomycin model (Kim et al., 2006) and *in vitro* (Tanjore et al., 2011), however studies utilising lineage tracing cast doubt on these results (Rock et al., 2011). Indeed a study by Hung *et al*, 2013,

mapped the fate of embryonic mesenchymal progenitors in murine lungs during tissue homeostasis and fibrotic injury and suggested the tissue resident mesenchymal cells known as pericytes were the major source of myofibroblast precursors alongside tissue fibroblasts in pulmonary fibrosis (Hung et al., 2013). Pericytes, also referred to as vascular smooth muscle cells, share a basement membrane with endothelial cells and regulate angiogenesis and vascular permeability in a number of organs (Hung et al., 2013, Bergers and Song, 2005). While Hung *et al* provided compelling evidence for the role of the pericyte as a myofibroblast precursor, the contribution of other cell types derived from the same mesenchymal progenitor cannot be ruled out. Furthermore, with regards to both the fibrocyte and the pericyte, there is no single specific cell marker to unequivocally identify these cell types (Hung et al., 2013).

While the relative contribution of fibrocytes, EMT, pericytes and local tissue fibroblasts in the pathogenesis of pulmonary fibrosis remains unclear, the central role of cytokines such as TGF-β is not disputed.

1.2.2 Transforming growth factor β (TGFβ)

TGFβ has been described as 'a master switch' in the induction of fibrosis (Willis and Borok, 2007). It is a multifunctional cytokine that regulates tissue morphogenesis and differentiation through effects on cell proliferation, differentiation, apoptosis and ECM production (Willis and Borok, 2007). It is chemotactic for fibroblasts, monocytes and macrophages (Zhao et al., 2002), modulating cell shape and arresting growth in vitro (Moustakas and Stournaras, 1999). TGF has been shown to stimulate the differentiation of α-SMA negative fibroblasts to α-SMA positive myofibroblasts in culture (Denys et al., 2008) and increase the number of stress fibres containing α-SMA by up to 60% in 3T3 cells (Chen and Raghunath, 2009, Moustakas and Stournaras, 1999). Furthermore, TGFβ has been shown to upregulate the transcription and activity of the ECM producing enzyme lysyl oxidase (LOX) in cardiac fibroblasts (Voloshenyuk et al., 2011) as well as the expression of several members of the LOX and matrix metalloproteinase (MMP) families in mechanically injured cruciate ligament fibroblasts (Xie et al., 2013).

Expression of active TGFβ in the lungs of rats induces a marked fibrotic response, whereas treatment of animals with TGFβ antagonists has been shown to prevent bleomycin-induced lung fibrosis in vivo (Zhao et al., 2002). TGFβ is upregulated in various spontaneous and experimental fibrotic diseases including idiopathic pulmonary fibrosis (Khalil et al., 1991).

1.3 Pulmonary fibrosis

Pulmonary fibrosis represents the endpoint of many diseases and is characterised by excessive and irreversible deposition of extracellular matrix in the lung parenchyma, leading to compromised ventilation and organ dysfunction.

Idiopathic pulmonary fibrosis (IPF) is the most common and severe form of the idiopathic interstitial pneumonias. It is a chronic and progressive disease which affects around 5 million people worldwide. The incidence of IPF in the UK and USA is increasing, accompanied by an increase in IPF mortality (Navaratnam et al., 2011). The mean age at presentation is 66 years, with a median survival of 2-5 years following diagnosis. Clinically, there is restriction on pulmonary function testing, reduced exercise tolerance and progressive dyspnoea.

Pathologically, IPF affects the basilar and peripheral areas of the lung and biopsies display the characteristics of usual interstitial pneumonia (UIP) (Armanios, 2012). These include clusters of fibroblastic proliferation termed 'fibroblast foci', which have long been thought of as the primary sites of cellular injury and repair (Winkler and Fowlkes, 2002, Ramos et al., 2001). These foci can be found at the ‘leading edge’ of the fibrosis, often bridging the gap between fibrotic and unaffected tissue in sections exhibiting spatial heterogeneity. This localisation drives the theory that these are discrete areas of recurrent epithelial injury, yet it has been argued that there is little evidence to support this claim (Cool et al., 2006). Cool et al 2006, showed that instead of representing isolated areas of lung injury, fibroblastic foci form an interconnected reticulum extending from the pleura and invading into the parenchyma (Cool et al., 2006). Thus the idea was introduced that IPF may be thought of more as a neoproliferative disorder with many of the functional features of

cancer including genetic abnormalities, disrupted cell signalling and uncontrolled proliferation (Vancheri, 2012).

This theory is further supported by the fact that medical treatment of IPF is currently of little benefit (Harari and Caminati, 2010, Lawson et al., 2008) although this is also the case with several other fibrotic lung diseases that do not share the pathological feature of fibroblastic foci. One such disease is the relatively novel clinicopathological entity termed pleuroparenchymal fibroelastosis (PPFE).

1.3.1 Pleuroparenchymal fibroelastosis (PPFE)

In 2002, The American Thoracic Society published consensus classifications of idiopathic interstitial pneumonias, aiding clinicians in their categorisation of fibrotic pulmonary diseases. Recently, the society published an update on these classifications (Figure 1-1) and introduced for the first time a group of rare entities including PPFE (Travis et al., 2013).

The term PPFE was appointed in 2004 to describe a predominantly upper zone distribution of pleural and subpleural fibrosis with elastosis, seen in a small cohort of patients. It was proposed that previous reports of IPF of upper lung lobes were consistent with PPFE, making the true extent of this rare condition difficult to determine (Frankel et al., 2004).

Clinically, PPFE patients have a lower body mass index and more severe restricted lung dysfunction than those with IPF. There may be chronic pleuritic pain as well as a high incidence of spontaneous pneumothorax (~30% patients) which makes lung biopsy very risky (Camus et al., 2014). On imaging, there is a dense peripheral rim of consolidation (fibrosis) with wedge-shaped pleural opacities extending along parenchymal septa into the interstitium (Camus et al., 2014).

1.3.2 Aetiology of fibrotic lung disease

Despite the precise ATS classification of the idiopathic interstitial pneumonias shown in Figure 1-1, there is very limited understanding of the aetiopathogenesis of these diseases. Genetic predisposition has been identified in some cases of IPF

(Armanios, 2012, Noth et al., 2013) and PPFE (Reddy et al., 2012, Azoulay et al., 1999). Host-specific factors including a propensity towards auto-immune reactions have also been implicated in disease pathogenesis, with high expression of non-specific auto-antibodies identified in some PPFE patients as well as links to autoimmunity following organ transplant (Frankel et al., 2004, Reddy et al., 2012).

Environmental factors such as smoking are likely to play a role in the pathogenesis of IPF (Horowitz and Thannickal, 2006), while historic exposure to alkylating drugs has been identified in several PPFE patients (Camus et al., 2014). Studies of viral respiratory tract infection in patients with IPF suggest an increased prevalence of past infection with herpes virus and Epstein-Barr virus among others (Lawson et al., 2008, Lok et al., 2001). Reddy *et al*, 2012, suggested that repeated inflammatory damage following recurrent respiratory infections in predisposed individuals could lead to PPFE and that airway centred injury could be key to disease pathogenesis (Reddy et al., 2012). Despite considerable research, many fibrotic lung diseases remain elusive not only in their aetiology and pathogenesis but also in their treatment (Chua et al., 2005).

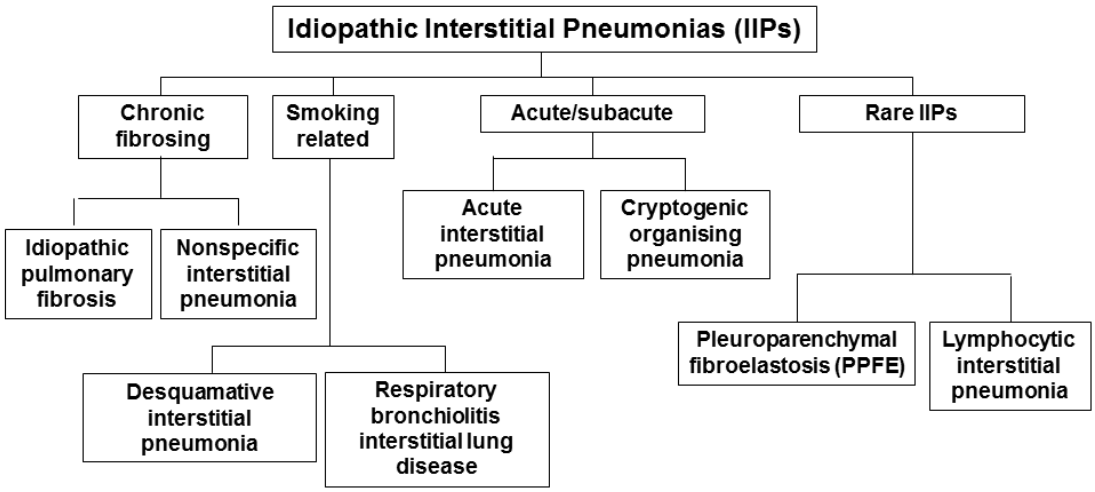

Figure 1-1: The idiopathic interstitial pneumonias (IIPs). Diagram categorising diseases collectively described as IIPs by The American Thoracic Society (Travis et al., 2013).

1.3.3 Anti-fibrotic therapies

Currently the only successful treatment for chronic fibrosing lung diseases such as IPF and PPFE is lung transplant, but even this has a limited impact on mortality, with less than half of transplanted IPF patients surviving beyond 5 years post-transplant (Mason et al., 2007). Over the past decade there have been at least 15 failed large scale clinical trials involving novel drug treatments for IPF. A few drugs have made it onto the market, but clinical improvement is generally marginal and it remains to be seen whether this will translate to improved survival (King et al., 2014, Richeldi et al., 2014). The process of taking a new therapy through each of the three phases of clinical trials as set out in current UK legislation is expensive and time consuming. Endpoint targets used to determine drug efficacy, such as a reduction in the rate of decline of lung function, are crude measurements which are slow to reflect changes in lung pathology and have poor sensitivity. Progress is hindered further by the lack of a translatable animal model with durable and persistent fibrosis (Williams et al., 2004).

1.3.4 Experimental animal models

At present, the most commonly used animal model in the study of IPF is that of the bleomycin-treated rodent. However, in this model there is spontaneous resolution of the lung injury four months after the intra-tracheal administration of bleomycin (Williams et al., 2004). While the repeated administration of bleomycin may overcome this issue (Degryse et al., 2010), a further problem is that the treatment outcomes used in murine model studies, such as the prevention or resolution of scar tissue, often do not translate to those sought in human trials i.e. reduction in the rate of decline of lung function or decreased mortality (Harari and Caminati, 2010).

Replacing the rapid and predictable experimentally-induced fibrosis of the rodent with that of a model that has progressed naturally over months to years holds obvious benefits to comparative IPF research. Moreover, growing awareness of the 3Rs ethical framework for the replacement, refinement and reduction of experimental animals further emphasises the need for a spontaneous alternative to the bleomycin model.

1.4 Potential spontaneous models of pulmonary fibrosis

Some of the earliest reports of insidious onset pulmonary fibrosis in veterinary species describe that induced by the chronic inhalation of dust particles or silicate pneumoconiosis. This condition has been reported in a number of domestic species as well as in zoo animals, but such reports are relatively rare (Brambilla et al., 1979, Hansen et al., 1989, Canfield et al., 1989, Schwartz et al., 1981). Although these may be valuable models in relation to human silicate pneumoconiosis, they are less relevant to IPF and their infrequency precludes any such utilisation. More recently there have been reports in the literature of IPF in the dog and cat (Williams et al., 2004, Corcoran et al., 1999). The disease in cats has been linked to a defect in type II pneumocyte biology, while canine IPF shows a breed predilection to West Highland white terriers. Thus there has been speculation as to the possible familial nature of IPF-like conditions in the dog and cat, but this is yet to be confirmed (Corcoran et al., 1999, Williams et al., 2004). Research in these species is limited by the relative rarity of pulmonary fibrosis as well as the lack of availability of biopsy and post mortem tissue (Corcoran et al., 1999).

Interstitial pneumonias in horses are equally uncommon and also provide a diagnostic challenge to veterinary surgeons. Various aetiologies have been implicated including pathogens, toxins and hypersensitivity reactions (Buergelt et al., 1986, Sweeney, Wong et al., 2008). Equine multinodular pulmonary fibrosis (EMPF), a progressive fibrosing interstitial lung disease of horses, was first described by Williams *et al*, 2007 and a strong association with herpesvirus was made. They demonstrated the presence of EHV5 in lung tissue from all 24 affected horses included in the study, using virus genera-specific PCR (Williams et al., 2007). As the name suggests, the gross pathology of this condition consists of multiple, discrete fibrotic nodules, mainly affecting the alveolar parenchyma (Williams et al., 2007). Lack of comparable pathological features, low incidence and size impracticalities prevent the use of EMPF as a model of human fibroproliferative disease.

1.4.1 Asinine pulmonary fibrosis (APF)

The final veterinary species in which an idiopathic interstitial fibrosing lung disease has been reported is the donkey. There are only four publications in the literature that refer to Asinine Pulmonary Fibrosis (APF), all of which were written in collaboration with The Donkey Sanctuary, Devon, which houses over three thousand donkeys (Thiemann and Bell, 2001, Thiemann, 2012, Morrow et al., 2010, Miele et al., 2014).

The Donkey Sanctuary is an internationally recognised charity that cares for the largest population of domestic donkeys in the world. All deceased donkeys at The Donkey Sanctuary undergo routine post-mortem examination within 24h of death or euthanasia, facilitating correlation between the clinical and pathological features of disease. Thiemann and Bell, 2001, were the first to report APF or Chronic Interstitial Fibrosing Pneumonia, as a common incidental finding of unknown aetiology, on post mortem examination at the Donkey Sanctuary (Thiemann and Bell, 2001). This was followed by an updated report in 2011 (Thiemann, 2012). Both of these reviews describe some of the clinical and pathological characteristics of APF, but as yet no systematic scientific study has been performed. A retrospective analysis of post-mortem findings of aged donkeys carried out at the sanctuary over a seven year period found that 35.2% of 1,444 donkeys were affected by APF (Morrow et al., 2010). However, the retrospective nature of this study and lack of supporting histopathology with regard to the classification of pulmonary fibrosis, pose questions as to the accuracy of this figure. In the majority of APF cases included in this study, pulmonary fibrosis was an incidental finding and was unrelated to the primary cause of death. The difficulties involved with diagnosis, and the lack of an effective treatment for this progressive and debilitating disease, make it a significant welfare concern (Thiemann and Bell, 2001, Thiemann, 2012).

Speculation has been made as to potential aetiologies of APF (Thiemann and Bell, 2001). In 2002, Kleiboeker *et al* reported an acute fibrosing interstitial pneumonia in seventeen donkeys in the USA and found two previously unrecognised herpesviral pathogens, AHV4 and AHV5, to be associated with the lung tissue from affected donkeys at post-mortem (Kleiboeker et al., 2002). However, a causal relationship has

not yet been confirmed, and it is unclear whether this is the same condition as that reported by The Donkey Sanctuary.

The high prevalence and localised population of APF affected donkeys at The Donkey Sanctuary, makes this potential model very accessible to scientific study. Furthermore, the size and anatomy of asinine lungs are much closer to those of the human than the murine equivalent, and diagnostic procedures such as bronchoscopy can be performed with relative ease in the standing asinine patient. At an international workshop (Coalition for Pulmonary Fibrosis) in Lafayette, Indiana in 2007, world leaders in human and animal pulmonary fibrosis identified APF as a potential model for IPF and highlighted the importance of further research into this disease.

1.5 Molecular imaging

As previously mentioned, it is not only the lack of a suitable animal model that impedes progress in the development of novel anti-fibrotic therapeutics, but also the lack of sensitive, real time information on the state of disease in patients undergoing clinical trials (Maharaj et al., 2013). Molecular imaging heralds the potential to reinvent the way in which therapeutic response to novel therapies is assessed, providing sensitive information on the real time dynamic activity of target molecules *in vivo* (Weissleder, 1999, Dorward et al., 2012) .

Molecular imaging allows temporal, structural and functional assessment of tissue *in vivo* through the exploitation of specific molecular targets and pathways to generate contrast. Since the sequencing of the human genome and recognition of the importance of molecular function in complex biological systems and disease processes, interdisciplinary collaborations between biologists, chemists and physicists have resulted in significant advances in the field of molecular imaging (Cassidy and Radda, 2005). A number of different imaging modalities exist, all of which have their own advantages and limitations (Figure 1-2).

Positron-emission tomography (PET) is the most commonly used molecular imaging technique in human disease (Dorward et al., 2012). It is based on the administration

and subsequent detection of a radioisotope combined with a biologically active compound that targets a specific biochemical event *in vivo*. The decay of this radioisotope emits a positron which produces high-energy photons detected by the PET scanner (Cassidy and Radda, 2005). There are reports of PET Fluorine-18 radiopharmaceuticals being successfully used to detect experimentally induced pulmonary fibrosis in rabbits (Jones et al., 1994, Wallace et al., 2002), but this success has yet to be translated to man. Furthermore, although PET provides good temporal resolution and a high sensitivity and specificity of contrast agents, spatial resolution remains poor (Cassidy and Radda, 2005). Combining PET with CT overcomes this problem to a certain extent by allowing correlation of PET signal with three dimensional anatomical information. However, PET requires significant financial investment and an onsite cyclotron as well as the intravenous injection of radioactive isotopes, limiting use to specialised centres (Hellebust and Richards-Kortum, 2012).

1.5.1 Optical molecular imaging

Optical molecular imaging is a relatively low cost technique that is widely used within laboratories and has the potential for application in a number of clinical settings (Dorward et al., 2012). It involves the detection of light which is generated by cells and/or tissue in relation to specific functional or molecular processes and heralds the opportunity to perform optical multiplexing whereby different wavelengths report on different targets of interest. Generally optical imaging utilises the visible and infrared regions of the electromagnetic spectrum, with the latter affording better tissue penetration and eliminating interference from tissue auto-fluorescence (Zhang et al., 2012). However, although near-infrared (NIR) wavelengths can be utilised to image at depths of several centimetres, the presence of cellular structures causes elastic scatter of photons, resulting in the diffusion of signal and loss of spatial resolution (Ntziachristos, 2006). One way of overcoming such problems in organs that are accessible to endoscopy such as the lung and gastrointestinal tract, is to utilise the emerging platform of confocal microendoscopy (Dorward et al., 2012).

1.5.2 Fibred confocal fluorescence microscopy

Fibred confocal fluorescence microscopy (FCFM) allows high resolution real-time *in vivo* visualisation of tissue at a cellular level and is a clinically applicable strategy (Figure 1-3). FCFM has been successfully utilised in a number of organ systems including the pulmonary tract, where the auto-fluorescence of elastin allows visualisation of tissue architecture (Fuchs et al., 2011, Thiberville et al., 2009b).

Pulmonary imaging via FCFM may be coupled with specifically engineered and targeted molecular contrast agents or Smartprobes. Smartprobes are exogenous contrast agents that fluoresce when activated by target biomarkers within the tissue of interest. Ultimately, the coupling of Smartprobes with FCFM enables minimally invasive visualisation of temporal and spatial alterations in the molecular characteristics of cells or tissue, with the potential to assess and monitor the benefits of novel molecularly targeted therapies (Goetz and Wang, 2010).

Figure 1-2: Table summarising common molecular imaging modalities. Reproduced from Dorward et al, 2012. Pharmacology and Therapeutics 135(2): 182-199, with permission from Elsevier

Imaging Modality	**Main Application**	**Spatial Resolution**	**Advantages**	**Disadvantages**	**Clinical Applications**	**Cost**
Bioluminescent	*In vivo*	Millimetres	High signal to noise ratio; Multiplex imaging; Good temporal resolution	Requires exogenous substrate and genetic manipulation of target cell or organism	Limited, likely to remain a pre-clinical tool.	+
Fluorescent	*In vivo, in vitro*	Micrometres	Multi-channel; NIR allows greater depth of penetration; Wide range of molecular probes	Scatter; Autofluorescence; Photobleaching; Surface weighting of images	Mainly pre-clinical use; Clinical applications in surgery, endoscopy and surface tissue imaging	+
Confocal microscopy	*In vivo, in vitro*	Micrometres	In vivo imaging with microendoscopic techniques; Intravital imaging	Small fields of view	Early stages of clinical use (bronchoscopy and endoscopy)	++
Positron emission tomography	*In vivo*	3-4mm (high resolution 1-2mm)	Highly sensitivity in hybrid imaging system (e.g. CT)	Short radionuclide half-life requires on-site cyclotron; Limited target-specific radionuclides available	In clinical use	+++

Single-photon emission computed tomography	*In vivo*	8-15mm (small animal machines <1mm)	Ability to perform multiplex imaging; Longer half-life of common radionuclides	Limited number of target-specific radionuclides available	In clinical use	+++
Magnetic resonance imaging	*In vivo*	100µm	Non-ionising radiation; Excellent spatial resolution	Specific molecular probes limited; Slow acquisition time; Low sensitivity for molecular imaging; High concentrations of contrast agents required	In clinical use — mainly structural imaging	++
Ultrasound	*In vivo*	Millimetres	Inexpensive; Highly portable; Useful in vascular imaging	Variable depth of penetration; Image quality operator dependent; lack of contrast agents	In clinical use — mainly structural imaging	+
Computed tomography	*In vivo*	100µm	Simultaneous acquisition of detailed structural information	Few contrast agents available for molecular imaging and high concentrations required	In clinical use — mainly structural imaging	+++
Hybrid systems	*In vivo*	Variable (application dependent)	Improves anatomical accuracy of information	Increases expense	PET/CT in clinical use	++

.

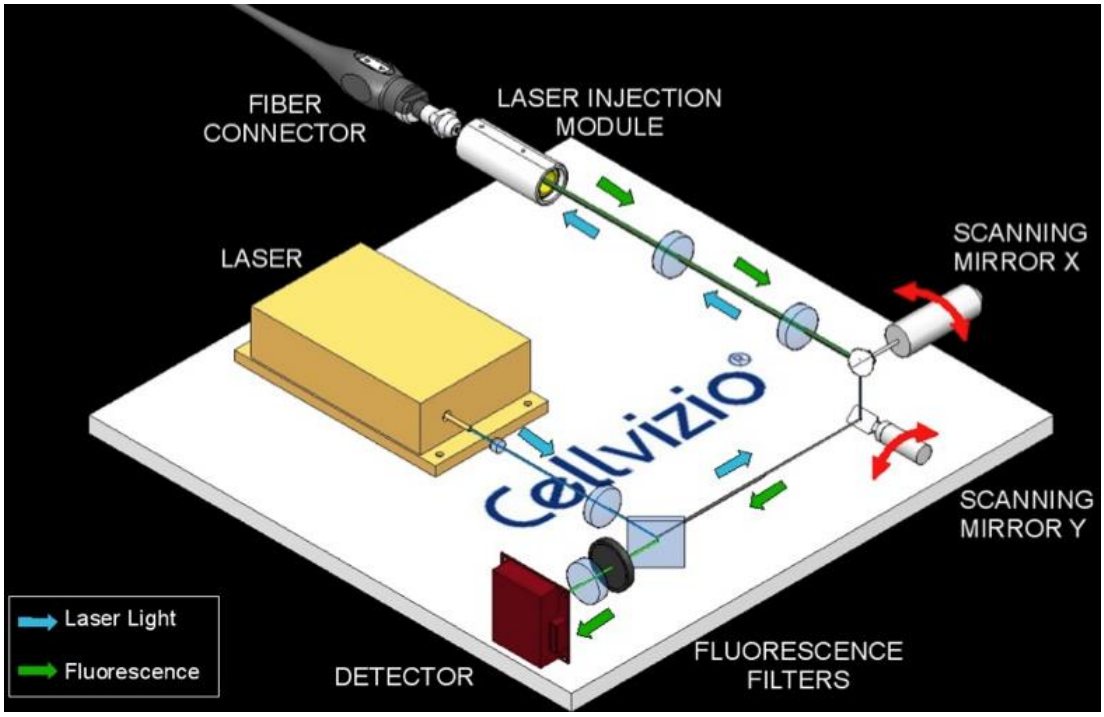

Figure 1-3: The FCFM system. The FCFM system (Cellvizio^{TM} –Lung, Mauna Kea Technologies, Paris, France) encompasses a fibreoptic mini probe, laser scanning unit and image acquisition software. The 1.4mm diameter mini probe (ProFlex^{TM} S-1500, Mauna Kea Technologies, Paris, France) is composed of a bundle of 30,000 laser fibres and is 3 metres in length. It has a field of view of 600µm, lateral resolution of 3µm and depth of focus of 0-50µm. The fibre bundle connects to the laser scanning unit which contains a 488nm laser source, scanned by two mirrors on the proximal surface of the fibre bundle. Each individual fibre core acts as a point source and point detector, transmitting the laser beam and collecting the returning fluorescent light emitted from the tissue. The system ensures the sequential injection of the laser beam into each fibre core and collects the returning fluorescent signal between 500nm and 650nm for imaging at a rate of 12 frames per second.

1.5.3 Smartprobes

While non-specific fluorescent dyes have their uses in biological science, including the ability to label cells and molecules *in vivo*, a Smartprobe must have an 'on/off' function in order to eliminate background fluorescence and generate good signal amplification in response to enzyme activity within a complex biological environment (Sapsford et al., 2006). This is generally achieved by manipulating the chemical properties of the reporting fluorophore. Subsequent activation of the probe under specifically designed conditions results in a significant increase in fluorescent intensity (Goetz and Wang, 2010).

An activatable Smartprobe may have a peptide, macromolecular, polymeric or nanoparticle base and there are specific advantages and disadvantages relating to each of these structures (Lee et al., 2010). Traditional techniques for the imaging of proteases often involve the use of fluorescently labelled monoclonal antibodies which bind in a very specific manner to the target of interest, but cannot inform on enzyme activity. More recently activatable antibody-based macromolecular imaging probes have been reported (Shimizu et al., 2011) that can overcome this problem. However, such Smartprobes are likely of limited use in the clinical setting due to the potential for adverse immunogenic reaction and their long plasma half- life (Goldsmith, 1997).

One alternative way of improving the target specificity of a Smartprobe is to incorporate nanoparticles into their structure. The large surface area and relative ease of manipulation renders nanoparticles as favourable carriers of activatable fluorescent probes (Minchin and Martin, 2010). Lee et al, 2009, utilised a polymeric nanoparticle based Smartprobe to inform on the protease activity of tumours in murine models (Lee et al., 2009). The probe was afforded targetability due to the enhanced permeation and retention effect, whereby macromolecules collect in solid tumours preferentially over normal tissue as a result of anatomical and pathophysiological differences. While the emerging prospect of utilising nanoparticles as molecular imaging tools has many potential benefits, the long-term

kinetics of nanoparticles are poorly understood, as is their potential for chronic toxicity (Minchin and Martin, 2010).

Peptide-based Smartprobes incorporating a protease substrate have been broadly used as molecular imaging tools *in vitro* and in murine models. Although these probes can often be limited by issues with signal specificity and stability (Lee et al., 2010), they remain a promising possibility with regards to achieving utility in man. Largely peptide Smartprobes utilise one of two techniques to achieve optical silencing in their un-activated state.

The first of these is a phenomenon known as fluorescence resonance energy transfer (FRET, see Figure 1-4). This describes the energy transfer from an electronically excited donor fluorophore to another chromophore (quencher) which acts as an acceptor when the molecules are held in close proximity (1-10nm) (Jares-Erijman and Jovin, 2003), resulting in optical silencing or quenching of fluorescent signal. FRET also relies on the overlapping donor excitation and acceptor absorption curves at the excitation wavelength. Enzymatic cleavage of the peptide sequence results in the release of the fluorophore and the emission of light upon excitation (Ntziachristos, 2006).

While the FRET Smartprobe structure is a long established method for achieving amplification of fluorescent signal, the dendrimer Smartprobe is a relatively new concept (Ellard et al., 2002). The dendrimer structure (see Figure 1-5) incorporates several branches, each containing a molecule of the chosen fluorophore which must have a small Stoke's shift. The Stoke's shift is the difference between the emission and excitation wavelengths of the fluorophore. The dendrimer thus consists of a high local concentration of fluorophore resulting in 'internal' quenching of the fluorescent signal. Hydrolysis of the probe allows the release of multiple fluorophores, resulting in signal amplification (Ternon et al., 2004).

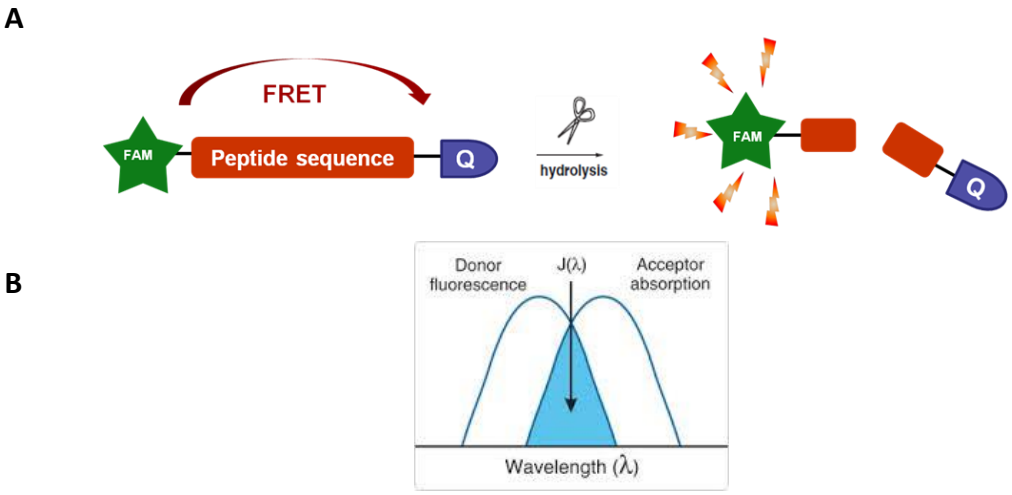

Figure 1-4: Basis of fluorescence resonance energy transfer (FRET). (A) Schematic diagram depicting the energy transfer that occurs between donor and acceptor chromophores when held in close proximity and the subsequent signal amplification that is achieved following hydrolysis of a FRET Smartprobe. (B) Schematic representation of the overlapping fluorescence and absorption spectra of the respective donor and acceptor chromaphores at the exciting wavelength, J. FAM= fluorescein, Q= quencher.

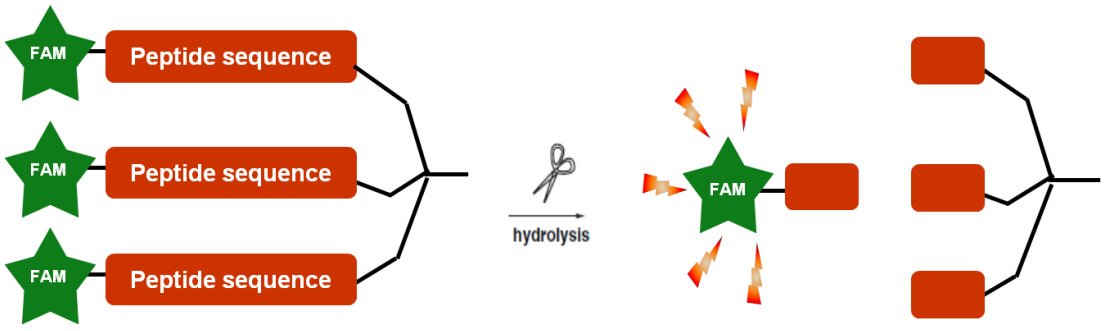

Figure 1-5: The dendrimer structure. Schematic diagram depicting the structure of the dendrimeric Smartprobes. Internal or vertical quenching occurs when multiple fluorophores with a small Stoke's shift are held in close proximity. Hydrolysis of the probe leads to release of the fluorophores and an amplification in fluorescent signal.

Fluorescein and derivatives thereof are commonly used in both dendrimer and FRET probes as they are inexpensive, have a high quantum yield and good solubility. However, the fluorescein dye falls within the visible light range, resulting in significant limitations, particularly with regards to *in vivo* use due to interference from tissue autofluorescence. Fluorescein is also sensitive to pH and the presence of endogenous quenchers such as haemoglobin and lipids further complicate *in vivo* application. As previously discussed, utilising a fluorophore in the NIR window (650-900nm) is one way of overcoming these issues (Tung, 2004, Sapsford et al., 2006).

As a member of the Pulmonary Optical Molecular Imaging Group, I was one of the biologists working on a multi-disciplinary project with the ultimate aim of synthesising Smartprobes for clinical application alongside FCFM. While dyes such as fluorescein (Fuchs et al., 2011) and methylene blue (Thiberville et al., 2009a) have been administered to patients either intravenously or topically in order to aid in the visualisation of pulmonary architecture on FCFM imaging of the lung, these dyes alone are non-specific. As yet there are no reports of Smartprobes for such application.

The premise of the study was that specifically designed small peptide Smartprobes would inform on the dynamic enzymatic activity of key players within the fibrogenic pathway and would be instilled into the lungs of patients in microdose amounts (<100µg). They would thus need to be non-toxic, safe, stable and fast acting and meet a specific target product profile (see Figure 5.3). However, the first step was to identify clinically relevant molecular targets with potential utility in the therapeutic monitoring of fibrogenic diseases. As such, lysyl oxidase (LOX) and matrix-metalloproteinase-9 (MMP-9) were investigated.

1.6 The lysyl oxidases

The Lysyl oxidases are copper dependent amine oxidases that play a central role in fibrogenesis (Molnar et al., 2003). They facilitate the covalent cross-linking found within elastin and collagen by catalysing the oxidative deamination of peptidyl-lysine and hydroxylysine residues (Figure 1-6), a step that is crucial to the mature

and functional extracellular matrix (Feres-Filho et al., 1995, Smith-Mungo and Kagan, 1998, Vora et al., 2010). Indeed, a disorder of connective tissue termed osteolathyrism that causes spinal curvature and paralysis, occurs when the lysyl oxidases are inhibited experimentally in rats by aminonitriles such as beta-aminopropionitrile (BAPN) (Barrow et al., 1974). There are five proteins within the lysyl oxidase family (LOXF): LOX, LOXL1, LOXL2, LOXL3 and LOXL4, all of which share the enzymatically active C-terminus and the cofactor lysine tyrosylquinone (Finney et al., 2014, Thomassin et al., 2005).

$$RCH_2NH_2 + O_2 + H_2O \longrightarrow RCHO + NH_3 + H_2O_2$$

Figure 1-6: The oxidative deamination of alkyl monoamines and diamines as catalysed by the lysyl oxidases (Palamakumbura and Trackman, 2002).

LOX is the most widely studied member of the LOXF family and has been shown to be expressed by a wide range of cell types in a number of organs, including fibroblasts, epithelial cells, smooth muscle cells, adipocytes, endothelial cells, osteoblasts and chondrocytes (Hayashi et al., 2004, Smith-Mungo and Kagan, 1998). The 46kDa LOX preproenzyme is synthesised by cells and transformed via signal peptide cleavage and N-glycosylation to the 50kDa LOX proenzyme which is then released and cleaved extracellularly to the 32kDa mature protein by bone morphogenetic protein-1 (Li et al., 1997, Finney et al., 2014).

LOX is important in lung development and is expressed in normal lung tissue (Poole et al., 1985, Barry-Hamilton et al., 2010). However, increased expression of LOX has been demonstrated in experimental models of pulmonary fibrosis (Machon et al., 2014, Borel et al., 2001, Counts et al., 1981) as well as in tumour biopsies from cancer patients. Indeed, LOX expression in certain tumours has been shown to correlate with poor survival and has thus been suggested as a therapeutic target (Erler et al., 2006).

Pathological activity of lysyl oxidase-like2 (LOXL2) has been shown by Barry-Hamilton *et al*, with increased expression of LOXL2 in the lung tissue of patients with IPF (Barry-Hamilton et al., 2010), while Chien *et al* found an association between serum LOXL2 levels and the progression of IPF (Chien et al., 2014). Furthermore, it has been shown that inhibition of LOXL2 can reduce lung fibrosis in the bleomycin model (Barry-Hamilton et al., 2010). As with LOX, the clinical relevance of LOXL2 also extends to tumour biology, with increased expression demonstrated in tumour biopsies from cancer patients, particularly in association with α-SMA positive fibroblasts. Inhibition of LOXL2 in a murine tumour model resulted in a reduction in cross-linked collagen, activated fibroblasts and tumour associated endothelial cells, culminating in reduced tumour volume (Barry-Hamilton et al., 2010).

It was this interest in the lysyl oxidases as potential therapeutic targets that inspired The Pulmonary Optical Molecular Imaging Group to investigate the possibility of developing a selective and sensitive fluorometric substrate probe to monitor enzymatic activity in complex biological systems.

1.6.1 Assays of LOX activity

For decades the most commonly used assays were based on LOX substrates containing tritiated lysine residues. The oxidative deamination of these residues by LOX resulted in the release of tritium ions and the subsequent production of tritiated water which could be quantified (Bedell-Hogan et al., 1993). The main disadvantage of this technique is that it utilises a discontinuous end point assay and therefore cannot inform on dynamic enzyme activity. Furthermore, the methodology is time-consuming and requires specialised equipment (Palamakumbura and Trackman, 2002).

The first fluorometric assay of lysyl oxidase activity utilised the hydrogen peroxide released from the reaction shown in Figure 1-6, to catalyse the oxidation of homovanillate in the presence of horseradish peroxidase (Trackman et al., 1981). The oxidisation of homovanillate yields a fluorescent product that gives a continuous read-out of enzyme activity. However, not only does the assay require the addition of

a LOX substrate and horseradish peroxidase as well as excitation with ultraviolet light, but it is also susceptible to interference from contaminating macromolecules in un-purified biological samples (Palamakumbura and Trackman, 2002, Trackman et al., 1981).

Other fluorescent reporters of amine oxidase activity have been designed either on a coumarin (Long et al., 2012) or resorufin scaffold (Zhou et al., 1997). The excitation wavelength for coumarin (λex 360nm) limits its applicability for cellular imaging due to its close proximity to the ultraviolet region. Amplex red (N-acetyl-3,7-dihydroxyphenoxazine) is a non-fluorescent derivative of dihydroresorufin that is converted to fluorescent resorufin on reaction with hydrogen peroxide in the presence of horseradish peroxidase (Zhou et al., 1997). This sensor has been utilised in a number of settings including the quantification of neutrophil nicotinamide adenine dinucleotide phosphate oxidase, monoamine oxidase (MAO), glucose oxidase and LOX (Zhou et al., 1997, Mohanty et al., 1997, Palamakumbura and Trackman, 2002). While providing a sensitive method for the detection of hydrogen peroxide, Amplex red is non-specific and as for the homovanillate method, relies on the addition of a substrate for the target enzyme (Rodriguez et al., 2010). It is also unlikely to be applicable *in vivo* and as yet no such utility has been reported (Li et al., 2014).

Thus there is a definite need for a sensitive fluorescent reporter of lysyl oxidase activity that can be utilised *in vivo*. In a recent publication, Li et al reported a novel probe for the fluorometric detection of MAO-A and MAO-B in vitro (Li et al., 2014). This utilised methyl fluorescein as the reporter and an amine oxidation/β-elimination mechanism to produce amplification of fluorescent signal in the presence of MAO-A and B. Alkylation of the two OH groups of the fluorescein derivative results in chemical ‘masking’ of the probe’s fluorescent signal in its un-activated state. Linkage of one of these hydroxyl groups to an amine oxidase substrate allows oxidation of the substrate in the presence of the target enzyme and subsequent spontaneous β-elimination of the resulting unstable aldehyde to yield the fluorescent molecule (Figure 1-7). The probe demonstrated a higher affinity for MAO-B over MAO-A, and was shown to have utility in a human breast cancer cell line.

While the probe synthesised by Li *et al*, 2014, has only been utilised to report on MAO activity, the incorporated amino-propoxy group may also be used as a substrate for LOX. Indeed, a fluorescent LOX Smartprobe, named TWB-219 (Figure 1-8), was synthesised by UoEDC prior to publication of the above manuscript and shared a similar structure (See Chapter 4). In order to be able to evaluate the utility of this probe with regards to the detection of LOX activity in complex biological environments, a potent inhibitor of LOX activity had to be identified.

1.6.2 Inhibitors of LOXF

β-Aminopropionitrile (BAPN) has been extensively used as the reference LOX inhibitor, with a reported IC_{50} of 10 μM (Narayanan et al., 1972, Barry-Hamilton et al., 2010, Li et al., 1997, Palamakumbura and Trackman, 2002). Although generally accepted to be a specific and irreversible inhibitor, this action had been shown to be time and temperature dependent and BAPN does appear to also have a lower affinity for inhibiting other oxidases (Tang et al., 1983, Mercier et al., 2009). BAPN has been shown to inhibit LOXL1 (Borel et al., 2001), LOXL3 (Lee and Kim, 2006) and LOXL4 (Ito et al., 2001), while inhibition of LOXL2 by BAPN is more controversial with mixed reports of success (Kim et al., 2011, Rodriguez et al., 2010). Over the last two decades various mechanism based selective inhibitors of LOX have been proposed as anti-fibrotic agents (Kagan and Gacheru, 1991, Nesbit, 2006, Burchardt et al., 2008, Nesbit, 2007, Apstein, 1996). Of these, the pyridazinone-based class are among the most potent (IC_{50} 0.005-0.07μM)(Apstein, 1996). Thus, compounds AMF-59 (Rudolf Schohe-Loop, 2006) and AMF-60 were synthesized in-house by UoEDC for application in inhibition studies (Figure 1-9).

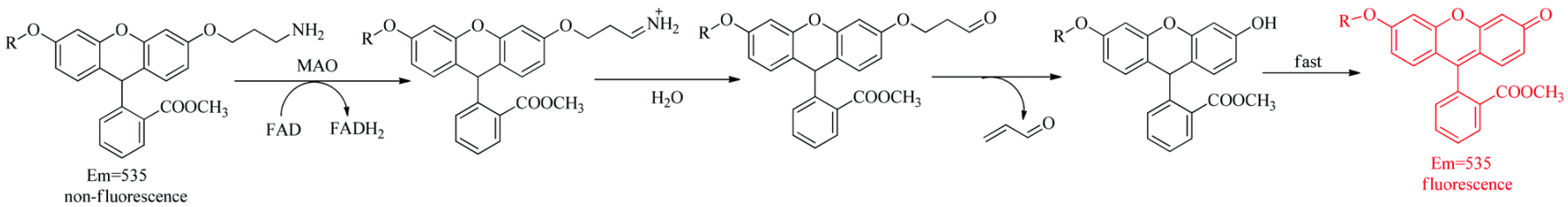

Figure 1-7: 'Design principle of the fluorescent probes for MAO'. Reproduced from Li, X., H. Zhang, et al., 2014. Organic and Biomolecular Chemistry 12(13): 2033-2036, with permission from The Royal Society of Chemistry.

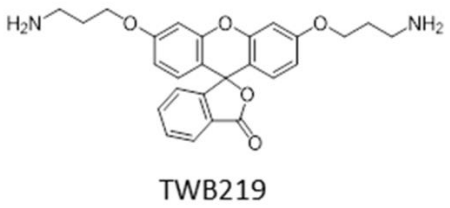

Figure 1-8: Structure of TWB-219. TWB-219 was synthesised by UoEDC for the detection of active lysyl oxidase.

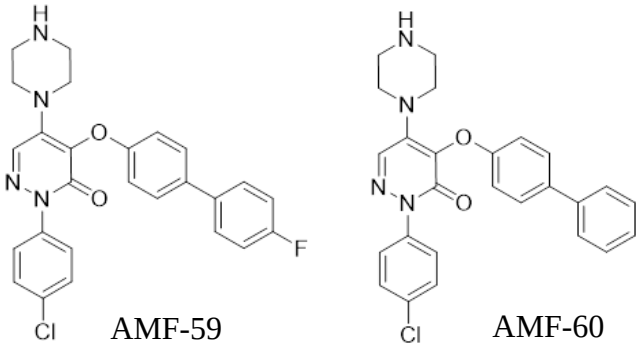

Figure 1-9: In-house LOX inhibitors. LOX inhibitor AMF-60 had been previously shown to have an IC_{50} of 3nM (Rudolf Schohe-Loop, 2006). AMF-59 was designed based on structure activity relationship of similar inhibitors where the introduction of 4-(p-fluorophenyl)phenol enhanced the potency of the inhibitor (Burchardt et al., 2008).

1.7 Matrix metalloproteinases

The second targets in the fibrogenic process identified by The Pulmonary Optical Imaging Group as potentially tractable for chemical targeting were the matrix metalloproteinases (MMPs), with particular focus on MMP-9. The matrix metalloproteinases are a family of zinc dependent protein and peptide hydrolases, 23 of which have been identified in the human genome (Tallant et al., 2010). These enzymes are either secreted by cells or bound to cell membranes (Itoh, 2015) and are collectively capable of degrading all ECM components including collagen and elastin (Woo et al., 2004). They are thus involved in a wide range of physiological processes from embryogenesis to bone resorption, tissue remodelling, angiogenesis and wound healing, but also play important roles in the proteolytic processing of proteins including other proteases, growth factors, hormones and cytokines (Tallant et al., 2010).

MMP activity is governed via transcription, secretion, activation, and inhibition (Massova et al., 1998). Genes encoding MMPs have been identified across all walks of life from plants and invertebrates to mammals, with an origin that may even trace

back to bacteria (Massova et al., 1998). Furthermore, in the vertebrate genome these genes are widely dispersed along different chromosomes. In the human genome the genes are distributed over 10 distinct chromosomes. While a cluster of 9 MMP genes including that encoding MMP-13 are located on chromosome 11, the functionally related gelatinases MMP-2 and MMP-9 map to chromosomes 16 and 20 respectively (Fanjul-Fernández et al., 2010). The majority of MMPs consist of a propeptide (~ 80 amino acids), a catalytic domain (~ 170 amino acids), a linker peptide and a hemopexin domain (~ 200 amino acids). However, evolution of the MMP family has resulted in the alteration of these domains allowing members to be separated into four different groups (Figure 1-10): archetypal MMPs including the collagenases and stromeolysins, the matrilysins, the gelatinases and finally the furin-activatable MMPs which include those that are bound to cell membranes (Fanjul-Fernández et al., 2010).

MMPs are expressed by fibroblasts, epithelial and endothelial cells as well as by inflammatory cells such as macrophages, lymphocytes, neutrophils and eosinophils (Woo et al., 2004). In general MMP expression is induced rather than being an inherent feature of these cells, with inciting agents such as inflammatory cytokines and bacterial lipopolysaccharides (Saren et al., 1996). The majority of MMPs are secreted in their inactive pro-form with the N-terminal pro-domain blocking the catalytic zinc ion at the active site cleft (Tallant et al., 2010). Removal of the pro-domain to reveal the active enzyme is catalysed *in vivo* by trypsin, plasmin, pro-hormone convertases, oxidation mechanisms and other MMPs as well as by mercurial compounds, chelating and alkylating agents *in vitro* (Tallant et al., 2010). In the case of MMP-9, the pro-form has a molecular weight of 92kDa and is cleaved to the active 82kDa form.

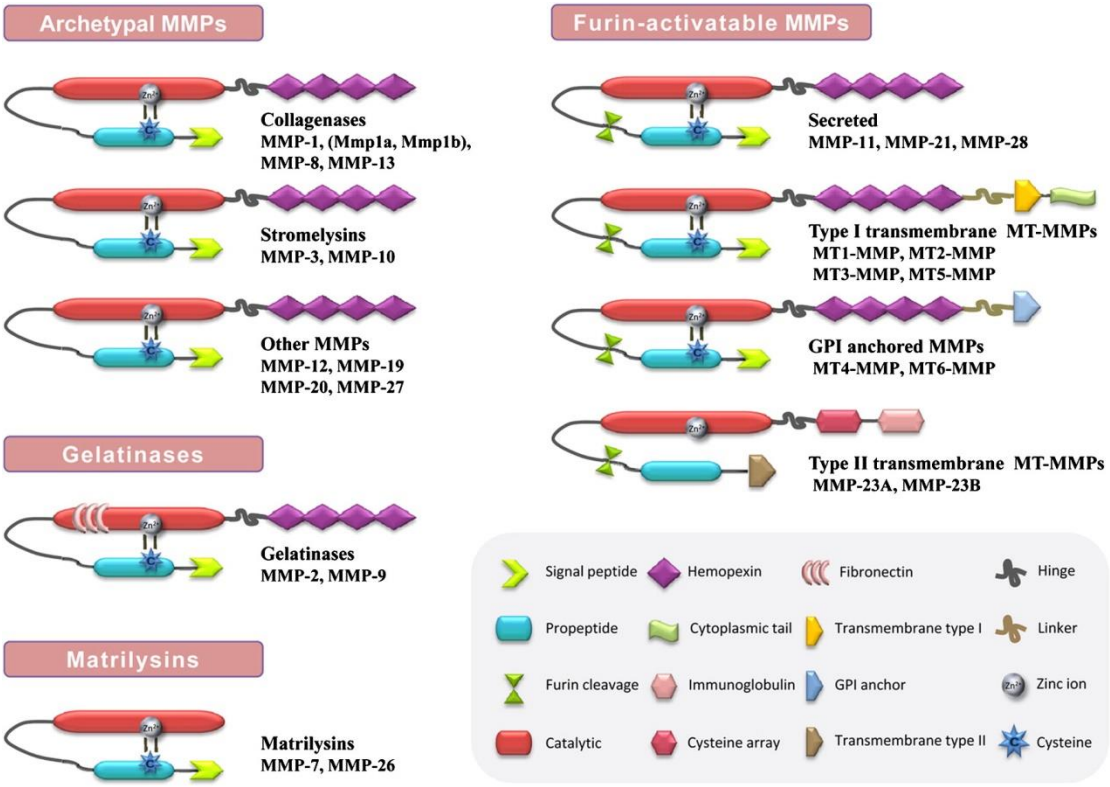

Figure 1-10: 'The mammalian family of matrix metalloproteinases.' 'Structural classification of MMPs based on their domain arrangement.' Reproduced from Fanjul-Fernández *et al*. 2010. Biochimica et Biophysica Acta (BBA) - Molecular Cell Research, 1803(1): 3-19, with permission from Elsevier.

Dysregulation of the proteolytic activity of MMPs contributes to the tissue damage seen in chronic inflammatory conditions such as arthritis, periodontitis, atherosclerosis and even Alzheimer's disease (Tallant et al., 2010). MMP overexpression is also integral to various cancer-associated processes from the facilitation of invasion and metastases via degradation of tissue and basement membrane, to tumourigenesis and neovascularisation (Overall and Lopez-Otin, 2002).

In several organs, including the lung, an imbalance between the synthesis and degradation of ECM molecules is thought to be central to the pathogenesis of fibrotic conditions. In interstitial pneumonias it is believed that the destruction of the subepithelial basement membrane results in increased permeability of alveolar walls and an influx of inflammatory cells culminating in intra-alveolar fibrosis (Suga and Iguchi, 2000). MMP-3,-7,-8 and 9 have been shown to be elevated in broncho-alveolar lavage (BAL) from patients with IPF, with the highest levels of MMP-9 (and MMP-8) in patients with rapidly progressive disease (McKeown et al., 2009, Suga and Iguchi, 2000). These findings along with the central role played by MMP-9 in several aspects of tumour progression (Farina and Mackay, 2014), led to the identification of MMP-9 as a Smartprobe target by The Pulmonary Optical Molecular Imaging Group.

However, as discussed above, MMP function reaches far beyond the degradation of ECM and the exact role that individual MMPs such as MMP-9 play in fibrosis remains poorly understood (Giannandrea and Parks, 2014). MMP-9 (along with MMP-2) has the ability to activate latent TGF-β (Yu and Stamenkovic, 2000), supporting the argument for a pro-fibrotic role (Lee et al., 2001). Studies have also demonstrated that interleukin-13 (IL-13) induced alveolar remodelling is MMP-9 dependent (Lanone et al., 2002). However, a study by Betsuyaku *et al,* found that fibrosis occurred in bleomycin treated mice irrespective of the presence of MMP-9 (Betsuyaku et al.), while Cabrera et al, 2007, reported attenuation of fibrosis in bleomycin-treated mice over-expressing human MMP-9 (Cabrera et al., 2007). It is entirely possible that MMP-9 has both pro-fibrotic and protective actions throughout the extensive array of molecular pathways that exist in the fibrogenic lung. It is also

worth noting that the results of studies utilising overexpression of MMP-9 should be interpreted with caution for a number of reasons including a relative imbalance between enzyme and substrate as well as an evasion of inherent regulatory mechanisms (Giannandrea and Parks, 2014).

One such regulatory mechanism is via the tissue inhibitors of metalloproteinases (TIMPs) of which there are four different forms (TIMP-1 to TIMP-4) capable of inhibiting active MMPs with relatively low selectivity (Tallant et al., 2010, McKeown et al., 2009).

TIMPs also play a role in the activation of pro-MMPs as well as exhibiting growth factor-like and apoptotic capabilities (Tallant et al., 2010). There is ongoing debate regarding the ratio of TIMPs to MMPs that exists in conditions such as IPF and the respective roles that each group of proteins plays in the pathogenesis of fibrosis. Selman *et al*, 2000, reported a higher expression of TIMPs compared to MMPs in IPF (Selman et al., 2000), a finding that was supported by others (Fukuda et al., 1998, Suga and Iguchi, 2000). A pro-fibrotic role of the relative TIMPs within a non-degrading collagen microenvironment was described, including the promotion of alveolar epithelial cell apoptosis, activation of pro-MMPs and promotion of myofibroblast growth (Selman et al., 2000). However, others have found elevated MMP/TIMP ratios in the BAL from IPF patients, suggesting a prevailing state of MMP activity (McKeown et al., 2009, Henry et al., 2002). It is very difficult to assess the true activity of MMPs in biological samples and an excess of MMPs over TIMPs does not necessarily correlate with an excess of MMP activity (Giannandrea and Parks, 2014). Furthermore, it is very possible that the ratio of MMPs to TIMPs is both dynamic and variable throughout different areas of the fibrotic lung. Indeed this is something that could be investigated by the use of fluorometric activity-based *in situ* imaging techniques.

1.7.1 MMP inhibitors

As the full extent and significance of the actions of MMPs within fibrotic disease and cancer begins to emerge, so does the importance of these enzymes as both therapeutic and imaging targets.

More than 50 MMP inhibitors have been investigated in cancer clinical trials alone, none of which have been successful (Vandenbroucke and Libert, 2014). Early MMP inhibitors were based on the cleavage site of collagen and the results of substrate specificity studies. Marimastat is one such first generation inhibitor which incorporates a hydroxamic acid zinc binding group capable of chelating the active site zinc ion within MMP molecules (Whittaker et al., 1999). It is a broad spectrum MMP inhibitor that has been used in several cancer clinical trials. This lack of specificity combined with a high rate of musculoskeletal side effects precluded the use of marimastat as an anti-cancer therapeutic despite positive results in animal models of human disease (Shepherd et al., 2002). One of the challenges faced by marimastat and other MMP inhibitors with regards to clinical trials is that the standard clinical trial endpoints for cancer patients, such as a reduction in tumour size, are not suitable for evaluating the effects of molecularly targeted cytostatic agents (Coussens et al., 2002).

MMP inhibitors have also received substantial interest within inflammatory disease processes. AZD1236, AstraZeneca, is a potent and reversible inhibitor of human MMP-9 and MMP-12, with lower selectivity towards MMP-2 and MMP-13 that was designed as therapy for chronic obstructive pulmonary disease. Once again it showed promising results in animal models, reducing haemorrhage and inflammation caused by administration of human MMP-12 into rat lungs (Magnussen et al., 2011). However, this success was not translated to clinical trials whereby a 6 weeks phase II trial did not reveal any evidence of drug efficacy, although adverse effects were minimal (Dahl et al., 2012).

A new generation of MMP inhibitors is emerging that exhibit structural specificity towards selected MMPs and reduced likelihood of inducing inadvertent off-target effects within the complex proteolytic pathways that exist *in vivo* (Vandenbroucke and Libert, 2014). This is achieved by targeting less well conserved sites distant to the catalytic domain (Schnute et al., 2010) or by utilising antibody-based inhibition (Devy and Dransfield, 2011).

1.7.2 Fluorometric assays of MMP-9 activity

It is clear from the discussion above that sensitive and dynamic endpoint targets are desperately needed to aid in the evaluation of MMP targeted therapeutics. Fluorometric Smartprobes specific to individual MMPs have the potential to provide a solution to this problem.

With regards to MMP-9, a number of different fluorometric assays currently exist. The first assay of MMP-9 activity involved the use of ^{14}C-labeled gelatin as a substrate (Harris Jr and Krane, 1972). This was followed by the synthesis of an activatable FRET probe for MMP-9 in 1988 which utilised the intrinsic fluorescence of the amino acid tryptophan (Stack and Gray, 1989) and also incoorporated a substrate sequence. However, it was not until 2001 that MMP activity was succsessfully measured *in vivo* (Bremer et al., 2001). Bremer *et al*, 2001, designed a NIR probe featuring a substrate sequence designed to confer MMP-2 selectivity and utilised it to image tumours in a murine model. However this probe which is now comercially available as MMPSense (PerkinElmer) is also cleaved by MMP-1,-7,-8 and -9 (Bremer et al., 2001). More recently, a cyanine based NIR probe that also demonstrated *in vivo* utility was proposed to be selective for MMP-2 and MMP-9 in tumour models (Jiang et al., 2004, Olson et al., 2009). This activatable probe comprises a substrate that is cleaved by MMPs to release a fluorescently labelled cell penetrating peptide which is capable of binding to and entering cells (Jiang et al., 2004). MMP-2 and MMP-9 selectivity of this probe was investigated by utilising MMP inhibitors as well as MMP-2/MMP-9 knockout murine models (Olson et al., 2009). Improved selectivity for MMP-2 was later conferred by the addition of an integrin αvβ3-binding domain as a co-targeting moiety (Crisp et al., 2014). However, a substrate based fluorescent Smartprobe with good selectivity for MMP-9 activity *in vivo* has yet to be synthesised.

1.8 Objectives and hypotheses

This thesis details my journey within the field of comparative pulmonary fibrosis from the study of spontaneous pulmonary fibrosis in a veterinary species to the evaluation of molecular imaging tools to aid in therapeutic monitoring of the disease

process. The study was inspired by the 'One Health' approach to medical science, with veterinary and medical scientists working together towards common goals.

The third chapter of this thesis represents the comprehensive characterisation of APF, with the overarching hypothesis that analysis of high resolution CT images of fibrotic asinine lungs and subsequent correlation with histopathological features would uncover comparative disease characteristics. A further goal was to evaluate techniques to aid veterinary clinicians in the diagnosis of APF which at present is often not detected until the late stages of disease when the donkey presents in respiratory distress. Thus the first section of Chapter 3 looks at the results of the systematic clinical examinations of a group of 22 donkeys with suspected respiratory disease. Sixteen of these donkeys were subsequently euthanased on humane grounds due to deterioration of their condition, facilitating correlation between clinical examination and post mortem findings.

The remainder of chapter 3 focuses on the results of HRCT and histopathological analysis of 32 *ex vivo* asinine lungs collected at routine necropsy examination. Review and subsequent scoring of the collected images and sections by expert radiologists and pathologists allowed identification of comparative features with striking similarity to the rare interstitial lung disease termed PPFE. Finally, investigation into potential inciting agents of APF was performed.

The clinical examination, HRCT and histopathological techniques utilised in chapter 3 are the mainstay of current disease diagnosis and monitoring in patients with fibrotic lung disease. While these techniques allow the meticulous characterisation of disease in relation to ATS guidelines, they provide static 'snap-shots' of pathology that cannot inform upon the dynamic state of the fibrogenic pathways targeted by novel anti-fibrotic therapies. As such, chapters 4 and 5 look at the expression of two potential therapeutic targets, LOX and MMP-9 within fibrotic asinine and human lung tissue, with the subsequent evaluation of targeted Smartprobes designed to monitor enzyme activity *in vivo*.

The overall hypothesis of chapter 4 was that a fluorogenic substrate peptide for LOX could rapidly report on enzymatic activity in *ex vivo* asinine and human lung tissue. The fluorogenic LOX Smartprobe, TWB-219, was thus evaluated utilising a range of plate reader and FCFM assays. The chapter begins with investigation into the expression of LOX and LOXL2 in murine cell lines with a view to developing a readily available source of active enzyme. Unfortunately preliminary experiments involving the incubation of cell supernatants with TWB-219 were unsuccessful due to high background fluorescence in cell culture medium. A range of experiments were then performed to investigate this problem and an alternative oxidase enzyme was used to achieve probe activation.

The remainder of chapter 4 focusses on the evaluation and subsequent use of *ex vivo* human and asinine lung tissue homogenate as a source of active LOXF for activation of TWB-219. It was important to show that signal amplification in the human tissue homogenate could be prevented by pre-incubation of the homogenate with potent LOX inhibitors. As such both BAPN and the in-house pyridazinone-based LOX inhibitors, AMF-59 and AMF-60 were used to demonstrate signal specificity. The report of a probe with a similar structure to TWB-219 as a reporter of MAO activity drove the need to confirm that signal amplification in tissue homogenate was not due to probe activation by MAO. As such, an experiment was performed whereby human tissue homogenate was pre-incubated with MAO-A and MAO-B inhibitors, clorgyline and pargyline, respectively, prior to exposure to TWB-219. Finally, the use of FCFM to detect activation of TWB-219 in *ex vivo* human and asinine lung tissue was investigated.

Chapter 5 follows the evolution of a Smartprobe for the detection of active MMP-9, with the central hypothesis that a fluorogenic substrate peptide for MMP-9 could rapidly report on enzymatic activity in biological samples including *ex vivo* human lung tissue. Testing this hypothesis once again involved the use of western blot and immunohistochemistry, this time with the addition of enzyme-linked immunosorbent assay (ELISA) and zymography techniques in order to establish MMP-9 expression in cell supernatants and asinine and human *ex vivo* lung tissue. Due to limited

availability of asinine tissue at this point in the study, *ex vivo* ovine cancer tissue was also explored as an alternative.

The chapter goes on to document a number of biological assays for the evaluation of a family of MMP Smartprobes with regard to the target product profile (Fig 5.3) including utility in *ex vivo* ovine and human lung tissue. Probe stability upon incubation with neutrophil supernatant and lysate, as well as off target enzymes elastase and plasmin, was also investigated. Final selection of a lead MMP Smartprobe involved performing enzyme kinetic assays and evaluating probe performance in *ex vivo* human lung tissue as determined by analysis of FCFM data.

1.8.1 Summary of central hypotheses

- Analysis of HRCT images of fibrotic asinine lungs and subsequent correlation with histopathological features will uncover comparative disease characteristics relevant to human fibroproliferative disease.

- A fluorogenic substrate peptide for LOX (TWB-219) can rapidly report on enzymatic activity in *ex vivo* asinine and human lung tissue.

- A fluorogenic substrate peptide for MMP-9 (SVC-186) can rapidly report on enzymatic activity in biological samples including *ex vivo* human lung tissue.

Chapter 2: Materials and Methods

2.1 Clinical assessment

Twenty-two donkeys with a history of demonstrating clinical signs of respiratory disease were examined at The Donkey Sanctuary, Devon, between March 2011 and January 2013. Donkeys were examined on up to 3 occasions at least 3 months apart as per an examination protocol that was designed specifically for the study (Appendix 7.2). If one of the donkeys was euthanased on humane grounds then post mortem reports were analysed and lungs were collected where possible.

2.1.1 Respiratory rate and effort

Respiratory rate was determined by counting number of breaths over 1 min, ideally observing the breathing pattern from a distance to avoid disturbing the donkey. Respiratory effort was scored using a system modified from one previously published (Rush et al., 1998) (Appendix Figure A2). The sum of respiratory effort and nostril flare scores was used to give a final score out of 8 for each donkey. Scores were agreed upon by two veterinary surgeons. If a donkey was examined more than once then the highest score was used. Data were analysed using GraphPad Prism 5 software (GraphPad Software, Inc., San Diego, and USA.) and a Mann Whitney-U test.

2.1.2 Thoracic ultrasound

Trans-cutaneous thoracic ultrasound was carried out when possible using a DP-6900 Vet machine (Mindray Medical International Ltd, China). When time constraints were an issue only one side of the thorax was imaged unless lesions were detected. Optimal thoracic ultrasound images were obtained if the hair over the donkey's thorax was clipped and the skin coated with isopropyl alcohol (67-63-0, Hayman Ltd, Essex, UK). If possible this was done for both sides of the thorax; however this was not always feasible due to the donkey's temperament or time constraints. In many cases, it was found that reasonable images could be obtained simply by parting the donkey's hair and applying isopropyl alcohol directly to the skin with a spray bottle.

2.1.3 Pulse oximetry

Pulse oximetry was carried out using a VitalStore Pulse Ox Module with Reflectance Probe (Vetronic Services Ltd, UK) respectively. The coccygeal artery was found to provide the most reliable point of contact for pulse oximetry measurements and the highest of 3 readings obtained with an 'A' rate signal was recorded.

2.1.4 Thoracic radiography

Thoracic radiography would have been useful to detect evidence of pulmonary fibrosis in donkeys presenting with signs of respiratory disease. However, The Donkey Sanctuary staff was unable to perform this technique due to a combination of equipment limitations and health and safety considerations.

2.2 Collection of asinine lung tissue

Whole lungs were collected from 32 aged donkeys during routine necropsy at two UK donkey sanctuaries (The Donkey Sanctuary, Sidmouth, Devon [n=31] and The Scottish Borders Donkey Sanctuary, St Boswells, Melrose, [n=1], between June 2009 and January 2013. Nineteen 'APF' lungs were selected because of grossly visible fibrosis, while 13 grossly unaffected 'control' lungs were selected at random. All donkeys included in the study were euthanised on humane grounds a maximum of 8 h prior to necropsy. The lungs were manually inflated, the trachea clamped and gross images photographed. Tissue samples were collected from each lung according to a standard protocol devised by Dr Du Toit and Prof McGorum (Appendix 7.1) and either snap frozen for future homogenisation or fixed into 10% buffered formalin (HT501128, Sigma-Aldrich, St Louis, MA, USA) before undergoing routine processing to paraffin blocks.

It should be noted that collection and processing of 12 lungs occurred prior to the commencement of this doctoral research and was performed by Dr Nicole Du Toit, The Donkey Sanctuary, Devon.

2.3 Retrospective analysis of clinical data

The Donkey Sanctuary's clinical databases were systematically reviewed for each of the donkeys included in the study. Any history of respiratory disease was recorded along with the results of routine terminal haematology and biochemistry when available. For the purposes of the study, a lower respiratory tract infection was considered if there was a record in the database of appropriate clinical signs, including abnormal lung sounds on auscultation, and a clinical improvement with antibiotic therapy.

2.4 High resolution computed tomography (HRCT) and digital photography

Eighteen whole inflated *ex vivo* lungs (11 APF, 7 control) were imaged using HRCT (Toshiba Aquilon One Toshiba Medical Systems, Tokyo, Japan or Siemens Somatom Volume Zoom, Siemens Aktiengesellschaft, Munich, Germany). The remaining lungs (8 APF, 6 control) were systematically sectioned transversely and photographed digitally.

2.5 Histopathology

Sections were stained with haematoxylin and eosin (H&E), Elastic Van Gieson (EVG) and Masson's Trichrome (MT). Histology sections were reviewed independently and blindly by 3 medical and veterinary pathologists with expertise in assessing lung disease. Histopathological features were described and documented for each animal. Staining was carried out by technicians in the histology laboratories at The Queen's Medical Research Institute, Edinburgh (QMRI) or The University of Edinburgh, Royal Dick School of Veterinary Studies (RDSVS).

2.6 Categorisation of lungs with regards to PPFE

Subsequent to the recognition that the pathological features of many APF lungs resembled those of human PPFE, the histological features were categorised as being 'consistent with' or 'inconsistent with' PPFE according to criteria described by Reddy et al, 2012 (Reddy et al., 2012). Cases were categorised as 'consistent with' PPFE on histology if (a) there was pleural thickening with associated subpleural intra-alveolar fibrosis and alveolar septal elastosis, or (b) intra-alveolar fibrosis was present but either not associated with pleural fibrosis, not predominantly subpleural or not in a dorsal lobe sample. 'Inconsistent with' PPFE was assigned to lungs that lacked the aforementioned features.

HRCT images were reviewed independently and blindly by an expert radiologist and were categorised as 'consistent with' or 'inconsistent with' PPFE according to criteria described previously (Reddy et al., 2012). Cases were categorised as 'consistent with' PPFE if there was (a) pleural thickening with associated subpleural fibrosis predominantly in the dorsal lung, or (b) dorsal lung pleural thickening and associated subpleural fibrosis but the distribution of fibrosis was not restricted to the dorsal lung or there was evidence of coexistent lung disease elsewhere. 'Inconsistent with' PPFE was assigned to lungs that lacked the aforementioned features. Overall, cases were assigned as 'PPFE-like' only if categorised as 'consistent with' PPFE on both imaging and histology.

2.7 Aetiological investigation

2.7.1 Special staining

Lung sections in which there was granulomatous inflammation were stained for acid fast bacteria using a standard Ziehl-Neelsen stain and for fungal hyphae elements using Grocott's methenamine silver and Periodic acid-Schiff stains. Sections containing multi-nucleated giant cells were stained for viral inclusions with Lendrum phloxine-tartrazine.

Staining was carried out by technicians in the histology laboratories at QMRI or RDSVS.

2.7.2 X-ray diffraction analysis

X-ray diffraction analysis was performed by Dr A.R.Gibbs, Environmental Lung Disease research Group, University Hospital Llandough, Penarth.

Formalin fixed wet lung tissue samples from 4 APF *ex vivo* lungs were pooled, digested in potassium hydroxide and then prepared for mineral particle analysis under transmission electron microscopy at a magnification of 20,000 and for energy dispersive x-ray analysis as described previously (Gibbs et al., 1994, Gibbs and Pooley, 1996). The mass of dust per gram of dry lung tissue was established. Both fibrous and non-fibrous particles were counted and typed.

2.7.3 Herpesviral PCR

Tissue samples from 12 lungs (6 APF, 6 controls) were collected into RNAlater (cat 76106, Qiagen N.V, Limburg, Netherlands) for deoxyribonucleic acid (DNA) extraction and subsequent polymerase chain reaction (PCR).

Herpesviral PCR was carried out by Dr R. Dalziel, The Roslin Institute, Edinburgh. Tissue samples were processed using the AllPrep DNA/RNA Mini Kit (Cat 80204, Qiagen N.V, Limburg, Netherlands) according to the manufacturer's instructions. Briefly, samples were homogenized using lysing tubes D in a FastPrep homogenizer (MP Biomedicals, Santa Ana, California). Where yields were low or of poor quality, samples were repeated. If the result was still low/poor then deoxyribonucleic acid (DNA) was extracted using the DNeasy Blood and tissue kit (Cat 69504, Qiagen, N.V, Limburg, Netherlands).

For investigation of the presence of herpesvirus, amplification of a region of the herpesvirus DNA polymerase gene was carried out using 100ng of DNA per reaction with two sets of nested degenerate primers as described in Kleiboeker *et al.* 2002. PCR products from 6 (3 APF, 3 control) samples were cloned into the TOPO®TA vector (Invitrogen, Thermo Fisher Scientific, Waltham, Massachusetts, USA),

sequenced (Genepool, Edinburgh) and Blastn (2.6.2) used to align the derived sequence against known herpesvirus sequences.

2.8 Culture of murine cell lines

Cell culture protocols and cell lines were obtained from Emma Scholefield. Murine NIH 3T3 fibroblasts and murine Raw 264.7 mouse monocyte macrophages (93061524 and 91062702 Sigma-Aldrich, St Louis, MA, USA) were maintained in 160mm^2 cell culture flasks (Corning Incorporated, Corning, USA) in Dulbecco's Modified Eagle's medium (DMEM, cat:11960-044, Thermo Fisher Scientific, Waltham, Massachusetts, USA) medium supplemented with 10% heat inactivated foetal bovine serum (FBS, Cat FB-1090, Biosera, Boussens, France), containing 1% L-glutamine and 1% penicillin/streptomycin (25030-024 and 15140-122, Thermo Fisher Scientific, Waltham, Massachusetts, USA), at 37˚C in a 5% CO_2 / 95% O_2 atmosphere. Cells were passaged every 3-5 days upon reaching approximately 70% confluence. The medium was removed and washed once with Dulbecco's PBS with calcium and magnesium (10440-091, Thermo Fisher Scientific, Waltham, Massachusetts, USA) prior to incubation with 5ml 0.5% trypsin-EDTA (25300-054, Thermo Fisher Scientific, Waltham, Massachusetts, USA) at 37˚C for 2-8min. In the case of the RAW 264.7 cells a cell scraper was sometimes required to assist in cell detachment. The trypsin-EDTA was then deactivated by dilution with 10ml of cell culture medium prior to centrifugation at 350g for 5min to remove the supernatant. Cells were then re-seeded at 1/10 dilution, equating to approximately 850,000 cells per flask. In order to preserve cells for future use, cells were frozen at approximately 8x10^{6}cells per 1ml of 60% culture medium with 10% Dimethyl sulfoxide (DMSO, cat:D2650, Sigma-Aldrich, St Louis, MA, USA) and an additional 30% FBS.

For the collection of cell supernatant, cells were seeded at approximately 20,000 per cm^2 and cultured to 70% confluence in 6 or 24 well plates then placed in starvation media prior to stimulation. Starvation media consisted of phenol red free DMEM (31053-044, Thermo Fisher Scientific, Waltham, Massachusetts, USA) supplemented with 1% L-glutamine and 1% penicillin/streptomycin and varying concentrations of either FBS or bovine serum albumin (BSA, A9418, Sigma-Aldrich,

St Louis, MA, USA). Cells were stimulated using varying concentrations of recombinant human tumour growth factor-β1 (TGF-β1, cat 240-B-002, R&D Systems Inc., Minneapolis, USA), recombinant murine interferon gamma (IFN-γ, cat 315-05, PeproTech, New Jersey, USA) and lipopolysaccharide from Escherichia coli 0127:B8 (LPS, L4516, Sigma-Aldrich, St Louis, MA, USA) for 6-48 h. Supernatants were then collected onto ice and centrifuged at 13,000 rpm for 20min at 4°C to remove any cell debris. Total cells per well that remained adhered to the cell culture trays were washed with Dulbecco's PBS without calcium and magnesium (14190193, Thermo Fisher Scientific, Waltham, Massachusetts, USA) then lifted using 0.5% trypsin EDTA and counted using a haemocytometer. This allowed any subsequent measurements of proteins within the supernatants to be expressed as mass per million cells. Prior to performing an ELISA, it was necessary to concentrate the supernatants using a vacuum concentrator (Jouan RC10.10, Thermo Fisher Scientific, Massachusetts, USA). Centrifugation tubes (Amicon Ultra-15, UFC905008, Merck Millipore, Billerica, MA, USA) were also used to concentrate the supernatant from 3T3 cells prior to western blot and zymography.

2.9 Cytometric bead array (CBA)

A CBA Mouse Inflammation Kit (552364, BD Biosciences, New Jersey, USA) was used to investigate the differences in inflammatory cytokines expressed by 3T3 and RAW cells following stimulation with TGFβ and LPS respectively. Cytokines measured were: interleukins 6, 10 and 12 (IL-6, IL-10, IL-12p70), IFNγ, tumour necrosis factor (TNF) and monocyte chemoattractant protein-1 (MCP-1). A vial of lyophilized Mouse Inflammation Standards was reconstituted in 2ml of Assay Diluent allowed to equilibrate at room temperature for 15min. An 8-point serial dilution was then performed ranging from 5000-20pg/ml along with a negative control consisting of assay diluent alone. The 6 individual tubes of capture beads were vortexed then combined using a 10µl aliquot of each bead per tube to be analysed.

Samples were diluted 1:200 in assay diluent before adding 50µl of sample or 50µl standard controls to each of the assay tubes containing 50µl of the mixed capture

beads. This was then combined with 50µl of Mouse Inflammation Phycoerythrin (PE) Detection Reagent containing PE-conjugated anti-mouse antibodies for each of the cytokines listed above. All tubes were incubated for 2h at room temperature protected from light, and then 1ml of Wash Buffer was added to each before centrifugation at 200g for 5min. The supernatant from each tube was removed and discarded prior to re-suspension of the bead pellet in 300ul Wash Buffer.

Analysis was performed on a BD FACS Calibur (BD Biosciences, New Jersey, USA) using FCAP Array software (641488, BD Biosciences, New Jersey, USA).

2.10 Isolation of neutrophils and monocytes from human blood using a Percoll gradient

Blood was collected from study volunteers by qualified phlebotomists or medical practitioners after obtaining signed consent. Blood preparations were sometimes performed by other members of the Lung Inflammation Group. The blood preparation protocol used was obtained from Prof Adriano Rossi.

To prepare the Percoll gradients, 3ml of 10X PBS (14200-075, Thermo Fisher Scientific, Waltham, Massachusetts, USA) was added to 27ml of Percoll® (P4937, Sigma-Aldrich, St Louis, MA, USA), to make up the Percoll stock. The stock was then diluted to 55%, 68% and 81% with PBS. The gradients were carefully layered just prior to use starting with 3ml of the 81% solution followed by 3ml of the 68% solution.

Whole blood was collected from the donor into 10% sodium citrate (W302600, Sigma-Aldrich, St Louis, MA, USA) in a 50ml BD falcon tube (BD Biosciences, Bedford, USA) then centrifuged at 350g for 20min with gentle brake and acceleration. The top layer (plasma) was then removed using a pastette and aliquoted into 10ml glass vial tubes containing 2.2% calcium chloride (C1016, Sigma-Aldrich, St Louis, MA, USA), before being incubated for one hour at 37˚C. The plasma plug was then removed leaving serum that could be added to culture media. 6ml of dextran (31392, Sigma-Aldrich, St Louis, MA, USA) was then added to the

erythrocyte layer and this was made up to 50ml with sodium chloride (UKF7124, Baxter International Inc., UK) and the tube inverted twice prior to being left to stand for 20 min at room temperature to allow sedimentation. The top layer was then removed and transferred to another 50ml tube without disturbing the buffy coat layer and topped up to 50ml with sodium chloride prior to centrifugation at 350g for 6 min. The top layer was then discarded and the cell pellet gently resuspended alongside 3ml of the previously prepared 55% Percoll gradient. This was then very carefully added on top of the other two Percoll layers using a pastette. Following centrifugation at 720g for 20 min, the monocyte then neutrophil layers were carefully removed and washed twice with PBS (without calcium and magnesium) centrifuging at 350g for 6 min. Cells were counted using either a haemocytometer or a NucleoCounter® NC-100™ (900-0004, ChemoMetec, Allerod, Denmark) and resuspended as required.

2.11 Culture of human blood monocyte macrophages

The protocol detailed below was adapted from one provided by Emma Scholefield. Cells were resuspended at $5x10^6$ cells/ml in Iscove's Modified Dulbecco's Media (IMDM, cat: 12440, Thermo Fisher Scientific, Massachusetts, USA) containing 1% pen/strep and plated out at 0.5ml per well into a 48 well plate. Plates were incubated for 1 hour at 37˚C before gentle washing x3 with the above media to remove any non-adherent cells. Medium was then replaced with IMDM containing 10% autologous serum in addition to the pen/strep. Cells were incubated at 37˚C in a 5% carbon dioxide/ 95% oxygen atmosphere and the media was replaced after 24h then every 48h. In order to investigate optimal culture and stimulation, a number of different factors were varied including length of culture prior to stimulation, starvation prior to stimulation, length of stimulation and means of stimulation. Cells were cultured for 5-7d prior to stimulation then washed x3 with PBS (+Ca+Mg) prior to overnight incubation in phenol red free IMDM supplemented with 1% pen/strep and either 0.5% BSA or autologous serum (1 or 10%). Cells were then stimulated for 6, 24 or 48h with either 10U/ml recombinant human IFNγ (cat PHC4031, Thermo Fisher Scientific, Massachusetts, USA) or LPS (100ng/ml, 500ng/ml or 1ug/ml).

Cells were viewed for changes in morphology and viability using a phase contrast microscope (Olympus 1M, Olympus Corporation, Tokyo, Japan) every 6- 24h. Supernatant was then collected and centrifuged at 4˚C for 5 min at 13,000rpm to remove any cell debris prior to snap freezing.

2.12 Stimulation of human neutrophils

A minimum of 40 million human neutrophils were resuspended at 20million cells/ml in warm sterile PBS (with calcium and magnesium) then divided into two tubes. One half was stimulated with calcium ionophore (A23187, Sigma-Aldrich, St Louis, MA, USA) at 37˚C for 30min while the unstimulated control was incubated in the same manner. Cells were then centrifuged at 350g for 5min prior to the supernatant being removed and snap frozen.

The cell pellets were again resuspended in PBS at 20million cells/ml before undergoing cell lysis with three cycles of rapid freeze thawing in acetone with dry ice. The lysate was centrifuged at 13,000rpm for 20 min at 4˚C to remove cell debris prior to snap freezing.

2.13 Collection and preparation of ovine tissue

Fresh ovine tissue was supplied by Dr Christina Cousens, The Moredun Research Institute, Edinburgh. Sheep with either naturally occurring or experimentally induced pulmonary andenocarcinoma (SPA) were culled for a research study being carried out by The Moredun Institute. Grossly unaffected, transitional and solid cancerous tissue sections were collected post mortem and transferred to The University of Edinburgh on ice. For plate reader experiments tissue was dissected into approximately $2mm^3$ sections and placed into a 96 well plate along with MMP buffer: 50mM Tris (T1503), 10mM $CaCl_2$ (C5080), 0.15M NaCl (S7653), 0.05% Brij 35 (B4184, Sigma-Aldrich, St Louis, MA, USA), pH 7, in a total volume of 60µl. For western blot, zymography and additional plate reader experiments, tissue was homogenised in PBS using a drill homogeniser (Bio-Gen PRO200 homogeniser, Pro-Scientific, Oxford, USA) prior to protein quantification (see 2.19). Sections of tissue were also fixed in 10% buffered formalin for immunohistochemical analysis.

2.14 Collection and preparation of human tissue

All human tissue was obtained with written informed patient consent via Dr Nik Hirani, and the study was approved by the Regional Ethic Committee. Human lung samples (patients aged 55-81 years) were obtained from the periphery of resections for lung carcinoma (n=12) or from surgical biopsies for investigation of interstitial lung disease (n=5). Fresh samples were placed immediately into transport medium (sodium chloride 0.9%, 1% pen/strep, 1% amphotericin B and 0.5% gentamicin (A2942 and G1272, Sigma-Aldrich, St Louis, MA, USA) at 4°C. For fibre confocal fluorescence microscopy (FCFM) imaging (see 2.28), tissue was further dissected to approximately $2mm^3$ sections and placed in a 96 well plate with MMP buffer (see 2.13) in a total volume of 60µl. A section of tissue was also fixed in 10% buffered formalin for immunohistochemical analysis, while the remainder was used for cell isolation or homogenised in PBS using a drill homogeniser (Bio-Gen PRO200 homogeniser, Pro-Scientific, Oxford, USA).

2.15 Culture of human primary lung fibroblasts and live cell imaging

The protocol detailed below was provided by Dr Nik Hirani. Tissue was carefully macerated on ice using a scalpel and agitated with 10mg/ml collagenase (C2674, Sigma-Aldrich, St Louis, MA, USA) in RPMI (31870-025, Thermo Fisher Scientific, Massachusetts, USA) for 1h at 37°C to give a single cell suspension. Cells were filtered in a 40µM cell strainer (BD Falcon, Thermo Fisher Scientific, Massachusetts, USA) then washed with culture media consisting of DMEM F12 +GlutaMAX™ (31331-028, Thermo Fisher Scientific, Massachusetts, USA) supplemented with 1% pen/strep and 10% FBS. Cells were then plated in 6 well plates and incubated at 37°C in a 5% CO_2/ 95% O_2 atmosphere for approximately 10d prior to refreshing the media and removing dead cell debris. At this stage fibroblasts have outgrown all other cell types. Upon reaching confluence cells were trypsinised and transferred to $75cm^2$ culture flasks (Costar®, Corning Inc., NY, USA). Cells were then passaged as required every 3-4d up to passage 10 essentially as described for NIH 3T3 cells above (see 2.8).

For live cell imaging cells were plated at 10-20,000 cells/ well in an 8-well chambered glass bottom plate (155409, Nunc™ Lab-Tek™ II, Thermo Fisher Scientific Inc., Waltham, USA). After approximately 12h cells were washed with and then incubated with phenol red free DMEM. Cells were then incubated for 1h at 37˚C with either 500uM or 1mM 3-Aminopropionitrile fumarate salt (BAPN, A76427, Sigma-Aldrich, St Louis, MA, USA) prior to the addition of 10uM or 50uM TWB-219 for a further 1.5h. Cells were washed x3 with phenol red free DMEM prior to imaging on a Leica TCS SP5 confocal microscope (Leica Microsystems, Wetzlar, Germany) in the same media.

2.16 Immunohistochemistry

Tissues were fixed in 4% paraformaldehyde (P/0840/53, Fisher Scientific, Leicestershire, UK) and embedded in paraffin prior to the cutting of 5µm sections. Paraffin embedding and microtome cutting of blocks was performed by technicians in the histology lab, QMRI. Immunohistochemistry was performed with the help of Debbie Mauchline, Mike Millar and Nancy Evans, Small University Research Facilities, QMRI. Rabbit polyclonal primary antibodies, LOX (ab31238), anti-LOXL2 (ab96233), α-SMA (ab15734, Abcam, Cambridge, UK) and anti-MMP-9 (AB19016, Merck Millipore, Billerica, MA, USA) were used along with a goat anti-rabbit horseradish peroxidase-linked secondary antibody for diaminobenzidine detection (Bond refined staining kit, Leica Biosystems, Nussloch, Germany). A BOND™ immunostaining robot (Leica Biosystems, Nussloch, Germany) was used. An isotype control consisting of a rabbit polyclonal immunoglobulin-G anti-green fluorescent protein antibody (A-11122, Invitrogen, Life Technologies, Carlsbad, CA, USA) was also carried out.

2.17 Immunocytochemistry

The protocol detailed below was provided by Dr Neil McDonald. Square glass coverslips were washed in heat treated and sonicated HCl and placed in 6-well plates prior to coating with 500µl poly-D-lysine hydrobromide (P6407, Sigma-Aldrich, St Louis, USA) for a minimum of 30min and washing x4 in sterile water.

Cells were then seeded at desired concentration. MDM were seeded at $20x10^6$cells per well (see 2.11) and cultured for 6-7d prior to stimulation with 100ng/ml LPS for approximately 24h. RAW and 3T3 cells were seeded at approximately $2x10^5$cells per well (see 2.8) and stimulated with either 500ng/ml LPS or 400pM TGFβ for 12h upon reaching ~70% confluence.

Slides were washed x3 in sterile PBS prior to 30min incubation with 4% paraformaldehyde and another wash sequence. All incubations from this point onwards were carried out at room temperature. Cells were then permeabilised in 0.1% Triton X 100 in PBS and once again washed x3 in PBS. A 1h blocking step was then carried out by incubating cells in a PBS solution containing 1% BSA and 5% FBS. Cells were washed x3 prior to a 1h incubation with the primary antibody (see 2.16) which was prepared at a 1:100 dilution in diluted blocking solution (PBS+ 0.5% BSA+ 2.5% FBS) in a total volume of 250µl per slide. A secondary control slide was always prepared, this involved incubation with diluted blocking solution alone. A thorough wash step (3x 5min agitation with PBS) was performed, followed by a 1h incubation (protected from light) with 250µl per slide of a 1:500 dilution of secondary antibody: Alexa-Fluor 546, goat anti-rabbit (A-11010, Fisher Scientific, Leicestershire, UK) in diluted blocking solution and 5µl/slide of Alexa Fluor 635 phalloidin (A34054, Thermo Fisher Scientific, Massachusetts, USA). A final wash sequence was performed prior to the final 5min incubation (protected from light) with a 1:1000 dilution (436nmol) of DAPI (D1306, Thermo Fisher Scientific, Massachusetts, USA) in PBS. Slides were washed once with PBS then removed from the plate so that the underside of each slide could be gently washed with deionised water prior to mounting. ProLong gold antifade reagent (P36934, Thermo Fisher Scientific, Massachusetts, USA) was used to mount the coverslips onto slides which were then stored in the fridge overnight (protected from light) with desiccant, prior to imaging on a Leica TCS SP5 confocal microscope (Leica Microsystems, Wetzlar, Germany).

2.18 Tissue homogenate supernatants

For the preparation of cell free supernatant from tissue homogenate, frozen asinine, ovine or human lung tissue was suspended in either RIPA lysis and extraction buffer (89900, Pierce, Thermo Fisher Scientific, Massachusetts, USA) with 10% protease inhibitor cocktail (P8340, Sigma-Aldrich, St Louis, MA, USA) or in PBS alone and homogenised (Bio-Gen PRO200 homogeniser, Pro-Scientific, Oxford, USA) on ice. Samples were centrifuged at 13000rpm for 15min at 4^{o}C and the debris-free supernatant collected. Total protein concentrations were determined using a Pierce™ BCA protein assay kit (Thermo Fisher Scientific, Massachusetts, USA) as detailed below. The samples were aliquoted and stored at -70^{o}C until further analysis.

2.19 Protein quantification

Protein quantification was performed using a BCA protein assay kit (Thermo Fisher Scientific, Massachusetts, USA). A series of dilutions ranging from 0- 2000µg/ml was made from the provided albumin standard to generate a concentration curve according to manufacturer's instructions and the working reagent was prepared by combing 1 part reagent B with 50 parts reagent A. Either 10 or 25µl of each standard and sample (either neat or diluted 1:10) was added in duplicate to a flat-bottomed 96well plate along with 200µl of the working reagent. The plate was agitated prior to incubation at 37˚C for 30min. The plate was allowed to equilibrate to room temperature prior to reading absorbance at 562nm on a Synergy™ H1 Hybrid Multi-Mode Microplate Reader (BioTek, Winooski, USA). Data was analysed using Microsoft Excel 2010 (Microsoft Corporation, Redmond, USA). A mean value was generated for each standard and sample following subtraction of background. Standard absorbance values were plotted on scatter plot of absorbance against protein concentration and a trend line was added. The equation for the trend line of the standard curve was used to calculate the total protein for each sample, giving a value in µg/ml.

2.20 Western blot

Results from the BCA were used to standardise protein loading for westerns. The protocol detailed below was provided by Emma Scholefield. Western samples were prepared at standardised protein concentration in NuPAGE® LDS sample buffer and NuPAGE® sample reducing agent (NP0008 and NP0009, Invitrogen Life Technologies, Carlsbad, CA, USA) before heating at 95°C for 5min. Samples were loaded onto Bis-Tris 4-12% gradient gels (NP032, Invitrogen Life Technologies, Carlsbad, CA, USA) with NuPAGE® MES SDS running buffer (NP002, Invitrogen Life Technologies, Carlsbad, CA, USA) and a voltage of 200V was applied for approximately 40min. Blots were then transferred to a nitrocellulose membrane using an iBlot® dry blotting system (Invitrogen, Life Technologies, Carlsbad, CA, USA). Blots were subsequently blocked in a 5% dried milk powder (Marvel, Premier Foods plc, UK) TBS tween solution: 15mM NaCl (S7653), 2mM Tris (T1503), 0.1% Tween 20 (P9416, all Sigma-Aldrich, St Louis, USA), pH 7.4, for 1h before washing and incubating overnight at 4°C with the primary antibodies listed in 2.16 above at a 1:1000 dilution. Blots were then washed and incubated at room temperature for 1h with a 1:5000 dilution of goat anti-rabbit IgG HRP conjugate (7074S, New England Biolabs Ltd., Hitchin, UK). Resultant bands were visualised by chemiluminescence (SuperSignal® West Pico Chemiluminescent Substrate, 34087, Thermo Fisher Scientific, Massachusetts, USA) and exposure of x-ray film.

Following initial visualisation, blots from tissue homogenates were stripped in Restore® stripping buffer (21059, Pierce, Thermo Fisher Scientific, Massachusetts, USA) for 5min prior to blocking as stated above and incubation with mouse monoclonal anti-beta-actin primary antibody (3700S, New England Biolabs Ltd., Hitchin, UK) overnight at 4°C. Blots were then incubated with goat anti-mouse HRP conjugate (7076S, New England Biolabs Ltd., Hitchin, UK) for 1h and visualised as detailed above.

2.21 Zymography

The protocol detailed below was provided by Dr Manuelle Debunne. Samples were prepared on ice at standardized protein concentrations in MMP buffer (see 2.13) and combined with Tris-SDS sample buffer (Novex, cat LC2676, Thermo Fisher Scientific, Massachusetts, USA) at a 1:1 ratio prior to loading at a total volume of 15-20µl per well into a precast 10% Zymogram (Gelatin) Gel (Novex, cat EC61755, Thermo Fisher Scientific, Massachusetts, USA). Recombinant MMP-9 (PF024, Merck Millipore, Billerica, MA, USA) and recombinant pro-MMP-9 (PF038 Merck Millipore, Billerica, MA, USA) were prepared in the same way at 2nM and 0.5nM respectively and 8µl of a migration standard (Novex Sharp prestained protein standard, cat LC5800, Thermo Fisher Scientific, Massachusetts, USA) was also loaded . The gel and diluted running buffer (Novex Tris-Glycine SDS, cat LC2675, Thermo Fisher Scientific, Massachusetts, USA) were pre-chilled to 4˚C and the gel was electrophoresed at 150V for approximately 90min at 4˚C. Gels were then removed and trimmed prior to incubation in pre-chilled and diluted renaturing buffer (Novex, Cat LC2670, Thermo Fisher Scientific, Massachusetts, USA) for 90min at 4˚C. Gels were rinsed with chilled distilled water then incubated at room temperature with pre-chilled developing buffer (Novex, Cat LC2671, Thermo Fisher Scientific, Massachusetts, USA) for 30min prior to overnight incubation at 37˚C in the same buffer. For negative control gels, either 2mM Ethylenediaminetetraacetic acid (EDTA, cat: E6758, Sigma-Aldrich, St Louis, MA, USA), 50µM marimastat (2631, Bio-Techne, Minneapolis, USA) or desired concentration of AZD1236 (AstraZeneca, London, UK, see 2.26) was added to the developing buffer. Gels were then rinsed with distilled water prior to staining with a colloidal blue staining kit (Novex, cat LC6025, Thermo Fisher Scientific, Massachusetts, USA) and imaging using a transilluminator (UVItec BXT-20M, UVItec Ltd, Cambridge, UK) and UVIpro software (UVItec Ltd, Cambridge, UK).

2.22 Band densitometry

Band densitometry was performed using Image J 1.48 (National Institute of Health, Maryland USA). Blots were scanned to a digital TIFF image that was then opened in

Image J. The region of interest was selected and cropped before converting to an 8 bit inverted and flattened image. The selection gel selection tool was then used to plot a graph of band density for each individual band selected. The area under each graph was calculated following the subtraction of background signal. The final band densitometry value for each well was then divided by the relevant actin band densitometry if available.

2.23 Enzyme-linked immunosorbent assay (ELISA)

Human and murine MMP-9 ELISA kits (DuoSet cat: DY911 and DY6718, Bio-Techne, Minneapolis, USA) were used according to standard guidelines. Capture antibodies were diluted to 1µg/ml in PBS and used to coat the wells of 96 well plates prior to overnight incubation at room temperature. Plates were washed three times with wash buffer: 0.05% Tween 20 (WA126, Bio-Techne, Minneapolis, USA) in PBS, pH 7.2-7.4, and blotted dry. Plates were then blocked with blocking buffer: 1% BSA, 0.05% NaN_3 (S2002, Sigma-Aldrich, St Louis, MA, USA) in PBS, for 1h prior to repeating the washing step detailed above.

Standards (recombinant human or mouse MMP-9) were prepared at 2-fold dilutions in reagent diluent: 1% BSA in PBS, pH 7.2-7.4, 0.2 µM filtered or 50mM Tris (T1503), 10mM $CaCl_2$. 0.05% Brij 35 (16005, Sigma-Aldrich, St Louis, MA, USA) pH 7.5, 0.2µM filtered, to give a 7- point standard curve with maximum concentrations of 2000pg/ml and 5000pg/ml respectively.

Samples and standards were added to the plates in duplicate at 50µl per well and incubated at room temperature for 2h. Cell supernatants and lysates were used neat while tissue homogenates were diluted 1:100 in reagent diluent. The plates were then washed as above prior to the addition of 50µl of detection antibody diluted to 100ng/ml in the appropriate reagent diluent and incubation at room temperature for a further 2h. The plates were washed again prior to the addition of 50µl of streptavidin-HRP solution and incubation for 20min. Stop solution (1M H_2S0_4, cat 320501, Sigma-Aldrich, St Louis, MA, USA) was added at 50µl per well prior to reading absorbance at 450nM.

Microsoft Excel, 2010 was used to plot the log of the standard MMP-9 concentrations versus the log of the optical density and the best fit line was determined by regression analysis.

2.24 MMP-9 activity assay (SensoLyte)

The SensoLyte 490 MMP-9 Assay kit (ANA71134, Cambridge Bioscience Ltd, Cambridge, UK) was used to determine the relative activity of MMP-9 in cell supernatants and lysates. Negative control samples were pre-incubated with either 200µM marimastat or 100µM sivelestat or both for 1h at room temperature. Any dilutions of inhibitors or recombinant enzymes were performed in MMP buffer (See 2.13). Recombinant MMP-9 was used at a final concentration of 30nM while purified neutrophil elastase (Human Sputum Leucocyte Elastase, cat SE563, Elastin Products Company Inc., Missouri, USA) was used at a final concentration of 2.5µg/ml.

The 5-((2-Aminoethyl)amino)naphthalene-1-sulfonic acid (EDANS) reference standard was diluted to a top concentration of 7.5µM in deionized water prior to performing a 7-point two fold series dilution.

Samples and standards (10µl) were loaded in duplicate into a white 384 well plate. Substrate was diluted in assay diluent then 5ul was added to each well to give a total well volume of 15µl and final substrate dilution of 1:200.

A fluorescent kinetic read was then recorded in the plate reader at Ex/Em 340/490, 37˚C for 1h. An endpoint read was taken at 1h for data analysis. Microsoft Excel 2010 was used to plot a concentration curve for the EDANS standard and results were quoted as relative concentration of EDANS cleaved from substrate.

2.25 Probe synthesis and MALDI analysis

All probes were synthesized by The Bradley Group, Department of Chemistry, University of Edinburgh, King's Buildings, UK (UoEDC). In order to instigate a system of probe identification within this group, all generated probes are coded with

the initials of the synthesizing chemist, followed by a chronological number corresponding to that scientist's work.

Probes were generally used at a working concentration of 10µM, although third generation probes were often used at concentrations of around 1µM. Matrix-assisted laser desorption/ionization time of flight mass spectrometry (MALDI –TOF) analysis was carried out with the help of members of The Bradley Group. MALDI spectra were acquired either on a Ultraflextreme MALDI-TOF (Bruker, Billerica, USA) or a Voyager-DE™ STR MALDI-TOF MS (Applied Biosystems, Thermo Fisher Scientific, Massachusetts, USA) with a matrix solution of sinapic acid (10 mg/mL, cat 49508, Sigma-Aldrich, St Louis, MA, USA) in a 50:50:0.1 solution of H_2O, acetonitrile (W7-1 and AC16765-0010, Thermo Fisher Scientific, Massachusetts, USA) and trifluoroacetic acid (L06374, Alfa Aesar, Johnson Matthey, Royston, UK) respectively. Sample was mixed with matrix at a ratio of 1:1 and 1µl was spotted onto the MALDI plate and dried prior to analysis.

2.26 TWB-219 background fluorescence: trouble shooting

In-house LOX probe TWB-219 was found to have a high background fluorescence in DMEM with no evidence of probe cleavage on MALDI analysis (see 2.25). In order to investigate this problem, the components of DMEM were reviewed and pyridoxine hydrochloride (vitamin B6), iron nitrate and riboflavin (vitamin B2) were identified as components with the potential to influence background fluorescence. Pyridoxine hydrochloride (P9755, Sigma-Aldrich, St Louis, MA, USA) was prepared at 1:10 dilutions from 4mM to 0.04nM (concentration in DMEM 0.0196mM), iron nitrate (Sigma-Aldrich, St Louis, MA, USA) was prepared at 1:10 dilutions from 0.1mg/ml to 0.1µg/ml (concentration in DMEM 0.1µg/l) and riboflavin (R9504, Sigma-Aldrich, St Louis, MA, USA) was prepared at 1:2 serial dilutions from 0.01mg/ml to 0.31µg/ml (concentration in DMEM 0.4ug/ml) all in PBS. All solutions were incubated with 10µM and 100µM TWB-219 in a clear 96-well plate in a total volume of 50µl at 37˚C for 1h and fluorescence was read continuously from the bottom in a plate reader at excitation 485/25, emission 530/20.

In order to assess the effect of pH on TWB-219, deionised water was prepared at pH 1-10 (at 37˚C) as determined by a pH meter (Sartorius Basic Meter, PB-11, Sartorius UK ltd, Surrey, UK), using hydrochloric acid (cat H1758, Sigma-Aldrich, St Louis, USA) and sodium hydroxide (cat S8045, Sigma-Aldrich, St Louis, USA) as necessary. The pH of PBS, LOX buffer: 25mM PIPES + 0.5% Triton X-100 (cat P6757 and X100 Sigma-Aldrich, St Louis, MA, USA) and DMEM were also measured. TWB-219 and carboxy-fluorescein (FAM, synthesised in-house) were prepared at 10µM in each of the pH solutions and buffers and incubated for 30min at 37˚C, reading fluorescence continuously at excitation 480nm, emission 530nm in a plate reader.

2.27 Plate reader assays

All plate reader assays were performed on a Synergy™ H1 Hybrid Multi-Mode Microplate Reader (BioTek, Winooski, USA) using Gen5 Data Analysis Software (BioTek, Winooski, USA) and Microsoft Excel for final analysis of data. Fluorescence was determined using monochromatic filters at Ex/Em 485/528nm, at 37˚C, with gain 25-50 depending on the probe being assessed.

Samples were generally loaded on ice into an opaque 384 well plate unless otherwise stated, in total volumes of around 15µl and the plate was centrifuged at 200g for 1min prior to analysis.

Recombinant MMPs used were either the catalytic domains: MMP-1,-2,-8,-9,-13 (Multipack-1, AK013, Enzo Life Sciences Ltd, NY, USA), MMP-3,-7,-10,-11,-12 (Multipack-2, AK014, Enzo Life Sciences Ltd, NY, USA) , the whole active enzyme: MMP-2 and -9 (Cat PF023, and PF024) or the pro-enzyme: MMP-9 and MMP-13 (Cat PF038 and 444287, Merck Millipore, Billerica, MA, USA). It was necessary to activate the pro-MMP-13 with 1mM 4-aminophenylmercuric acetate (APMA, A9563, Sigma-Aldrich, St Louis, MA, USA) for 2h at 37°C prior to use. All recombinant MMPs were used at a final concentration of 30nM and were diluted in MMP buffer (see 2.13 above).

Other enzymes included purified human sputum leukocyte elastase (SE563, Elastin Products Company Inc., Missouri, USA) which was used at 2.5µg/ml in elastase assay buffer: 0.05 M sodium acetate (S2889, Sigma-Aldrich, St Louis, MA, USA) pH 5 containing 0.1 M NaCl (S5886, Sigma-Aldrich, St Louis, MA, USA) and diamine oxidase (DAO) from porcine kidney (D7876, Sigma-Aldrich, St Louis, MA, USA) which was used at various different concentrations in LOX buffer (see 2.26 above). Purified human plasmin (P1867, Sigma- Aldrich, St Louis, MA, USA) was also used at 30nM in MMP buffer.

MMP inhibitors included Inhibitor I (444278-500UG, Merck Millipore, Billerica, MA, USA) which selectively inhibits MMP-9 at low concentrations (IC_{50} 5nM), marimastat (2631, Bio-Techne, Minneapolis, USA) a pan-MMP inhibitor and AZD1236 (AstraZeneca, London, UK) which has a reported selectivity for MMP-9 and MMP-12. Samples were incubated with inhibitors at either room temperature or 37˚C for a minimum of 30min.

LOX inhibitors used included 3-Aminopropionitrile fumarate salt (BAPN, A76427, Sigma-Aldrich, St Louis, MA, USA) and the in-house LOX inhibitor AMF-59 which was synthesised in-house by Dr Fernandez of the Bradley Group. LOX inhibitors were diluted as required in LOX buffer and incubated with samples for 1h at 37˚C prior to assays.

Sodium diethyldithiocarbamate trihydrate (DETCA, cat 228680, Sigma-Aldrich, St Louis, MA, USA) was used as an inhibitor of diamine oxidase activity and was diluted to a working concentration of 100mM prior to incubation with enzyme for 30min at room temperature.

Sivelestat (3535, Bio-Techne, Minneapolis, USA) was used to inhibit neutrophil elastase by incubating samples for 1h at room temperature at a final concentration of 100µM.

2.28 Calculating Km and Kcat

The Michaelis-Mentan constant (Km), Vmax and Kcat were calculated for recombinant MMP-2, MMP-9 (whole active enzyme) and MMP-13 (activated pro-enzyme), using the three third generation MMP probes as substrates (see Figures 5-35 and 5-36). Probes were prepared at 1:2 dilutions ranging from 20µM to 2.44nM and incubated with 30nM (whole active MMP-2 and -9) or 3nM (activated pro-MMP-13) enzyme (see 2.27 above) in MMP buffer (see 2.13) in a 384 well plate in a total volume of 10µl.

The kinetic was performed in the plate reader at 37˚C for 30min. Data were transferred to Microsoft Excel 2010, where graphs of probe concentration against time were plotted. The 'SLOPE' function in Excel was then used to determine the linear regression value or velocity for each substrate concentration. Velocity was then plotted against substrate concentration in Graphpad Prism 5 and the Michaelis-Mentan function was used to calculate Km and Vmax (Figure 5-35). To calculate the Kcat (the number of times each enzyme site converts substrate to product per unit time), the equation Vmax= Kcat x Et, where Et is the concentration of enzyme active sites, was used.

2.29 FCFM

The FCFM system used was a Cellvizio^{TM} –Lung device (Mauna Kea Technologies, Paris, France) incorporating a 1.4mm diameter mini probe (ProFlex^{TM} S-1500, Mauna Kea Technologies, Paris, France). Experiments were performed with the help of Ahsan Akram and Chesney Michels.

Human tissue samples (approximately 5mm diameter) were incubated in 96 well plates with either MMP or LOX buffer (see 2.13 and 2.26 respectively) +/- inhibitors (100µM marimastat or 1mM BAPN for MMP and LOX probes respectively) at 37°C for 1h in a total volume of 100µl.
Videos were taken at baseline for intrinsic pulmonary autofluorescence and at 30-90min following addition of probe. Images were taken for each sample for a minimum of 60sec, giving rise to over 700 frames per video.

Whole *ex vivo* asinine lungs were connected via a cuffed endotracheal tube to a positive pressure mechanical ventilator. A video endoscope was then used to navigate to a region of interest within the *ex vivo* lung. The endoscope was secured within a bronchus before the miniprobe was passed down the working channel of the endoscope and advanced into the alveolar tissue. 200µM TWB-219 was then instilled in a total volume of 1ml in PBS. Images were taken for a minimum of 2min, giving rise to over 1000 frames per video. Videos were taken at baseline for intrinsic pulmonary autofluorescence and at 15-30min following addition of probe.

Analysis of videos was by Cellvizio™ Viewer (Cellvizio™ Viewer 3.8.3, Mauna Kea Technologies, Paris, France) with a region of interest across the entire field of view (430 x 307 nm) for all frames and the mean frame fluorescence was calculated for each frame. Mean frame fluorescence was then used to calculate the overall mean fluorescence for each video. Each individual experiment for probe +/- inhibitor was corrected to the corresponding autofluorescence for that patient sample. The means (+/-SEM) for each experiment are reported and analysis was by a Mann Whitney U test by GraphPad Prism version 5.00 for Windows, GraphPad Software, San Diego California USA.

2.30 Statistical analysis

Statistical analysis was performed using Graphpad Prism 5 software (GraphPad Software, Inc., San Diego, USA.) after selecting an appropriate statistical test for each data set. The test used is specified in the legend of relevant figures.

Chapter 3: Characterisation of Asinine Pulmonary Fibrosis

3.1 Abstract

Asinine Pulmonary Fibrosis (APF) is a spontaneous syndrome of aged donkeys with high prevalence (35%). No previous detailed characterisation of APF has been previously performed. The objective of this chapter of my thesis was to characterise the clinical, gross and histopathological features of APF in order to begin to elucidate disease pathogenesis and determine if there are similarities to recognised patterns of human pulmonary fibrosis.

Whole lungs were collected from 32 aged donkeys at routine necropsy, following euthanasia on humane grounds. Gross examination revealed pulmonary fibrosis in 19 donkeys (APF cases), while 13 (controls) had grossly normal lungs. Eighteen whole inflated *ex vivo* lungs (11 APF, 7 controls) were imaged with high resolution computed tomography (HRCT), while the remainder were sectioned and photographed. Tissue samples were collected from all lungs for histopathological evaluation using a standardised protocol. HRCT images and histology sections were reviewed independently and blindly. Lung tissue was analysed for herpes virus, fungal hyphae, mycobacteria and dust content.

Ten of 19 APF lungs were categorised as being 'consistent with' a recently identified human interstitial pneumonia termed pleuroparenchymal fibroelastosis (PPFE) according to previously defined histological and imaging criteria (Reddy et al., 2012). All 10 PPFE-like lungs had marked pleural and subpleural fibrosis, predominantly within the upper lung zone, with accompanying intra-alveolar fibrosis and elastosis. Asinine herpesvirus (AHV) DNA was ubiquitously present within control and APF lung tissue. No other aetiological agents were identified.

Many cases of APF share key pathological and imaging features with human PPFE. Consequently, further study of APF may help elucidate the aetiopathogenesis of this emerging human disease.

3.2 Introduction

Pulmonary fibrosis represents the endpoint of many diseases and is characterised by excessive and irreversible deposition of extracellular matrix in the lung parenchyma, leading to compromised ventilation and organ dysfunction. Despite considerable research, many fibrotic lung diseases remain elusive in terms of aetiology, pathogenesis and treatment (Chua et al., 2005). One such disease is pleuroparenchymal fibroelastosis (PPFE), a rare but emerging condition with poor survival (see Chapter 1.3.1) characterised by pleural and subpleural elastotic fibrosis of the upper lung lobes with intra-alveolar fibrosis (Travis et al., 2013). Progress in the research of PPFE and other idiopathic fibrotic lung diseases is hindered by the lack of a translatable animal model with durable and persistent fibrosis (Williams et al., 2004).

Asinine Pulmonary Fibrosis (APF) is a syndrome that is sparsely documented, yet a prevalence of 35% at routine necropsy was reported in a UK cohort (Morrow et al., 2010). Very little is known about this chronic, potentially debilitating and currently untreatable idiopathic condition.

The paucity of information with regard to APF highlights the need for a comprehensive and systematic scientific characterisation of the disease process. Such characterisation would not only benefit the welfare of donkeys, but could also hold translational relevance to human fibroproliferative disease. The use of high resolution computed tomography (HRCT) is central to the current diagnostic evaluation and monitoring of human pulmonary fibrosis patients, thus equivalent characterisation of APF could identify potential comparative features. The subsequent histopathological correlation with HRCT findings will complete the pathological characterisation of APF affected lungs and facilitate further comparisons with human fibroproliferative disease.

Therefore, the objective of this chapter was to perform the most comprehensive systematic characterisation of APF to date in order to address the hypothesis that

APF is a useful spontaneous model of pulmonary fibrosis that shares histopathological and imaging characteristics with human disease.

3.3 Results

3.3.1 Clinical assessment

Sixteen donkeys (8 APF, 8 control) of the 22 that were examined using the study examination protocol (Appendix 7.2) were subsequently euthanised on humane grounds during the timeframe of the study (Figure 3-1). These comprised 7 females and 9 castrated males (Figure 3-2).

Clinical features of individual APF donkeys that were euthanised due to severe respiratory disease included tachypnoea, increased respiratory (particularly inspiratory) effort and abnormal findings on thoracic auscultation including crackles and wheezes (Figure 3-4). Mean respiratory rate of APF donkeys was not significantly different to that of controls (26 versus 15, p= 0.07, two-tailed t-test).

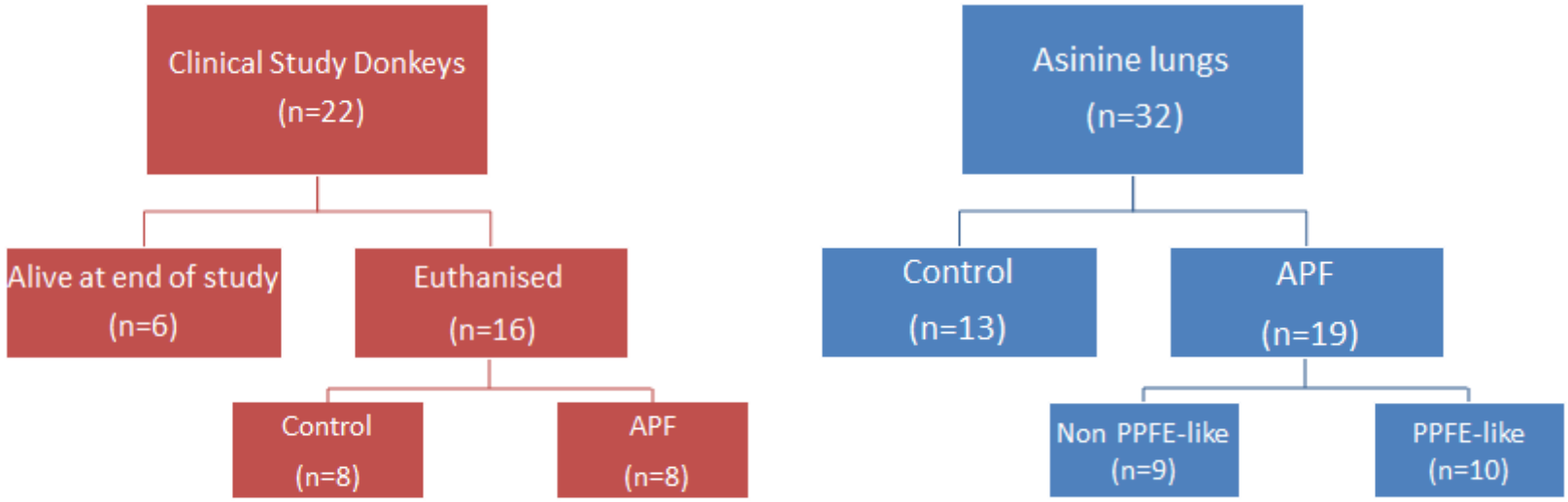

Figure 3-11: Flow diagrams showing classification of clinical study donkeys and lungs collected at necropsy.

Figure 3-12: Table summarising clinical findings for study donkeys

Case No or Name	Reason for euthanasia	U/S results	Pulse ox	RR	Auscultation	Respiratory effort score	Nostril flare score	Total resp score	Responsive to RAO medication	Comments	PM
1	Resp disease	Hypoechoic subpleural lesions	90% post ex	60	NAD	2	2	4	No	Mainly insp effort	APF
3	Resp disease	Hypoechoic subpleural lesions	ND	24	Insp/exp crackles and exp wheeze	4	3	7	No	More exp effort	APF
5	Resp disease	Hypoechoic subpleural lesions	93%	16	Insp+exp wheeze, exp and insp crackles	3	2	5	Yes	Exp effort	APF
10	Resp disease	Hypoechoic subpleural lesions	99%	24	Insp wheeze and squeak	2	2	4	No	More insp Effort	APF
12	Resp disease	Diffuse comet tails	ND	24	Insp wheeze and exp crackles	2	3	5	No	Exp effort	APF
Beauty B.	Resp disease	Diffuse comet tails	97%	16	Exp crackles	3	3	6	Yes	Insp and exp effort	APF
Dandelion	Resp disease	Areas with numerous comet tails	100%	20	Insp crackles and exp tracheal wheeze	2	3	5	Yes	Insp and exp effort	APF (lung periphery)

Dan	Resp disease	Hypoechoic subpleural lesions	100%	28	Exp wheezes and crackles over trachea, some tracheal collapse palpated	3	3	6	Yes	Insp and exp effort	APF
Randy RSPCA	Resp disease	Some comet tails	100%	36	NAD	1	2	3	Yes	Rapid shallow respiration	Chronic bronchiolitis, no fibrosis
Geoffrey D	QOL	Diffuse comet tails	98%	8	Increased breath noise audible over trachea and tracheal collapse palpated	2	1	3	Yes	NAD	Tracheal collapse. Lungs NAD
Sally	Tracheal collapse	Some comet tails	ND	12	NAD	2	1	3	Yes	NAD	Tracheal collapse, Lungs NAD
Jacko Eire	QOL	Diffuse comet tails	100%	10	Inspiratory crackles	2	2	4	Yes	NAD	No fibrosis
Phoebe	QOL	Diffuse comet tails	98%	8	NAD	2	1	3	Yes	Insp and exp effort	Lungs NAD
Jacko M	Tracheal collapse	Some comet tails	ND	10	NAD	1	1	2	Yes	ND	Lungs NAD
Pinocchio	Sarcoids	Occasional comet tail	ND	18	NAD	2	2	4	No	ND	Lungs NAD

Katie B	QOL	Occasional comet tail	100%	16	NAD	2	1	3	Yes	More exp effort	Lungs NAD

PM= post mortem results, Resp= respiratory, Insp= inspiratory, Exp= expiratory, QOL= poor quality of life, NAD= no abnormalities detected, RAO= recurrent airway obstruction, ND= not done

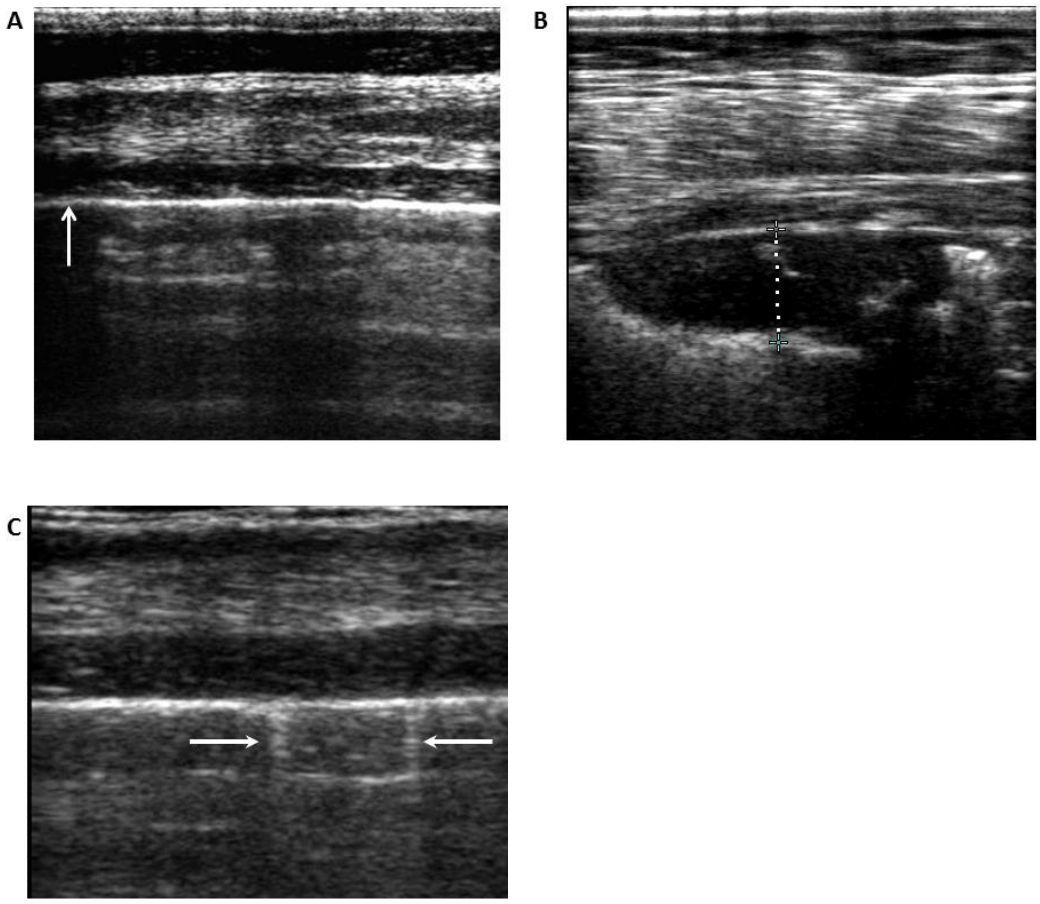

Figure 3-13: Pre-mortem thoracic ultrasonogram images from donkeys included in the clinical study (Miele et al., 2014). Image A is representative of a normal pleural interface (arrow). The top of the image represents the skin surface. Image B was recorded from a donkey with APF (confirmed at post mortem), note the hypoechoic sub-pleural lesion (dotted line = 1.27cm). Image C is an example of 'comet tail artifacts' (arrows) originating from the visceral pleural surface which was a common finding in the majority of donkeys scanned and indicates irregularities of the visceral pleura and sub-pleural parenchyma. Image C reproduced from Thiemann, 2012. Veterinary Education, 24(9) 469-478, with permission from Wiley. ©2011 EVJ Ltd.

Figure 3-14: Pulmonary auscultation of a clinical study donkey with APF. Pulmonary auscultation was performed on all 22 donkeys included in the clinical study and any abnormal respiratory sounds were noted. Donkeys were also scored for inspiratory/expiratory effort and nostril flare.

Nostril flare and respiratory effort scores were significantly increased in APF donkeys (p= 0.0031 and 0.0182 respectively, Mann-Whitney U). The sum of respiratory effort and nostril flare scores for each donkey was also significantly increased in the APF donkeys (mean 5.3) compared to the controls (mean 3.1), p=0.0017, Mann-Whitney U. Of the 8 APF donkeys, 5 had an increased inspiratory effort (3 of these also had expiratory effort) while the remaining 3 had mainly expiratory effort. An increased expiratory effort was also recorded in 2/8 control donkeys.

Blood oxygen saturation was only consistently found to be reduced (<98%) in 3/12 donkeys, all of which had pulmonary fibrosis on post mortem examination. A post exercise blood oxygen saturation was only successfully measured via pulse oximetry in one of these donkeys and this showed an 8% reduction from resting measurement.

In 5 of the 8 donkeys with APF that underwent thoracic ultrasound in the weeks prior to euthanasia, hypo-echoic sub-pleural lesions (suspected fibrosis) were imaged (Figure 3-3), with multiple comet tails being detected in the three remaining cases. It should be noted that the subsequent post mortem examination indicated that fibrotic lesions in at least one of these three cases were located in lung regions that are inaccessible to transthoracic ultrasonographic examination.

There was no significant difference in the documented occurrence of lower respiratory tract infection between APF (9/19) and control (2/13) donkeys, Fisher's exact p=0.13.

3.3.2 Asinine lungs collected at necropsy

A total of 32 asinine lungs were collected at necropsy (Figure 1). Ages of APF (median 31 years, range 14-53) and control (28 years, 4-36) donkeys were not significantly different (Mann Whitney, p>0.05). The typical asinine lifespan is 30 years. Donkeys comprised 12 neutered males and 20 females.

Relevant clinical details of APF and control donkeys are summarised in Figures 3-5 and 3-6 respectively. In 50% of the APF cases, the pulmonary pathology was an incidental finding at post mortem examination. Of the remaining 9 cases, recorded

clinical signs consistent with respiratory disease had been on-going for a period of 1 week to 5 years. Common treatments received by donkeys with on-going respiratory disease included oral clenbuterol (β-2 agonist bronchodilator), oral prednisolone and/or inhaled beclometasone and inhaled salbutamol. These medications are commonly used in the management of recurrent airway obstruction (RAO) in donkeys and horses.

Ten of 19 APF lungs were categorised as being 'PPFE-like' (Figure 3-1 and 3-7), having features 'consistent with' PPFE on both pathology and imaging (7 on HRCT; 3 on photographed images of sectioned lungs).

Figure 3-15: Table summarising the signalment of APF donkeys (Miele et al., 2014)**.**

Case No.	APF suspected pre-mortem?	PPFE?	Age (years)	Sex	Indication for euthanasia	History of respiratory infection	Relevant treatments
1	Yes	No	19	F	Severe respiratory disease	Yes (3 episodes)	Intermittent oral clenbuterol, oral dembrexine, and beclometasone and salbutamol inhalers for 1 year prior to euthanasia
2	No	No	34	MN	Chronic laminitis	No	NA
3	Yes	Yes	53	MN	Severe respiratory disease	No	Oral clenbuterol for 2 weeks prior to euthanasia

4	No	Yes	34	F	Laminitis	Single episode <2years prior to euthanasia	NA
5	Yes	Yes	31	MN	Severe respiratory disease	Yes (4 episodes)	Intermittent oral clenbuterol, oral dembrexine, and inhaled beclometasone and salbutamol for 5 years prior to euthanasia
6	No	Yes	30	F	Liver disease	Single episode 3years prior to euthanasia	NA

7	Yes	Yes	38	F	Severe respiratory disease	No	Intermittent oral clenbuterol, oral prednisolone, and inhaled beclometasone and salbutamol for 4 months prior to euthanasia
8	Yes	No	28	F	Severe respiratory disease	Yes (single episode commencing 10d prior to euthanasia)	Intermittent oral clenbuterol, dembrexine and prednisolone for 6 months prior to euthanasia

9	Yes	Yes	34	F	Severe respiratory disease	Yes (2 episodes, 4 months prior to euthanasia)	Intermittent oral clenbuterol and dembrexine for 3 years prior to euthanasia
10	Yes	Yes	23	F	Severe respiratory disease	No	Inhaled beclometasone and salbutamol for 1 week prior to euthanasia
11	Yes	No	14	MN	Severe respiratory disease	Yes (single episode commencing 1 month prior to euthanasia)	Inhaled beclometasone and salbutamol and oral prednisolone for 1 month prior to euthanasia

12	Yes	No	28	F	Severe respiratory disease	Yes (3 episodes within 1 year of euthanasia)	Intermittent oral clenbuterol and prednisolone for 1year prior to euthanasia
13	No	Yes	30	F	Nasal haemangiosarcoma	No	NA
14	Yes	No	37	F	Severe respiratory disease	No	Course of oral clenbuterol and dembrexine 8 months prior to euthanasia
15	No	No	34	MN	Laminitis	No	NA
16	No	Yes	30	F	Arthritis	No	NA
17	No	No	31	F	Blindness and poor QOL	No	NA
18	No	Yes	32	MN	Impaction colic	Single episode 11yrs prior to euthanasia	NA

19	No	No	25	F	Poor QOL (hypoproteinaemia, tachypnoea, tachycardia, dull)	No	NA

NA= not applicable, F= female, MN=castrated male, QOL= quality of life, NA= not applicable

Figure 3-16: Table summarising the signalment of control donkeys.

Case No.	Age (years)	Sex	Indication for euthanasia	History of respiratory infection	Relevant treatments
20	23	F	Liver fibrosis	Yes (single episode 2 years prior to euthanasia)	Oral clenbuterol and dembrexine 2 years prior to euthanasia
21	21	MN	Liver disease	No	NA
22	31	F	Neoplasia	No	NA
23	4	MN	Sarcoids	No	NA
24	20	F	Laminitis	No	NA
25	4	MN	Sarcoids	No	NA
26	36	MN	Impaction colic	No	NA
27	27	F	Impaction colic with pancreatitis and hyperlipaemia	No	NA
28	28	F	Chronic arthritis	No	NA
29	29	MN	Laminitis	No	NA

30	34	MN	Chronic foot problems	No	NA
31	30	F	Chronic liver disease & severe sudden onset dyspnoea (chronic tracheal collapse)	Yes (several episodes within 15 years of euthanasia, mainly related to chronic sinusitis)	Intermittent oral clenbuterol and dembrexine
32	30	F	Laminitis	No	NA

F= female, MN=castrated male, NA= not applicable

Figure 3-17: Table summarising the classification of APF lungs with regards to PPFE (Miele et al., 2014).

Case No.	Imaging Type	Imaging Classification	Histology Classification	Overall Classification
1	HRCT	Inconsistent	Inconsistent	Inconsistent
2	HRCT	Consistent	Inconsistent	Inconsistent
3	HRCT	Consistent	Consistent	Consistent
4	HRCT	Consistent	Consistent	Consistent
5	HRCT	Consistent	Consistent	Consistent
6	HRCT	Consistent	Consistent	Consistent
7	HRCT	Consistent	Consistent	Consistent
8	HRCT	Inconsistent	Inconsistent	Inconsistent
9	HRCT	Consistent	Consistent	Consistent

10	HRCT	Consistent	Consistent	Consistent
11	Digital	Inconsistent	Inconsistent	Inconsistent
12	HRCT	Consistent	Inconsistent	Inconsistent
13	Digital	Consistent	Consistent	Consistent
14	Digital	Consistent	Inconsistent	Inconsistent
15	Digital	Consistent	Inconsistent	Inconsistent
16	Digital	Consistent	Consistent	Consistent
17	Digital	Consistent	Inconsistent	Inconsistent
18	Digital	Consistent	Consistent	Consistent
19	Digital	Inconsistent	Inconsistent	Inconsistent

3.3.3 Gross post mortem findings

All APF lungs had some grossly visible fibrosis of the visceral pleura and/or subpleura on the dorsal /costal surface. This was often symmetrical and characterised by multifocal to coalescing vermiform cream/grey lesions that caused visible restriction to pleural expansion on manual lung inflation (Figure 3-8). The majority of APF lungs (16/19) also had a degree of fibrosis of the ventral or diaphragmatic lung surface which was again symmetrical and often very pronounced. A ventral 'skirt' of fibrosis was sometimes present around the circumference of the right and left caudal lobes (Figure 3-8C). Three of the APF lungs had evidence of pleural adhesions: 2 over the ventral lung surface and one over the dorsal surface. In severe (presumed chronic) cases, bands of grey scar tissue (fibrosis) were also evident on the cut surface of the lung parenchyma, while in more acute cases a mottled appearance was evident (Figure 3-9), thought to indicate an alveolar inflammatory infiltrate.

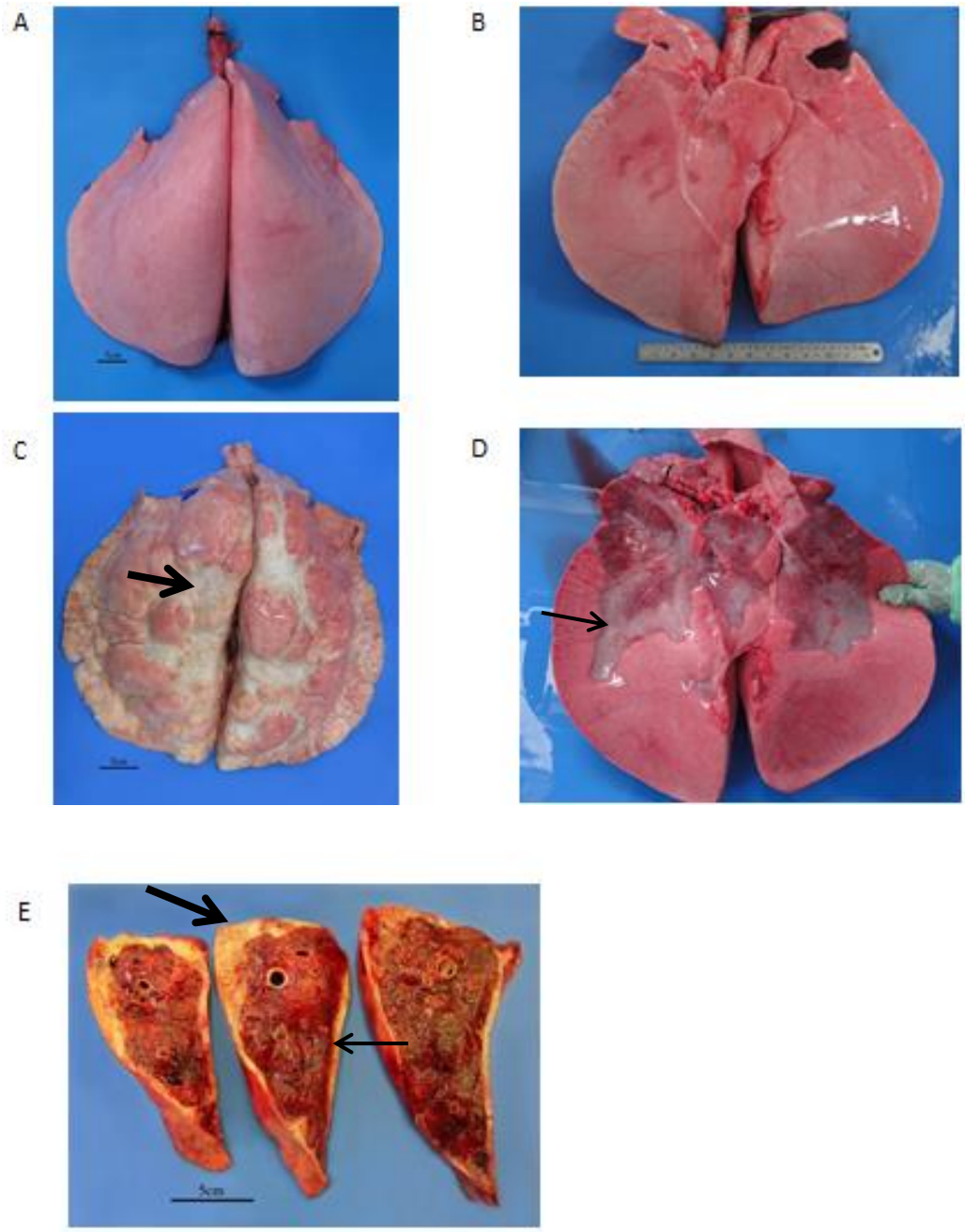

Figure 3-18: Gross pathological features of APF (Miele et al., 2014). Photographs of the dorsal (A and C) and ventral (B and D) surface of inflated control (A and B) and APF (C and D) lungs. Where HRCT was not available, lungs were sectioned vertically prior to digital imaging (E). Note the extensive dorsal pleural fibrosis (large arrows) in (C) and (E). In severe cases there was also pronounced fibrosis of the ventral (diaphragmatic) lung surface (D and E, small arrows). Scale bar = 5cm.

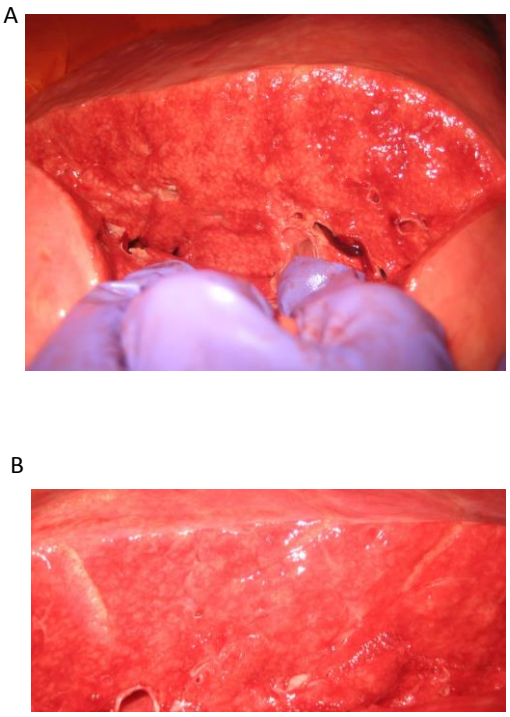

Figure 3-19: Cut surface of APF lungs. (A) Dorsal cut surface of *ex vivo* lung from an APF donkey. Note the pale subpleural infiltrate (presumed alveolar) extending into the interstitium. (B) Diaphragmatic cut surface of *ex vivo* lung from the same animal. Note the pale thickened interlobular septae extending from the pleural surface.

3.3.4 Histopathology

Histological features of both control and APF lungs included frequent haemosiderophages and occasional areas of mild anthracosis (Figure 3-10). The presence of alveolar oedema was a feature of one control and 4 APF lungs and was generally considered to be an agonal change. While alveolar histiocystosis and peri-bronchiolar/peri-vascular accumulation of lymphocytes (lymphoid follicles) were evident in 6/13 control lungs, these features were more prominent in APF lungs, occurring in all APF donkeys (Figures 3-10 and 3-15).

Expansion of the pleura with fibrous tissue (collagen) was a significant finding in all but one APF lung. In the majority of APF cases the fibrosis extended into the subpleura and interstitium along inter-lobular septae (Figure 3-11). Peri-bronchiolar and peri-vascular accumulation of lymphocytes and plasma cells was present in all APF lungs, with peri-bronchiolar fibrosis also being a consistent feature (15/19, Figure 3-11). Epithelial cells lining alveolar walls within areas of fibrosis often showed type II pneumocyte hyperplasia (Figure 3-12) and the presence of multinucleated giant cells and/or foamy macrophages was frequently noted within the alveolar spaces (15/19). In some cases organising fibrin was also present (Figure 3-16). Another common observation was the spatial heterogeneity of many of the sections, with a sharp demarcation between fibrotic and normal interstitium (Figure 3-12).

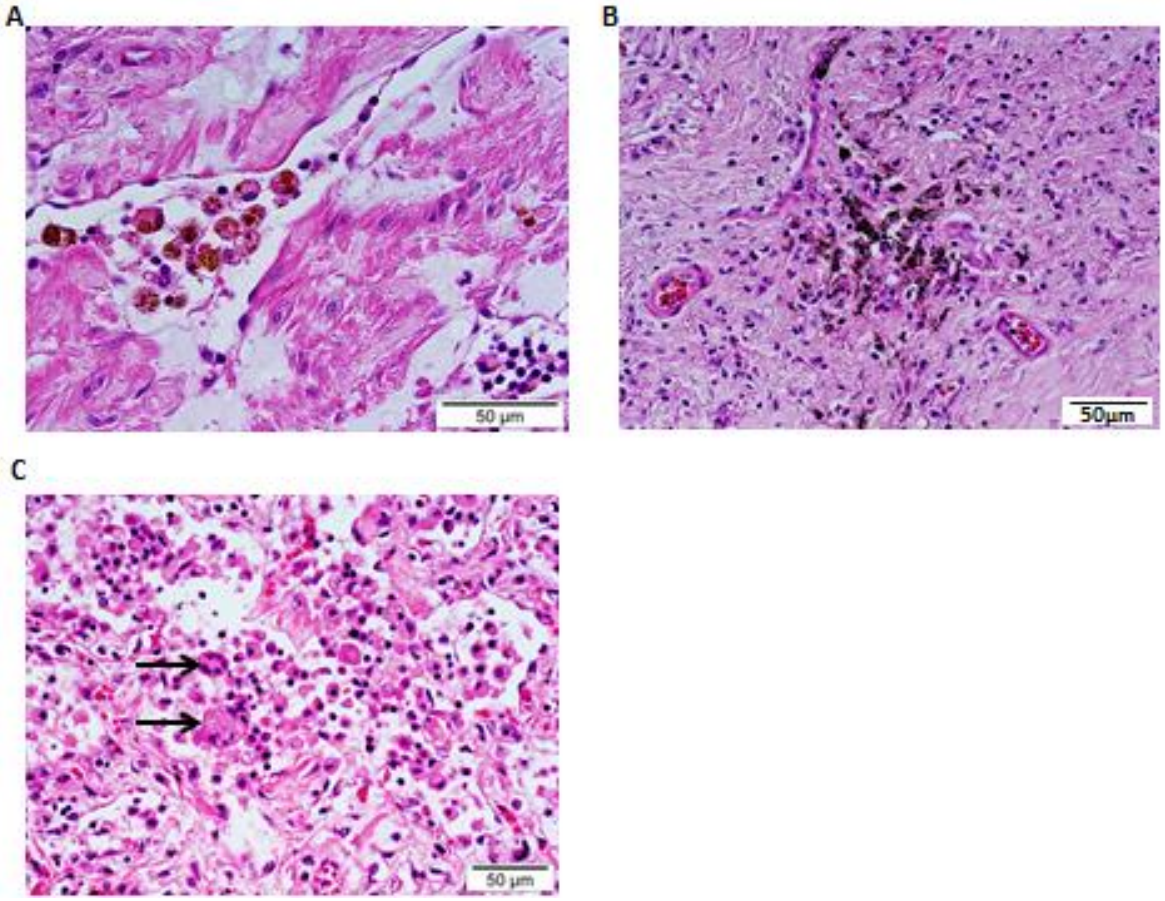

Figure 3-20: Common histological features of asinine lungs. Haemosiderin and haemosiderophages (A) were common findings in both control and APF lungs. Areas of anthracosis (B) were also present in both control and APF lungs, while alveolar histiocytosis (C) was more marked in APF lungs and the presence of giant cells (arrows) was more common (80% of APF lungs vs 14% control lungs). APF lungs, H&E.

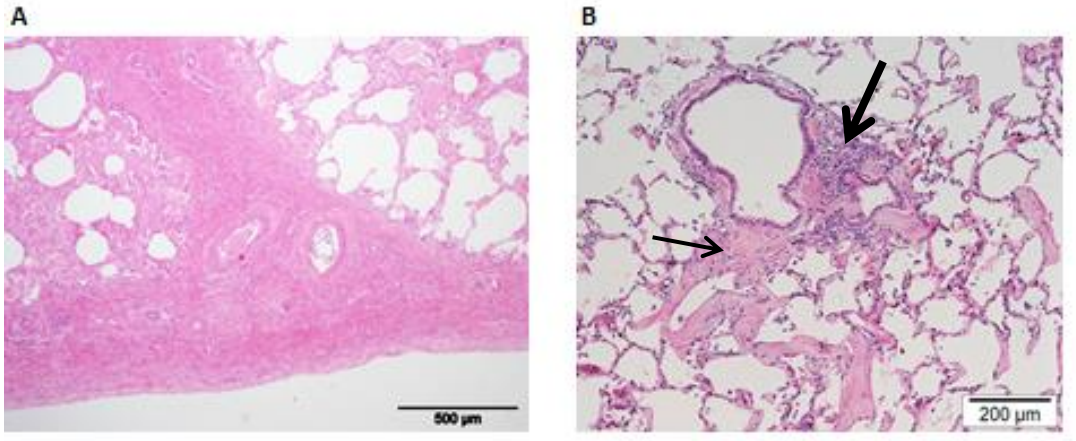

Figure 3-21: Common histological features of APF lungs (Miele et al., 2014). Subpleural fibrosis often extended into the pleural parenchyma along thickened interlobular septa of APF lungs (A). Peri-bronchiolar inflammation (large arrow) and fibrosis (small arrow) was also a common feature of APF (B). H&E.

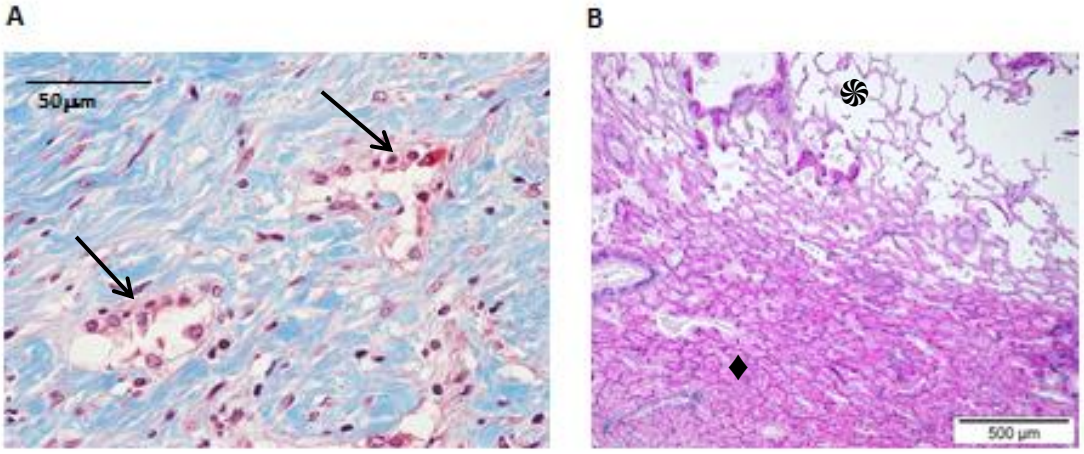

Figure 3-22: Common histological features of APF lungs. (A) Type II pneumocyte hyperplasia or bronchiolisation (arrows) was a consistent feature within areas of fibrosis. Collagen deposition is stained in blue with MT stain. Spatial heterogeneity (B) was also a consistent feature of APF. The EVG stained section shows the contrast between aerated (֍) and fibrotic (♦) lung tissue.

3.3.5 Comparative classification (with regards to PPFE)

Honeycombing and fibroblastic foci, key features of human IPF, were not detected in the APF lungs. However, staining with Elastin Van Gieson (EVG) revealed features consistent with human PPFE (Figure 3-14). Following scoring of the 19 APF lungs with regards to both histopathological and imaging features, 10 lungs were identified as 'PPFE-like' (Figure 3-7). Each of these had grossly visible visceral pleural fibrosis on the dorsal /costal surface with no involvement of the parietal pleura. As donkeys are quadrupeds, the dorsal lung equates to the human upper zone. Histologically, all 10 'PPFE-like' lungs had dorsal pleural and subpleural fibrosis with subpleural intra-alveolar fibrosis and elastosis evident on EVG stained sections (Figure 3-14). Other common features (Figure 3-13) included septal and bronchiolocentric fibrosis with lymphoplasmacytic bronchiolitis as previously discussed, along with vascular remodelling and occasional large clusters of macrophages and plasma cells sometimes resembling granulomatous inflammation (Figure 3-15).

All 9 APF lungs classified as 'inconsistent with' PPFE on histology had pleural, subpleural or septal fibrosis in at least one section. In 4/9 of these lungs the fibrosis was focussed around alveolar walls, with similarities to a non-specific interstitial pneumonia-type pattern rather than to PPFE (Figure 3-16). Importantly, all 9 lungs lacked the intra-alveolar fibrosis previously reported to be a feature of PPFE (Frankel et al., 2004), but the majority (7/9) had marked intra-alveolar mononuclear cell infiltrates with fibrin deposition (Figure 3-16).

Figure 3-23: Table summarising the features of 'PPFE-like' lungs (Miele et al., 2014).

Imaging (digital and HRCT)		**Histology**	
Feature	**Frequency**	**Feature**	**Frequency**
Pleuroparenchymal thickening predominant in upper zones	10/10	Pleural and subpleural fibrosis with intra-alveolar fibrosis and elastosis in dorsal lung sections	10/10
Subpleural fibrosis	10/10	Inter-lobular septal fibrosis	10/10
Ventral fibrosis	7/10	Bronchocentric fibrosis	8/10
Parenchymal bands	7/7	Lymphoplasmacytic bronchiolitis	10/10
Traction bronchiectasis	7/7	Venous and arterial intimal fibrosis	9/10
“Ground glass” opacity	4/7	PPFE pattern in ventral lobe biopsies	2/6
Bronchocentric consolidation	5/7	Granulomatous inflammation	3/10
		Pleural ossification/calcification	1/10

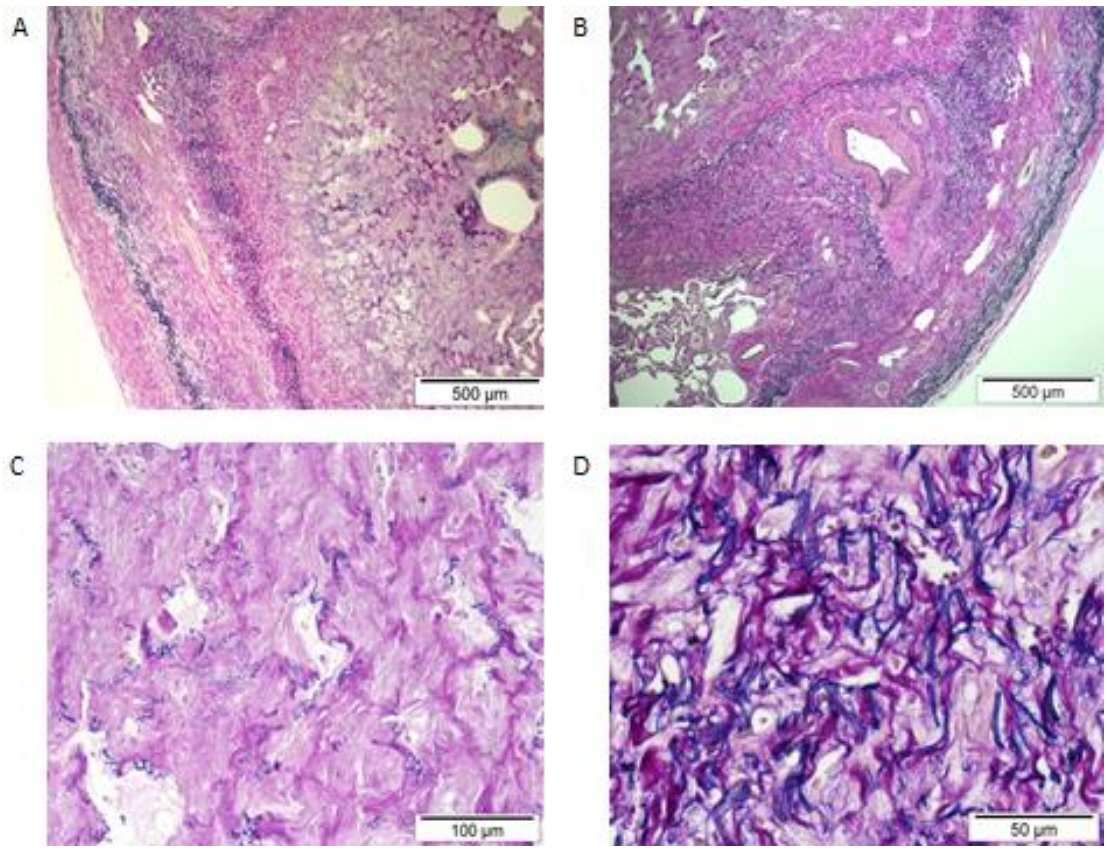

Figure 3-24: Histology of 'PPFE-like' asinine lungs (Miele et al., 2014). (A) Pleural and subpleural fibrosis with alveolar septal elastosis and intra-alveolar fibrosis, EVG. (B) Disarray of the pleural elastin with a band of fibrosis extending from the subpleura along an interlobular septum, EVG. (C) Higher powered view of an area of intra-alveolar fibrosis, EVG. (D) High power view of an area of diffuse elastosis, EVG.

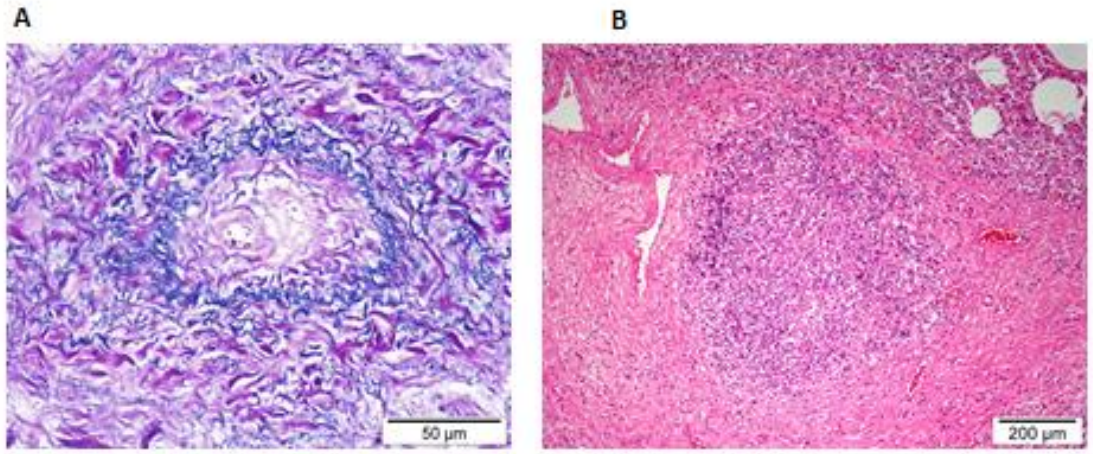

Figure 3-25: Histologic features of 'PPFE-like' asinine lungs (Miele et al., 2014). Sections from asinine lungs scored as consistent with PPFE. (A) Intimal fibrosis and elastosis of an entrapped vessel, EVG. (B) An aggregate of lymphocytes and macrophages within an area of fibrosis that displays many of the features of granulomatous inflammation, H&E.

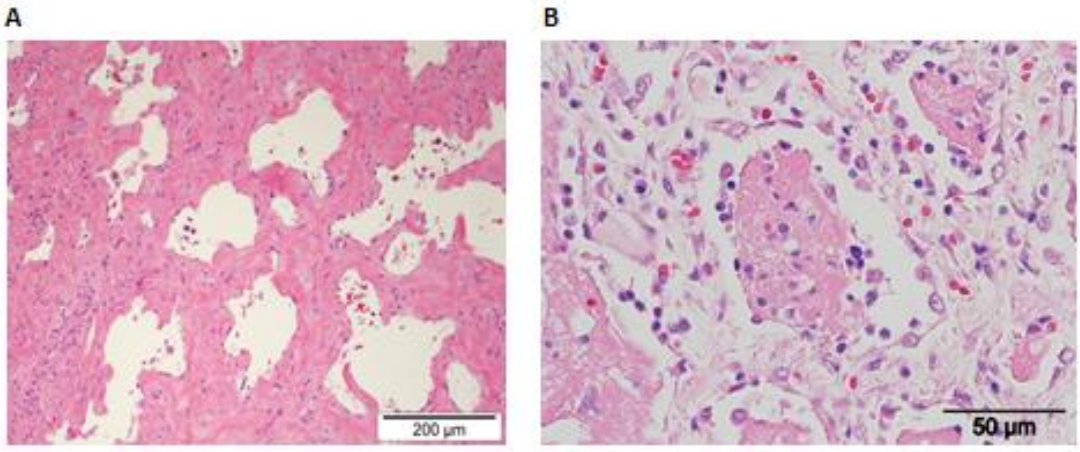

Figure 3-26: Histologic features inconsistent with PPFE (Miele et al., 2014). Sections of APF tissue classified as 'inconsistent with' PPFE demonstrating fibrosis of the alveolar walls with conservation of alveolar architecture (A) and alveolar deposition of fibrin (B), H&E.

3.3.6 HRCT imaging

All 7 'PPFE-like' lungs which had undergone HRCT had pleuroparenchymal thickening (max 5-32mm compared to <2mm in controls) of the dorsal lung lobes with associated subpleural consolidation consistent with established fibrosis. The consolidation extended from the subpleural region along parenchymal bands (Figure 3-17). In 2/7 lungs the fibrosis was relatively superficial and confined solely to uppermost zones of the dorsal lung surface. The other 5 cases had consolidation extending along parenchymal bands into mid and ventral zones, and often radiating out to surround adjacent bronchi. Features of coexistent disease identified on HRCT included primary bronchiectasis and "ground glass" opacity. Traction bronchiectasis was present to varying degrees in all 7 cases (Figure 3-13). "Ground glass" change was a feature of 4/7 lungs, although some of this was attributed to collapse of dependent parenchyma in the inflated ex vivo tissue, an artefact also noted in 3/7 control lungs.

Four of 19 lungs were classified as 'inconsistent with' PPFE on imaging (HRCT n=2; photographic n=2). Two of these had small amounts of dorsal pleural and subpleural fibrosis that was either asymmetrical or considered not to be a predominant feature. One had a predominantly ventral distribution of fibrosis, while the other showed diffuse "ground glass" opacity (Figure 3-18).

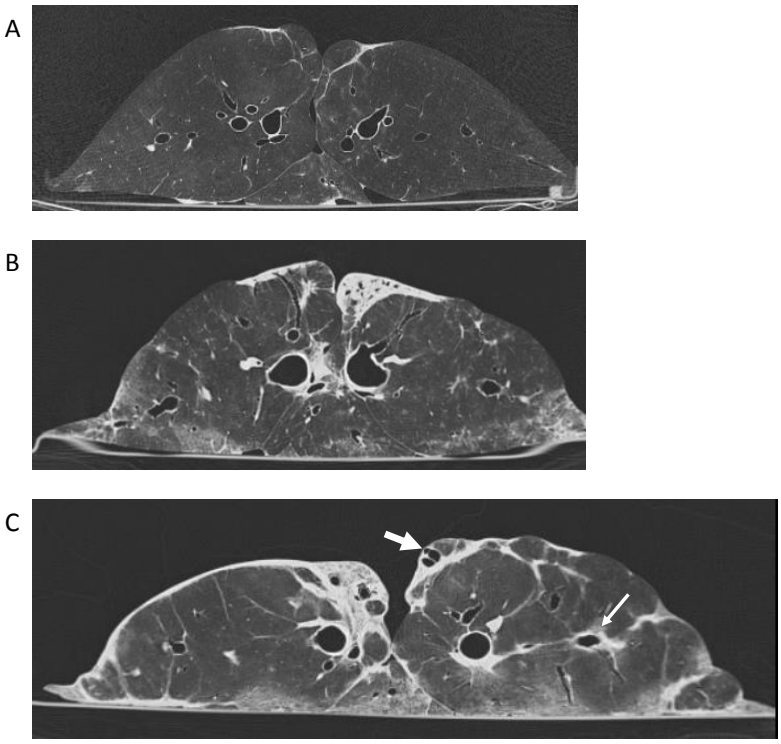

Figure 3-27: Cranio-caudal HRCT images of 'PPFE-like' inflated *ex vivo* APF lungs (Miele et al., 2014). Pathology ranged from mild dorsal pleural fibrosis extending along parenchymal bands (A) to thick rinds of pleural fibrosis encasing the dorsal surface of the lung (C). Also note the traction bronchiectasis (large arrow) and bronchocentric fibrosis (small arrow) (C).

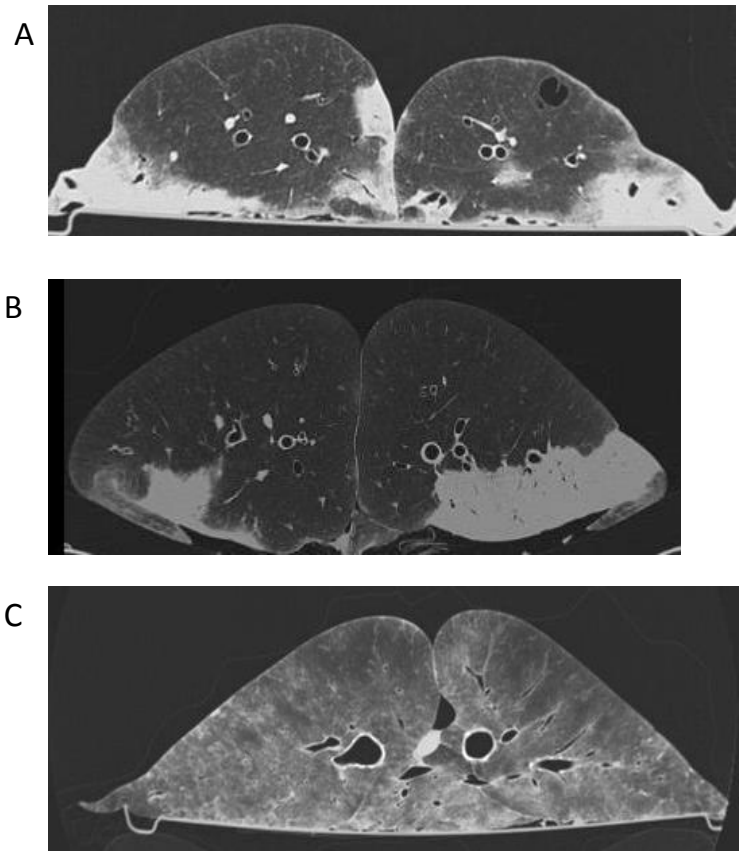

Figure 3-28: HRCT images of inflated *ex vivo* APF lungs classified as 'inconsistent with' PPFE on both imaging and histology (Miele et al., 2014). Images A and B show a predominantly ventral distribution to the fibrosis whereas image C demonstrates diffuse "ground glass" change. Image B reproduced from Thiemann, 2012. Veterinary Education, 24(9) 469-478, with permission from Wiley. ©2011 EVJ Ltd.

3.3.7 Aetiological investigations

Acid fast bacteria, viral inclusions (Figure 3-19) and fungi were not identified in APF lung sections with special staining.

Amplification products were detected following PCR for herpesvirus in all 12 cases tested (see Chapter 2.7.3). Herpesviral sequences were identified in all 6 of the PCR products that underwent nucleotide sequencing, with 5 sequences mapping to AHV-5 and 1 to AHV- 4.

X-ray diffraction analysis revealed a dust burden of 6.98mg/g dry lung. Small numbers of fibrous particles were identified: talc 0.28 and silica 0.14 million fibres/g dry lung. The percentages of non-fibrous particles were calcium silicate 95, potassium silicate 2, kaolin 1, muscovite 1 and silica 1. No asbestos fibres were found. Slides were examined under polarised light to look for the presence of crystalline particles and to assess the extent of their co-localisation with dust-laden macrophages (Figure 3-20). While co-localisation was occasionally identified, the overall dust burden was not considered to be significant with regards to potential calcium silicate toxicity.

3.3.8 Immunohistochemistry and western blotting

Western blot of homogenised asinine lung tissue showed increased expression of α-SMA in fibrotic compared to unaffected tissue from APF lungs and to control donkey lung homogenates ($p<0.05$, Mann Whitney, Figure 3-21). On immunohistochemistry, α-SMA staining in control tissue was restricted to the smooth muscle surrounding the airways and pulmonary vasculature. In APF lung tissue, staining was often concentrated around the alveolar septae (Figure 3-22) and was spatially heterogeneous in nature. Histological features representative of fibroblastic foci were not identified but abundant myofibroblasts were detected within fibrotic areas of APF lungs. See chapters 4 and 5 for further immunological analysis of asinine tissue.

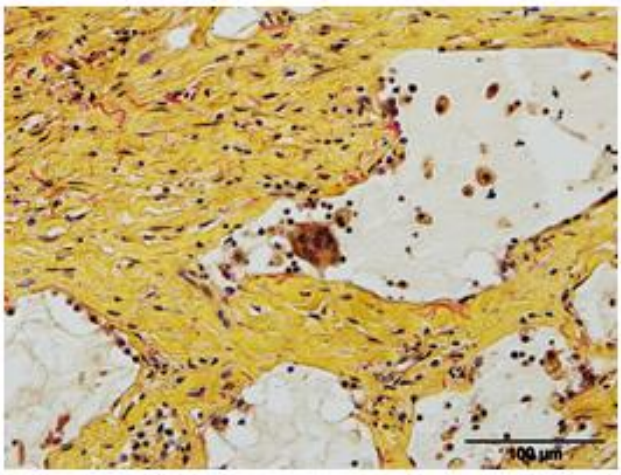

Figure 3-29: Additional staining did not detect the presence of pathogens. Phloxine-tartrazine staining of APF lungs did not reveal any evidence of viral inclusions.

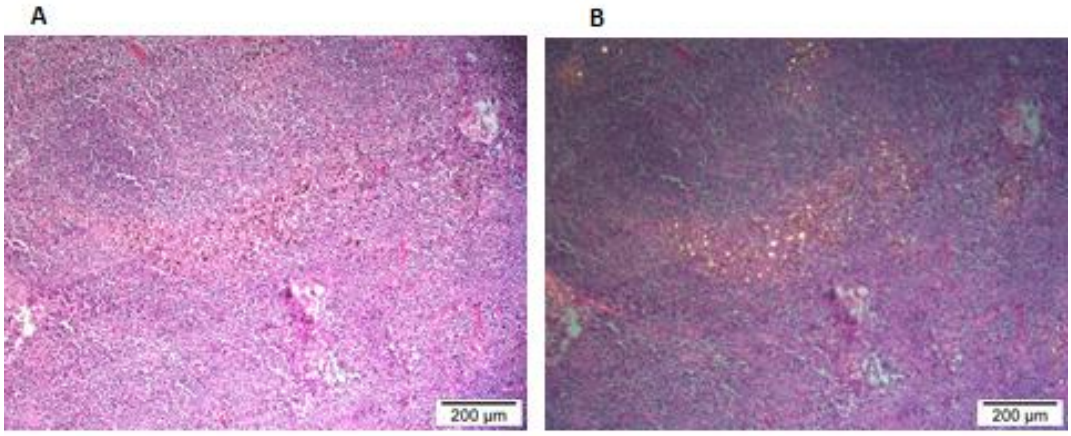

Figure 3-30: Polarised light revealed crystalline material within sections of bronchial lymph node. Section of bronchial lymph node from an APF affected donkey under bright-field (A) and polarised light (B), H&E. Note the illumination of crystalline particles within an area of anthracosis (B).

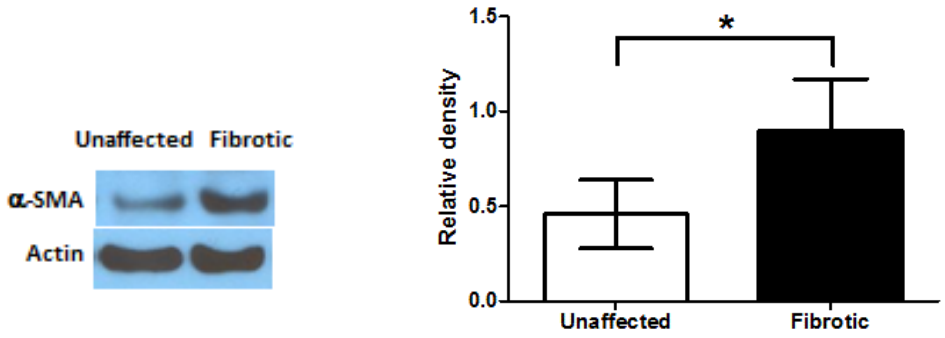

Figure 3-31 Western blot demonstrates increased expression of α-SMA in APF lung tissue. Sections of APF and grossly unaffected lung were homogenised for western blot analysis of α-SMA expression. Band densitometry revealed significantly increased expression in the fibrotic tissue (* p= 0.0317, Mann Whitney), n= 5 unaffected and 3 fibrotic.

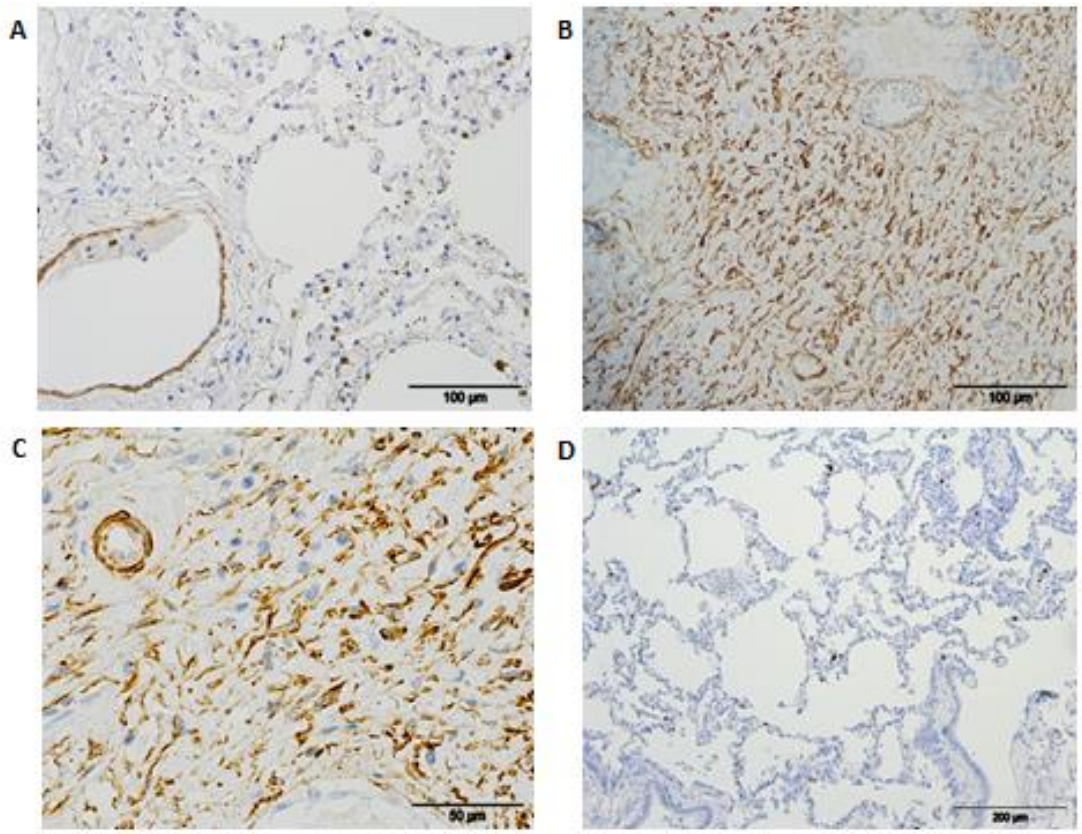

Figure 3-32 Immunohistochemistry of asinine lung supports results of western blot. Representative images of α-SMA immunohistochemistry of control (A) and APF (B-C) lungs. α-SMA in control tissue (A) was concentrated within the smooth muscle cells lining blood vessels and airway walls, and there was no evidence of a myofibroblast population within the alveolar interstitium. α-SMA was more diffuse within the fibrotic tissue (B) with frequent myofibroblasts lining the alveolar walls (C). GFP control (D) did not show any DAPI staining although haemosiderin appears as dark brown deposits.

3.4 Discussion

Chronic respiratory disease in UK donkeys often goes undetected and is thus a common incidental finding at necropsy. This is mainly due to the sedentary and stoic nature of donkeys in the UK and is compounded by the rarity of coughing as a clinical sign in this species. When APF is presented pre-mortem it is often not until the advanced stages, the clinical signs are variable and non-specific, and the animal is frequently in respiratory distress. The difficulties involved with diagnosis and the lack of an effective treatment for this progressive and debilitating disease, make it a significant welfare concern (Thiemann, 2012, Thiemann and Bell, 2001).

This is the most comprehensive study of a spontaneous large animal model of pulmonary fibrosis to date. In support of the 'One Health' initiative, it was envisaged that this project would be of benefit to both veterinary and medical fields in that aiding the diagnostic and pathological evaluation of APF could in turn help to instigate an advance in knowledge with regard to PPFE.

The study explored the use of a respiratory scoring system to aid the veterinary surgeon in the diagnosis of APF. Similar scoring systems have been used successfully in the literature, particularly with regards to recurrent airway obstruction (RAO)(Rush et al., 1998, Costa et al., 2000). While case numbers in this study were relatively low, donkeys with APF had a significantly higher respiratory score than those with grossly normal lungs as determined on necropsy.

Consistent with previous descriptions (Thiemann and Bell, 2001) this study found that increased inspiratory effort, although not seen in every case, was highly suspicious of APF. It was noted that 3/8 APF donkeys also had an increased expiratory effort which may have been due to coexisting RAO (Figure 3-12). Generally the increased expiratory effort seen in RAO is more readily detected than the subtle change in respiratory pattern observed in APF cases. It should also be noted that similar to findings in the horse, this study confirmed that although it seems

that RAO and APF can occur simultaneously, pulmonary fibrosis was not a consistent feature of donkeys presenting with chronic RAO (Figure 3-2).

Prior to the commencement of this research project, thoracic ultrasound was generally not used in the diagnosis of potential APF cases at The Donkey Sanctuary. With a detection rate of over 60% in this study, it was a technique that proved to be very useful and is one that will hopefully be continued to be utilised by the veterinary surgeons at The Donkey Sanctuary. However, given that the number of donkeys subjected to thoracic ultrasound with subsequent availability of necropsy reports was low, the diagnostic utility of thoracic ultrasound for the detection of APF does require further evaluation. Thoracic radiography is not currently performed in the diagnosis of APF at The Donkey Sanctuary and although likely to prove useful, it was not possible to evaluate as a diagnostic technique during the course of this project.

APF was first reported as a common incidental necropsy finding of donkeys resident at The Donkey Sanctuary back in 2001 (Thiemann and Bell, 2001). Reported gross and histopathological findings were consistent with those detailed here, including a wide spectrum of pleural, subpleural and septal fibrosis extending into the interstitium of dorsal lung fields, with more diffuse and ventral changes in severely affected cases. Peribronchial cuffing and multifocal aggregates of mononuclear cells on histopathology were also described along with the presence of haemosiderophages as a common finding. The authors suggested that severe dyspnoea may result in increased capillary fragility and haemorrhage (Thiemann and Bell, 2001). However that would not account for the frequent haemosiderophages observed in the lungs of control donkeys in this study. The role of cellular senescence in pulmonary pathology is an emerging field and senescent endothelial cells have been shown to be more susceptible to oxidative stress resulting in endothelial dysfunction (Podlutsky et al., 2010). It is possible that aged asinine lungs are generally more susceptible to pulmonary capillary haemorrhage even in the absence of grossly evident disease.

The presence of intra-alveolar fibrosis and alveolar septal elastosis as a histopathological feature of donkeys with pulmonary fibrosis has not previously been reported, most likely because such features are less striking in the absence of EVG staining. In this study, over 50% of donkeys with APF displayed the key imaging and pathological characteristics of human PPFE, an emerging and likely previously misdiagnosed disease. While the donkey may seem an implausible candidate with which to share pathological features of pulmonary disease, of all the domestic species, the subgross anatomy of the equine lung and visceral pleura most closely resembles that of humans (McLaughlin Jr and Tyler, 1961).

APF lungs were classified as 'PPFE-like' only if they had features considered 'consistent with' PPFE (Frankel et al., 2004) on both histology and imaging. In this respect, a greater proportion of APF lungs were classified as 'consistent with' PPFE on HRCT (82%) compared to histology (58%). It is possible that some of the 9 lungs classified as 'inconsistent with' PPFE on histology represent an earlier stage of 'PPFE-like' disease. Seven of these had intra-alveolar mononuclear inflammatory infiltrates with organising intra-alveolar fibrin which is a likely prelude to intra-alveolar fibrosis (Figure 3-16B). Furthermore, the marked spatial heterogeneity in extent and pattern of fibrosis meant that 'PPFE-like' pathology may have been missed as a result of unrepresentative sampling in some cases.

Imaging of 'PPFE-like' lungs indicated that, although all had the characteristic predominantly dorsal distribution of lesions, 7/10 lungs also had pleural and subpleural fibrosis in the mid and ventral pulmonary parenchyma. Similarly, Reddy et al, 2012 reported that 6/12 PPFE lungs had interstitial lung disease in lobes distant from the upper zone on HRCT (Reddy et al., 2012). Furthermore, 6/12 lungs had areas of consolidation and 1/12 had bronchiectasis. In the present study, HRCT identified "ground glass" opacity in 4/7 'PPFE-like' lungs and traction bronchiectasis in all 7 lungs. The presence of bronchocentric consolidation in HRCT images of 5 of these 7 lungs further supports the proposal that chronic airway disease could be key to PPFE pathogenesis (Reddy et al., 2012). Bronchocentric changes were also evident histologically, with all 10 'PPFE-like' lungs having variable lymphoplasmacytic bronchiolitis, and 8/10 having areas of bronchocentric fibrosis. A

patchy lymphoplasmacytic infiltrate was a feature of the PPFE cases reported by Frankel et al, 2004(Frankel et al., 2004), while Reddy et al, 2012, found bronchocentric fibrosis in 11/12 PPFE cases, with all 12 cases having focal non-specific chronic inflammation with lymphoid follicle accumulation (Reddy et al., 2012).

Frequent lymphoid follicles were a feature of all APF lungs (including those consistent with PPFE) and almost half of the control lungs. Lymphoid follicles are generally accepted to be an indication of chronic respiratory disease and are found in chronic obstructive pulmonary disease (COPD) as well as in equine RAO (van der Strate et al., 2006, Robinson, 2001). There has been speculation that they may reflect an autoimmune component to the disease process (Feghali-Bostwick et al., 2008), and non-specific autoantibodies have been detected in PPFE cases (Reddy et al., 2012). It would have been very interesting to investigate the presence of auto-antibodies in the sera of donkeys included in the study and this is a potential area of future work.

Other features of PPFE shared by asinine 'PPFE-like' lungs included perilobular fibrosis (10/10) and venous and arterial intimal fibrosis (9/10) (Thiemann and Bell, 2001, Reddy et al., 2012). Vascular changes in asinine lungs were considered to reflect secondary intimal invasion by the surrounding fibrosis, rather than a primary vasculopathy.

While granulomatous inflammation is not a key accepted feature of PPFE, it has been detected in PPFE cases (Reddy et al., 2012) and was an additional feature of 3/10 'PPFE-like' lungs. Along with mycobacterial and fungal pneumonias, granulomatous inflammation is also a feature of hypersensitivity pneumonitis, silicate pneumoconiosis and inhalation pneumonia among other pulmonary diseases (Mukhopadhyay and Gal, 2010). Neither mycobacteria nor fungi were identified in the granulomatous lesions in the asinine lungs.

Pleural fibrosis is a feature of asbestos-induced pulmonary fibrosis (Bergin et al., 1994). Inorganic fibre content of the asinine lung tissue was minimal and there was

no evidence of asbestos fibres. The presence of non-fibrous dust particles such as calcium silicate was unsurprising considering the grazing habits of donkeys and likely reflected local soil composition. Potential toxicity of calcium silicate is thought to be minimal (Bolton et al., 1986) and the dust burden of the asinine tissue was not considered to be significant.

The significance of elastosis within fibrotic asinine tissue is unclear. Elastosis and upregulation of elastin gene expression occurs in a murine model of pulmonary fibrosis (Hoff et al., 1999), and in humans, progressive vascular fibroelastosis occurs in idiopathic interstitial pneumonias and correlates with a poor prognosis in usual interstitial pneumonia (Parra et al., 2007). An overall increase in both collagen and elastin with alveolar septal elastosis has been documented during the late phase of adult respiratory distress syndrome and in usual interstitial pneumonia (Negri et al., 2000).

Reddy et al, 2012, reported that 7/12 PPFE patients had a history of recurrent lower respiratory tract infections, leading the authors to postulate the contribution of such infections to the pathogenesis of PPFE. Respiratory disease in donkeys often goes undetected for reasons mentioned previously and it is highly probable that donkeys in this study may have suffered from undiagnosed respiratory tract infections. Additionally, it should be noted that respiratory tract infections are particularly common in young equids and that the available histories for donkeys included in this study rarely covered periods beyond 10yr prior to death (Thiemann and Bell, 2001). Despite this, 3/10 ‘PPFE-like cases’ had a history that included a single episode of suspected lower respiratory tract infection, while a further 2 cases had received antibiotic treatment for a suspected lower respiratory tract infection on 2 or more occasions. Further investigation is required to determine whether donkeys with PPFE-like disease had preceding recurrent lower respiratory tract infections.

In the horse, a progressive fibrosing interstitial lung disease termed Equine Multinodular Pulmonary Fibrosis (EMPF) is associated with equine herpesvirus 5 infection. Similarly asinine herpesvirus 4 and 5 (AHV-4, AHV-5) were implicated in an acute fibrosing interstitial pneumonia in 11 donkeys in North America and in a

pyogranulomatous pneumonia in a mare (Williams et al., 2007, Kleiboeker et al., 2002, Witte et al., 2012). Kleiboeker et al (2002) described multifocal to coalescing nodules of fibrosis scattered throughout the lung parenchyma in the most severely affected of the 11 donkeys, a pattern similar to that seen in EMPF and quite different to the pathology described herein for APF. However, as in this study, multinucleated giant cells were reported as a common feature (Kleiboeker et al., 2002). Although present in some viral pneumonias, multinucleated giant cells are also abundant in several other pulmonary diseases such as chronic hypersensitivity pneumonitis and asbestosis (Prieditis and Adamson, 1996, Ohtani et al., 2005).

Kleiboeker et al (2002) detected herpesviral DNA in lung homogenate in all 11 affected donkeys but not in 6 control animals (Kleiboeker et al., 2002). This differs from the current findings whereby lung homogenates from 6 APF and 6 control donkeys were positive for herpesviral DNA on PCR, with all 6 samples sequenced corresponding to that of AHV-4 or-5. The role of AHV-4 and -5 in APF thus warrants further study.

3.5 Conclusion

Systematic clinical examination of donkeys with suspected respiratory disease and the use of a respiratory scoring system, along with thoracic ultrasound, may be used to distinguish between cases of APF and the more common RAO, with which there appears to be some overlap with regards to clinical signs and response to treatment.

The ubiquitous presence of gamma herpesvirus in the study population of donkeys warrants further investigation with regard to its potential role in the aetiology of APF as does the significance of recurrent respiratory tract infections.

Elastosis is a previously unreported histopathological feature of APF and this study demonstrated that over 50% of donkeys with APF share key imaging and pathological characteristics of human PPFE. Hence the interdisciplinary study of these conditions may help to accelerate learning and elucidate disease aetiopathogenesis.

Chapter 4: Evaluation of a Smartprobe for the Detection of Lysyl Oxidase

4.1 Abstract

Aberrant fibrogenesis is a feature of many diseases in multiple organ systems. The lysyl oxidase family of enzymes are central to tissue homeostasis and elevated lysyl oxidase activity is implicated in fibroproliferation as well as in cancer stroma. The fluorogenic LOX Smartprobe, TWB-219, synthesised by the UoEDC, was evaluated and shown to generate a 3- fold increase in fluorescence following probe activation in *ex vivo* human lung tissue. The strategic use of inhibitors demonstrated signal specificity in this model and preliminary experiments utilising FCFM to detect probe signal were promising. However, problems with background fluorescence and reaction time limit the *in vivo* potential of TWB-219.

4.2 Introduction

Fibrogenesis is a prominent feature of several lung diseases ranging from adult respiratory distress syndrome in intensive care to chronic obstructive pulmonary disease and interstitial lung diseases (Demedts and Costabel, 2002). The global impact of these diseases is huge, incurring significant financial burden (Lozano et al., 2013). As previously mentioned, treatment options are very limited and monitoring of disease progression also remains a challenge as there are no rapid bedside biomarkers that can detect active fibroproliferation (Wynn and Ramalingam, 2012). Blood biomarkers offer poor molecular specificity for lung pathology while invasive pulmonary biopsy provides only a 'snap-shot' of information as the analysis of fixed tissue cannot inform on the dynamic enzyme activity that exists *in vivo* (Chen and Raghunath, 2009).

As previously discussed, the lysyl oxidase family (LOXF) is important in several fibrotic diseases as well as in cancer progression (Erler et al., 2006, Barry-Hamilton et al., 2010, Chien et al., 2014, Trivedy et al., 1999). Of the 5 members of the LOXF, two in particular have been the basis of extensive investigation and therapeutic

targeting: LOX and LOXL2 (Erler et al., 2006, Barry-Hamilton et al., 2010, Chien et al., 2014).

As the potential for the lysyl oxidases as therapeutic targets becomes clear, there is a discernible need for the development of selective and sensitive oxidase substrates to monitor enzymatic activity in complex biological systems. As yet fluorescent spectroscopy methods have been unable to provide a reporter probe for LOX activity *in vivo*.

With this in mind, the activity based fluorescent Smartprobe, TWB-219 was synthesized in-house by UoEDC (Figure 4-1). The probe was based on the concept that the chemical "masking" of the polar functionalities of fluorescein with suitable groups can suppress fluorescence and facilitate cell permeability (Dickinson et al., 2010). It was hypothesised that upon incubation of TWB-219 with an appropriate oxidase, the two amino groups would be oxidised to give the bis-aldehyde, followed by β-elimination to release acrolein and the fluorescent reporter fluorescein. Thus TWB-219 would report on LOXF activity in biological samples through signal amplification. In order to test this hypothesis a potent inhibitor of LOXF activity was required. As such the in-house pyridazinone-based inhibitors AMF-59 and AMF-60 were also synthesised and evaluated.

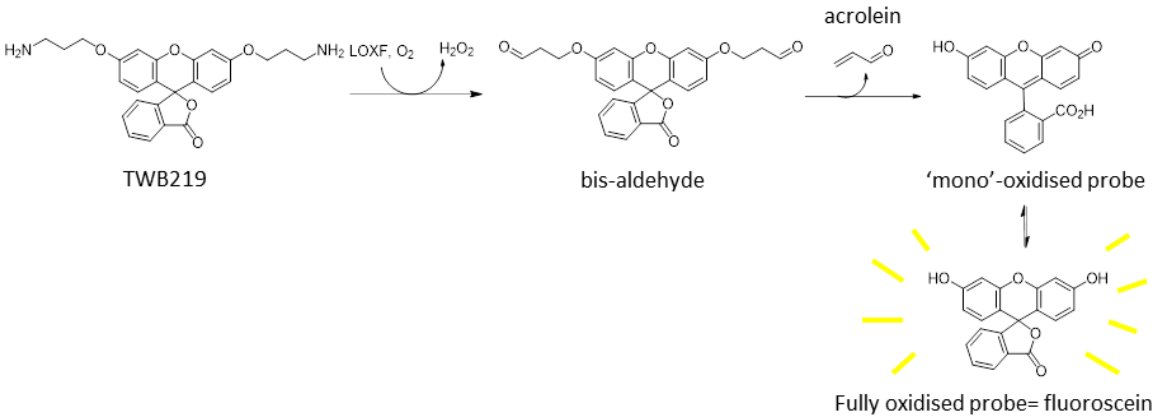

Figure 4-1: **Activation of TWB-219 by LOXF.**

4.3 Results

4.3.1 Developing a cellular model of LOX production

The production of LOX by fibroblasts in culture was investigated in order to generate a readily available *in vitro* model to facilitate the evaluation of the LOX optical imaging probe.

Considerable time was spent optimising the cell culture conditions of murine NIH 3T3 embryonic fibroblasts with regards to stimulation with TGFβ. It was confirmed that 24h stimulation of 3T3 cells with TGFβ resulted in increased expression of lysyl oxidase and monocyte chemoattractant protein-1 (MCP-1) on western blot and cytometric bead array (CBA) respectively (Figure 4-2). Furthermore, pre-stimulation starvation with BSA resulted in increased expression of LOX and MCP-1 compared to starvation with low concentrations of FBS. There was a notable increase in α–SMA and LOXL2 immunofluorescence in 3T3 cells stimulated with TGFβ compared to controls, although this was not quantified (Figures 4-3 and 4-4). It should be noted that no difference in LOX expression was observed by immunocytochemistry (Figure 4-5) or Amplex red fluorescence (data not shown) between stimulated and non-stimulated cells.

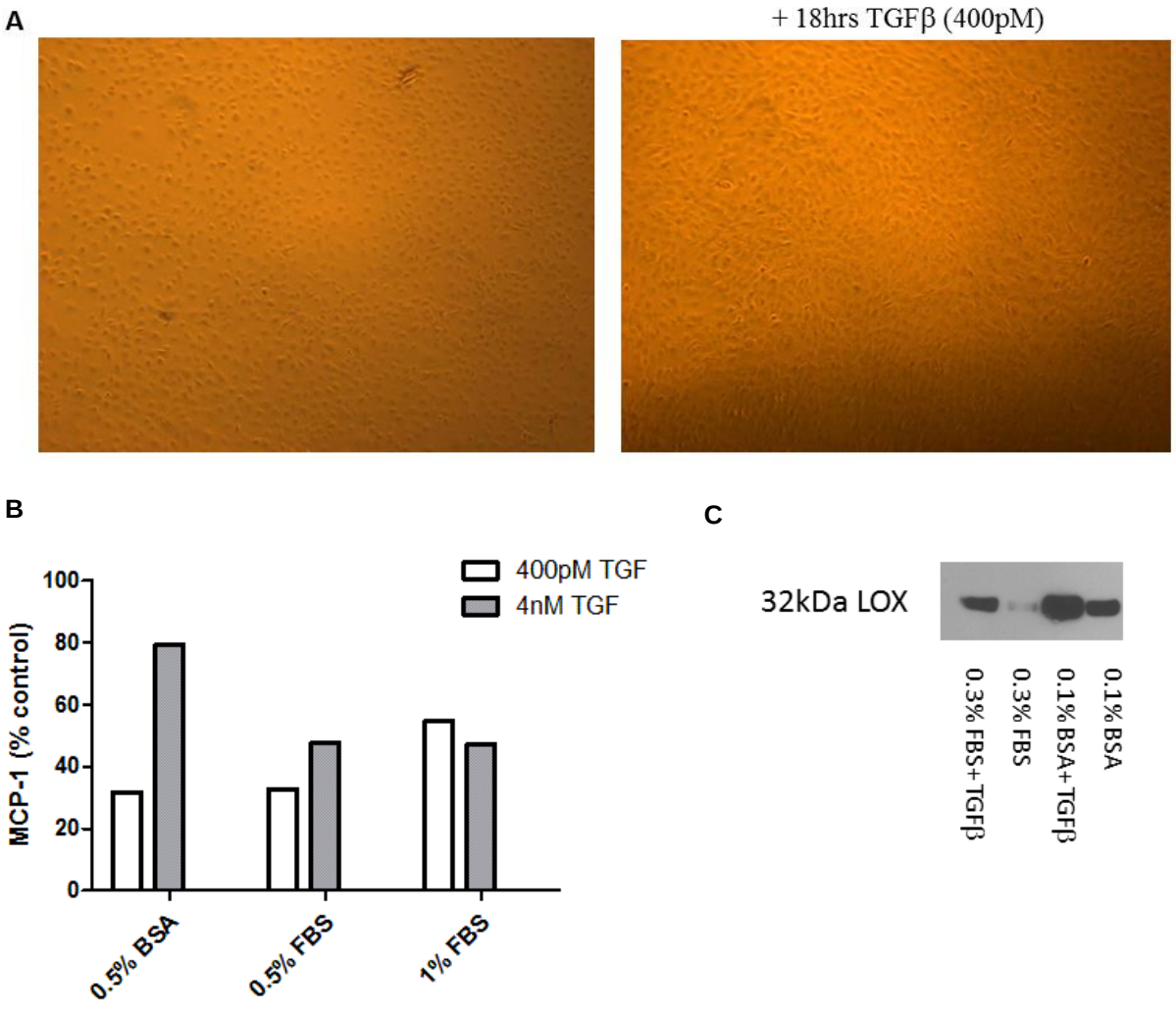

Figure 4-2: Serum starvation of murine NIH 3T3 cells results in greatest activation following stimulation with TGFβ. Phase images (A), Cytometric bead array results (B) and western blot (C) of murine 3T3 fibroblasts stimulated with TGFβ under varying conditions. Cell morphology was monitored following stimulation with TGFβ and changes observed included transformation from square to spindle shaped cells and focus-forming (A, x5 lens). (B) Serum starvation of cells (0.5% BSA) prior to the addition of 4nM TGFβ resulted in the greatest stimulation as determined by production of monocyte chemoattractant protein-1 (MCP-1), representative of n=2. Western blot demonstrated increased expression of LOX in cells stimulated with 400pM TGFβ, again with greatest expression in serum free conditions (C, representative of n=3).

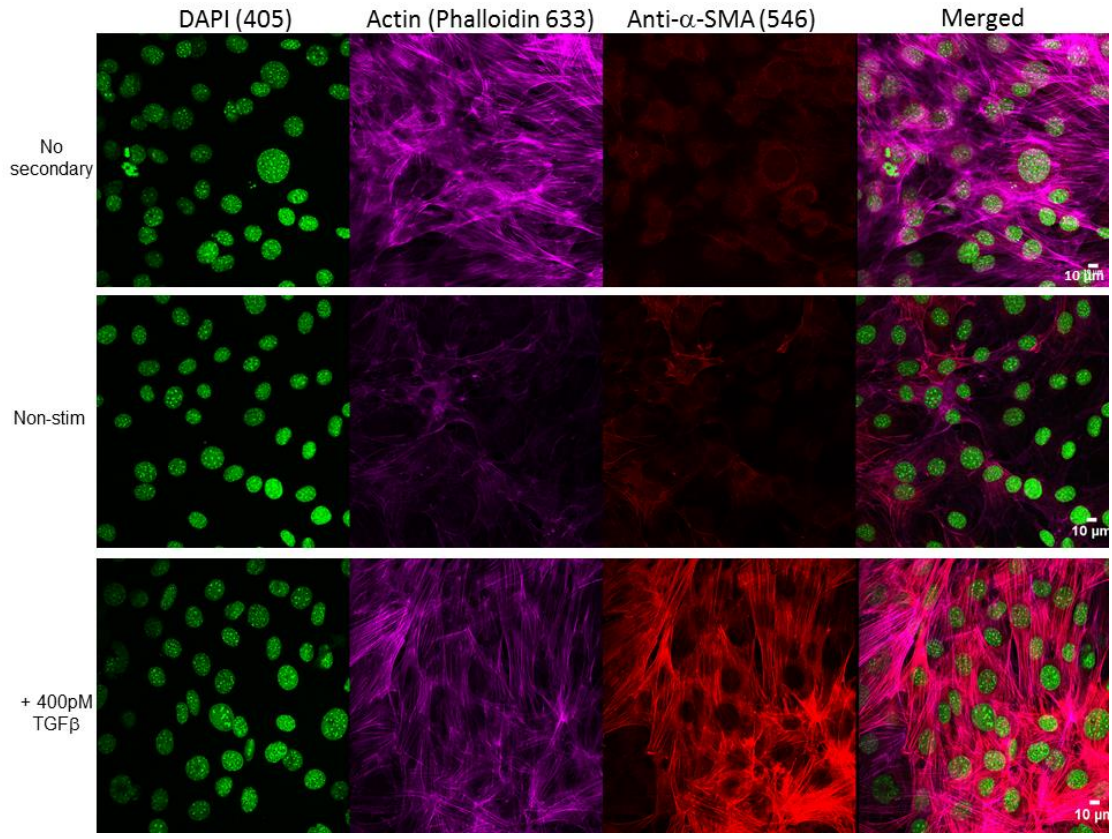

Figure 4-3: α-SMA expression in murine NIH 3T3 fibroblasts increases with TGFβ stimulation. Immunocytochemistry of α-SMA in 3T3 fibroblasts. Note the increase in α-SMA expression in cells stimulated overnight with TGFβ (representative of n=3). No α-SMA expression was seen in murine A549 epithelial cells stimulated with TGFβ (data not shown). DAPI stains cell nuclei, phalloidin stains F actin.

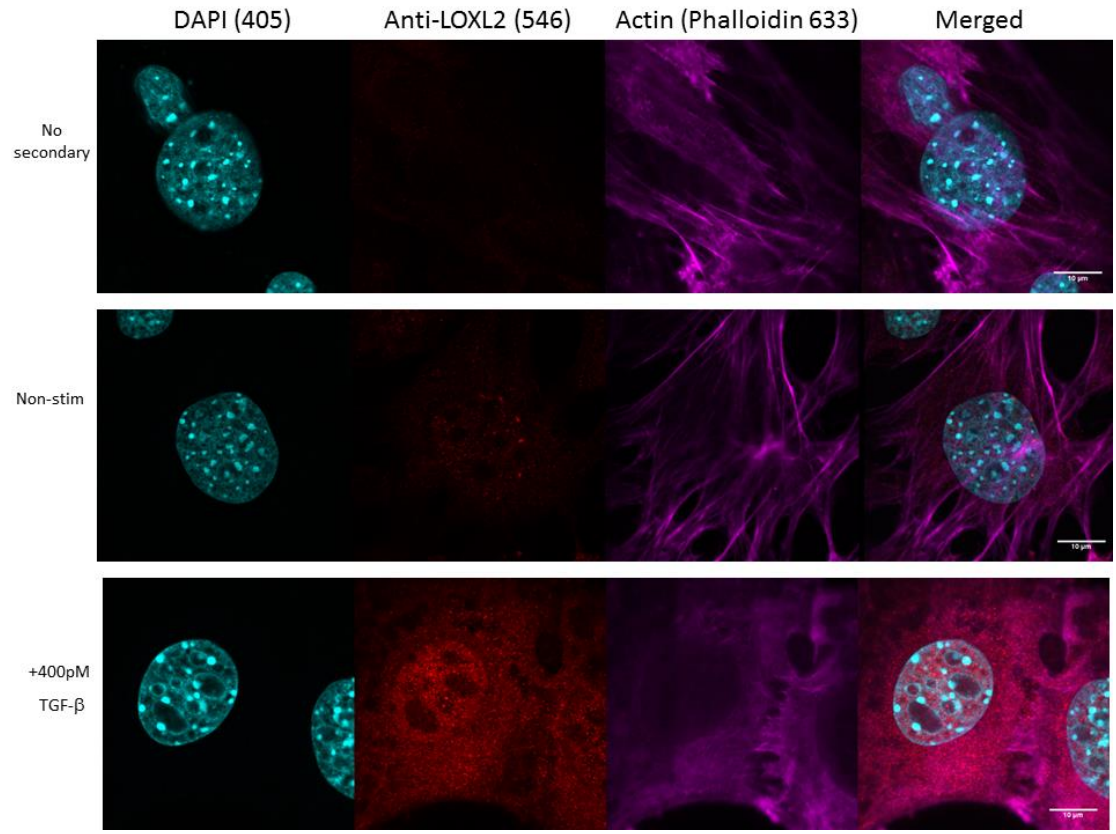

Figure 4-4: Lysyl oxidase-like 2 (LOXL2) is expressed in murine 3T3 fibroblasts stimulated with TGFβ. Immunocytochemistry for LOXL2 in 3T3 fibroblasts. Increased LOXL2 expression was seen in cells stimulated overnight with TGFβ (representative of n=3, bar=10μm). DAPI stains cell nuclei, phalloidin stains F actin.

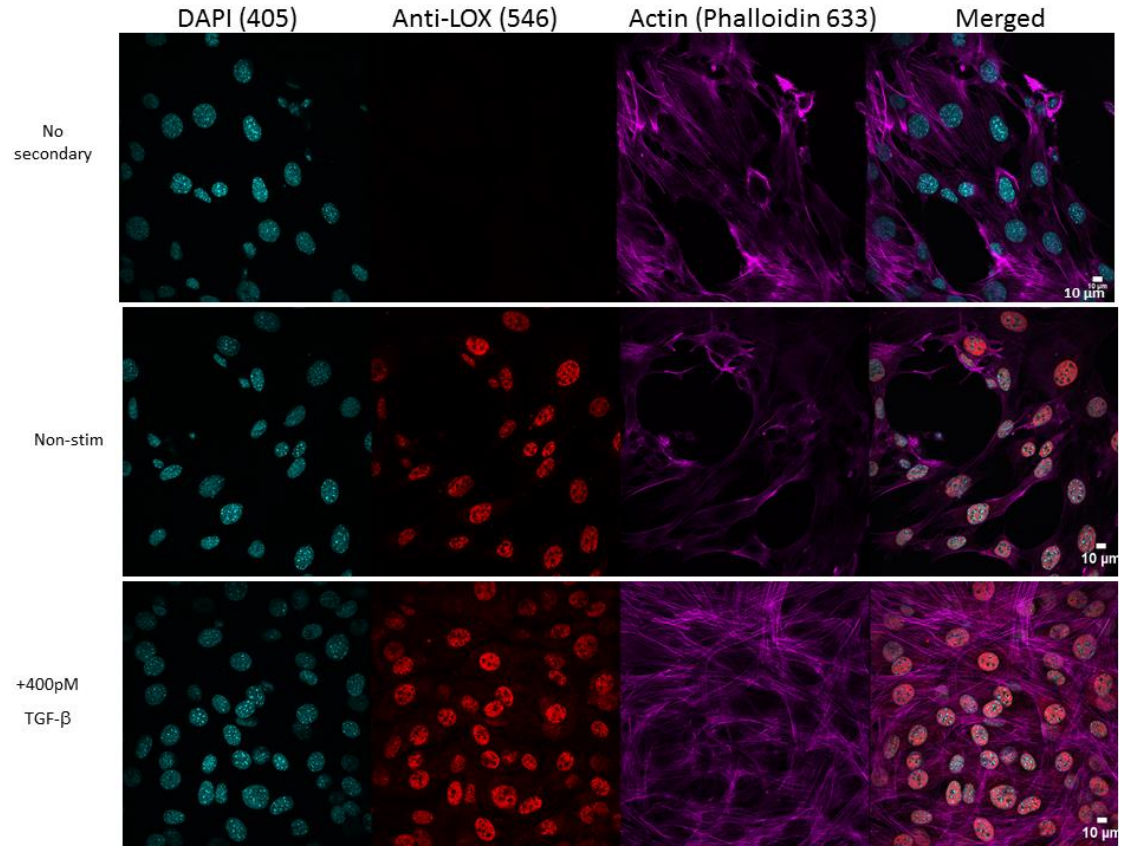

Figure 4-5: LOX is expressed in murine 3T3 fibroblasts. Immunocytochemistry confirmed expression of LOX in 3T3 fibroblasts but no difference in expression was observed following overnight stimulation with TGFβ (representative of n=2, bar=10µm). DAPI stains cell nuclei, phalloidin stains F actin.

4.3.2 Preliminary evaluation of TWB-219

It was quickly observed that TWB-219 had a relatively high background fluorescence that gradually increased over time. This increase was particularly marked in cell culture media such as Dulbecco's Modified Eagle's medium (DMEM, Figure 4-6). Matrix-assisted laser desorption/ionization (MALDI) analysis of the probe following incubation with DMEM did not reveal any evidence to indicate probe activation and various potential components of the media including riboflavin (vit B2) and iron nitrate (ferric acid) as well as changes in pH were eliminated as potential causes of the increased signal (Figure 4-6). As a result of this problem, it was difficult to utilise cell supernatants as a model to evaluate probe activation and no increase in fluorescence was observed (data not shown). Although probe signal was detected in live primary human fibroblasts in the absence of cell culture media, the signal was not inhibited by beta-aminopropionitrile (BAPN, Figure 4-7).

As resources did not allow the isolation of LOX from bovine aorta and recombinant LOX was both expensive and unreliable with regards to activity, it was necessary to source an alternative enzyme to assess probe activation. The action of the probe is such that it has the potential to be activated by any amine oxidase. Thus, diamine oxidase (DAO) was chosen as a cheap and readily available option.

It was established that optimal probe activation was achieved using 10µM probe (rather than 100µM) with high concentrations of enzyme and that the reaction could be inhibited by sodium diethyldithiocarbamate (DETCA, Figure 4-8). However, the reaction was relatively slow, with probe signal beginning to emerge at around 20min and continuing to increase beyond 2h incubation. Furthermore when MALDI analysis was performed on the final assay products, it was noted that the greatest peak equated to the mono-oxidised rather than di-oxidised probe (Figure 4-8D).

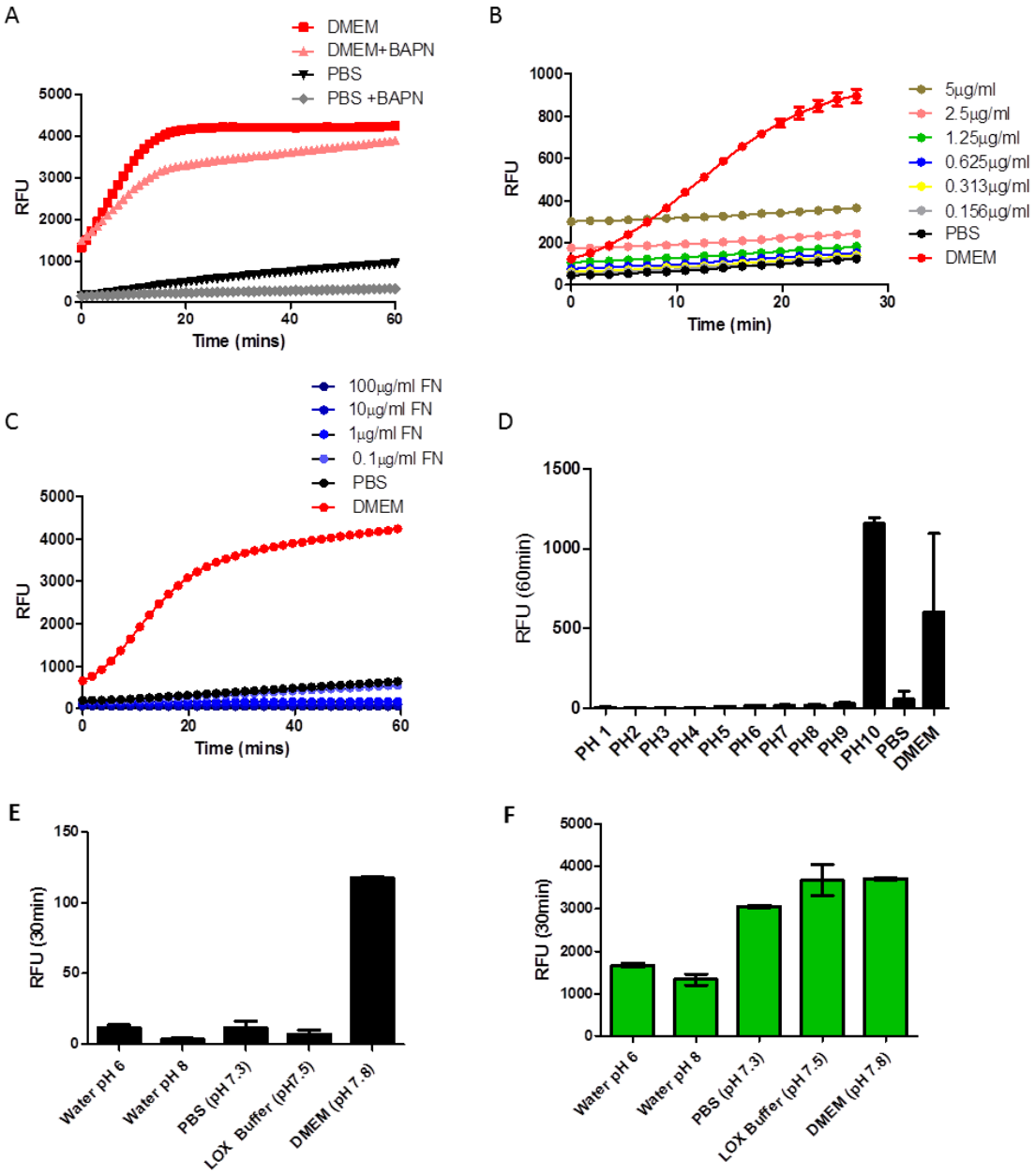
A
DMEM
DMEM+BAPN
PBS
PBS +BAPN
RFU
Time (mins)
B
5µg/ml
2.5µg/ml
1.25µg/ml
0.625µg/ml
0.313µg/ml
0.156µg/ml
PBS
DMEM
RFU
Time (min)
C
100µg/ml FN
10µg/ml FN
1µg/ml FN
0.1µg/ml FN
PBS
DMEM
RFU
Time (mins)
D
RFU (60min)
PH 1
PH2
PH3
PH4
PH5
PH6
PH7
PH8
PH9
PH10
PBS
DMEM
E
RFU (30min)
Water pH 6
Water pH 8
PBS (pH 7.3)
LOX Buffer (pH7.5)
DMEM (pH 7.8)
F
RFU (30min)
Water pH 6
Water pH 8
PBS (pH 7.3)
LOX Buffer (pH 7.5)
DMEM (pH 7.8)

Figure 4-6: **Investigating increased background fluorescence of TWB-219 in Dulbecco's Modified Eagle's medium (DMEM).** (A) TWB-219 (10µM) was added to phenol red free DMEM or PBS +/- beta-aminopropionitrile (BAPN, 500µM) and incubated at 37° C for 1h. Note the increase in fluorescence (RFU) in the presence of DMEM over the first 20min of incubation, kinetic plot is mean of 3 replicates, representative of n=3. 10µM TWB-219 was then incubated with varying concentrations of riboflavin (B) and iron nitrate (C) in PBS at 37°C for 30 and 60 minutes respectively. Note that the background fluorescence of TWB-219 in DMEM was higher than in the presence of riboflavin and iron nitrate (FN). Error bars indicate SD, n=3. (D) Bar chart of 10µM TWB-219 incubated with water at a range of different pH for 1h. Only at very alkaline pH did the background fluorescence of TWB-219 increase, error bars represent SD, n=4. The fluorescence of 10µM TWB-219 (E) and 10µM fluorescein (F) following 30min incubation with different media was then investigated. It can be seen from graph E that the background fluorescence of TWB-219 in DMEM was much higher than in other media of similar pH. This was not the case with fluorescein (F). Error bars represent SD, n=2.

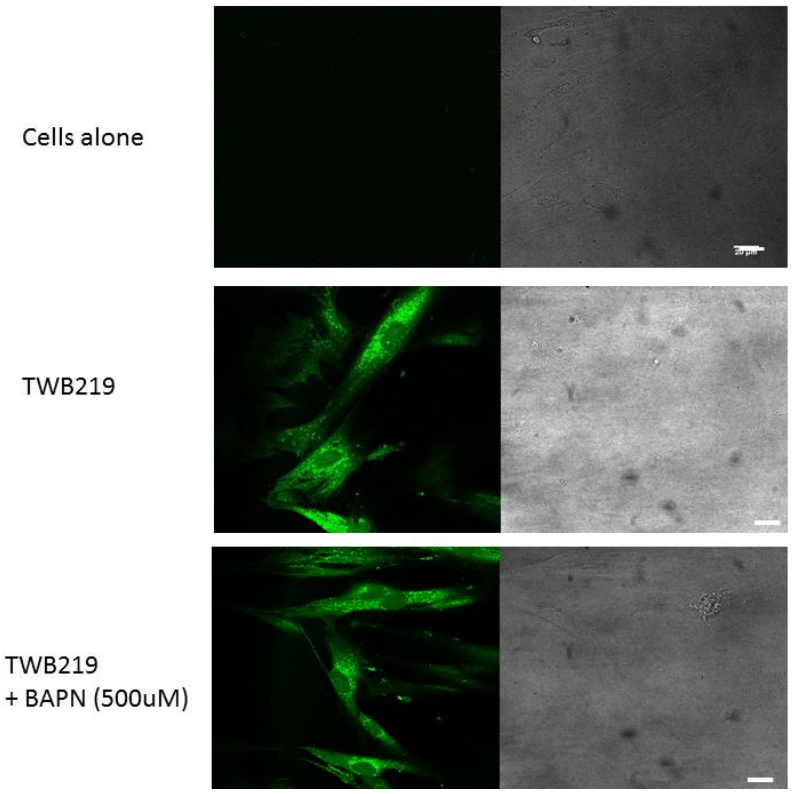

Figure 4-7: TWB-219 on live primary human lung fibroblasts. Fibroblasts were grown in 8 well chambers until they reached 70% confluence. Cells were then incubated with 50µM TWB-219 for 1h prior to washing with PBSx3 and imaging on confocal. There was no reduction in fluorescence in cells that had been pre-incubated with 1mM BAPN for 1h prior to the addition of probe. n=3, bar= 20µm. It should be noted that no fluorescence was observed in cells incubated with free fluorescein dye (10µM) and that results were confirmed using flow cytometry (data not shown).

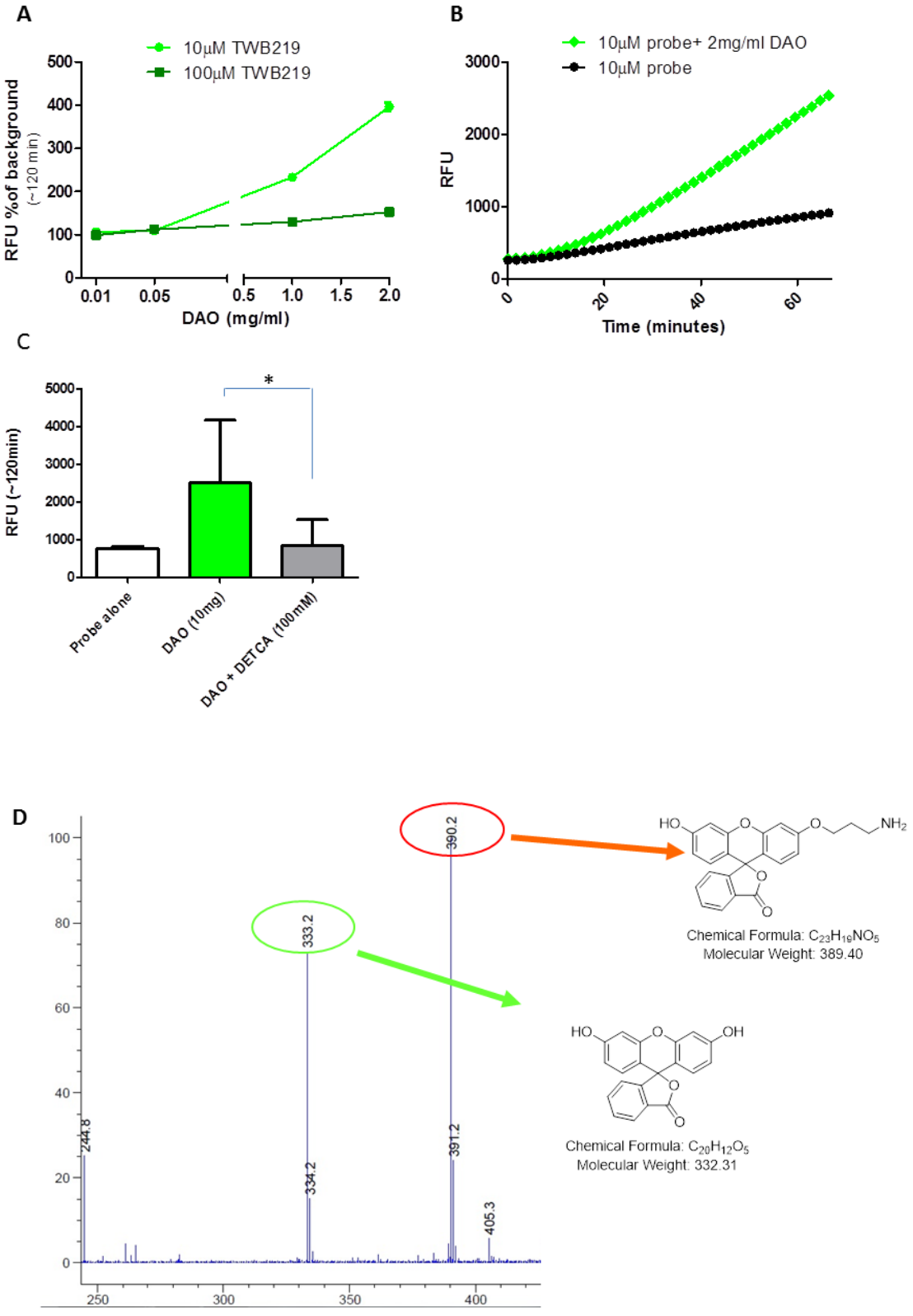
A
10µM TWB219
100µM TWB219
RFU %of background
(~120 min)
DAO (mg/ml)
B
10µM probe+ 2mg/ml DAO
10µM probe
RFU
Time (minutes)
C
RFU (~120min)
Probe alone
DAO (10mg)
DAO + DETCA (100mM)
D
390.2
333.2
334.2
391.2
405.3
244.8
Chemical Formula: C23H16NO5
Molecular Weight: 389.40
Chemical Formula: C20H12O5
Molecular Weight: 332.31

Figure 4-8: TWB-219 is activated by diamine oxidase (DAO). TWB-219 (10 and 100μM) was incubated with different concentrations of DAO at 37°C for 2h (A) and the greatest signal to noise ratio was achieved with the lower concentration of TWB-219. The reaction was slow with signal appearing after about 20min incubation (B), data representative of n≥3. (C) When DAO was pre-incubated with 100mM sodium diethyldithiocarbamate (DETCA), a copper chelator, for 10min at 37°C, there was a significant reduction in probe signal. n=4, * p=0.045 paired t test. (D) Probe cleavage by DAO was confirmed by MALDI, although the highest peak corresponded to only partially oxidised probe as highlighted in red (fully oxidised probe is highlighted in green).

4.3.3 Developing an *ex vivo* model

As DAO was not the intended target enzyme for TWB-219, it was necessary to try to establish a model of LOX production that did not involve the use of cell culture medium. As such, the expression of LOX and LOXL2 was confirmed in aged human lung tissue using western blot and immunohistochemistry (Figure 4-9). Homogenised human lung tissue was thus deemed an appropriate model to evaluate the utility of TWB-219. Incubation of TWB-219 with human lung homogenate resulted in a 2-3 fold increase in fluorescence. Importantly, probe activation was completely inhibited in a concentration dependent manner by pre-incubation of homogenate with BAPN and in-house inhibitors AMF-59 and AMF-60 (Figure 4-10). The minimum concentration of BAPN and AMF-60 found to have a significant inhibitory effect was 62.5µM (Mann Whitney p= 0.0286), whereas the minimum concentration of AMF-59 found to have a significant inhibitory effect was 15.6µM (Mann Whitney p= 0.0286).

To further prove molecular specificity in the human tissue, the potential contribution of mono amine oxidases (MAO) to TWB-219 activation was negated by the fact that clorgyline (MAO-A inhibitor) and pargyline (MAO-B inhibitor) did not cause any significant reduction in fluorescent signal (Figure 4-11) thus confirming that MAO is not cleaving TWB-219 in this model.

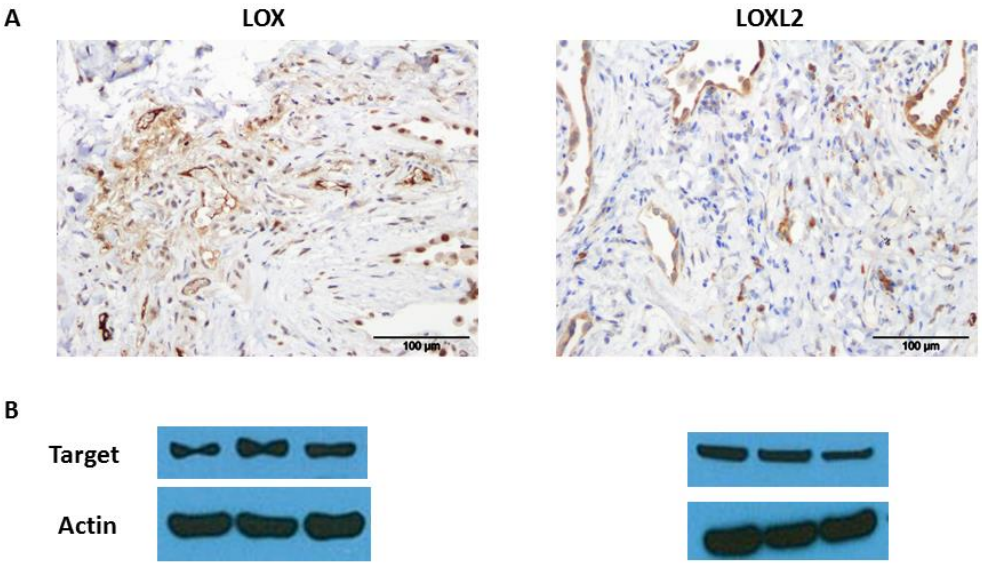

Figure 4-9: LOX and LOXL2 are expressed in aged human lung tissue. Immunohistochemical analysis (A) and western blot (B) of LOX and LOXL2 expression in aged human lung tissue. Strongest bands for LOX were around 50kDa, consistent with the glycosylated pro-lysyl oxidase, but mature 32kDa LOX was also present in several samples (not shown). Data representative of a minimum of n=3.

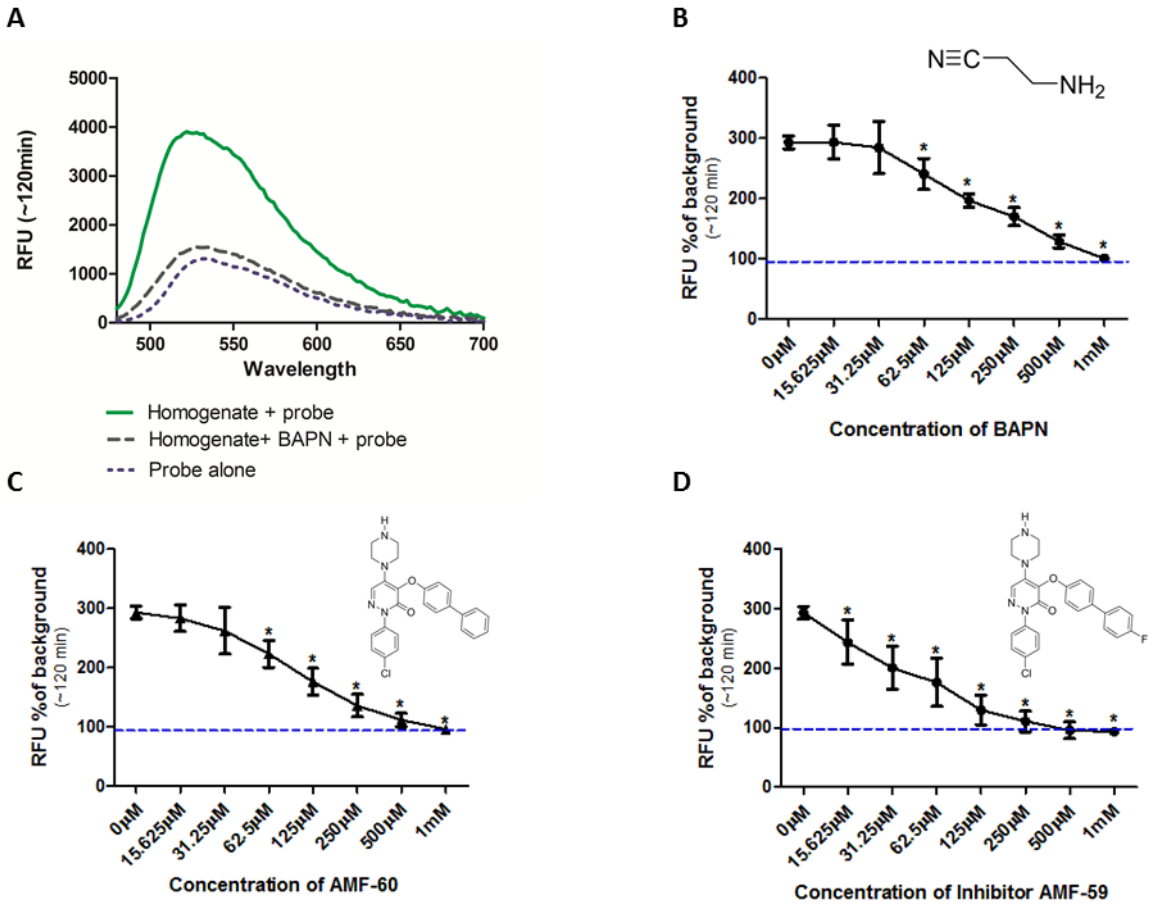

Figure 4-10: TWB-219 is specifically activated in the presence of aged human lung tissue homogenate. (A) Fluorescent intensity of 10μM TWB-219 after 2h incubation with aged human lung tissue homogenate (solid line). Spectra were recorded at λex =450nm. (B-D) Human lung homogenate was pre-incubated with 2 fold dilutions of inhibitors at 37°C for 1h prior to the addition of 10μM TWB-219. The line graphs show the resultant fluorescence presented as percentage of background fluorescence after 2h incubation of the reaction (n=3). The minimum concentration of BAPN (B) and AMF-60 (C) found to have a significant inhibitory effect was 62.5μM (Mann Whitney p= 0.0286), whereas the minimum concentration of AMF-59 (D) found to have a significant inhibitory effect was 15.6μM (Mann Whitney p= 0.0286). The dotted line represents background fluorescence of TWB-219, error bars show standard deviation.

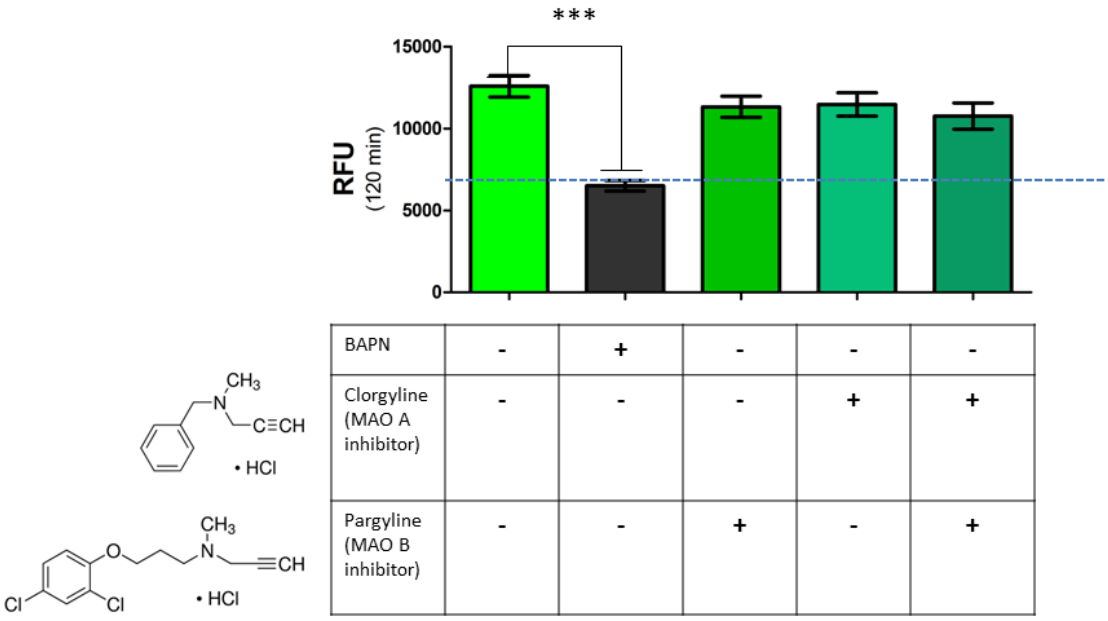

Figure 4-11: TWB-219 is not activated by monoamine oxidase in human lung homogenate. Human lung homogenate was pre-incubated in triplicate with 500µM BAPN, MAO- A inhibitor, clorgyline and/or MAO- B inhibitor, pargyline at 37°C for 1 h prior to the addition of 10µM TWB-219. The bar charts show the mean resultant fluorescence after 2h incubation of the reaction (n=3). ****p*<0.001, one way ANOVA, dotted line represents background fluorescence of TWB-219, error bars show standard error of the mean.

4.3.4 Fibre confocal fluorescence microscopy (FCFM)

Having evaluated probe target specificity in human lung homogenate, whole sections of lung tissue were incubated with TWB-219 in the presence of BAPN or buffer and the resultant fluorescence was imaged using FCFM. Again an increase in fluorescent signal over background was observed and this was significantly inhibited by BAPN (Figure 4-12).

Finally, in order to evaluate probe fluorescence in a ventilating lung, the *ex vivo* asinine lung model was used. As with human tissue, expression of LOX and LOXL2 as well as α-SMA was demonstrated using immunohistochemistry and western blot (Figures 4-13 and 4-14). Although not formally quantified, there was increased expression of both LOX and LOXL2 in fibrotic compared to control lung tissue on immunohistochemistry and a trend towards increased LOX expression in fibrotic tissue on western blot. A significant increase in fluorescent signal was detected following instillation of TWB-219 into the ventilating fibrotic asinine lung (Figure 4-15).

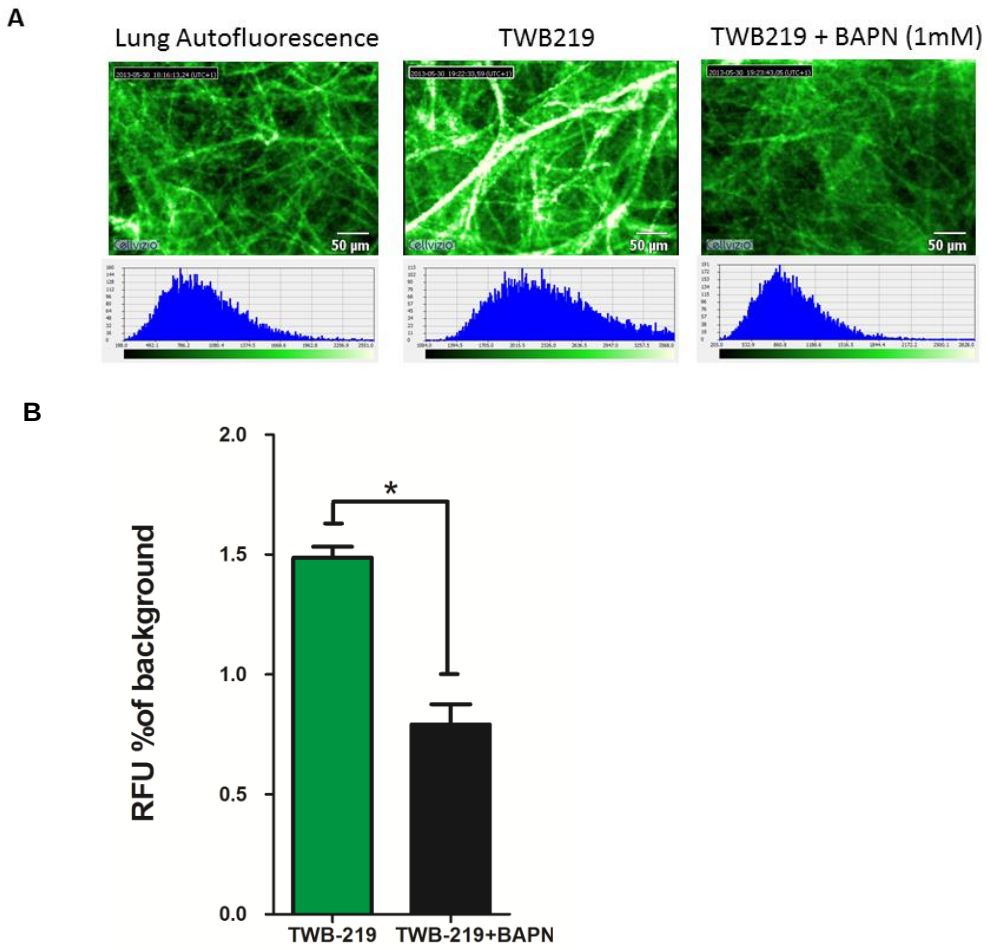

Figure 4-12: TWB-219 can be used alongside FCFM to demonstrate LOXF activity in whole ex vivo human lung tissue (A) Representative single frame images generated by FCFM on fresh sections of aged human lung tissue following incubation with 10µM TWB-219. The graph (B) represents the mean auto-fluorescence of each 60sec imaging period adjusted for tissue auto-fluorescence (n=4). Note the significant reduction in fluorescence on incubation with the lysyl oxidase inhibitor, BAPN (*p = 0.0286, Mann Whitney).

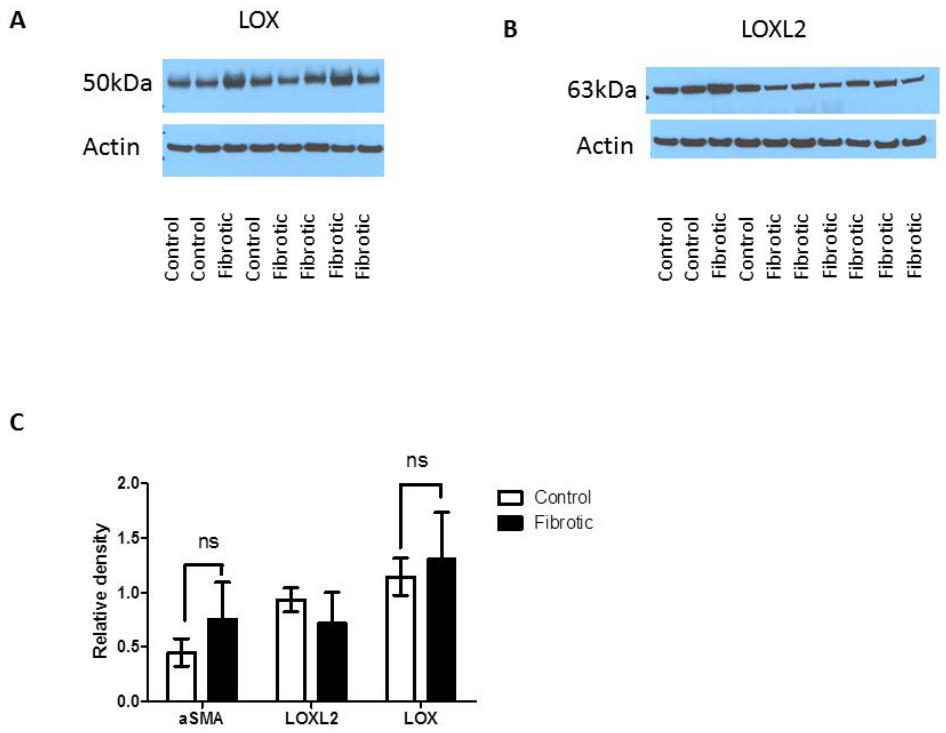

Figure 4-133: LOX and LOXL2 are present in aged donkey lung tissue as shown by western blot. Western blot showing LOX (A) and LOXL2 (B) expression in control and fibrotic asinine lung tissue. Bands for LOX were around 50kDa, consistent with pro-LOX. (C) Westerns were quantified using band densitometry analysis.

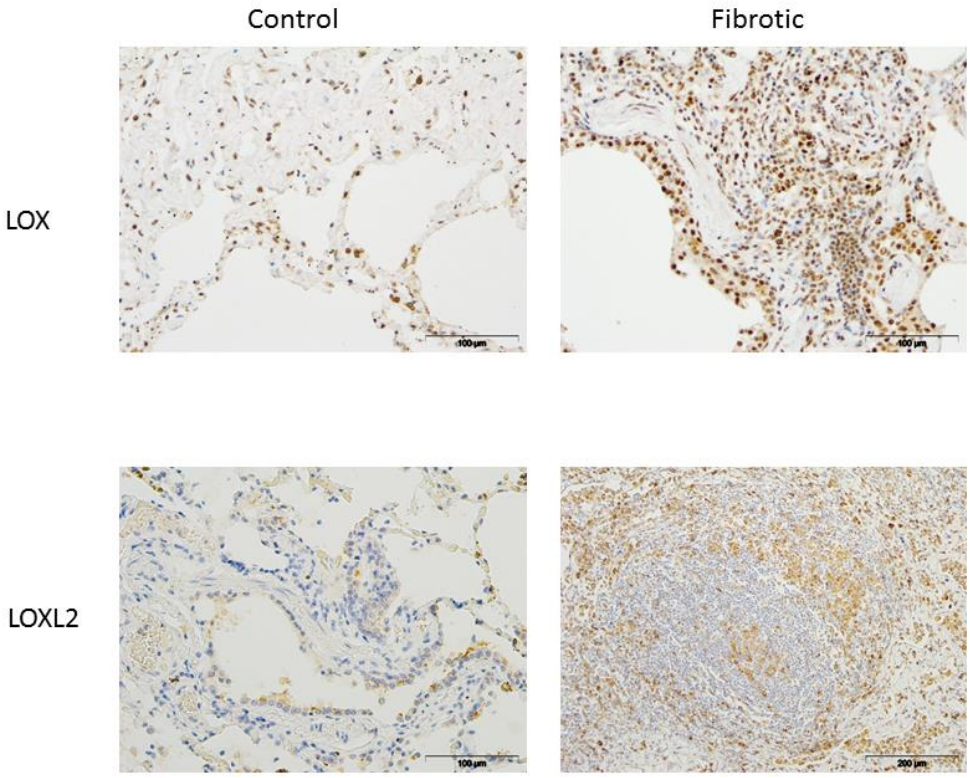

Figure 4-14: Immunohistochemical analysis of asinine lung tissue revealed increased expression of LOX and LOXL2 in fibrotic vs control sections. LOX expression was noted in a range of cells including fibroblasts, epithelial and endothelial cells and the staining was mainly nuclear. LOXL2 showed a different pattern of expression with staining focussed within the cytoplasm of the same cell types. Bar= 100µm.

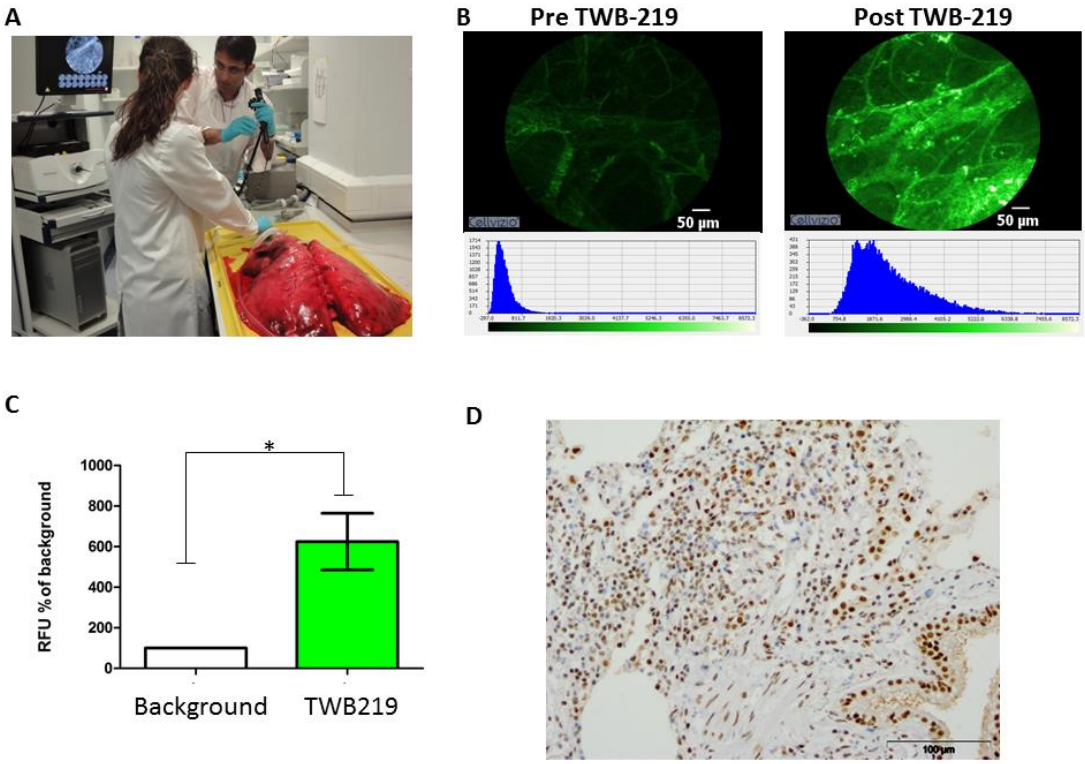

Figure 4-15: TWB-219 can be used to image LOXF activity in a ventilating *ex vivo* lung model of spontaneous fibrogenesis. (A-C) Catheter instillation of 200µM TWB-219 into a whole fibrotic ventilating *ex vivo* asinine lung (A) results in a significant increase in fluorescent signal (B-C, **p*= 0.0313, Mann Whitney, n=3). Target tissue was then evaluated for LOX expression using immunohistochemistry (D, bar=100µm).

4.4 Discussion

LOX has been shown to be produced by human dermal fibroblasts in culture, with maximal enzyme activity in the cell supernatant towards the end of the rapid growth phase of proliferation (Layman et al., 1972). NIH 3T3 cells were chosen for this study as they have also been shown to express LOX and were readily available (Li et al., 1997). It was hypothesised that the 3T3 cells would produce more LOX and LOXL2 in their activated state following stimulation with TGFβ.

In order to confirm activation of the 3T3 cells, monocyte chemotactic protein-1 (MCP-1) and α-SMA were used as indicators of cell stimulation alongside assessment of cell morphology. MCP-1 has been shown to be expressed at high levels in certain cancers (Graves et al., 1989, Negus et al., 1995, Lu et al., 2006) and in IPF (Iyonaga et al., 1994) among other diseases. It is produced by a number of different cell types including fibroblasts and attracts monocytes and lymphocytes but not neutrophils to sites of inflammation (Baggiolini et al., 1997).

α-SMA is accepted as a marker of activated fibroblasts or myofibroblasts, the expression of which can be increased by stimulation with TGF-β (Desmoulière et al., 1993). Both α-SMA and MCP-1 were increased in the 3T3 cells in this study following 24h stimulation with TGFβ, while western blot demonstrated increased LOX expression in the supernatant of stimulated 3T3 cells as hypothesised. There was greater activation and LOX expression in cells that were starved of serum prior to stimulation with TGFβ. Serum starvation is frequently used prior to cell stimulation in order to halt cell growth at an optimal confluence and synchronise all cells to enter G0 phase (Woessner et al., 1991, Iyer et al., 1999). It is also necessary to eliminate the contribution of growth factors contained within the serum in order to maximise cell stimulation from TGFβ (Roberts et al., 1988).

However, despite serum starvation an increase in LOX expression following stimulation with TGF β was not detected on immunocytochemistry (ICC). The pattern of immunostaining for LOX on fluorescent ICC of 3T3 cells was mainly nuclear as described previously (Li et al., 1997) with the presence of distinct non-

staining vacuoles within the nuclei. While there was faint cytoplasmic staining, there was no evidence of the presence of LOX within the extracellular space. This is likely due to the culture time being insufficient for the formation of extracellular matrix to which the enzyme adheres (Li et al., 1997). Wakasaki and Ooshima, 1990, using a monoclonal antibody raised against human LOX in mouse hybridoma cells, described the expression of LOX as fine filamentous staining within the cytoplasm of cultured human dermal fibroblasts on ICC (Wakasaki and Ooshima, 1990). Li *et al*, 1997 used a rabbit polyclonal antibody raised against bovine aorta which had been previously shown to be specific for LOX produced by 3T3 cells (Li et al., 1995, Li et al., 1997). Interestingly the pattern of staining shown by Wakasaki and Ooshima was very similar to the staining observed in this study following incubation of live primary human lung fibroblasts with TWB219 (Figure 4-7). It is difficult to speculate on the validity of the findings of Wakasaki and Ooshima, 1990, however, the presence and activity of LOX in the isolated nuclei of smooth muscle cells stained by Li *et al* 1997 was confirmed using the tritium release technique (Li et al., 1997).

Both of the studies discussed above demonstrated expression of LOX within fibroblasts without prior stimulation of the cells (Li et al., 1997, Wakasaki and Ooshima, 1990) and it is therefore likely that LOX is inherently expressed in the 3T3 cells. Interestingly, the expression of LOXL2 by 3T3 cells was also mainly nuclear on ICC with the addition of variable cytoplasmic staining. Furthermore, expression increased upon stimulation with TGFβ. While this has not previously been shown in the literature, Saito et al 1997, showed that stimulation with TGFβ increased levels of LOXL2 messenger RNA in foetal lung fibroblasts (Saito et al., 1997).

Regarding results of immunohistochemical analysis of human and asinine lung tissue, expression was found to be consistent with previous reports that found LOX and LOXL2 staining in fibroblasts, smooth muscle, endothelial and epithelial cells in murine tissue (Wakasaki and Ooshima, 1990) and in the lungs of mice exposed to bleomycin (Barry-Hamilton et al., 2010) respectively. Details regarding the specific localisation of the staining within cells was not reported in the articles referenced

above but this study found LOX staining to be mainly nuclear with LOXL2 pertaining to a more cytoplasmic distribution consistent with findings on ICC.

Barry-Hamilton et al, 2010 found LOXL2 expression in healthy human tissue to be minimal or absent. LOXL2 expression in the lungs of control human and asinine patients in this study was variable and was most likely a reflection of variations in subclinical pathology of the aged lungs. Unfortunately lung tissue from young healthy patients was not available from either species but would obviously have provided more representative control populations.

It was out with the scope of this study to purify LOX from bovine aorta as documented previously (Kagan et al., 1979). As such, models of potential LOX production were investigated. The interference of cell culture media with TWB-219 prevented the use of cell culture models, thus it was necessary to utilise tissue models of LOX production, relying on LOX inhibitors to prove the specificity of TWB-219. As previously stated, BAPN has been used extensively in the literature as a specific inhibitor of LOX activity with an IC^{50} of 10µM (Narayanan et al., 1972, Li et al., 1997, Barry-Hamilton et al., 2010, Palamakumbura and Trackman, 2002), although the pyridazinone-based class of inhibitors appear to be more potent (IC^{50} 0.005-0.07µM) (Tolleshaug et al., 2007). In the human ex vivo tissue homogenate assay with TWB-219, BAPN was found to have an IC^{50} of around 125µM while the IC^{50} of the in-house pyridazinone-based inhibitor AMF-59 was around 30µM (Figure 4-10). These values are understandably higher than those determined by inhibition of purified LOX enzyme in the literature. Indeed other studies also used higher concentrations of BAPN to inhibit LOX activity in cell culture models (Li et al., 1997).

As well as showing that probe activity could be completely inhibited by BAPN and in-house inhibitors (AMF-59 and AMF-60), the potential contribution of MAO to activation of TWB-219 in the human lung tissue model was negated by the fact that clorgyline (a MAO-A inhibitor) and pargyline (a MAO-B inhibitor) did not cause any significant reduction in fluorescent signal (Figure 4-11). Furthermore, BAPN

does not inhibit MAO (Wilmarth and Froines, 1991), thus confirming that MAO does not cleave TWB-219 in the *ex vivo* human tissue model.

Results of immunohistochemistry and western blot have shown that both LOX and LOXL2 are present within the homogenates of aged human and asinine lung. While the expression of other members of the LOXF within the lung tissue has not been investigated, it is certainly possible that they are present at low levels and contribute to the fluorescent signal observed following incubation with TWB-219. Assessing the specificity of TWB-219 to individual members of the LOXF family is a potential goal for future work, which may involve exploiting the use of specific inhibitor based imaging agents.

The reaction of TWB-219 with both porcine DAO and human lung homogenates was slow, taking around 20min for an increase in fluorescent signal to become evident and plateauing at around 60min. Alternative techniques for measuring LOX activity in biological samples are also slow, with Amplex red taking at least 30min (Palamakumbura and Trackman, 2002) and the tritium release method continuing at a linear rate for up to 12h (Layman et al., 1972). The Amplex red assay was investigated as a possible positive control for TWB-219, however results were found to be inconsistent, with a high background fluorescence in various different buffers. This is consistent with the findings of Barry-Hamilton *et al* (Reddy et al., 2012).

The slow reaction time and high background fluorescence of TWB-219 does limit the applicability of the probe with regard to *in vivo* use, however preliminary experiments utilising TWB-219 in combination with FCFM in *ex vivo* tissue models were promising. A significant increase in fluorescent signal over background was detected following the local intrapulmonary delivery of TWB-219 into fibrotic regions of whole ventilating *ex vivo* asinine lung that were subsequently confirmed to express LOX (Figure 4-15). The next stage would be to deliver a LOXF inhibitor such as BAPN to the area of interest prior to probe installation and to compare fluorescent signal increase over background in areas with and without inhibitor.

4.5 Conclusion

The activity-based fluorescent probe, TWB-219 synthesised by the UoEDC, has been evaluated with regard to biological activity and application. The activation of the probe by LOXF was confirmed in human lung homogenate and also in *ex vivo* human lung tissue. Furthermore, probe activation was inhibited in the presence of a specific LOX inhibitor, thus confirming target specificity and validating the hypothesis that TWB-219 can be used to report on LOX activity in biological samples. The probe also showed potential utility in the ventilating size-relevant asinine model of lung fibrogenesis alongside FCFM, although further work is required to demonstrate specificity in this complex biological environment. Unfortunately, despite these positive results, problems with high background fluorescence and slow reaction times meant that TWB-219 was unlikely to fulfil the requirements for eventual *in vivo* use (see Figure 5-3) and thus further probe evaluation was discontinued in favour of the more promising Smartprobes introduced in Chapter 5.

Chapter 5: Evaluation of Optical Imaging Probes for the Detection of MMP-9

5.1 Abstract

The matrix metalloproteinases are fundamental to the fibrogenic process in chronic respiratory diseases and cancer. In this chapter I demonstrate MMP-9 expression in cell culture and *ex vivo* lung tissue models and show the evolution of fluorogenic reporters of enzyme activity, culminating in a lead MMP probe. This probe can detect active MMPs in *ex vivo* aged human lung tissue and is applicable alongside the cutting edge imaging technique fibred confocal fluorescence microscopy. While this ambitious project has encountered many challenges, both historic and ongoing, there remains the potential for the lead MMP probe to inform on dynamic MMP activity *in vivo* and thus be of clinical utility in patients at the bed-side.

5.2 Introduction

As previously discussed, the matrix metalloproteinases (MMPs) are a family of zinc endoproteinases that degrade components of extracellular matrix (ECM) including collagen and elastin. Imbalance between synthesis and degradation of ECM molecules in local lung microenvironment is thought to be central to the pathogenesis of IPF and increased MMP-8 and MMP-9 expression has been demonstrated in BAL from rapidly progressive IPF patients (McKeown et al., 2009). MMP-9 also has several important roles in tumour biology including loss of the ECM tissue architecture and local invasion (Farina and Mackay, 2014).

While the LOX probe TWB-219 was based on the silencing and subsequent activation of fluorescein via alterations in chemical side-chains, the MMP group of probes relied on quenching of signal in their un-activated state either via FRET or the use of a dendrimeric structure (Figures 1-4 and 1-5).

The first reported fluorescent probes for the detection of MMP-9 were based on a peptide FRET system incorporating the fluorescent amino acid tryptophan (Stack and Gray, 1989, Netzel-Arnett et al., 1991). These were closely followed by the more fluorescent and more optimally quenched coumarin based FRET probes (Knight et

al., 1992). Since then several other fluorogenic MMP probes have been documented based on a FRET system, but the majority have limited utility *in vivo* due to poor specificity and stability (Ryu et al., 2011).

In order to synthesise an MMP probe with good selectivity for MMP-9 over other MMPs, collaborators in the UoEDC reviewed substrate sequences previously shown to be cleaved by MMP-9. The active site amino-acid sequence of the 3-branched fluorescein dendrimer TWB-140 had been previously reported to have specificity for MMP-2 and -9 (Prudova et al., 2010) (Figure 5-1). While the sequence used in the fluorescein/methyl red linear FRET, SVC-16, was a combination of sequences from previously identified peptides with MMP-9 selectivity (Figure 5-1 and 5-2).

In total, 48 MMP probes were synthesised in-house by UoEDC. Each of these was evaluated using a range of biological assays, the outcome of which influenced further chemical modifications, finally leading to the selection of a lead probe sequence and structure. It is out-with the scope of this chapter to introduce all of the probes, instead a select few that demonstrate the biological and chemical evolution of the project will be discussed (Figure 5-2).

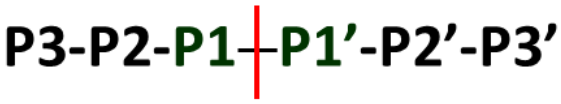

Amino acid	MMP selectivity								TWB-140	SVC-16
	2/9	1/9	2/9	2/9/13	13>7	2/9	13> 1/8	1/2/3 /7/9		
P3	P	P	P	P	P	P	P	P	P	P
P2	K	Cha	L	L	L	L	Cha	L	K	F
P1	G	G	G	G	S	G	G	G	G	G
P1'	L	Cys(Me)	L	V	L	M	Nva	L	L	M
P2'	K	H	A	R	T	W	H	W	K	K
P3'	G	A	G	G	M	S	A	r	G	A

Figure 5-1: Sequence selection. Table showing how the active site amino acid sequences for the two first generation MMP probes was selected from commercial MMP probes and sequences previously documented in the literature (Ryu et al., 2011, Jiang et al., 2004, Prudova et al., 2010, Nagase and Fields, 1996, Overall and Lopez-Otin, 2002). Data included in this table were provided by Dr Sunay Chankeshwara.

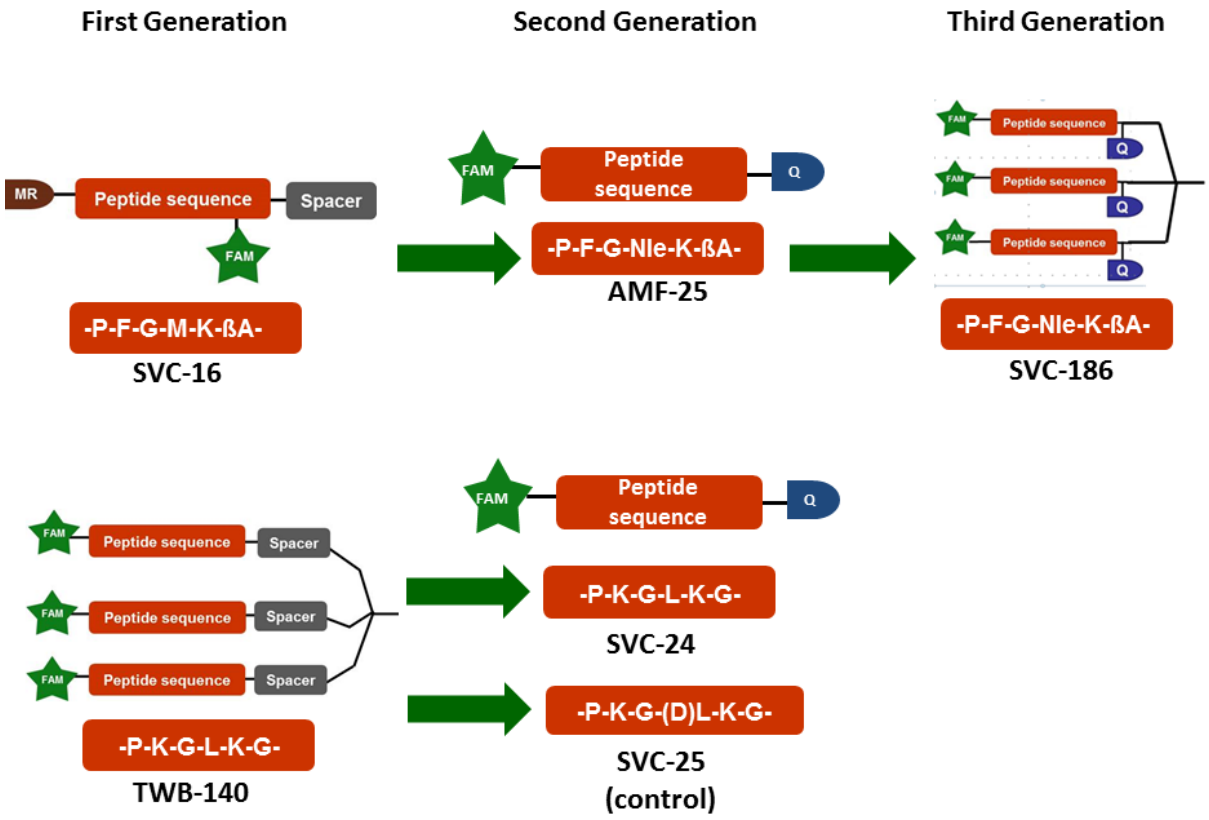

Figure 5-2: Probe evolution and structure. Schematic diagrams representing the structural evolution of the MMP probes included in this thesis. Probe sequences are shown in the red boxes underneath the schematics.

The over-arching hypothesis of this work was that MMP-9 activity in biological samples could be sensitively and specifically measured using in-house fluorogenic reporter peptides, supporting the potential for *in vivo* application.

I will thus begin the chapter by reviewing the evaluation of a number of cell culture models and *ex vivo* lung tissue with regards to the expression of MMP-9, utilising western blot, immunocytochemistry/immunohistochemistry, ELISA and zymography. I will then show the biological assessment of a commercially available MMP assay that was initially purchased as a positive control for probe validation assays.

I will summarise the results of relevant biological assays on selected probes, set out according to a pre-defined target product profile (Figure 5-3). I will firstly introduce the use of recombinant MMP-9 to assess background fluorescence and signal amplification or signal to noise, in conjunction with MMP inhibitors. I will then show the assessment of probe selectivity utilising a panel of recombinant MMP enzymes, followed by the evaluation of probes in *ex vivo* tissue (ovine and human) and assessment of probe stability following incubation with off target enzymes elastase and plasmin. Finally, I will use the results of experiments carried out lead probe to demonstrate the calculation of relevant enzyme kinetics as well as utility in human *ex vivo* tissue in conjunction with fibred confocal fluorescence microscopy (FCFM).

The challenges faced by this large multi-disciplinary project were great and centred around the previously discussed limitations of fluorogenic substrate probes *in vivo.* Furthermore, FCFM is a relatively novel optical molecular imaging modality that, while requiring further validation in the scientific literature, also challenges current conceptions and protocols with regards to the monitoring of disease processes.

Target Product Profile

- **Soluble in PBS or saline**
- **Stable**
- **Good signal to noise**
- **Target specificity as demonstrated by inhibition of signal**
- **Stable against off target enzymes**
- **Utility in relevant *ex vivo* tissue model**
- **Utility in *ex vivo* human tissue**
- **Utility in conjunction with FCFM**
- **Non-toxic in pre-clinical models**

Figure 5-3: Target product profile (TPP). Summary of the main requirements or TPP for the selection of a lead MMP probe following biological evaluation.

5.3 Results

5.3.1 Optimising a cell culture model of MMP-9 production

In order to establish a cell culture model to assist in preliminary probe evaluation, MMP-9 expression in 3T3 fibroblasts, RAW macrophages and human monocyte derived macrophages (MDM) was investigated. Optimisation of culture conditions for 3T3 cells is described in chapter 4. While ICC did not show an obvious difference in MMP-9 expression between control and stimulated 3T3 cells, an increase in total MMP-9 following a 6h incubation with TGFβ and active MMP-9 following 24h incubation with TGFβ was demonstrated by ELISA and zymography respectively (Figure 5-4).

With regard to RAW cells, it was determined via cytometric bead array (CBA) that stimulation with lipopolysaccharide (LPS) was necessary in order to increase tumour necrosis factor- α (TNF-α) and interleukin-6 (IL-6) production. However, it was not necessary to starve cells prior to stimulation and similar results were obtained regardless of LPS concentration and length of exposure (data not shown). As with the 3T3 cells, there was no discernible difference in MMP-9 expression between control and stimulated RAW cells on ICC. However, a significant increase in total MMP-9 was demonstrated in cells stimulated with LPS for 24h compared to control on ELISA (Figure 5-5). Unfortunately the concentration of MMP-9 produced was not sufficient for bands of active enzyme to be detected on zymography.

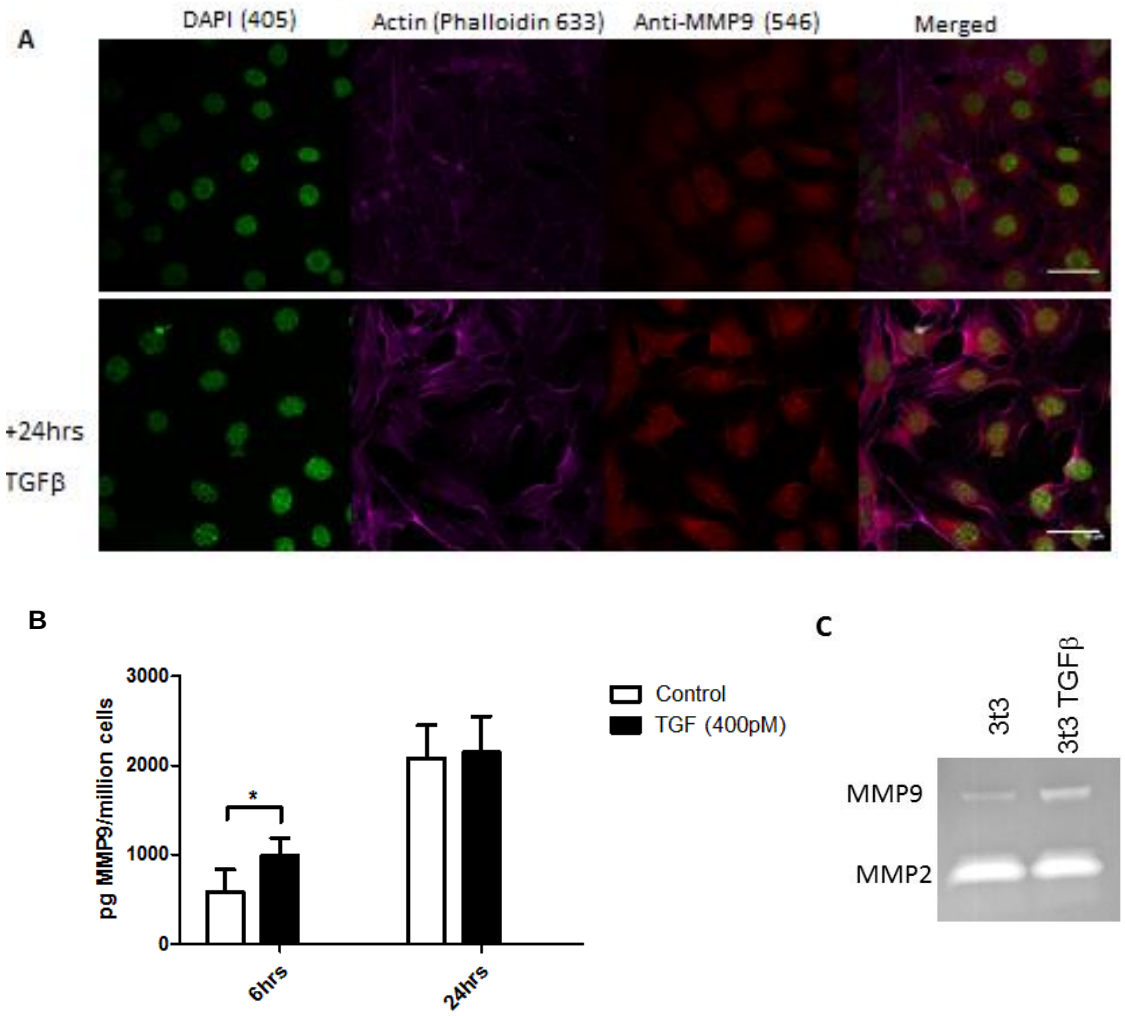

Figure 5-34: MMP9 expression in murine NIH 3T3 fibroblasts.
Immunocytochemistry (A) shows expression of MMP9 in unstimulated 3T3 cells and following stimulation with 400pM TGFβ. DAPI stains cells nuclei and phalloidin stains F-actin filaments, representative images of n=4, bar= 50µm. ELISA (B) showed that there was no increase in total MMP9 in the supernatant of 3T3 cells stimulated with TGFβ for 24h, but a significant increase was seen in cells stimulated for 6 h (error bars represent SD, n=4, *p=0.04, two tailed t test). (C) Active 82kDa MMP9 was increased in the supernatant of cells stimulated with 400pM TGFβ for 24h as shown by zymography (representative of n=3).

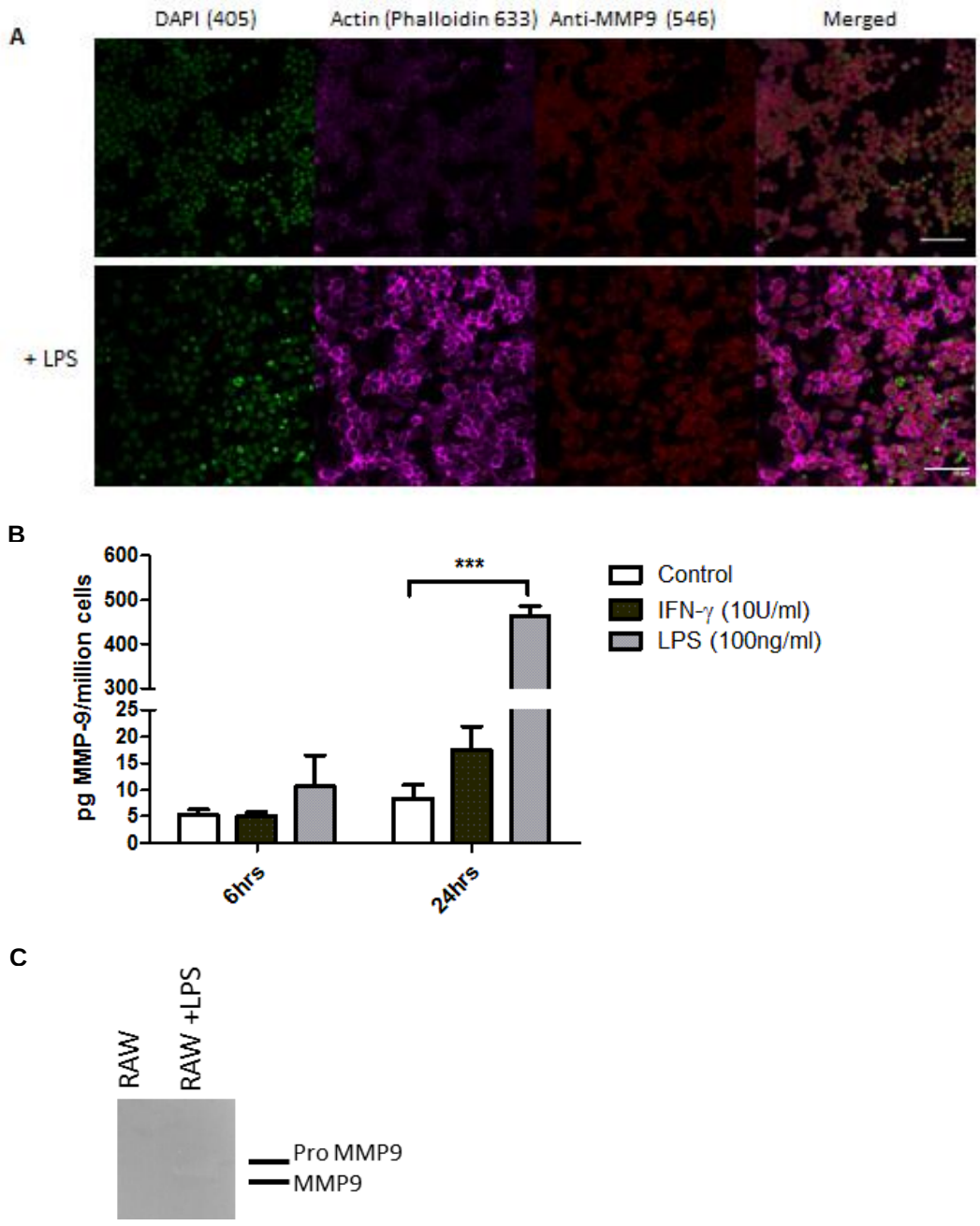
A
DAPI (405)
Actin (Phalloidin 633)
Anti-MMP9 (546)
Merged
+ LPS
B
pg MMP-9/million cells
600
500
400
300
25
20
15
10
5
0
***
6hrs
24hrs
Control
IFN-γ (10U/ml)
LPS (100ng/ml)
C
RAW
RAW +LPS
Pro MMP9
MMP9

Figure 5-5: MMP-9 expression in murine RAW 264.7 macrophages. `. Immunocytochemistry (A) shows expression of MMP-9 in unstimulated RAW 264.7 cells and following 24h stimulation with 100ng/ml LPS (images representative of n=2). DAPI stains cell nuclei and phalloidin stains F-actin filaments. ELISA showed that there was no increase in total MMP-9 in the supernatant of RAW cells (B) stimulated with either IFN-g or LPS for 6h, but a significant increase was seen in cells stimulated with LPS for 24h (error bars represent SD, n=4, ***$p<0.0001$, two tailed t test). (C) Concentration of active MMP-9 in RAW cell supernatant was not sufficient to be detected on zymography (representative of n=2).

To investigate optimal culture of MDM, cells were cultured for 5-7d prior to stimulation with varying concentrations of LPS in different starvation conditions for varying lengths of time. Cell morphology was monitored closely to assess viability and reactivity. Starvation of cells during stimulation with LPS was not found to affect the total MMP-9 in cell supernatant. Similarly no difference was seen with varying concentrations of LPS either on ELISA or ICC (data not shown). While there was a trend towards increased MMP-9 in the supernatant of cells after 24h compared to 6h (both stimulated and control), this difference was not significant (Figure 5-6) and there was no difference between 24 and 48h stimulation. Zymography confirmed the presence of active 82kDa MMP-9 in the supernatant of both LPS stimulated and control MDMs.

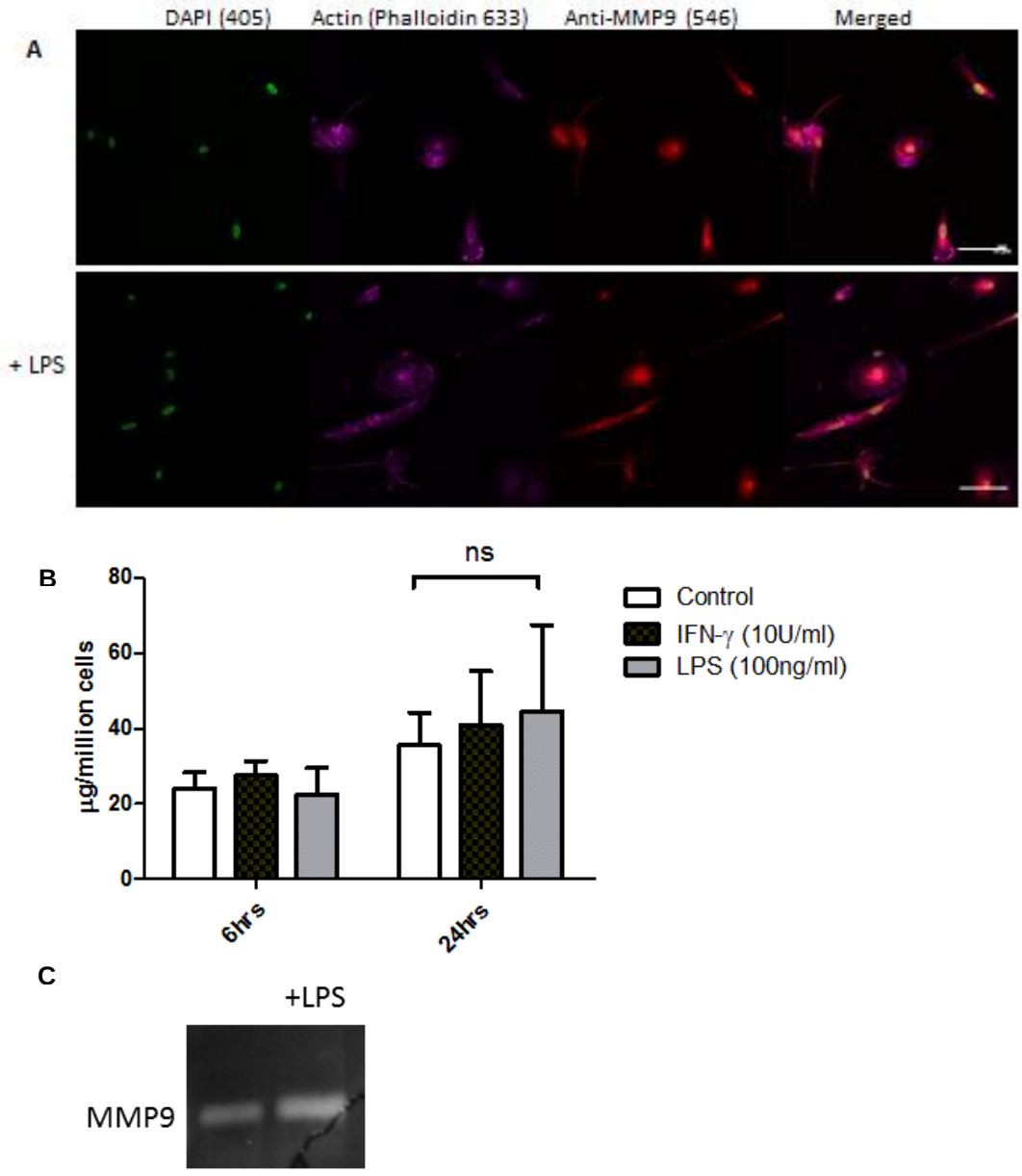

Figure 5-6: MMP-9 expression in human monocyte derived macrophages (MDM). (A) ICC showed expression of MMP-9 in MDM cells with no difference in expression following 24h stimulation with 100ng/ml LPS (representative images of n=2). DAPI stains cell nuclei; phalloidin stains F-actin filaments. (B) ELISA showed that there was no significant difference in total MMP-9 in the HMDM supernatant with either 6 or 24h stimulation (error bars represent SD, n=3, two tailed t test). (C) Zymography showed increased expression of 82kDa MMP-9 in the supernatant of MDM cells stimulated with 100ng/ml LPS for 24h (n=1).

5.3.2 Developing *ex vivo* tissue models of MMP9 production

Having investigated cell culture models of MMP-9 production, the next step was to establish an *ex vivo* tissue model. During early probe evaluation, the donkey model (See Chapters 3 and 4) was readily available and a trend towards increased MMP-9 expression was demonstrated in fibrotic asinine lung tissue compared to age matched controls on western blot, although there was substantial variability between samples (Figure 5-7). Immunohistochemistry was also performed on tissue sections from fibrotic and control donkeys, including a negative control and isotype control for each run of slides (Figure 5-8). MMP-9 was expressed in both control and fibrotic asinine tissue. On zymography, the most prominent bands were around 92kDa, consistent with pro-MMP-9. Again there was no significant difference between control and fibrotic samples.

As the project progressed it became difficult to acquire further donkey tissue due to staffing issues at The Donkey Sanctuary. As such, it was necessary to investigate other potential *ex vivo* tissue models that were more accessible. Ovine lung tissue from sheep with pulmonary adenocarcinoma (OPA) was therefore evaluated using immunohistochemistry, western blot and zymography.

OPA is a spontaneous neoplastic disease induced by the infection of alveolar epithelial cells with Jaagsiekte sheep retrovirus leading to neoplastic transformation (Scott et al., 2013). OPA is endemic in the UK and has been proposed as a model for human bronchocarcinoma (Palmarini and Fan, 2001). As for the donkey, MMP-9 expression in OPA tissue was substantial but variable (Figure 5-9). The pros and cons of each large animal *ex vivo* model are summarised in Figure 5-10.

Finally, the presence of MMP-9 in aged human lung tissue either from grossly normal areas of lung lobectomies (control) or biopsies of interstitial lung disease (fibrotic) was confirmed using the same techniques as above (Figures 5-11 to 5-13). Once again sample variability was evident within each group and while there were trends towards increased expression in fibrotic lung, differences were not significant.

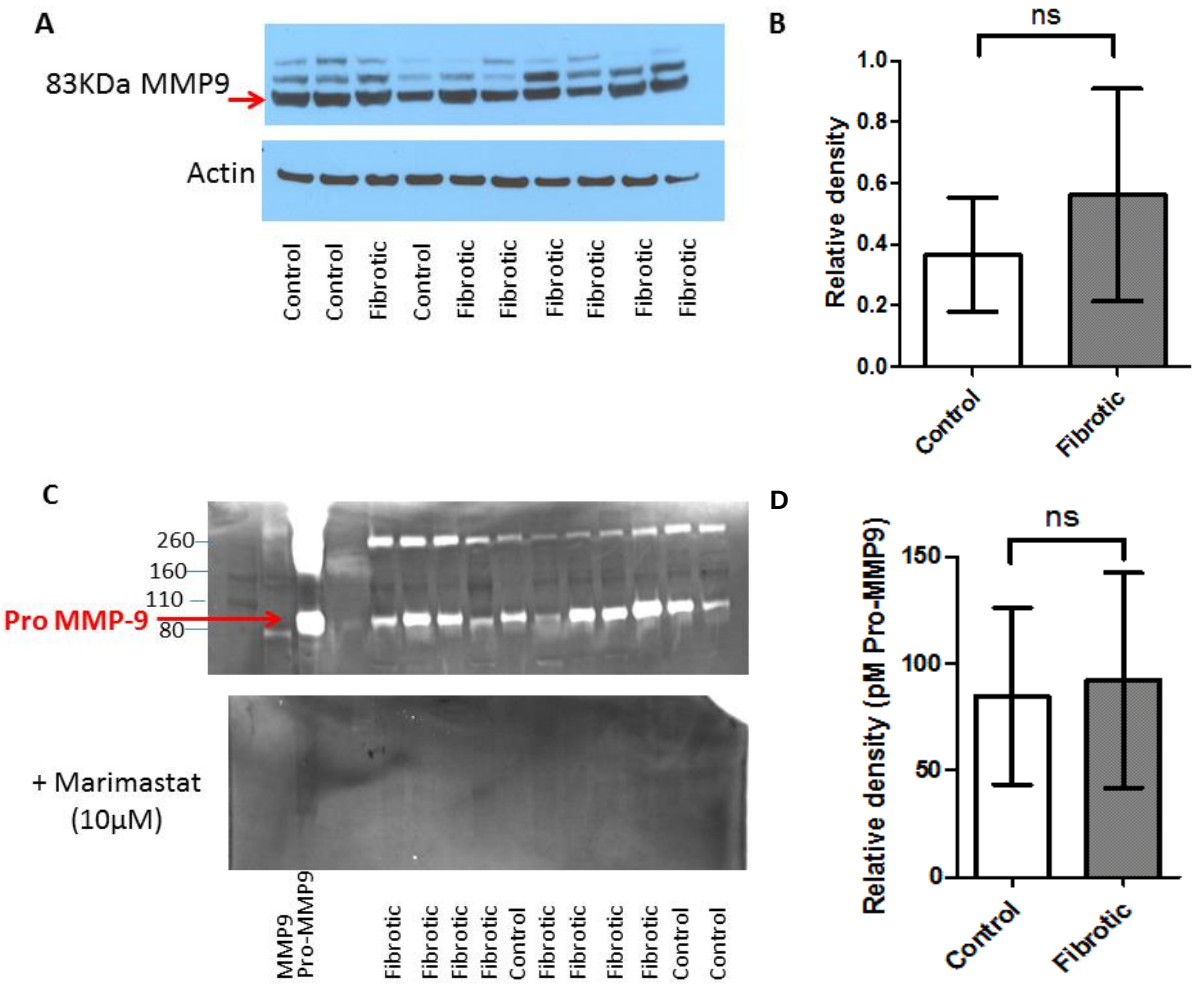

Figure 5-7: MMP-9 is expressed in asinine lung tissue. (A) Western blot on homogenate from control and fibrotic asinine lung was analysed using relative density of bands (B). (C) Zymography shows that expression of pro-MMP-9 is variable within both fibrotic and control tissue as confirmed by analysis of relative density (D). Marimastat was used as a control as it inhibits MMP-9 activity. Error bars represent SD, representative of n=3.

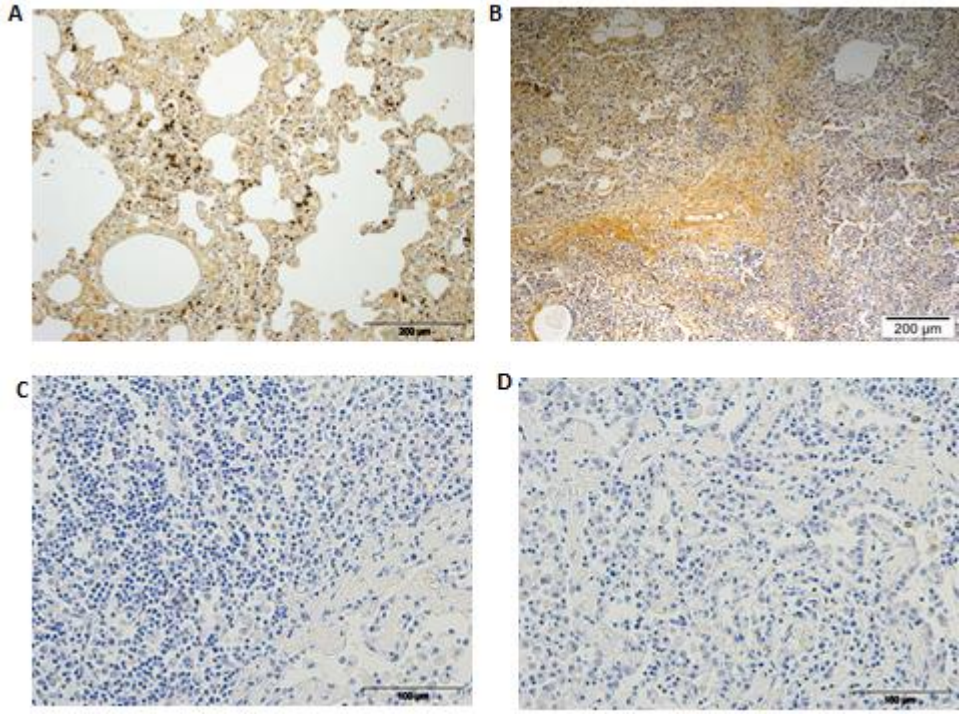

Figure 5-8: Immunohistochemical analysis of MMP-9 expression in asinine lung tissue. Immunohistochemistry for MMP-9 showed that MMP-9 was expressed in lung tissue sections from both control (A) and APF (B) donkeys. Negative controls without primary antibody (C) and GFP controls (D) were also performed. Representative images of a minimum of n=3.

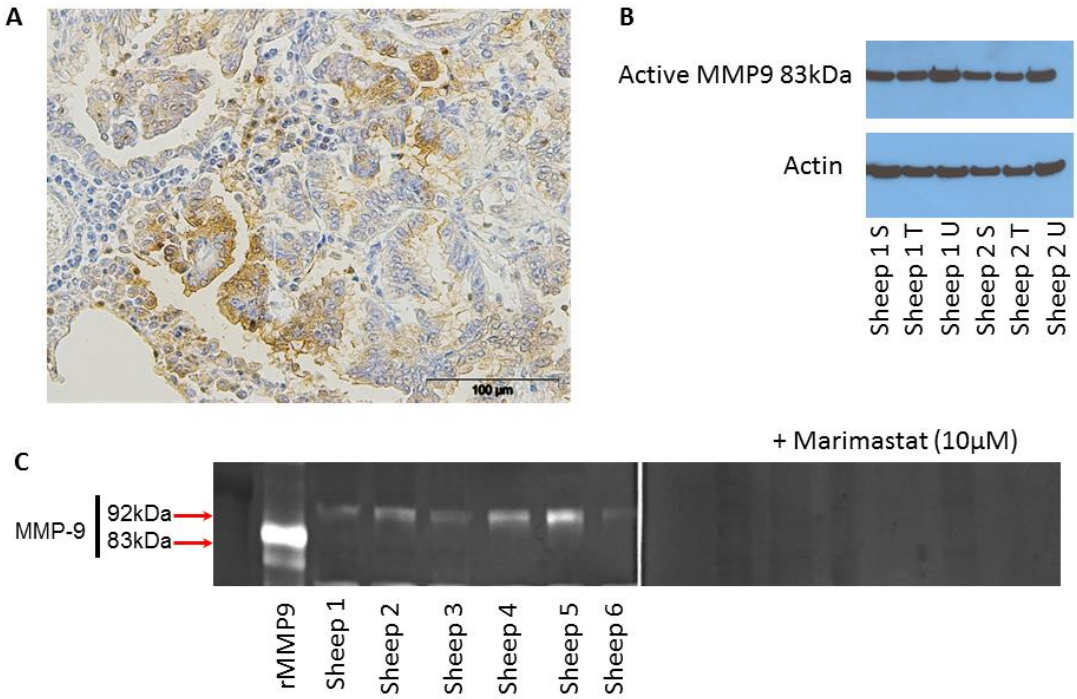

Figure 5-9: MMP-9 is expressed in lung tissue from sheep with ovine pulmonary adenocarcinoma (OPA): Immunohistochemistry (A) and western blot (B) demonstrate expression of MMP9 in OPA lung tissue, while zymography (C) confirms that pro-MMP-9 is present in the transitional lung tissue homogenate used in (B) as well as in 4 other transitional tissue samples from different sheep. Renaturing the zymography gel in the presence of marimastat inhibits MMP9 activity. n ≥3, S= solid tumour, T= transitional tissue, U= grossly unaffected tissue.

Factor	Donkey	Sheep
Spontaneous disease	✓	✓
Lungs fresh	X	✓
Readily available	X	✓
Expression of MMP-9	✓	✓

Figure 5-10: Table summarising the advantages and disadvantages of *ex vivo* donkey (APF) and sheep (OPA) tissue.

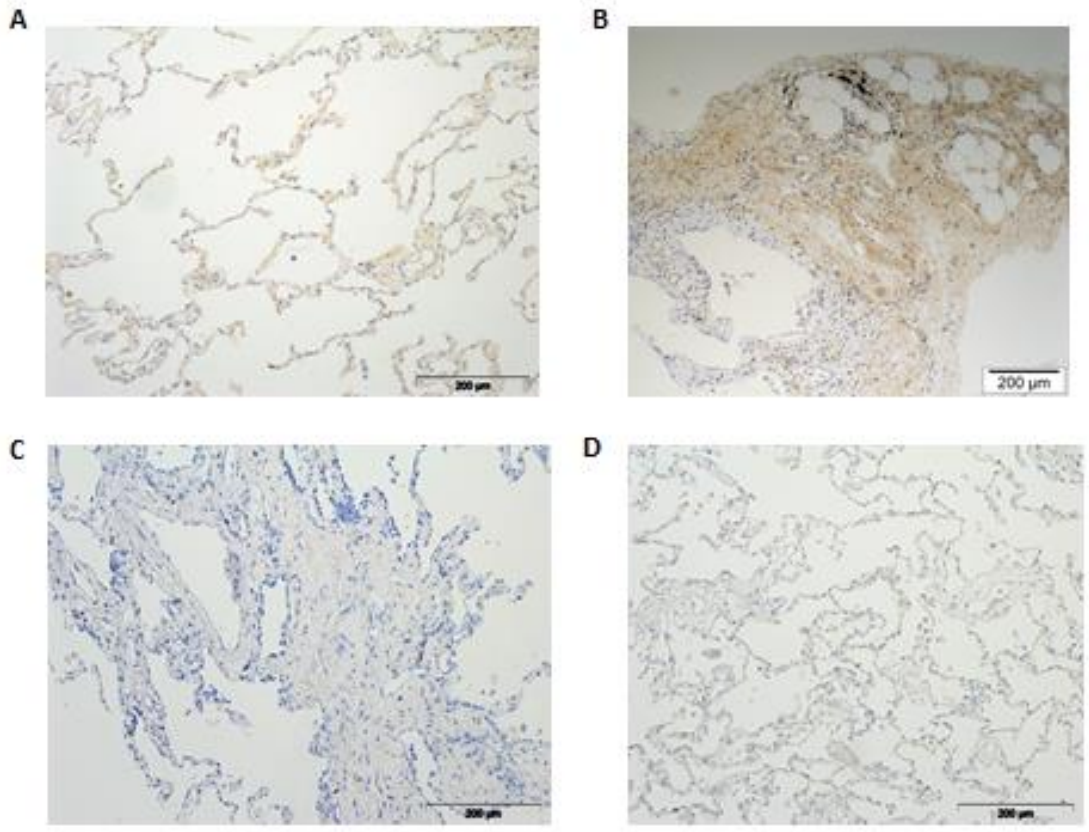

Figure 5-11: MMP-9 is expressed in aged human lung tissue.
Immunohistochemistry demonstrated increased expression of MMP-9 in fibrotic (B) compared to control (A) human lung tissue from aged patients. Negative controls without primary antibody (C) and GFP controls (D) were also performed. Data representative of a minimum of n=3.

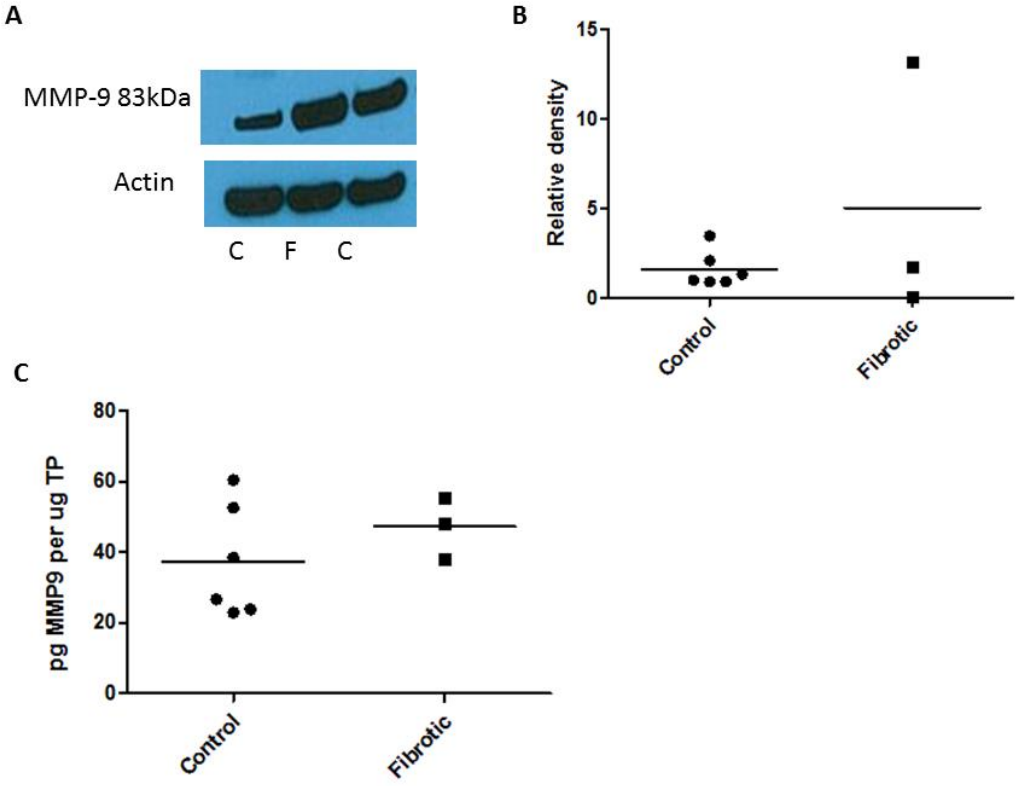

Figure 5-12: Total MMP-9 in aged human lung tissue homogenate. (A, B) Western blot confirmed the expression of MMP-9 in human tissue homogenate, with no significant difference between control and fibrotic samples on analysis of relative density (B). Mann Whitney, n=3. (C) ELISA confirmed there was no difference in MMP-9 expression between control and fibrotic samples (two tailed t test).

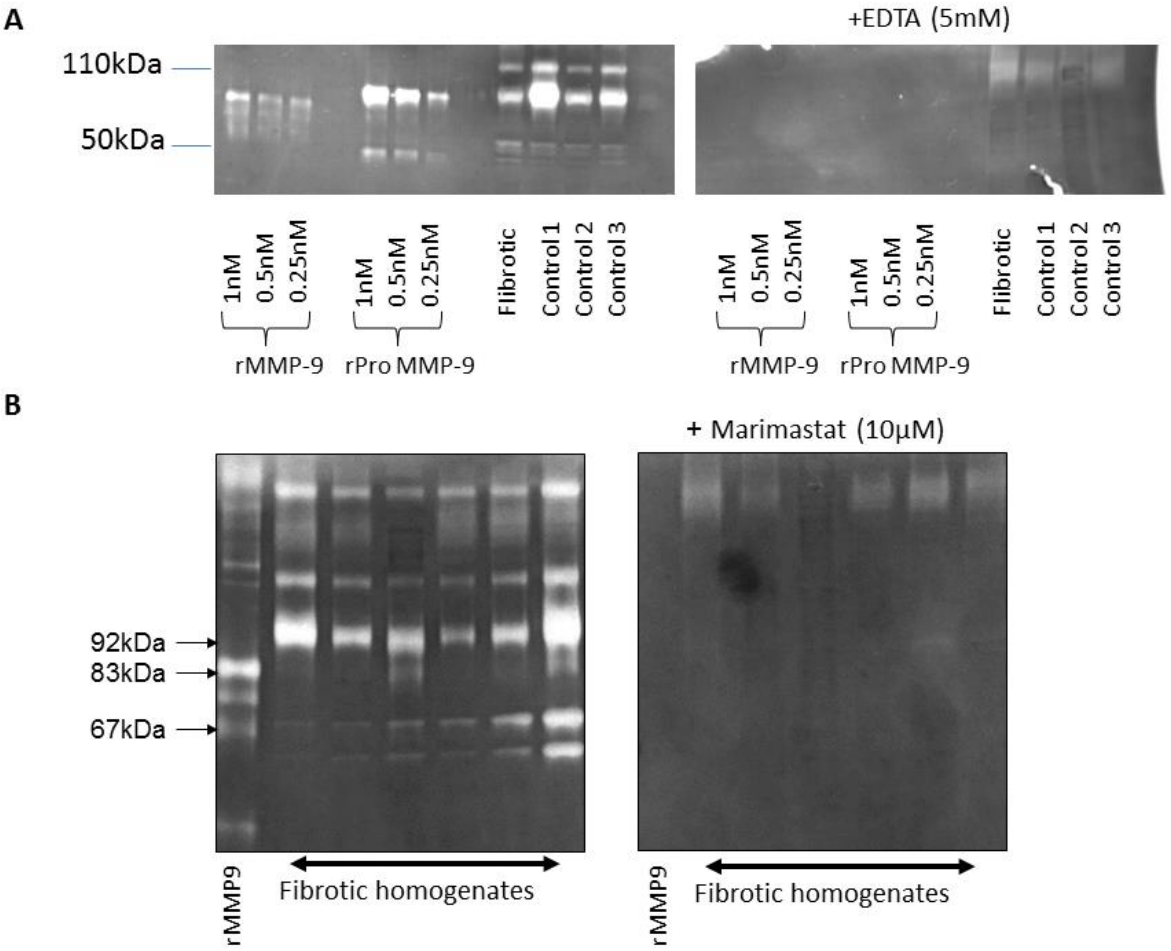

Figure 5-13: Active MMP-9 expression in human lung homogenate. (A) Zymography gel showing bands from various concentrations of recombinant MMP-9 and pro-MMP-9 as well as bands from human lung homogenate corresponding to pro-MMP9. The addition of EDTA at the renaturing stage collates zinc and prevents activation of MMP-9. (B) Zymography showing expression of pro-MMP-9 and active MMP-9 (fainter bands) in fibrotic human lung tissue homogenates. The addition of marimastat at the renaturing stage also causes inhibition of enzyme activity.

5.3.3 Commercial MMP-9 activity assay

Prior to beginning the biological evaluation of the in-house MMP probes, it was decided to investigate the potential for a positive control probe to feature in validation experiments. SensoLyte® is a commercially available assay for the detection of MMP-9 in biological samples that utilises an activatable fluorescent peptide (Figure 5-14). The commercial probe was tested against recombinant MMP-9 and purified leucocyte elastase as well as cell supernatants and lysates including those collected from human blood neutrophils which are known to express MMP-9 (Kjeldsen et al., 1994).

While the signal generated by probe cleavage in the presence of recombinant MMP-9 was completely inhibited by pan-MMP inhibitor marimastat, there was very little inhibition of fluorescent signal following pre-incubation of the neutrophil samples with the same inhibitor. Instead a dramatic inhibition of signal was observed in samples that had been pre-incubated with the neutrophil elastase inhibitor sivelestat, suggesting that it was in fact elastase rather than MMP-9 that was cleaving the commercial probe in the neutrophil samples. While this sensitivity to elastase precluded the use of the SensoLyte assay as a control for in-house probes, it did help to reinforce the importance of robust probe screening against biologically relevant off-target enzymes.

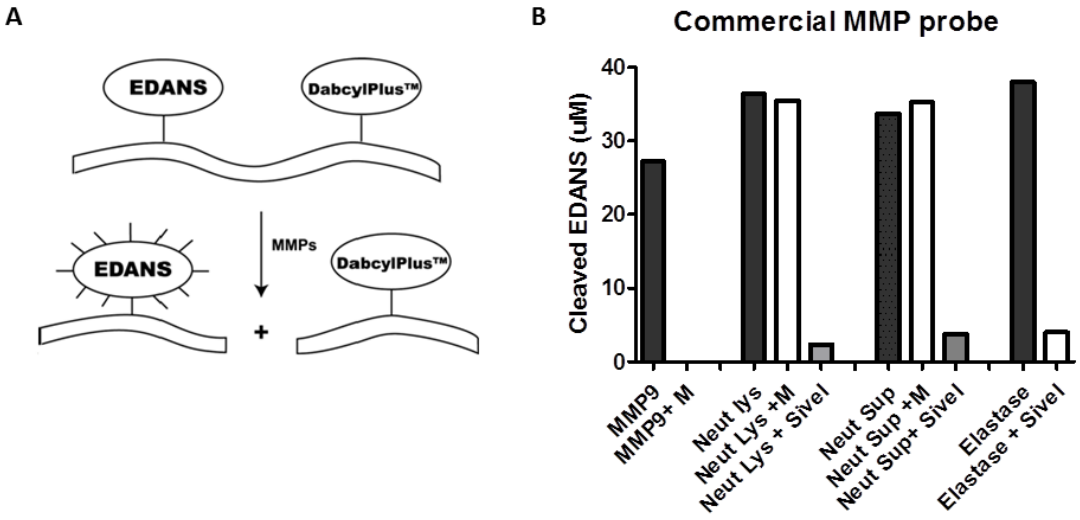

Figure 5-14: Commercial MMP probe is sensitive to neutrophil elastase. Schematic diagram (A) shows the cleavage of the SensoLyte® MMP-9 substrate to give fluorescent 5-((2-Aminoethyl)amino)naphthalene-1-sulfonic acid (EDANS). The bar chart (B) shows the cleavage of the SensoLyte® MMP-9 substrate by neutrophil lysate, neutrophil supernatant and purified leucocyte elastase (2.5µg/ml). Note that EDANS signal is not inhibited by pre-incubation of the neutrophil lysate/supernatant with marimastat (20µM) but is inhibited by sivelestat (100µM), indicating that it is neutrophil elastase rather than MMPs that is causing cleavage of the MMP9 substrate. (Bars represent mean of two readings, representative of n=3). M= marimastat, Lys= lysate, Sivel= sivelestat.

5.3.4 Preliminary evaluation of in-house MMP probes

The initial probe, TWB-140, was a three branched dendrimer comprising three fluorescein (FAM) molecules (Figures 5-2 and 5-15). It was quickly observed that the dendrimer had a high background fluorescence (Figure 5-16), therefore a linear FRET probe (SVC-016) that incorporated the quencher methyl-red, was also synthesised based on a different cleavage sequence (Figures 5-1, 5-2 and 5-17). A probe concentration of 10μM was chosen as this was consistent with optimal performance in previously published probes of similar structure (Avlonitis et al., 2013) and was shown to generate high signal to noise in the presence of recombinant MMP-9 (Figure 5-18A). In order to eliminate differences in background fluorescence when comparing signal to noise between these probes, increase in fluorescence was displayed as percentage of background fluorescence. This demonstrated that there was greater signal amplification from SVC-016 in the presence of recombinant MMP-9 than there was from TWB-140 (Figure 5-18).

The next step was to demonstrate that the observed increase in fluorescence was due to probe cleavage by MMP-9. This involved pre-incubating recombinant enzyme with an MMP-9 inhibitor prior to the addition of probe. Three different MMP-9 inhibitors were used: marimastat, a pan MMP inhibitor, Inhibitor I, an MMP-9 specific inhibitor and AZD 1236, a MMP-9 and MMP-12 inhibitor (Figure 5-19). It was demonstrated that all three inhibitors could inhibit probe signal with recombinant enzyme in a concentration dependent manner. As well as proving signal specificity via the use of inhibitors, it was also important to demonstrate probe cleavage via matrix-assisted laser desorption/ionization (MALDI) analysis (Figure 5-20).

As seen in Figures 5-7, 5-9 and 5-13, marimastat had already proved to be an excellent inhibitor of MMP-9 activity in donkey, ovine and human lung tissue respectively. In order to assess the performance of AZD1236 in human lung tissue, zymography gels were incubated in varying concentrations of inhibitor and complete inhibition of MMP-9 activity was achieved at 4.6uM AZD1236 (Figure 5-21).

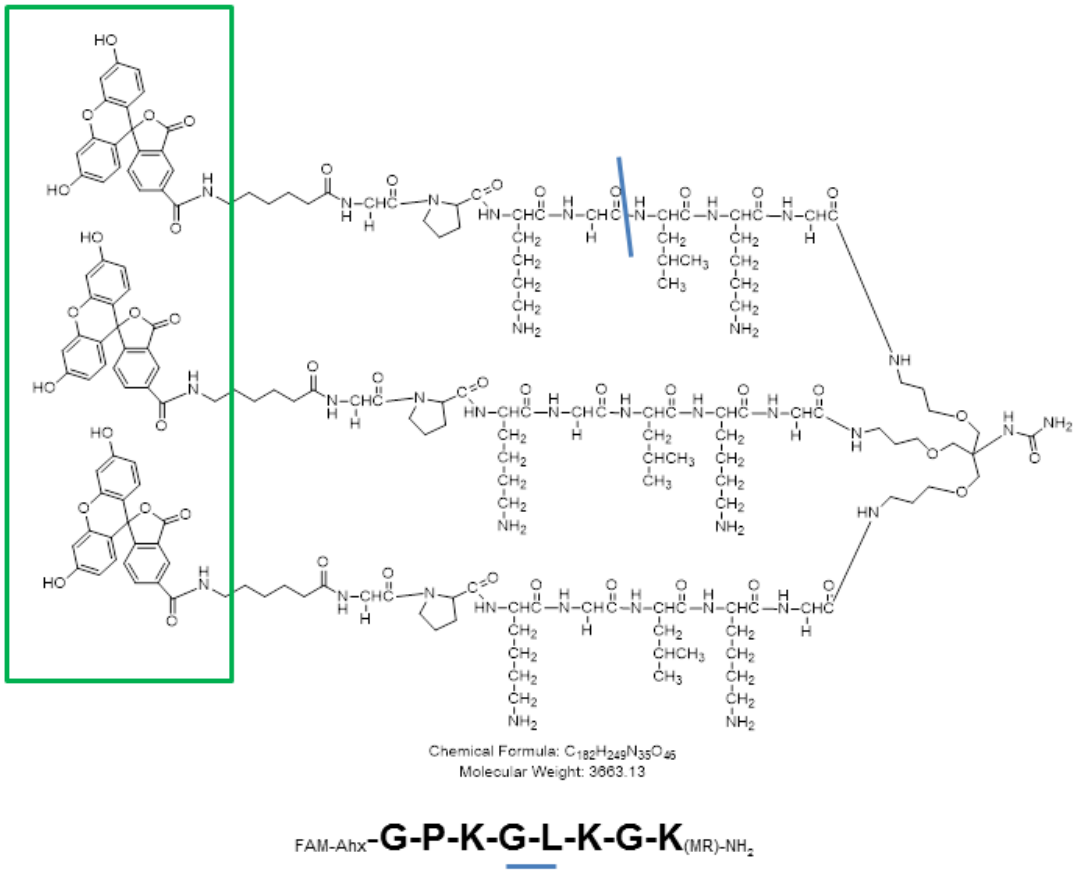

Figure 5-15: Chemical structure of first generation dendrimer MMP-9 probe, TWB-140. The amino acid sequence at the cleavage site is written below the chemical structure. Blue lines indicate the site of specific cleavage by MMP-9, while the green box highlights the three fluorescein molecules.

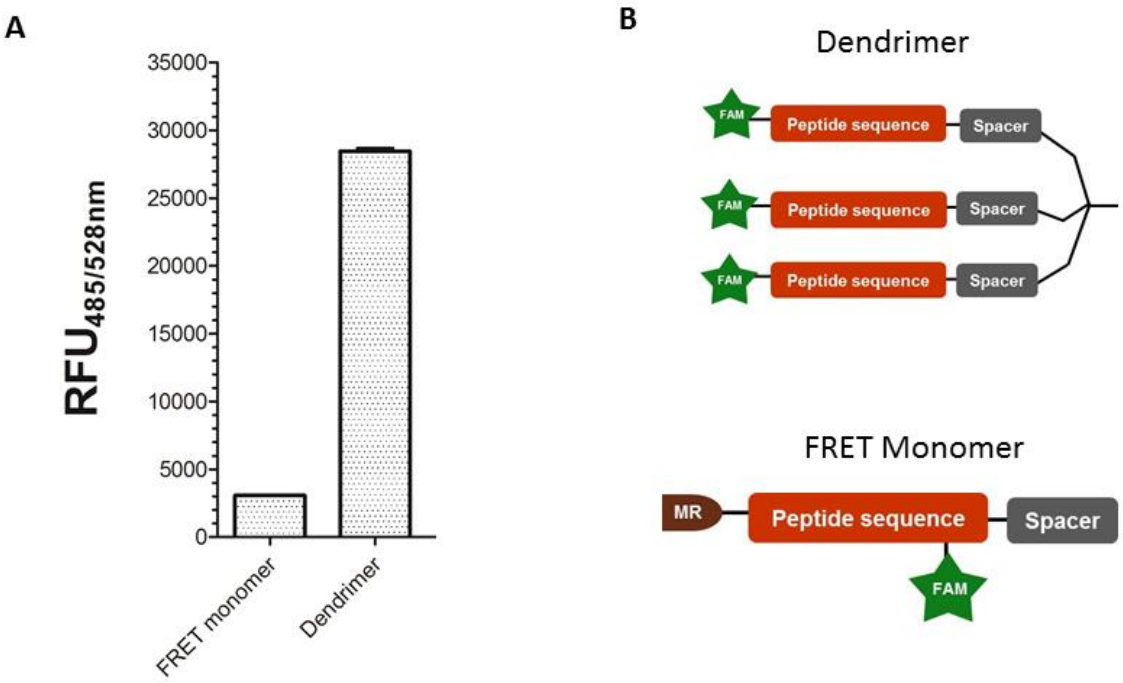

Figure 5-16: The first generation FRET monomer is more effectively quenched than TWB-140 (dendrimer). Bar chart (A) shows that the background fluorescence of TWB-140 is approximately six times that of the FRET monomer SVC-016 (probes at 10µM, representative of n=4). Schematic diagrams (B) show the basic structures of the two probes. Schematic images were provided by Dr Sunay Chankeshwara and Dr Alicia Megia-Fernandez.

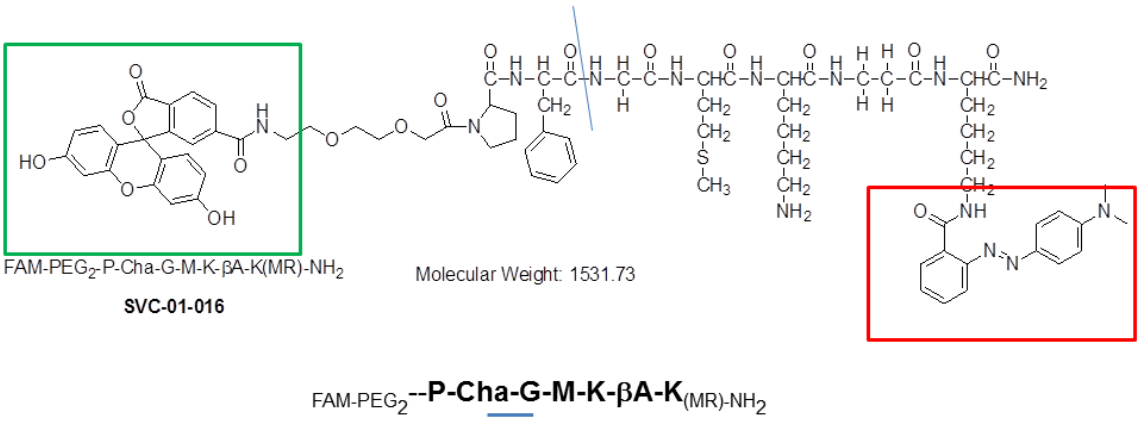

Figure 5-17: Chemical structure of first generation FRET monomer MMP-9 probe, SVC-016. The amino acid sequence at the cleavage site is written below the chemical structure. Blue lines indicate the site of specific cleavage by MMP-9, the green box highlights the fluorescein molecule and the red box highlights the methyl red.

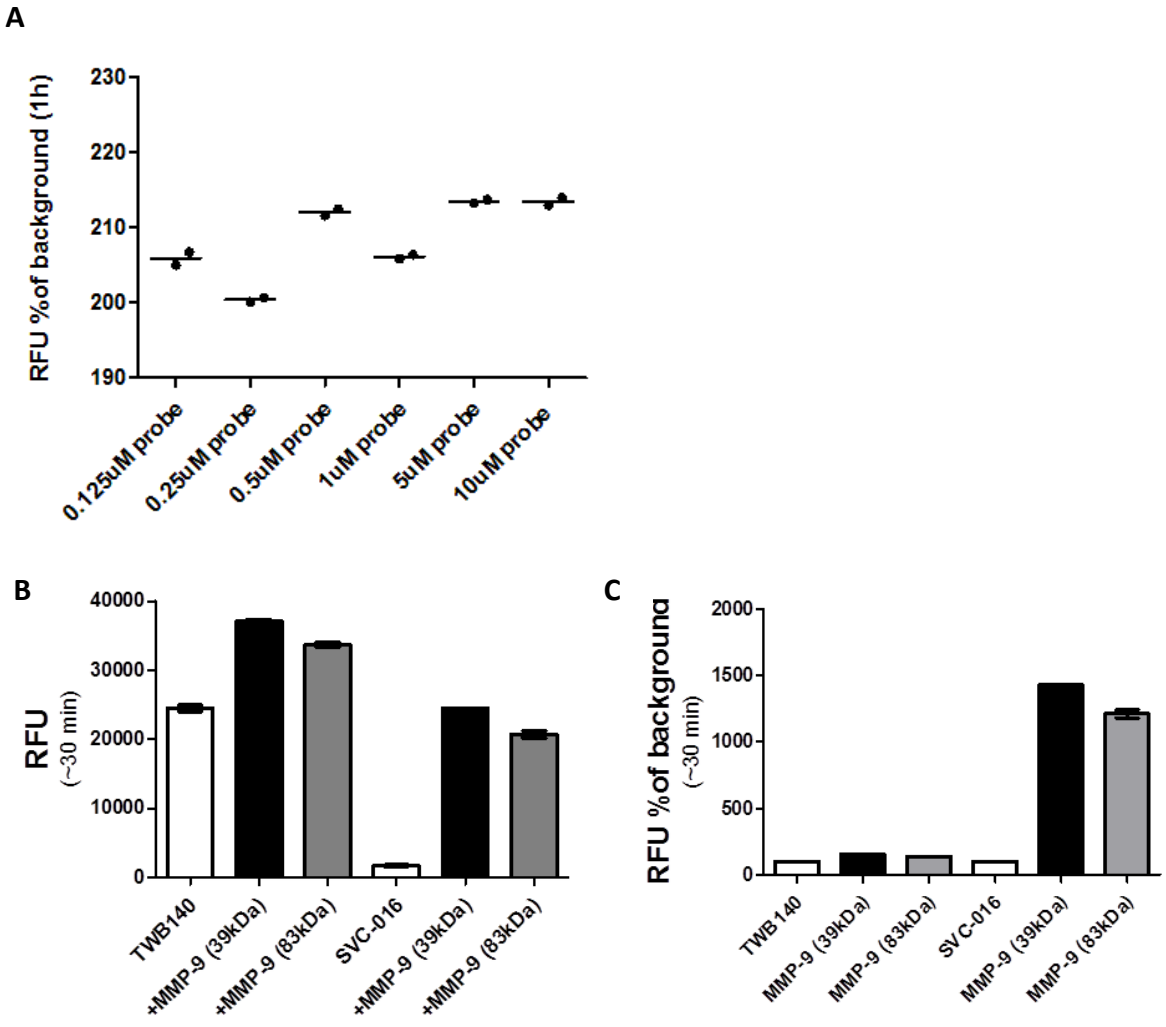

Figure 5-18: Standardising plate reader results to relevant background fluorescence allows comparison between probes. (A): A probe concentration of 10uM was chosen following the determination of signal to noise generated from incubating different concentrations of TWB-140 with 30nM recombinant MMP-9 (39kDa), n=1. Graph (B) shows the relative RFU of 10µM TWB-140 and 10µM SVC-016 following 30 min incubation with recombinant MMP-9 enzymes (30nM). Standardising RFU to background fluorescence for each probe (C) shows that SVC-016 has a much greater signal to noise. Experiment performed in duplicate, error bars represent SD, representative of n=3.

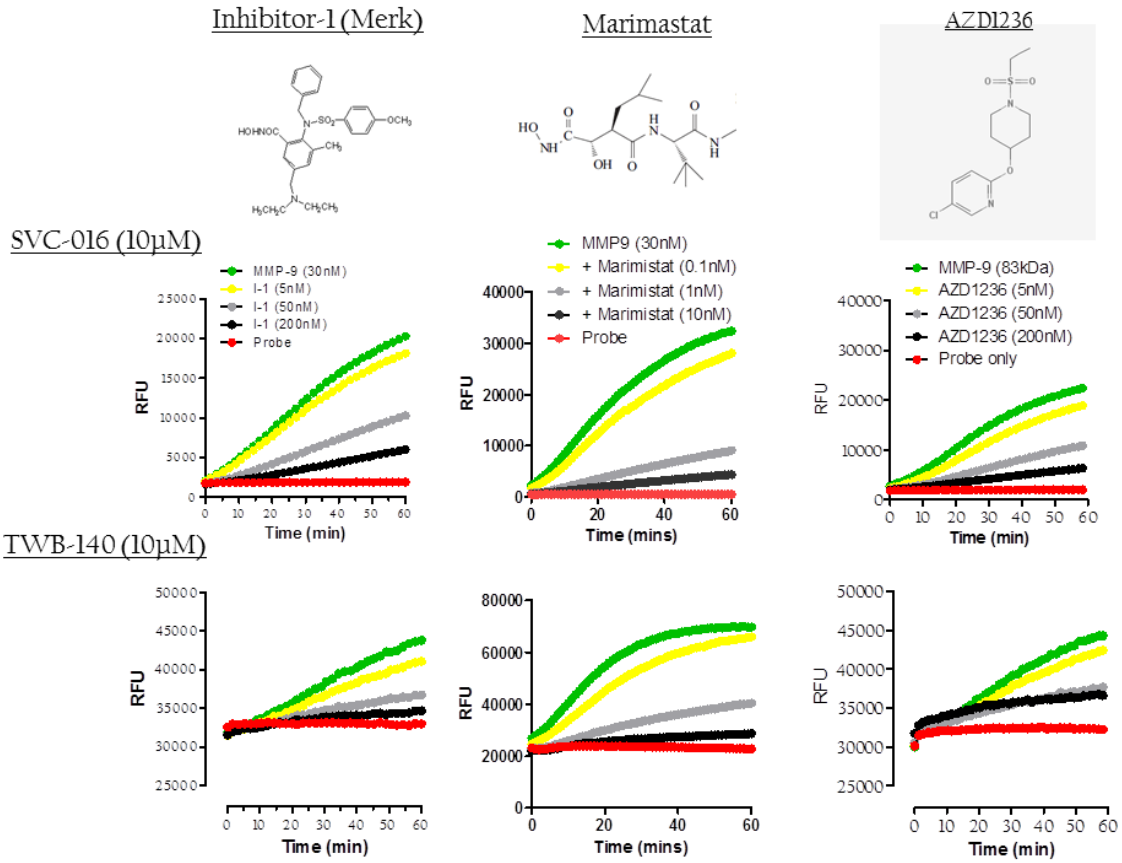

Figure 5-19: First generation MMP-9 probes are inhibited in a concentration dependent manner by specific inhibitors. Kinetic plots of relative probe fluorescence in the presence of recombinant MMP-9 following pre-incubation with increasing concentrations of Inhibitor-I (a MMP-9 specific inhibitor at low concentrations), marimastat (pan MMP inhibitor) and AZD1236 (MMP-9 and MMP-12 inhibitor). Graphs represent mean fluorescence of three replicates.

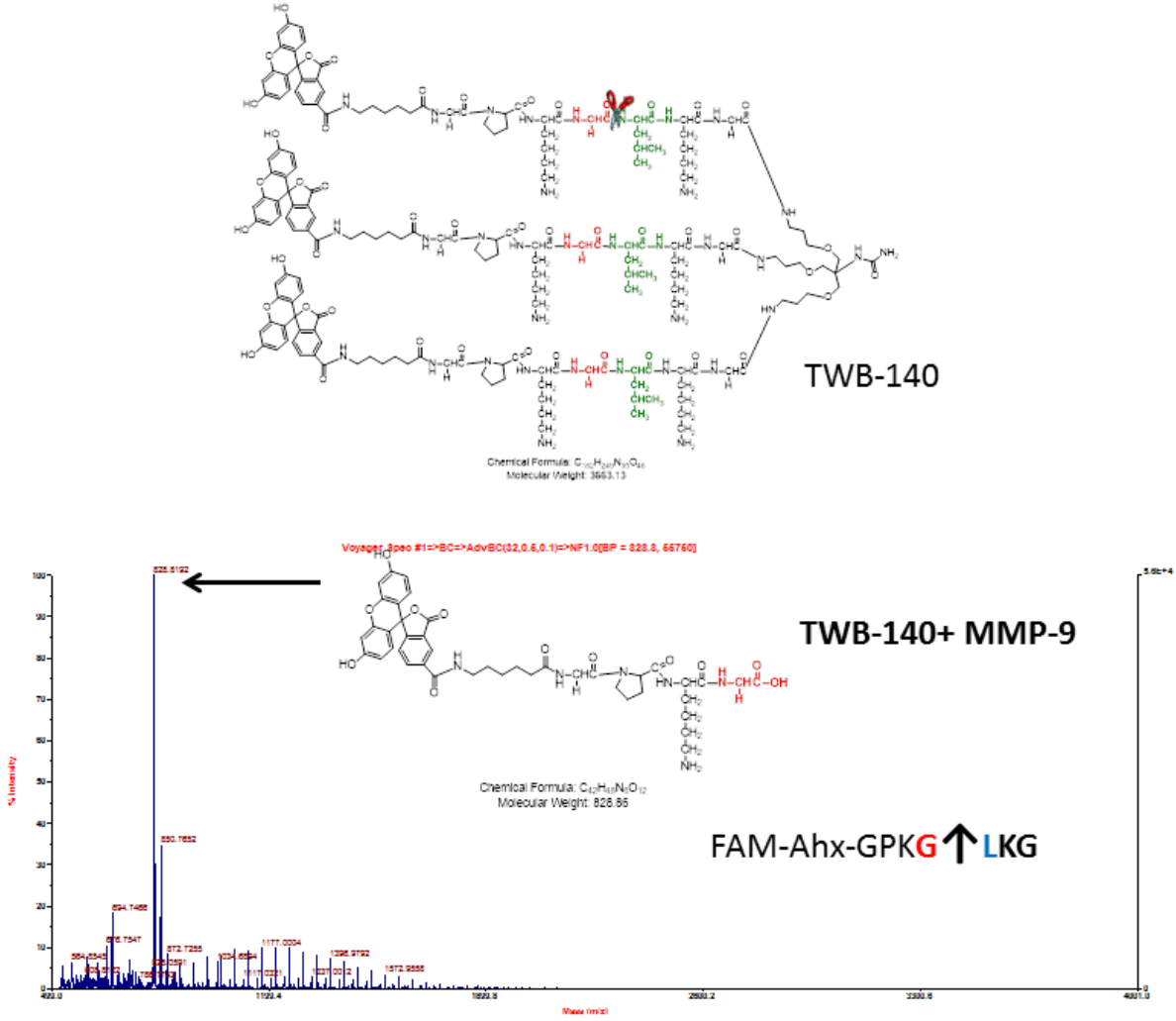

Figure 5-20: MALDI analysis confirms specific cleavage of TWB-140 following incubation with recombinant MMP-9. TWB-140 (10µm) was incubated with 30nM recombinant MMP-9 for 2h and the reaction products were stored on ice prior to MALDI analysis. The MALDI trace shows a peak at 828.86, corresponding to the molecular weight of a cleaved branch of TWB-140.

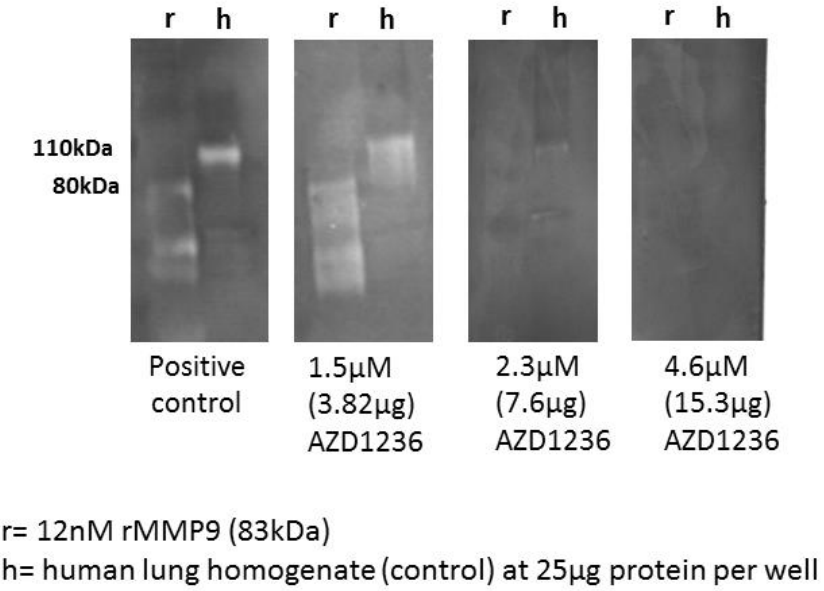

Figure 5-21: AZ1236 inhibits MMP-9 in human tissue in a concentration dependent manner. Zymography gels were loaded with recombinant MMP-9 and human lung tissue homogenate. Gels were then cut and each section incubated with a different concentration of AZD1236 during the enzyme renaturation phase. Complete inhibition of pro-MMP9 in human tissue was achieved at 4.6µM AZD1236. n=1

5.3.4.1 Evaluating probe selectivity for MMP-9 over other MMPs

In order to assess the affinity of each probe as a substrate for MMP-9, the probes were tested against a panel of recombinant catalytic domain MMP enzymes. This revealed that the two probes could also be cleaved by MMP-2, MMP-9 and MMP-13, although again SVC-016 displayed a greater signal to noise for each of these enzymes (Figure 5-22). To try to overcome the issue of high background fluorescence with TWB-140, a linear FRET (SVC-24) was synthesised with the same cleavage sequence (Figure 5-2). A control probe (SVC-25) was also created, which contained a D-amino acid at the cleavage site. Furthermore, an alteration was made to SVC-16 whereby the amino acid methionine was replaced with nor-leucine in order to improve probe stability (AMF-25). As shown in Figure 5-22, SVC-24 had a similar pattern of activation to TWB-140 against the panel of MMP enzymes but the signal amplification was greater. As expected, there was no cleavage of SVC-25 in the presence of any of the enzymes (data not shown). At this point it was accepted that the in-house probes would not be selective for MMP-9.

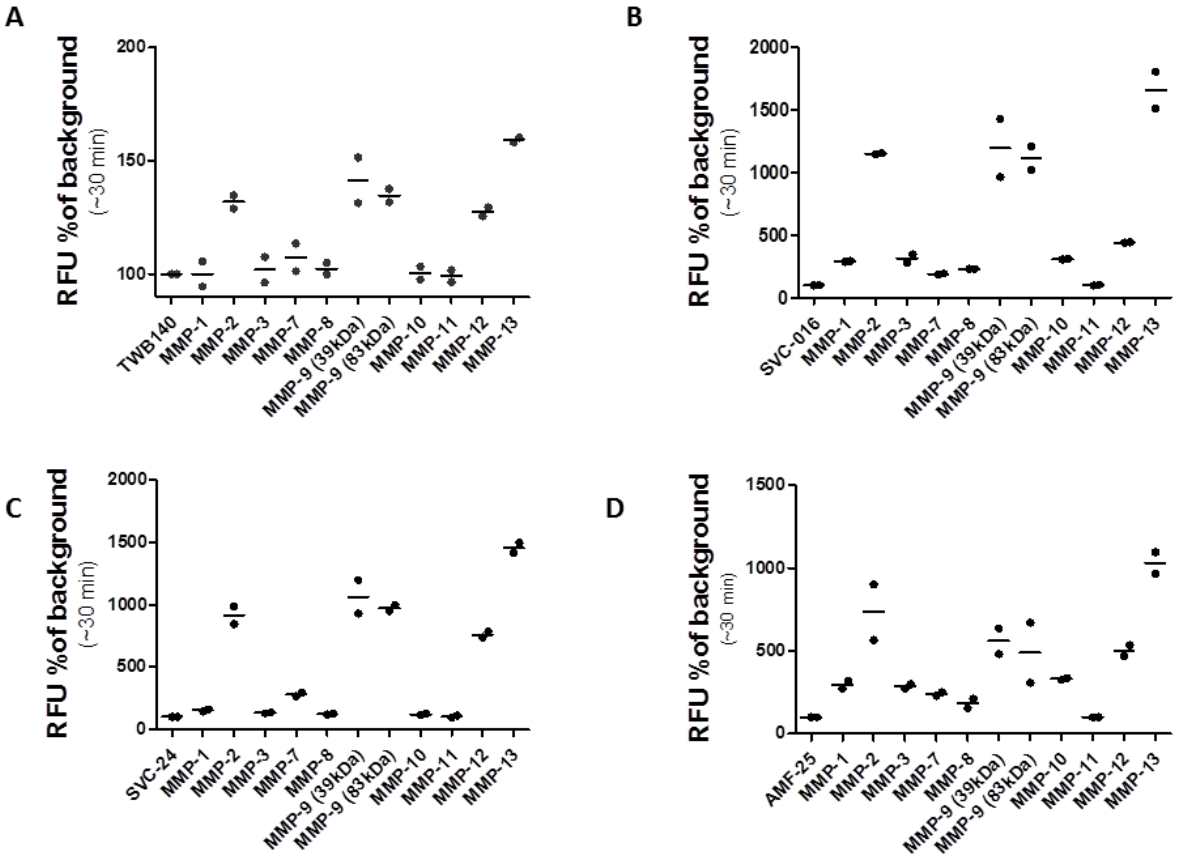

Figure 5-22: Probes are cleaved by MMP-2, -9, -12 and -13. Bar charts representing percentage of background fluorescence following 30 min incubation of 10µM probe with 30nM recombinant catalytic domain MMP enzymes. An increase in fluorescence is observed following incubation with MMP-2, -9, -12 and -13 in each of the probes (A-D), with MMP-13 producing the greatest signal to noise ratio. Bars represent the mean of two experimental replicates. n=3 for enzymes of interest (MMP-2, -9, -12 and -13).

5.3.5 Evaluation of probes in *ex vivo* tissue models

5.3.5.1 Ovine pulmonary adenocarcinoma (OPA) tissue

Initially both 2mm sections of OPA tissue and cell free tissue supernatant were incubated with the second generation probes in the plate reader in order to compare the results from different tissue preparation techniques. From Figure 5-23 it can be seen that all probes showed increased fluorescence in solid cancerous tissue compared to grossly unaffected tissue from the same animal. Results were similar between tissue and homogenate, other than for SVC-24 which showed a significant reduction in fluorescence upon incubation of solid tissue homogenate with marimastat but not in whole tissue. It should be noted that it was not necessary to normalise fluorescence to background as all of the second generation probes were linear FRETs with the same background fluorescence. MALDI analysis was done on the supernatant from the whole tissue wells, and a small peak representing the cleaved fraction of SVC-24 was detected with solid tissue (Figure 5-24). MALDI did not detect any cleavage of SVC-25 or AMF-25 either specific or otherwise, despite the increase in fluorescence in the presence of solid tissue/homogenate.

5.3.5.2 Human *ex vivo* tissue

In order to optimise conditions for MALDI analysis, small (approximately 2mm) human tissue sections were incubated with the probes rather than using homogenate. As shown in Figure 5-25, there was increased probe signal in control compared to fibrotic tissue, although the increase was not significant ($p=0.163$, unpaired t test). There was a significant increase in fluorescence over background with SVC-24 and AMF-25 in both control and fibrotic tissue, although significant signal inhibition was only achieved with SVC-24 in fibrotic tissue, most likely due to control sample variation. When results from control and fibrotic tissue were combined (Figure 5-25C), a significant reduction in fluorescence from SVC-24 was achieved in the presence of marimastat. Cleavage of SVC-24 and AMF-25 was confirmed by MALDI (Figure 5-26) and absence of cleaved probe in the presence of marimastat was also confirmed. An unexplained increase in fluorescence of SVC-25 (control probe) was observed, but inhibition of signal was not significant and there was no evidence of probe cleavage on MALDI.

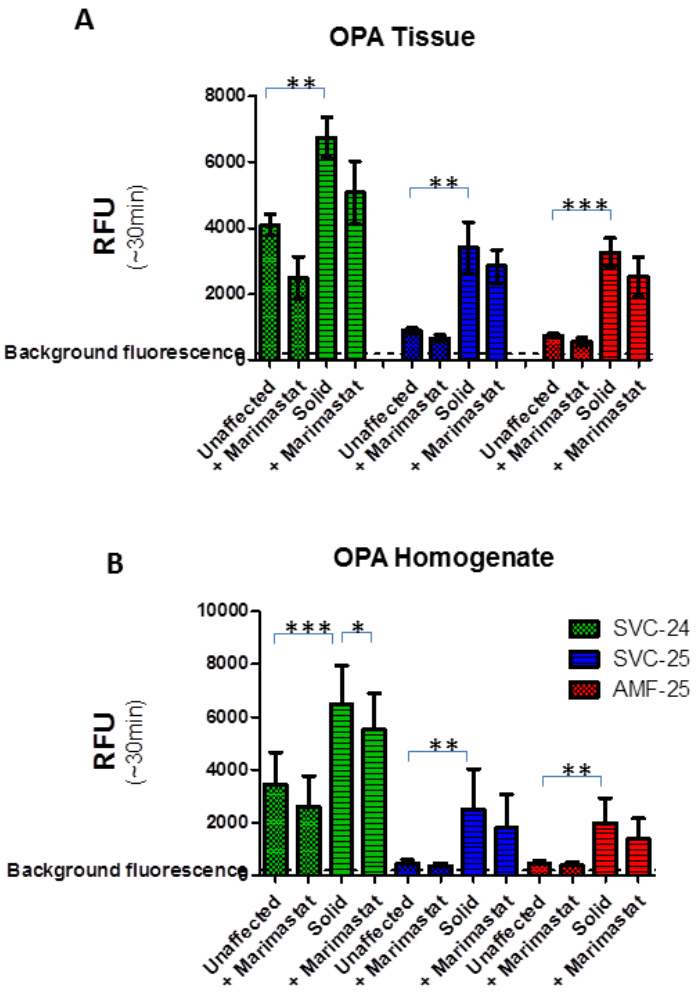

Figure 5-23: Probe signal is increased in cancerous lung tissue from sheep with OPA. Second generation probes (10µM) were incubated with either 2mm sections of whole tissue (A) or tissue homogenate (B) from ovine lungs. Selected tissue was either grossly normal in appearance (unaffected) or from an area obviously affected by the tumour (solid). After 30min incubation all probes showed increased fluorescence in solid compared to unaffected tissue including the control probe SVC-25. Significant signal inhibition by marimastat (20µM) was only achieved with the homogenised tissue and SVC-24 (B). Experiment (A) was performed in duplicate, n=5, error bars represent SEM. Graph (B) was a single well experiment, n=5, error bars represent SD. *p<0.05, **p<0.01, ***p<0.001, one way ANOVA.

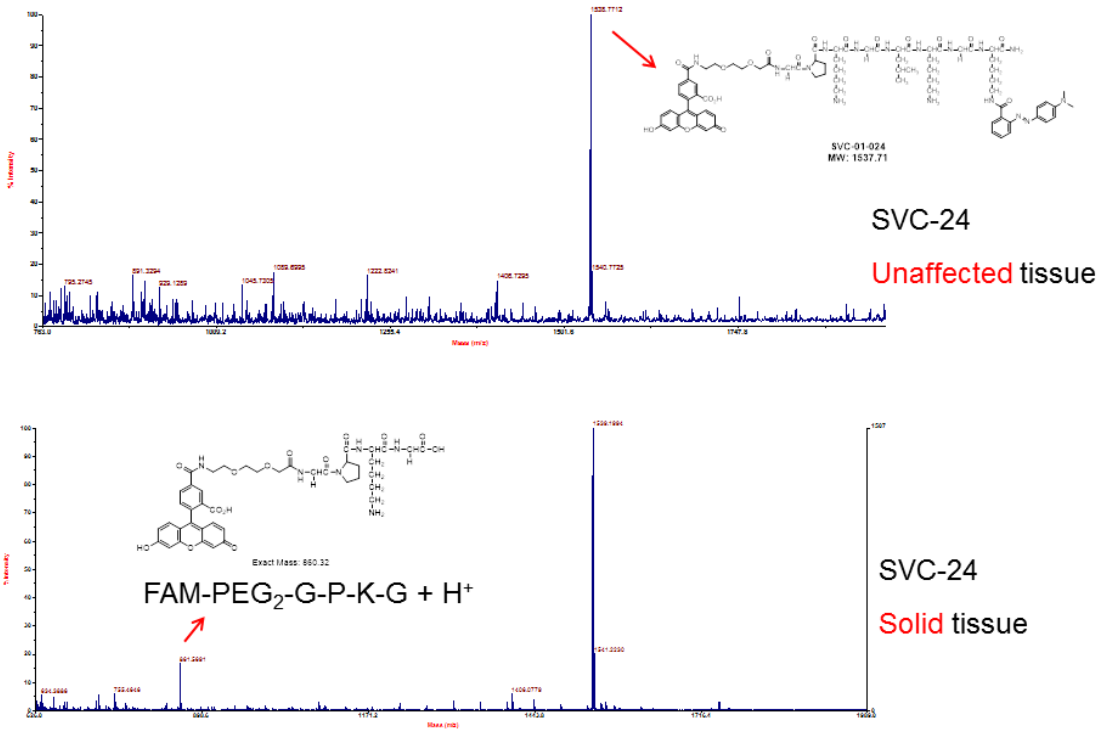

Figure 5-24: MALDI analysis confirmed cleavage of SVC-24 following incubation with solid OPA tissue. Grossly unaffected and solid OPA tissue sections were incubated with SVC-24 for 2h. The reaction products were then analysed by MALDI. The top plot from unaffected tissue shows a peak representing intact probe only, while in the presence of solid tissue an additional small peak was seen at 860, representing the cleaved fraction of probe.

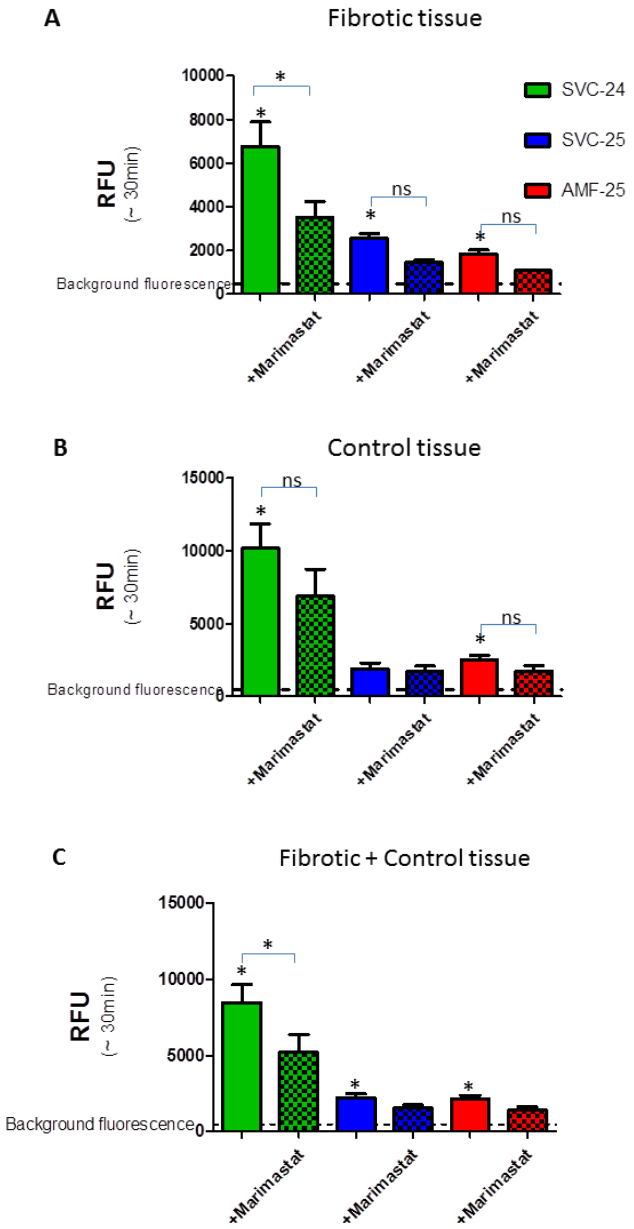

Figure 5-25: Probes are cleaved in the presence of aged human lung tissue. Bar charts of probe fluorescence following 30min incubation of 10µm probe with 2mm sections of fibrotic (A) and control (B) aged human lung tissue. There is a significant increase in fluorescence of all three probes in the presence of fibrotic tissue and a significant reduction in signal of SVC-24 in tissue pre-incubated with 20µM marimastat (A). Similar trends were present when results from control and fibrotic experiments were combined (C). All probes at 10µM, n=3 for fibrotic and control samples, error bars represent SEM, * <0.05, one sided t-test (increase over background) and One Way ANOVA.

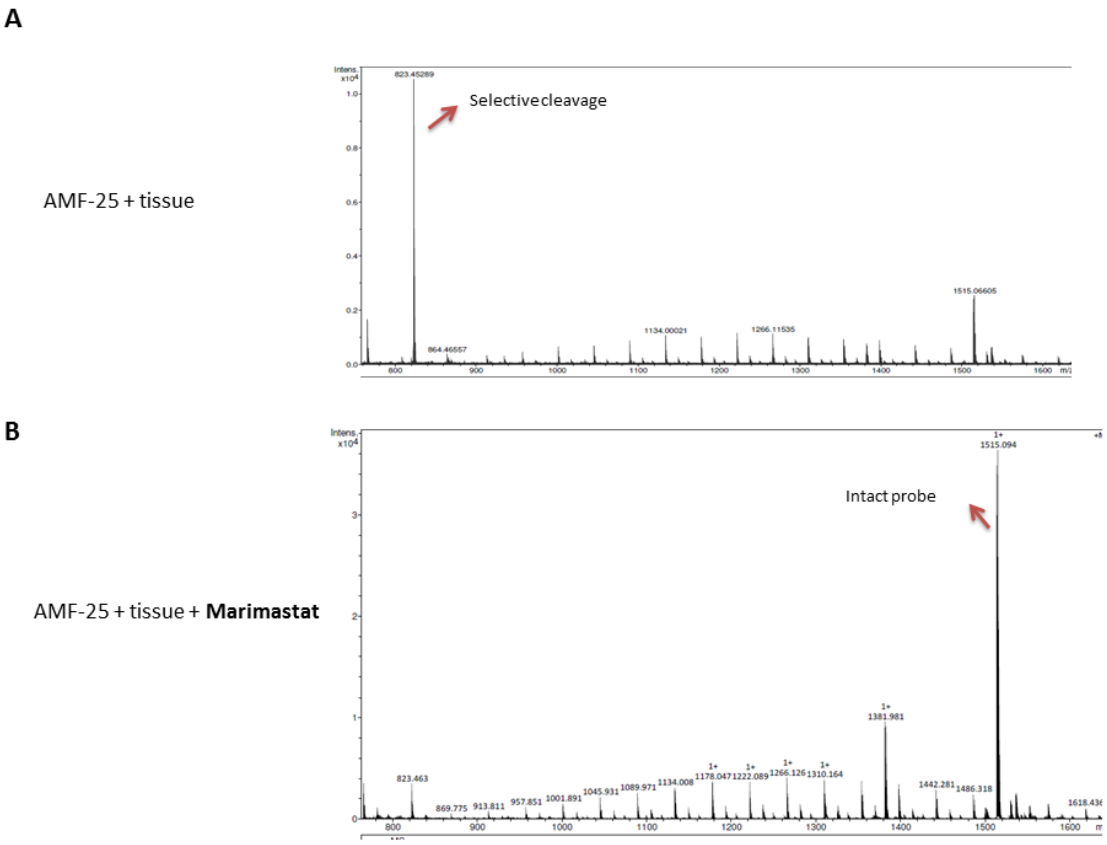

Figure 5-26: MALDI confirms cleavage of AMF-25 in the presence of fibrotic human tissue and inhibition of cleavage by marimastat. Following 2h incubation of sections of human tissue with AMF-25 the supernatant was collected and MALDI analysis performed. There was a peak at 823, corresponding to the molecular weight of the cleaved probe (A) but this peak was absent in the supernatant from tissue that had been pre-incubated with 20µM marimastat (B). Instead a peak at 1515 was noted, corresponding to intact probe. Representative of n=3.

5.3.6 Investigating off target probe cleavage

The in-house MMP probes were incubated with purified leucocyte elastase in order to begin to assess susceptibility to off-target enzymes. MALDI analysis of the reaction products did not detect any probe cleavage (Figure 5-27) other than in the case of TWB-140 which showed a peak that corresponded to the molecular weight of a side chain cleaved distal to the active site (Figures 5-28) i.e. non-specific probe cleavage. Therefore SVC-24 and AMF-25 were stable in purified leucocyte elastase.

Neutrophil lysates and supernatants were then incubated with the second generation MMP-9 probes (AMF-25, SVC-24 and SVC-25) either in the presence or absence of marimastat and/or sivelestat. A previously validated (Avlonitis et al., 2013) in-house activatable probe for neutrophil elastase (NA129) that had a similar FRET monomer structure to the second generation probes was used as a positive control (Figure 5-29). NA129 showed a threefold increase in fluorescence in the presence of neutrophil lysate and the signal was inhibited by sivelestat but not marimastat. However, despite having a similar linear FRET structure to NA129, all of the second generation probes were stable in the neutrophil lysate and supernatant (Figure 5-30).

Plasmin was later identified as another relevant off target enzyme and was used to evaluate the signal specificity of third generation probes. It was demonstrated that the amino acid sequence of SVC-24 was plasmin sensitive (data not shown).

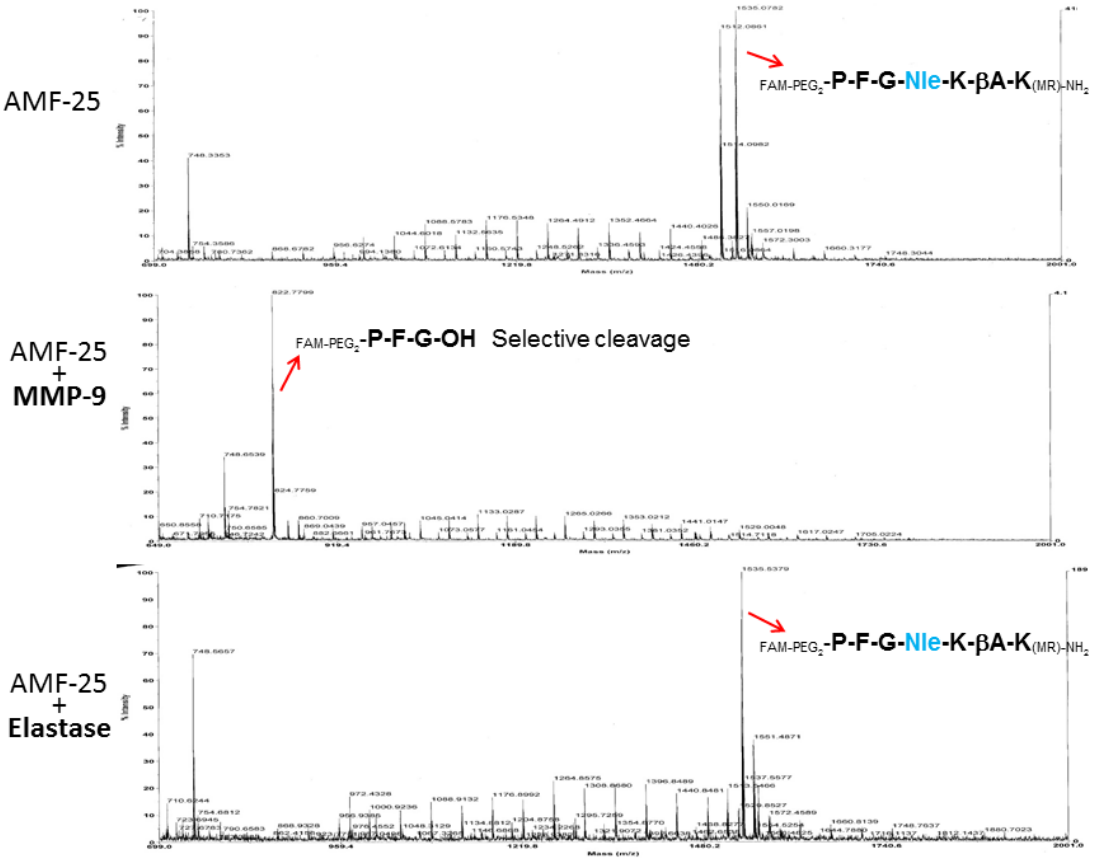

Figure 5-27 MALDI analysis confirmed stability of AMF-25 in the presence of purified leucocyte elastase. MALDI analysis was performed on the reaction products following two hour incubation of AMF-25 with recombinant MMP-9 (30nM) and elastase (2.5ug/ml). While there was a peak at 822 representing the molecular weight of the FAM fragment of the cleaved probe following incubation with MMP-9, this peak was not observed on incubation with elastase. Similar results were obtained with SVC-24 and SVC-25.

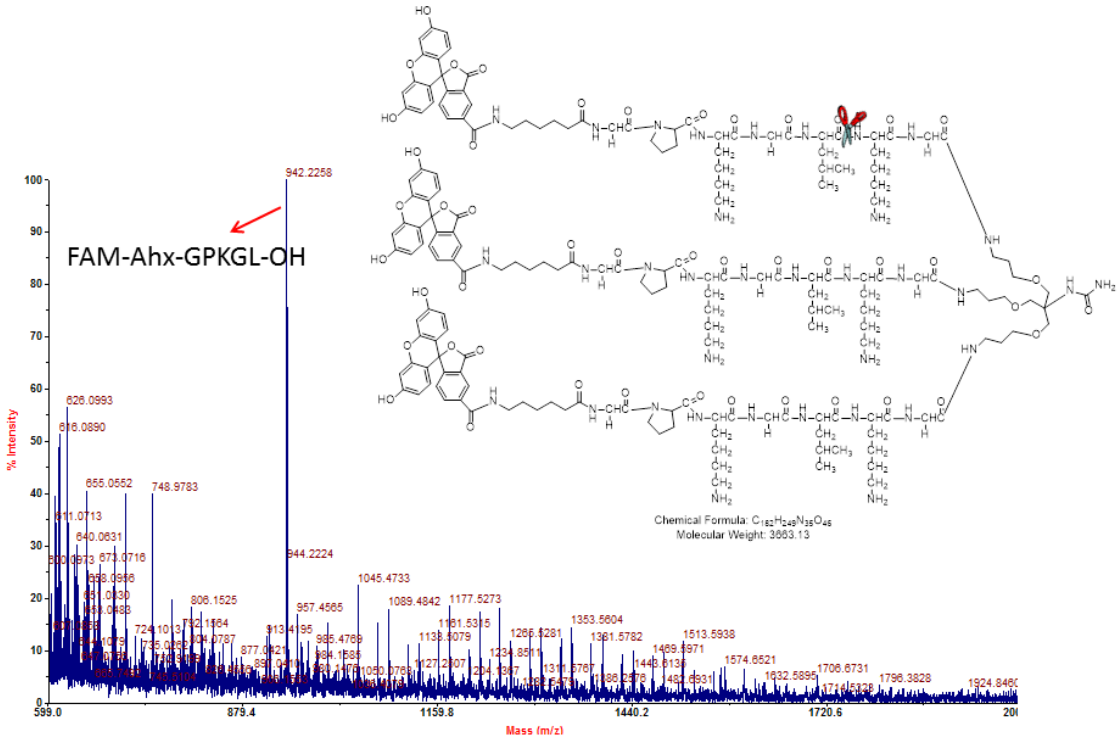

Figure 5-28: MALDI analysis demonstrated non-specific cleavage of TWB-140 following incubation with purified leucocyte elastase (2.5µg/ml). MALDI plot shows a peak at 942, corresponding to the molecular weight of the FAM fragment of TWB-140 when cleaved between leucine and lysine. This is unexpected cleavage was distal to the MMP9 cleavage site and is therefore classed as non-specific.

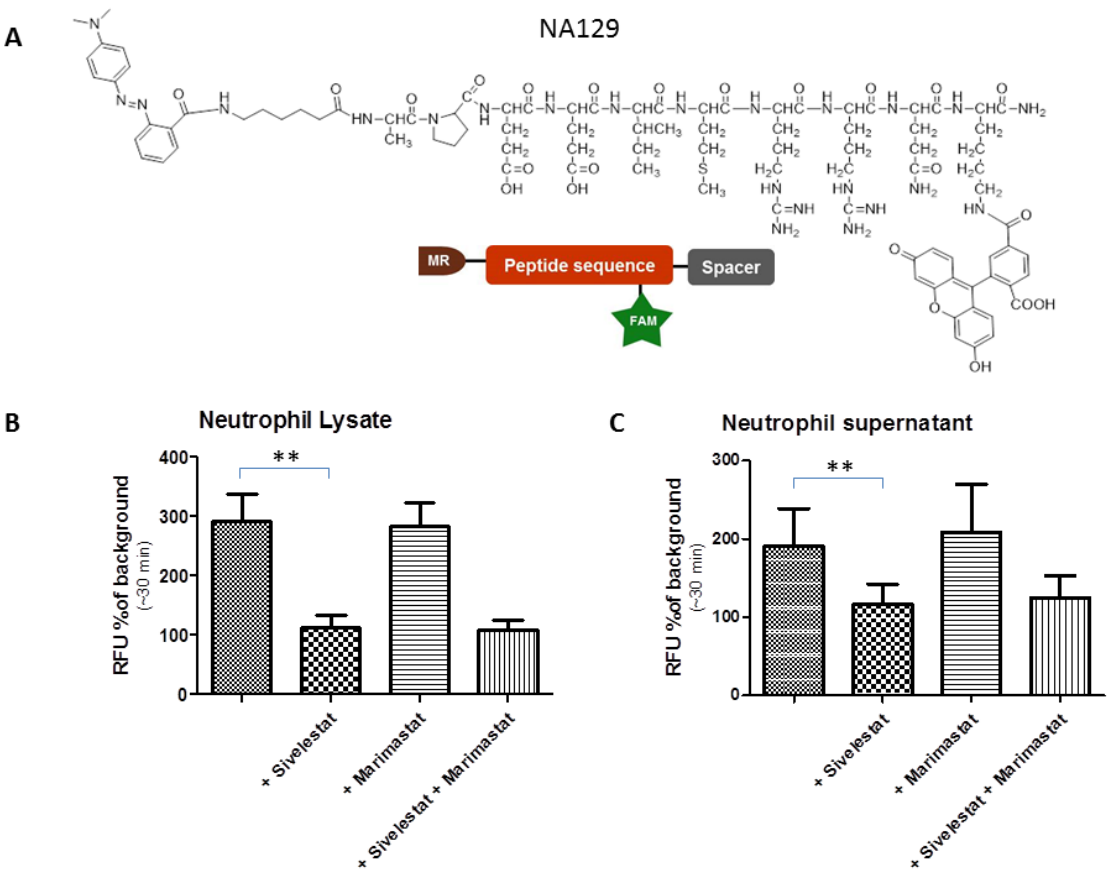

Figure 5-29: Elastase probe was used as a positive control for specificity experiments. 10µM of a previously validated (Avlonitis et al., 2013) in-house probe for neutrophil elastase, NA129 (A) was added to neutrophil lysate (B) and supernatant (C) that had been pre-incubated with 20µM marimastat and/or 100µM sivelestat. There was increased signal to noise in neutrophil lysate compared to supernatant (p=0.0152, Mann Whitney) following 30min incubation with probe, and signal was almost completely inhibited in samples pre-incubated with sivelestat. n=3, error bars represent SD, ** p< 0.01.

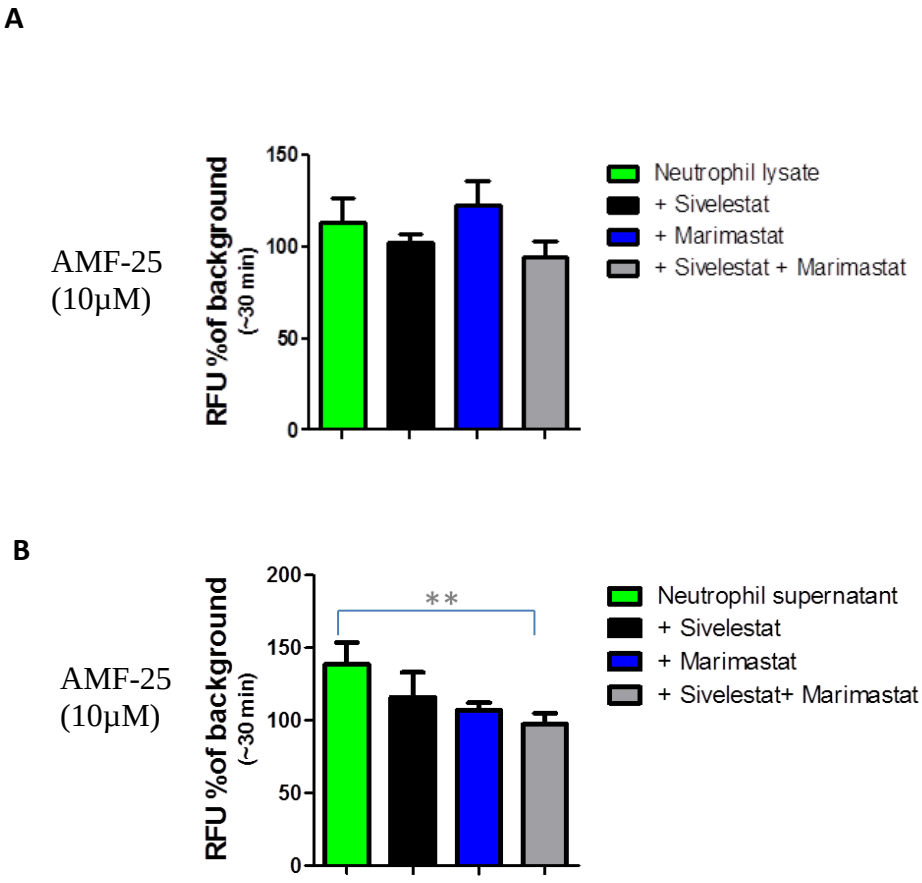

Figure 5-30: Neutrophil lysate and supernatant were used to assess probe specificity. AMF-25 was incubated with neutrophil lysate (A) and supernatant (B) which had been pre-treated with 20µM marimastat +/- 100µM sivelestat. Error bars represent SD, n=3. (C) Corresponding MALDI spectra from (A) demonstrating stability of AMF-25 following incubation with neutrophil lysate. Similar results were obtained with SVC-24 and SVC-25.

C **AMF-25 + buffer**

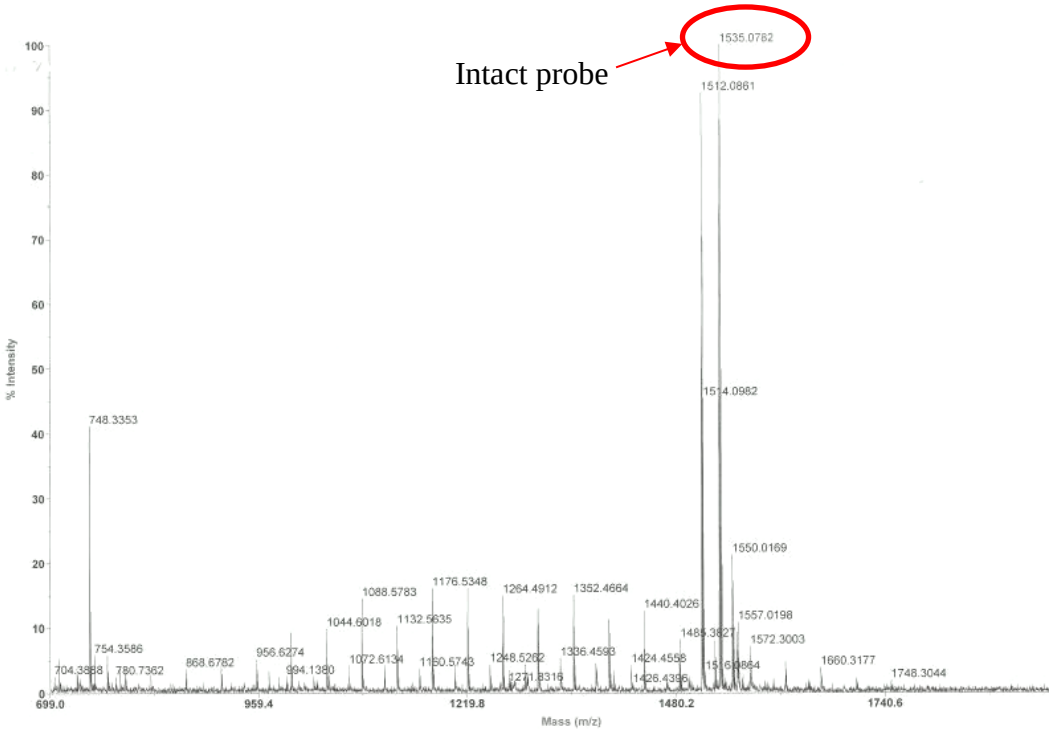

AMF-25 + neutrophil lysate

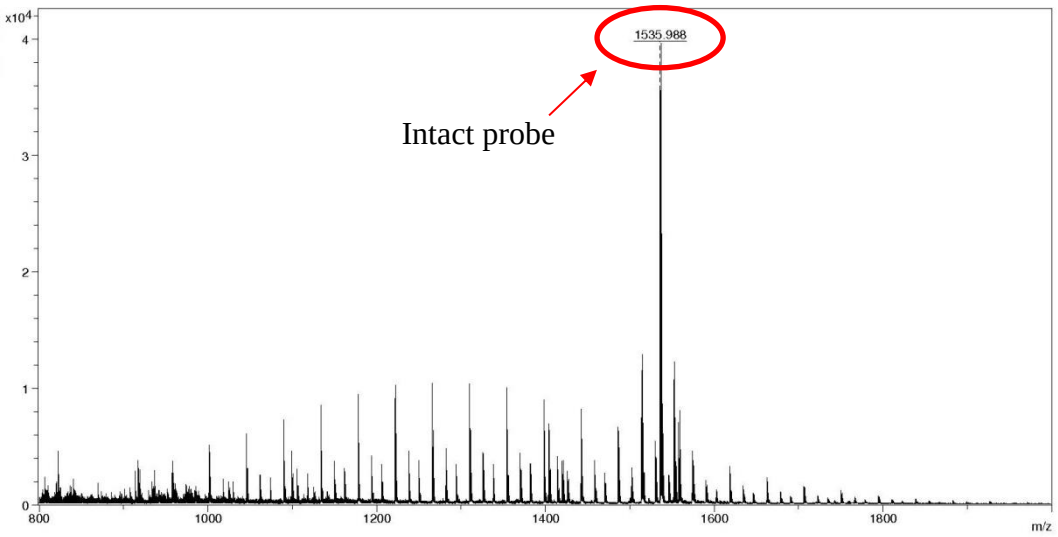

5.3.7 Third generation probes

In order to improve signal to noise amplification while maintaining a low background fluorescence, it was decided to synthesise a third generation of probes that utilized the amino acid sequences of SVC-24 and AMF-25 in an alternative structure. Thus FRET dendrimer versions of the linear probes were synthesized (Figure 5-31). As anticipated, the new probes had a low background fluorescence (Figure 5-32) and good signal to noise (Figure 5-33). While the third generation probes showed selectivity for MMP-13 at the 5min incubation time-point, it was found that a similar fluorescent signal was achieved with MMP-2 and MMP-9 following a 2h incubation (Fig 5-33 B).

As previously mentioned, the cleavage sequence of SVC-24 was found to be sensitive to plasmin, thus the plasmin stable third generation probe SVC-186, derived from AMF-25, was chosen to take forward for further evaluation (Fig 5-34). The Km and Kcat of recombinant MMP-9, MMP-2 and MMP-13 with SVC-186 was calculated (Figures 5-35 and 5-36). While a similar Km was calculated for MMP-9 and MMP-13, the Kcat of MMP-13 was much higher, consistent with the results of selectivity experiments.

The final test for SVC-186 was to utilize fibred confocal fluorescence microscopy (FCFM) to detect signal amplification in human lung tissue biopsies (Figure 5-37). While signal to noise was not as high as anticipated, analysis of the data was relatively crude and it is envisaged that future analysis will utilize specific algorithms to achieve a more sensitive result. Despite this crude analysis and the interference of tissue auto-fluorescence etc., a significant inhibition of signal was observed in tissue that had been pre-incubated with inhibitor. Further evaluation of SVC-186 with *ex vivo* tissue models and off-target enzymes is required.

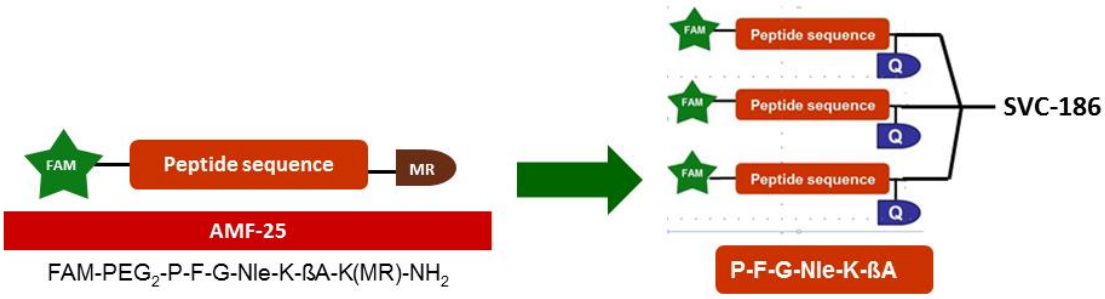

Figure 5-31: Probe evolution and structure of third generation MMP probe SVC-186. A FRET dendrimer (SVC-186) comprising three molecules of fluorescein was synthesised utilising the same sequence as AMF-25.

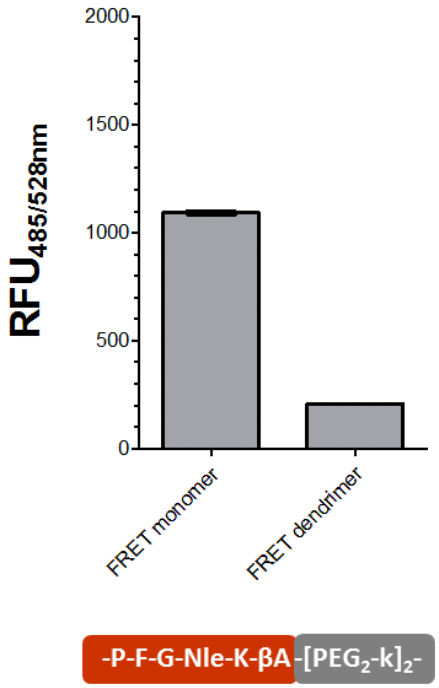

Figure 5-32: Third generation FRET dendrimer MMP probe (SVC-186) has a low background fluorescence. Background fluorescence of FRET monomer (AMF-25) vs third generation FRET dendrimer (SVC-186) incoorporating the same cleavage sequence. Probes were used at 10µM, experiment performed in duplicate, representative of n=3. This experiment was carried out by Dr Chesney Michels.

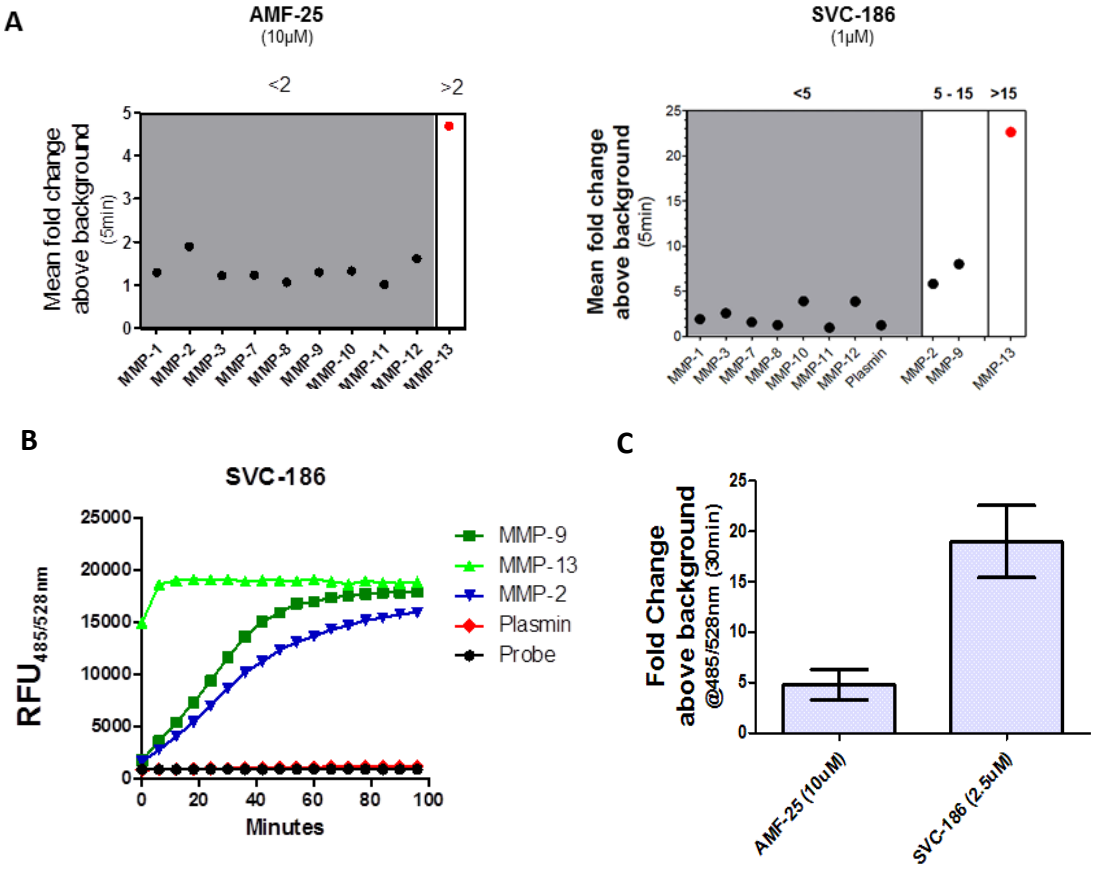

Figure 5-33: MMP specificity and signal to noise of second vs third generation probes. (A) Dot plots of fold increase in fluorescence above background following 5 minute incubation of probes with a panel of recombinant MMPs +/- plasmin (30nM). The 5min time-point was chosen to reflect the reading time of the signal with regards to potential *in vivo* application. There was an increase in signal to noise with the third generation FRET dendrimers SVC-186. This experiment was performed by Dr Chesney Michels and was only performed once due to limited supply and cost of recombinant enzymes. (B) 2h time-course demonstrating fluorescence of roughly equimolar concentrations of SVC-186 incubated with selected recombinant MMPs and plasmin. (C) Bar chart showing fold change in fluorescent signal above background following 30min incubation of probes with recombinant MMP-9, n=3, error bars represent standard deviation.

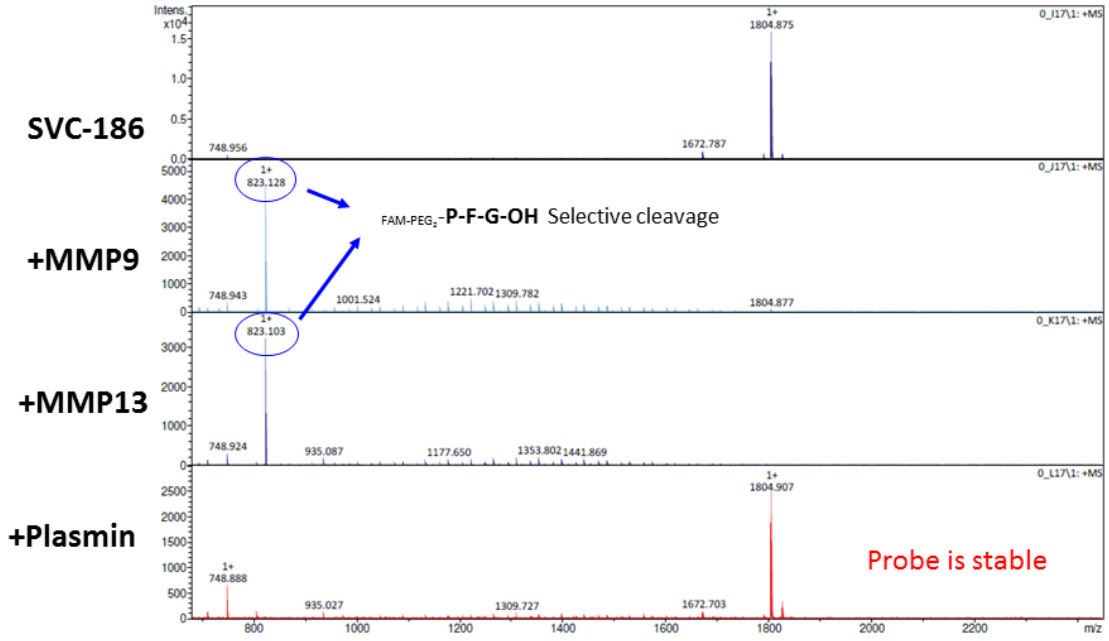

Figure 5-34: MALDI analysis confirmed that SVC-186 is plasmin stable.
MALDI analysis was performed on the reaction products following 2h incubation of 3rd generation FRET dendrimer probe, SVC-186 with recombinant MMP-9, MMP-13 and plasmin (30nM). Peaks at 823 represent specifically cleaved probe fragments following incubation with recombinant MMPs. There was no cleavage of SVC-186 following incubation with plasmin.

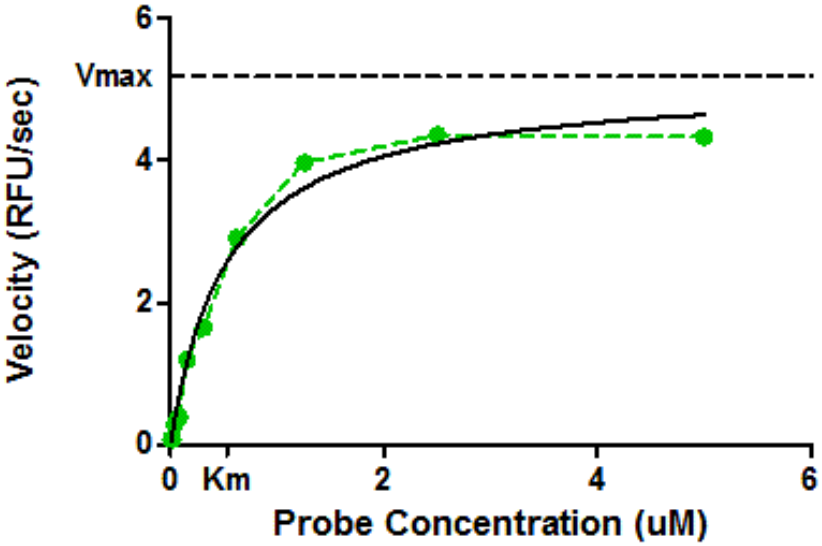

Figure 5-35: Calculating the Km. Graph of velocity against probe concentration generated for the calculation of the Michaelis-Menton constant (Km) of MMP-9 when a third generation MMP probe was used as a substrate. The Km is the concentration of substrate at which the velocity is half that of the maximum reached (1/2 Vmax).

	MMP2				MMP9				MMP13			
	V_{max} (µmol/sec)	K_m (µmol)	K_{cat} (sec^{-1})	K_{cat}/K_m	V_{max} (µmol/sec)	K_m (µmol)	K_{cat} (sec^{-1})	K_{cat}/K_m	V_{max} (µmol/sec)	K_m (µmol)	K_{cat} (sec^{-1})	K_{cat}/K_m
SVC -186	6.93	0.75	231	308	7.38	**0.46**	**246**	534.78	13.15	0.47	4383.3	9326.171

Figure 5-36: Enzyme kinetics of key recombinant enzymes with third generation probe SVC-186. The Vmax and Km were calculated for recombinant MMP-2, MMP-9 and MMP-13 using SVC-186 as the substrate. Kcat was calculated using the equation Vmax=KcatEt where Et is the concentration of enzyme active sites. Mean values of n=3.

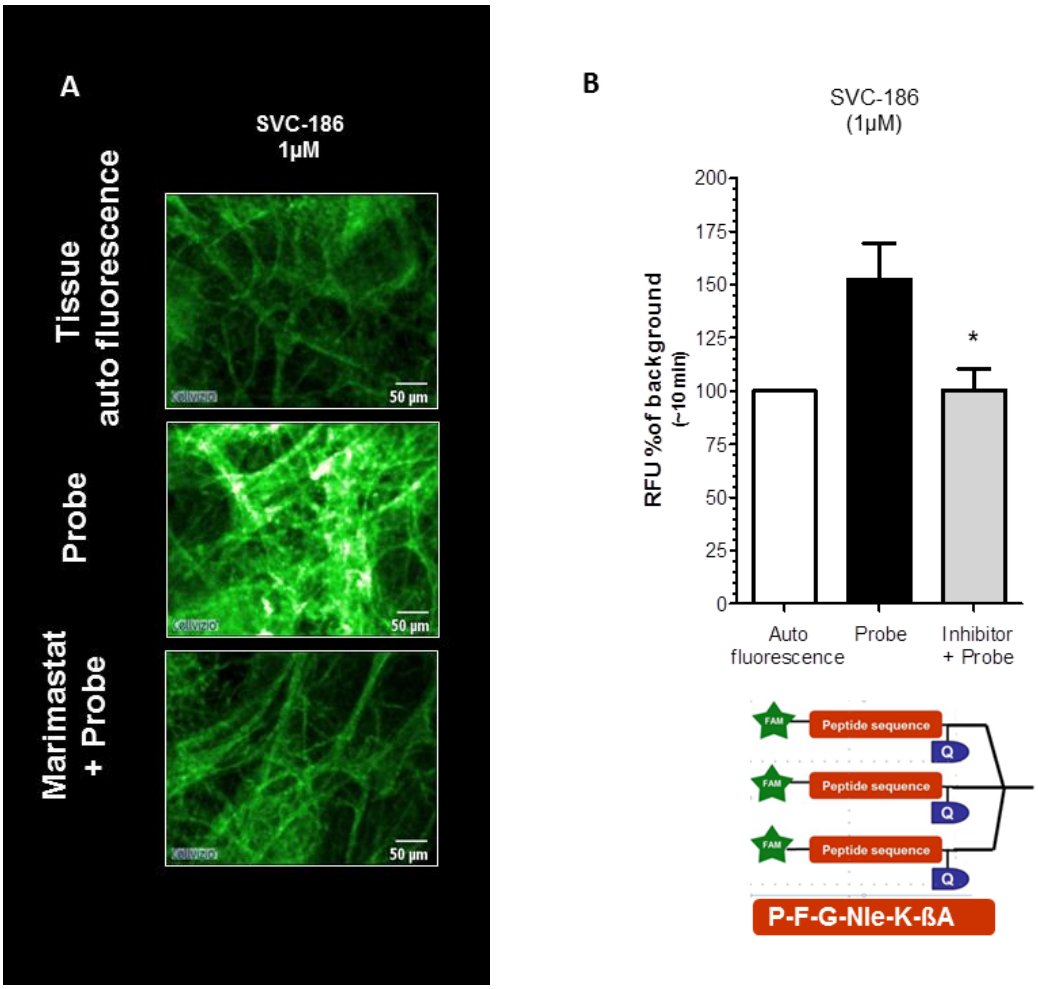

Figure 5-37 Fibred confocal fluorescence microscopy (FCFM) can be used to detect changes in probe fluorescence on incubation with *ex vivo* aged human tissue. (A) Single frame images taken by FCFM prior to and following 10min incubation of probe with sections of human tissue. Data were also obtained from tissue that had been pre-incubated with 100µM marimastat. (B) Bar charts represent percentage of background fluorescence detected by FCFM averaged over a 1min period of imaging. Significant signal inhibition was achieved. n=5, error bars represent SEM, *p < 0.05, Mann Whitney.

5.4 Discussion

5.4.1 Expression of MMP-9 in cell culture and *ex vivo* tissue models

In order to produce a readily available model of MMP-9 production for the evaluation of in-house MMP probes, the expression of MMP-9 in 3T3, RAW 264.7 and MDM cells was investigated.

It was determined by ELISA and zymography that 3T3 cells secrete MMP-9 both in the absence of and following stimulation with TGF-β (Figure 5-4). TGF-β has been used previously to stimulate MMP production in human cruciate ligament fibroblasts (Xie et al., 2013) as well as lung fibroblasts (Ramirez et al., 2011). MMP-9 production has also been demonstrated by zymography in BALB 3T3 cells following 18h stimulation with TNF-α (Mon et al., 2006), yet others have failed to show MMP-9 production by NIH 3T3 either in control cells or those stimulated with bacterial endotoxin using the same technique (Herrera et al., 2014). With regards to zymography, cell supernatants used in this study had been concentrated and it is likely that this is required in order to meet the minimum concentration of MMP-9 required for detection by zymography.

MMP-9 has been previously shown to be expressed by RAW 264.7 cells, with a marked increase in expression following stimulation with LPS (Lone, Woo et al., 2004). Findings of Lone, 2014, were consistent with ELISA data from this study (Figure 5B) in that increased stimulation time resulted in increased expression of MMP-9 (Lone, 2014). Increased expression following stimulation with LPS was not consistently evident on ICC (Figure 5-5A) but was complicated by the difficulties in quantifying increases in fluorescence using this technique (Waters, 2009). It is likely that the concentration of MMP-9 present in the cell supernatants was not sufficient to be detected by zymography.

Results regarding the expression of MMP-9 in MDM (Figure 5-6) were consistent with the literature in that cells were found to inherently express and release MMP-9 (Saren et al., 1996). Furthermore IFNγ has been shown to have no effect on MMP-9 production (Saren et al., 1996). Interestingly, freshly isolated human peripheral blood

monocytes have also been shown to produce MMP-9 but the amount released doubles following differentiation into macrophages after 7d culture (Saren et al., 1996).

Although a trend towards increased expression of MMP-9 in MDM stimulated for 24h-48h with LPS was observed in this study, the 4-fold increase reported in the literature (Saren et al., 1996) was not observed. It is possible that the concentration of LPS used was not sufficient to generate such expression (100ng/ml vs 5µg/ml). Another possibility is that cells were already producing maximal levels of MMP-9 and were thus unresponsive to further stimulation (Lepidi et al., 2001). Despite this promising MMP-9 production, the in-house MMP probes did not produce an inhibitable fluorescent signal following incubation with MDM supernatant. This could have been due to insufficient concentration of MMPs, interference from the culture medium or due to the presence of TIMPs within the supernatant. There is also an issue with regards to the intrinsic variability of cells from different donors (Cassol et al., 2006).

The active 82kDa form of MMP-9 is less frequently detected in the literature than the 92kDa pro-MMP-9 (Demedts et al., 2005, Roomi et al., 2009). TIMP-1 forms a stable complex with the MMP-9 pro-enzyme as well as binding to the catalytic site of active MMP-9 (Kim et al., 2012). An area of future work would be to investigate expression of TIMP-1 in MDM as well as in human and asinine tissue by reverse zymography as it may prevent MMP-9 from cleaving the MMP probes in cell culture and tissue models.

While both the 92kDa pro-MMP-9 and the active 82kDa MMP-9 were detected by a combination of western blot and zymography on human, asinine and ovine tissue, higher molecular weight forms were also detected, one between 110-130kDa and one at around 250kDa. Such findings are common in the literature and are thought to represent heterodimer complexes with other MMPs, macroglobulin (Snoek-van Beurden and Von den Hoff, 2005) or neutrophil-associated lipocalin (NGAL) (Kim et al., 2012, Raulo et al., 2001, Atkinson and Senior, 2003). Interestingly, sodium dodecyl sulfate causes the dissociation of TIMPs from MMPs which can result in a

misleadingly high level of MMP-9 activity (Snoek-van Beurden and Von den Hoff, 2005). Another important acknowledgment is that pro-MMP-9 undergoes autocatalytic cleavage during the development phase of zymography thus enabling it to digest the gelatin matrix (Frankowski et al., 2012). Aminophenylmercuric acetate (APMA) is commonly used to convert pro-MMP-9 to the 82kDa form prior to performing zymography (Snoek-van Beurden and Von den Hoff, 2005) and although this was attempted during the course of the study, such activation was not observed.

MMP-9 expression is minimal in healthy lung tissue (Atkinson and Senior, 2003, Ohnishi et al., 1998) but has been shown to be expressed by bronchial and alveolar epithelial cells, fibroblasts, smooth muscle cells and endothelial cells (Atkinson and Senior, 2003). In IPF, MMP-9 is upregulated and is predominantly expressed by alveolar macrophages (Lemjabbar et al., 1999), neutrophils and epithelial cells (Dancer et al., 2011, Fukuda et al., 1998) but has also been shown to be expressed by pulmonary fibroblasts on immunohistochemistry (Selman et al., 2000).

Although there was a trend towards increased expression of MMP-9 in fibrotic asinine and human tissue compared to control tissue in this study, the increase was not as great as hypothesised. This may reflect the nature of the control tissue used, in that both asinine and human control tissue were obtained from aged patients likely suffering from a range of subclinical pulmonary pathology. Fukuda *et al*, 1998 also found MMP9 to be expressed in the lung tissue of ‘control’ patients using western blot, zymography and immunohistochemistry (Fukuda et al., 1998). As in this study the control biopsies were taken from areas remote from cancer from the lungs of aged smokers and were thus not representative of healthy control tissue. It should also be noted that while MMP-9 was chosen as a clinically relevant target with regards to the potential monitoring of fibrogenic processes, it is accepted that it is unlikely to be the best single biomarker for fibrosis.

5.4.2 Probe structure and specificity

Investigation of the *ex vivo* models discussed above highlighted the need for a reporter of MMP-9 activity that could be utilised *in vivo*. A number of probes were synthesised by UoEDC with this aim in mind, representing a range of different

scaffold structures and cleavage sequences. The initial dendrimer probe (TWB-140) was found to have greater background fluorescence and reduced signal to noise amplification than the linear FRET (SVC-16, Figures 5-16 and 5-18). It should be noted however that although equimolar concentrations of probe were used to compare background fluorescence of the two probes, this did not equate to equimolar concentrations of fluorophore. An alternative way of comparing probe fluorescence would thus have been to use 3 times more of the single fluorescein monomer probe. However, for operational ease it was decided to use equimolar probe concentrations in the majority of instances regardless of the relative concentrations of fluorophore present. This is also the approach that is generally used in the literature (Avlonitis et al., 2013, Ternon et al., 2004).

In order to confirm signal specificity, it was necessary to demonstrate inhibition of observed fluorescence from the in-house probes (Figure 5-19). Marimastat is a synthetic hydroxymate pan-MMP inhibitor that fits tightly into the active site of the MMP enzyme, chelating the zinc atom (Brown, 1999). Marimastat is documented to have an IC_{50} of 3nM for MMP-9 which is consistent with findings in this study (Brown, 1999). Inhibitor I is a cell-permeable and reversible inhibitor with increased selectivity towards MMP-9 (IC_{50} 5nM) over MMP-13 (IC_{50} 113nM) and MMP-1 (IC_{50} 1.05µM) (Levin et al., 2001). The reported IC_{50} of Inhibitor I for MMP-9 is approximately 10 fold lower than that achieved in this study utilising recombinant MMP-9 and SVC-016 (Figure 5-19). This discrepancy is likely due to differences in the enzyme used (recombinant vs cell isolated) as well as the detection system. AZD1236 is an inhibitor reported to show selectivity for MMP-9 (IC_{50} 4.5nM) and MMP-12 (IC_{50} 6.1nM) *in vitro* (Dahl et al., 2012) with a 10-15 fold lower selectivity to MMP-2 and MMP-13. This study found it to have a similar IC_{50} for recombinant MMP-9 as Inhibitor I (Figure 5-19), although higher concentrations were required to inhibit MMP-9 activity in human tissue as determined by zymography (Figure 5-21).

Successful inhibition of probe cleavage generated by recombinant MMP-9, utilising the inhibitors discussed above, confirmed the specificity of probe signal in this assay but did not inform on the potential of other MMPs to cleave the probes.

As shown in Figures 5-22 and 5-33, while MMP-9 had a good affinity for each of the in-house probes tested, the probes were not selective when tested against a panel of recombinant MMP enzymes. MMP-13 produced the greatest signal to noise with each of the probes and MMP-2 and MMP-12 also demonstrated good affinity. Although it was the aim of this project to synthesise a Smartprobe that was specific for MMP-9, the above results were not unexpected particularly with regards to lack of specificity between MMP-2 and MMP-9. As well as having a high degree of structural similarity, MMP-2 and MMP-9 act upon the same major substrates and as yet no fluorescent substrate based assay has been reported that is capable of exclusively detecting one of these two gelatinases (Ryu et al., 2011). MMP-13 has the broadest substrate specificity of all of the collagenases and the highest degree of gelatinase activity by over 40-fold (Ravanti et al., 1999).

While MMP-2 activity has been shown to be increased in IPF, MMP-13 was not detected either by immunohistochemistry or PCR within the lung tissue of IPF patients (Selman et al., 2000). An area of future work is to determine the level of MMP-13 expression in the human *ex vivo* tissue used in this study. If MMP-13 expression is truly negligible then the in-house probes could still have the potential to report on MMP-9 activity in the lungs of patients with IPF. However, another potential application of the probes would be the detection of MMP-13 in cancer tissue as MMP-13 has been identified as a predictor of malignant behaviour and as a therapeutic target in certain tumours (Chang et al., 2009, Kudo et al., 2012).

As previously mentioned (Chapter 1.7.2), a dual targeted fluorescent peptide for MMP-2 which incorporated both a substrate sequence and an integrin αvβ3-binding domain was reported to have improved selectivity for MMP-2 over MMP-9 compared to a peptide composed of the substrate alone (Crisp et al., 2014). It may be that a similar approach could be utilised to improve probe specificity to MMP-9.

5.4.3 Probe stability against off-target enzymes

In order for the final MMP probe to have successful *in vivo* utility, it must have demonstrated stability against biologically relevant off-target enzymes. Thus the human neutrophil model was utilised both as a source of MMP-9 and as a source of

off-target enzymes such as neutrophil elastase (Bentwood and Henson, 1980) . Pro-MMP-9 secreted by neutrophils is free of TIMPs and is therefore readily cleaved to its active form (Ardi et al., 2007). The pro-MMP-9 is known to be activated by proteinases such as trypsin, plasmin and other MMPs (Ogata et al., 1992, Tallant et al., 2010). Interestingly human neutrophil elastase is also thought to be capable of cleaving the MMP-9 pro-domain as well as degrading TIMP-1 (Jackson et al., 2010).

Second generation probes (AMF-25, SVC-24 and SVC-25) were found to be stable following incubation with purified leucocyte elastase as well as neutrophil lysate and supernatant (Figures 5-27 and 5-30), while TWB-140 showed non-specific cleavage with purified elastase (Figure 5-28). Results were somewhat unexpected in that there was no evidence of specific cleavage by MMPs present in the neutrophil products in any of the probes tested. MALDI analysis of enzymatic reactions in biological samples can be challenging and it is possible that probe fragments of lower molecular weight could have been missed (Kang et al., 2000, Kang et al., 2001).

It is acknowledged that although the active site of the lead third generation probe (SVC-186) was the same as that of AMF-25; it is not guaranteed that stability against elastase would be conferred. Thus an area of future work is to evaluate the stability of the third generation probe SVC-186 to neutrophil elastase.

One off target enzyme that was used to challenge the third generation probes was recombinant plasmin. Plasmin is very proteolytic, with functions such as the degradation of fibrin, fibronectin and laminin, as well as the activation of pro-MMPs including MMP-2 and -9 (Martínez-Rizo et al., 2010). It has also been used to evaluate the signal specificity of MMP probes in the literature (Jiang et al., 2004). The stability of SVC-186 following incubation with plasmin, as opposed to the non-specific cleavage seen with the SVC-24 derivative, was one of the main factors in the identification of SVC-186 as the lead probe.

5.4.4 *Ex vivo* OPA tissue model

This study demonstrated for the first time that there is a high level of MMP-9 expression in OPA tissue (Figure 5-9). Unfortunately there was a lack of available

healthy ovine tissue with which to compare MMP-9 expression and this is a potential area of future work should this model be utilised further. While there was an increased probe signal to noise in solid cancerous tissue compared to grossly unaffected tissue, there was once again a discrepancy between the results of plate reader assays and MALDI analysis. Specific cleavage of SVC-24 was detected following incubation with solid cancerous tissue, however cleavage of AMF-25 and SVC-25 (control probe) were not detected despite significant increases in fluorescence. Again it is possible that there was an issue with MALDI analysis, but it is also possible that a non-specific increase in fluorescence was being observed. This theory is supported by the relatively poor signal inhibition following the addition of marimastat. A similar phenomenon was observed with SVC-25 in human tissue.

Interestingly there was increased probe signal to noise and inhibition of signal with marimastat following incubation of SVC-24 with ovine tissue homogenate compared to sections of whole tissue. This could be due to increased concentration of bioavailable MMPs within the homogenate as well as problems with probe penetration in the case of the tissue. However, it was found that MALDI analysis of the reaction products in the buffer surrounding the whole tissue was less problematic than analysis of the tissue homogenate as it minimised interference from background peaks.

5.4.5 *Ex vivo* human tissue model

No reports on the utilisation of a fluorogenic probe to demonstrate MMP activity in human lung tissue could be found in the literature. This study demonstrated an increase in fluorescence following the incubation of in-house MMP probes with aged *ex vivo* human tissue and significant signal inhibition with marimastat as determined by plate reader and FCFM (Figures 5-25 and 5-37).

The results of initial plate reader assays of probe incubation with human tissue (Figure 5-25) were somewhat surprising in that there was no significant difference in fluorescent signal achieved between control and fibrotic tissue. However, once the results of ELISA and zymography have been taken into account (Figure 5-12 and 5-13 respectively) it is understandable that there was little difference in fluorescent

signal between the two groups. It would be very interesting to compare results with those from truly healthy human lung tissue, but such tissue is very rarely available.

5.4.6 SVC-186

The lead MMP probe (SVC-186) is silent in its un-cleaved state both as a result of FRET (through the presence of the quencher methyl-red) and internal quenching due to the dendrimeric structure and close proximity of the FAM molecules. Internally quenched, enzymatically cleaved dendrimer peptides incorporating several FAM molecules have been synthesised previously for the detection of human neutrophil elastase (Avlonitis et al., 2013). One such probe, a 6-branched dendrimer containing 6 fluorescein molecules was found to have improved signal to noise compared to an equimolar concentration of a 3-branched dendrimer of the same peptide sequence, with better quenching and a further 2-fold increase in fluorescent signal (Avlonitis et al., 2013). In the literature a 3-fluorophore/1-quencher dendrimer had a lower background fluorescence and increased signal to noise than a single-fluorophore/single-quencher equivalent (Ternon et al., 2004). However these probes utilised the fluorophore dansyl which is not subject to internal quenching due to its long Stoke shift (Ternon et al., 2004). Dendrimer probes containing small Stoke shift fluorophores that also incorporate a quencher into their structure have not yet been reported in the literature, thus SVC-186 is completely novel.

As well as being optimally quenched, SVC-186 demonstrated a high signal to noise ratio with regard to the detection of MMP-9 and resistance to off –target enzyme plasmin (Figures 5-33 and 5-34). While further evaluation of SVC-186 stability towards other biologically relevant of-target enzymes is required, initial results were promising and enzyme kinetic studies of the most relevant recombinant MMPs with regards to probe selectivity, further supported the position of SVC-186 as ‘lead probe’ (Figure 5-36). However, care should be taken when interpreting the results of kinetic studies quoting the catalytic efficiency (Kcat/Km) of different enzymes. While this value can be a useful way of comparing the affinity of a particular enzyme towards different substrates (such as the in-house probes), it should not be used to

compare the affinity of different enzymes towards the same substrate (Eisenthal et al., 2007).

A further note of caution with regards to the interpretation of results relates to the issue of probe solubility. All probes were fully soluble in 100% DMSO but it was occasionally noted that precipitation of probes occurred following dilution with buffer at high probe concentrations. It is possible that this problem could have been rectified by utilising lower probe concentrations, but probe solubility could also be further optimised.

5.5 Conclusion

This chapter of work documents the evolution of a novel fluorogenic substrate reporter of MMP activity, SVC-186. The expression of MMP-9 in cell culture and *ex vivo* tissue models has been demonstrated and SVC-186 has successfully detected MMP activity in human lung tissue biopsies, something that has not been previously reported in the literature. Furthermore, SVC-186 has been shown to be stable following incubation with the off target enzyme plasmin. While further evaluation of this probe is required, preliminary results indicate that it has the potential to report on MMP activity *in vivo* and to aid in clinical decision making at the bedside.

Chapter 6: Concluding Remarks and Future Studies

6.1 Introduction

A recurring theme throughout this thesis has been challenging the way in which scientists traditionally approach the study of disease aetiopathogenesis and progression. Inspired by the 'One Health' initiative, the overall objective of this thesis was to perform the first comprehensive characterisation of APF and generate data with translational relevance to medical science. This in turn would highlight the potential for the study of spontaneous models of disease within the field of veterinary medicine as opposed to traditional experimental models. The second half of my thesis focussed on challenging current conceptions with regards to the therapeutic monitoring of the disease process. While this ambitious project was faced with several limitations and it is acknowledged that a great deal of work still requires to be done, the foundations have been set for future development and the ultimate goal of producing an MMP Smartprobe for *in vivo* use in a clinical setting.

6.2 Overall conclusions

6.2.1 Characterisation of APF

Results of the clinical aspect of the APF study, although limited by the size of the study cohort, did reveal some areas of interest. Firstly the relationship between RAO and APF certainly warrants further investigation as does the potential to characterize the breathing pattern observed in cases of APF. This study has shown that thoracic ultrasound can be used to aid in the diagnosis of APF and distinguish cases from those suffering from RAO.

Just over 50% of APF lungs included in the *ex vivo* part of the study shared key imaging and histopathological features with PPFE. Obviously this leaves a large proportion that was unaccounted for. As previously suggested it is possible that the histopathological changes observed in many of these lungs represented an early stage in the disease process or that the tissue sampling was not representative of the pathology of the lung as a whole. It should also be considered that if we were to take a cross section of *ex vivo* human lungs that had gross evidence of fibrosis, then we

would be likely to see a wide range of different diseases (Figure 1-1), so it seems logical that donkeys might possess similar disease diversity.

The genetic diversity within the resident donkey population at The Donkey Sanctuary is unknown and it is entirely possible that there is a familial predisposition to APF as has been suggested for both IPF and PPFE. Even so, environmental factors will undoubtedly play a role. Half of the APF donkeys had a history of lower respiratory tract infections, the significance of which remains to be determined, while AHV-4 and -5 were found to be ubiquitously present in a representative sample of APF and control lungs.

6.2.2 Imaging of LOX

While the evaluation of LOX Smartprobe TWB-219 faced several limitations (see 6.2.3) it also yielded some positive results. I have shown that a three-fold increase in fluorescent signal can be achieved in aged human lung homogenate and that this signal can be completely inhibited by pre-incubating the homogenate with either BAPN or the more potent in-house inhibitor AMF-59. However, the slow activation time and high background fluorescence of TWB-219 limits potential *in vivo* application and does not meet the pre-defined target product profile.

6.2.3 Imaging of MMP-9

The challenge faced with regard to the synthesis of a substrate based Smartprobe that was selectively activated by MMP-9 was a very difficult one that has yet to be achieved. The lead MMP probe SVC-186 had a novel FRET dendrimer structure that was rapidly cleaved by MMP-13 but also demonstrated good affinity for MMP-2 and -9. Probe sequence and structure optimization was the result of an extensive amount of work driven by constant cross-talk between biologists and chemists within The Pulmonary Optical Imaging Group. SVC-186 fulfilled the requirements of the target product profile, with low background fluorescence, good signal to noise and rapid activation time and although further work is required with regards to off-target stability, preliminary results are promising.

6.3 Study limitations

6.3.1 Characterisation of APF

With regards to the clinical investigation of donkeys with suspected respiratory disease, the available history was often limited to the time that the donkey had been resident at the Sanctuary, which in some cases was only a few months. Furthermore, clinical notes were variable in their detail and were often subjective. It was therefore very difficult to accurately assess the true extent of historic LRT infections in study donkeys. It is also accepted that the criteria used to determine the occurrence of an historic LRT infection were not pathognomonic and could be applicable to other conditions. It should also be noted that viral infections would be unlikely to respond to antibiotic therapy. The number of donkeys included in the study (both pre and post mortem) was limited by a number of factors including the workload of the veterinary surgeons and pathologists at The Donkey Sanctuary, time constraints imposed by the limited study period and the fact that I was not based at The Sanctuary to facilitate data collection. A wider study population would obviously have been preferred given the high degree of variability, particularly with regards to the clinical study data.

Preparation of the *ex vivo* asinine lungs prior to shipping was relatively crude, in that the lungs were manually inflated and it was therefore not possible to standardise the degree of inflation between lungs. The distance between the tissue processing site in Edinburgh and The Donkey Sanctuary, Devon meant that the lungs were also not as well preserved at the time of HRCT and tissue sampling as I would have liked. Furthermore, while HRCT and histopathology of the lung tissue provided very valuable information that would not be possible to attain from a live donkey, there were limitations to the use of *ex vivo* tissue. Firstly it was sometimes difficult to distinguish between artefactual post-mortem consolidation on HRCT and true consolidation such as that detected in fibrotic lungs. Similarly, peri-mortem changes were often evident on histopathology and this was something that had to be taken into account during interpretation of tissue sections. It should also be noted that evaluation of HRCT images and histopathology sections was mainly qualitative rather than quantitative as well as being fairly subjective. Finally, it was not the intention of this study to propose the donkey as a widely available model for the

assessment of potential anti-fibrotic therapies, but to draw attention to the advantages of studying a spontaneous model of disease and the potential for interdisciplinary collaborations between veterinary and medical scientists.

6.3.2 Molecular imaging: LOX

As previously stated, one of the major limitations with regards to the evaluation of a Smartprobe for the detection of active LOX was the lack of a suitable recombinant or purified enzyme. Thus validation experiments relied on the use of LOX inhibitors to demonstrate knock-down of fluorescent signal in human lung tissue homogenate. The results of these experiments could only be analysed utilizing data from kinetic fluorescent reads obtained on the plate reader as MALDI analysis of the reaction products was unsuccessful. As previously mentioned, MALDI analysis of complex biological samples can be challenging due to the sheer volume of components over a wide concentration range (Szájli et al., 2008).

The experiment involving the delivery of TWB-219 into a ventilating *ex vivo* asinine lung was purely exploratory and requires refinement, including the prior installation of a LOX inhibitor to show knock-down of signal. In many ways evaluation of TWB-219 was cut short to allow efforts to be focused on the more promising MMP probes with regards to target product profile (Figure 5-3). Had this not been the case, further experiments would have also involved the assessment of probe stability following incubation with off-target enzymes such as neutrophil elastase and plasmin. The contribution of different members of the LOXF to the signal amplification generated by TWB-219 in human lung homogenate is also yet to be determined.

6.3.3 Molecular imaging: MMPs

With regards to the MMP probe it should be acknowledged that the original objective of developing a Smartprobe that was specific to MMP-9 was not achieved. Instead, the lead probe SVC-186 is cleaved rapidly by MMP-13, with MMP-9 and MMP-2 resulting in a more gradual increase in fluorescent signal (Figure 5-33B). However the results of the experiments shown in Figure 5-33 highlight the limitations of using individual time points with regards to the quantitative analysis of fluorescent signal,

as the relative outputs following incubation of SVC-186 with each of the recombinant MMPs mentioned above are very different depending on the incubation time used. However it is most likely to be the earlier time points that are ultimately most relevant to future *in vivo* utility. As with TWB-219, the relative contribution of different MMPs to signal amplification in *ex vivo* human lung tissue has not been determined but may be possible via the use of more specific inhibitors for individual MMPs.

6.3.4 *Ex vivo* assays

The limitations relating to the lack of true control asinine and human tissue, both in the evaluation of enzyme expression and in probe assays has already been discussed. However, it is also accepted that while LOX, LOXL2 and MMP-9 are integral to the fibrogenic process, increase in their expression is not diagnostic of fibrosis nor are they necessarily optimal molecular markers of fibrogenesis when measured in isolation. However, this does not limit their utility with regards to the monitoring of the response of diseased tissue to specifically targeted molecular anti-fibrotic therapies. Potential utility within the field of cancer resection and therapeutic monitoring also needs to be explored.

There are inherent limitations regarding the translation of results obtained in *ex vivo* tissue to those expected *in vivo*. The lack of perfusion and progressive ischaemia and cell death leads to changes in tissue pH and the cessation of metabolic and physiochemical processes (Ong et al., 2013), all of which are likely to have substantial effects on probe activation. The use of a perfused and ventilating *ex vivo* lung model would overcome some of these issues and plans to establish such a model at The University of Edinburgh are underway.

6.3.5 FCFM

A fundamental limitation of all of the probes evaluated during the course of this study, with regards to *in vivo* use, is their excitatory wavelength of 488nm which is subject to interference from tissue autofluorescence and endogenous quenchers. However, having utilized the inexpensive and readily available fluorescein dye for sequence validation and structural optimization of the lead MMP Smartprobe,

substituting fluorescein for a NIR dye would be relatively straight forward. The FCFM system used throughout this study was limited to one colour (480nm) but a 660nm system has since been acquired and work is underway to produce a multiplex FCFM system (Proteus).

FCFM is also limited to use in organs that are accessible via endoscopy and, unlike techniques such as PET that inform on the whole organ, FCFM gives a very localized yet high resolution image with a depth of only 50µm. The latter two issues can be overcome to a certain extent by taking multiple videos from different locations throughout the lung and by advancing the mini-probe deeper into the alveolar space as required.

The final limitation of FCFM experiments was the lack of pre-validated data quantification techniques for this relatively novel imaging system. Thus as previously mentioned, the data analysis performed in this study was relatively crude and did not take into account the issue of blank frames and motion blur that inevitably occur during movement of the FCFM mini-probe within tissue. Furthermore, the scope of data produced by the FCFM system reaches beyond a fluorescent readout, with the detection of changes in tissue architecture and cellular infiltrates. Potential solutions to these issues will be discussed below.

6.4 Future directions

6.4.1 APF

The ubiquitous presence of gamma herpesvirus in the study population of donkeys warrants further investigation with regard to its potential role in the aetiology of APF. In-situ hybridisation to determine whether herpesviral DNA co-localises with fibrotic lesions as well as quantitative real-time PCR for a number of equine and asinine herpesviruses both on nasal swabs and tissue sections may uncover an association between herpesviral infection and APF. Other areas of future work include expanding on the epidemiological data collected from APF cases and analysing serum samples for the presence of auto-antibodies.

6.4.2 Molecular imaging: LOX and MMPs

Assessing the specificity of TWB-219 and SVC-186 to individual members of the LOX and MMP families respectively, is a potential goal, which may involve exploiting the use of specific inhibitor-based imaging agents.

The high affinity of the lead MMP probe, SVC-186, for MMP-13 could expand the potential clinical utility of the probe. For example, MMP-13 has been shown to be over-expressed in breast cancer (Sendon-Lago et al., 2014, Kim et al., 2014) and squamous cell carcinoma (Vincent-Chong et al., 2014) among other tumours and is thus a potential therapeutic target in oncology. It would be very interesting to evaluate probe performance in cancer biopsy tissue, particularly with regards to levels of enzyme expression in relation to distance from tumour margins. With this in mind, having shown no evidence of toxicity in an in-house toxicology panel, SVC-186 is currently undergoing further validation alongside large scale clinical grade manufacture with a view to beginning phase 1 clinical trials.

The establishment of primary fibroblast cell lines from human lung tissue biopsies occurred quite late in the course of this study and as such this was an under-utilised resource which I believe has a lot of potential for future exploitation. Optimising protocols for live cell imaging of cells pre-incubated with both LOX and MMP probes is thus another area of future work.

6.4.2.1 FCFM

An aim of ongoing work within The Pulmonary Optical Molecular Imaging Group is to develop specific algorithms to remove blank frames, reduce motion blur and distinguish between different patterns of florescent signal such as those produced by cells versus those produced by tissue structures. Work into the production of dual probes whereby two different fluorophores within a single Smartprobe are used to report on two different molecular targets at different wavelengths, is also ongoing. The potential for multiplexing, whereby multiple targets are assessed on multiple wavelengths is huge and we are yet to scratch the surface of the potential of FCFM.

Chapter 7: Appendix

7.1 Sampling protocol for *ex vivo* asinine lung tissue

APF affected lungs: collect approximately 3cm x 3cm x 1cm samples from (a) a grossly fibrotic area, (b) an apparently unaffected area, and (c) a region representing the junction between grossly fibrotic and unaffected tissue.

Collect this series of 3 samples both from cranial (between V1 and D1 as shown in figure A1), mid (between D2 and V2) and caudal lung (between V3 and D3) regions of either lung.

Also collect one sample of lung (from anywhere) containing a larger airway (0.5-1 cm diameter) as well as a bronchial or mediastinal lymph node. Record the region of lung from where each sample is collected. There will be a total of 11 lung samples from APF donkeys.

Control lungs; collect approximately 3cm x 3cm x 1cm samples from the cranial (between V1 and D1), mid (between D2 and V2) and caudal lung (between V3 and D3) regions of either lung. Also collect one sample of lung (from anywhere) containing a larger airway (0.5-1 cm diameter) and a sample of bronchial or mediastinal lymph node. Record region of lung from which each sample is collected. There will be a total of 5 samples from control donkeys.

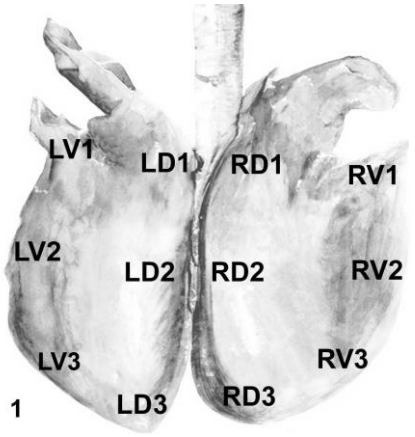

Figure A1: Diagram depicting regions of lung as discussed in sampling protocol.

7.2 Examination protocol and record sheets

Name: **Age:**

Sex: **Farm:**

Housing:

Current Bedding:

Current feed:

Height: **Weight:**

Body condition score:

Last wormed:

Result of last worm egg count:

Lung worm positive?:

History of respiratory disease, cough or nasal discharge?:

Clinical tracheal collapse?:

Mucous membrane colour:

Nasal discharge?:

SMLN enlargement?: **Respiratory rate:**

Respiratory Effort score:

Nostril Flare score:

Respiratory pattern/ character:

Heart rate/Pulse rate: **Rectal Temperature**

Other Diagnostics

Thoracic ultrasound?: **Yes** **No**

Recent blood sample?: **Yes** **No**

Endoscopy?: **Yes** **No**

BAL?: **Yes** **No**

Nasopharyngeal swab?: **Yes** **No**

Oxygen Saturation (highest A reading obtained with pulse oximeter):

Site used to measure oxygen saturation:

Tracheal Auscultation and Palpation

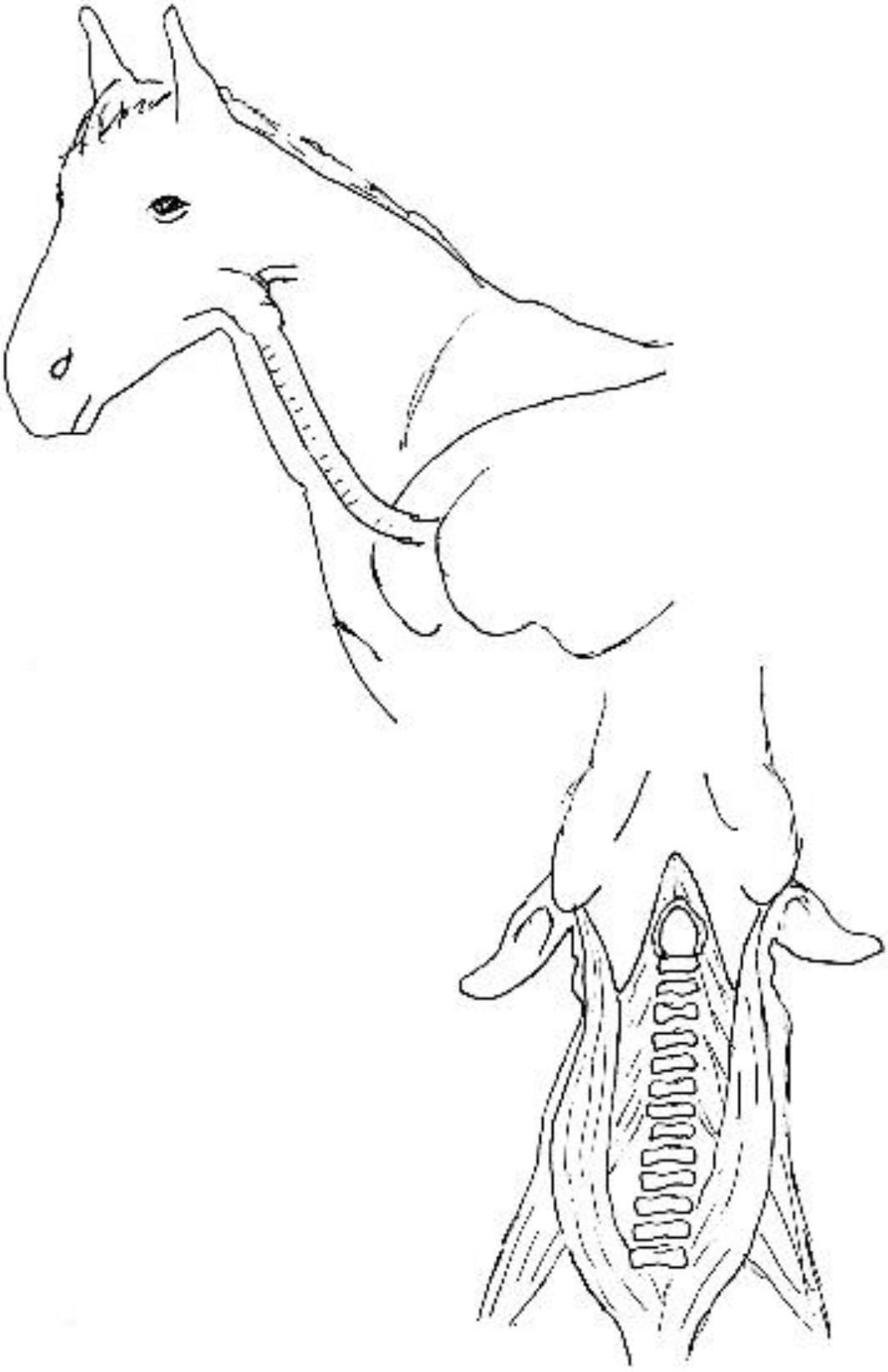

Auscultation Record Sheet

Right

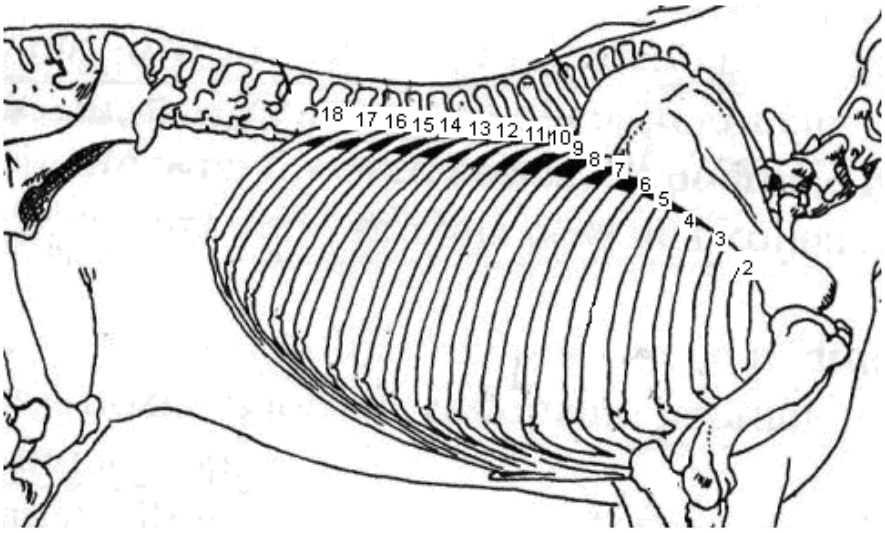

Left

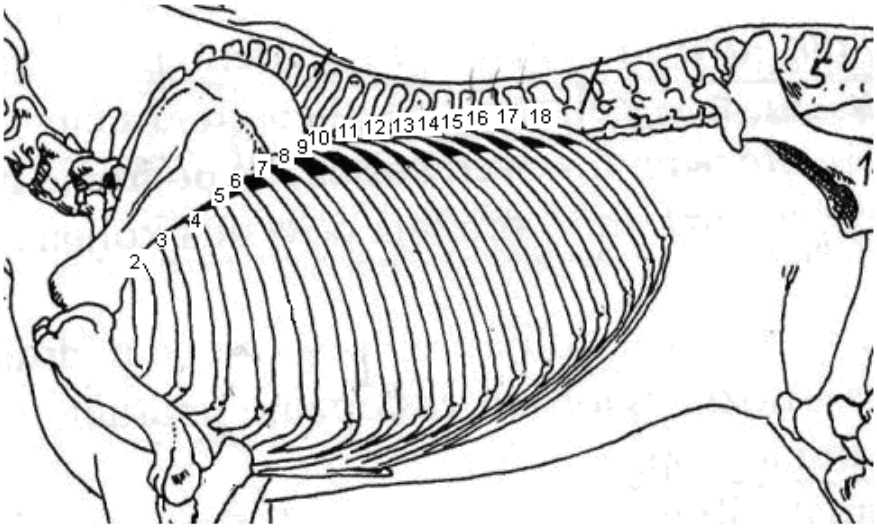

WI=wheeze inspiratory, WE =exp wheeze, CI=insp crackle, CE=exp crackle, IA=area of increased audibility, RA=reduced audibility

Ultrasonography Record Sheet

Right

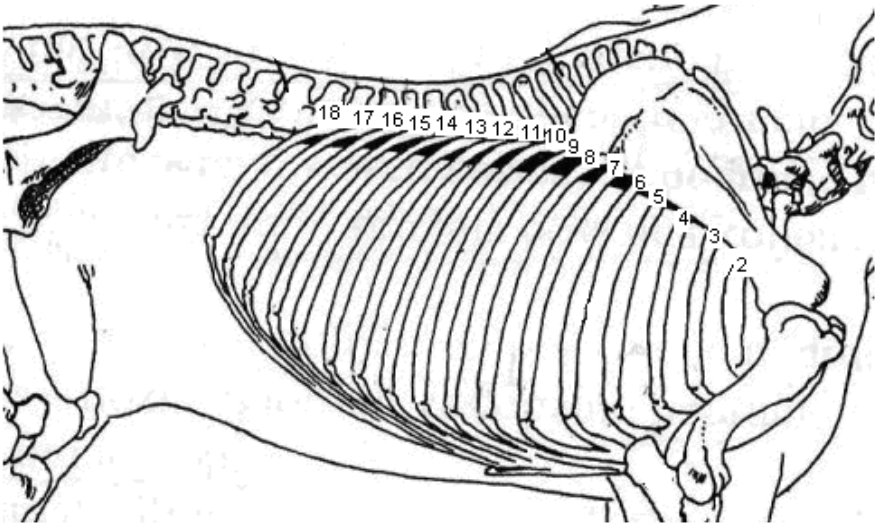

Left

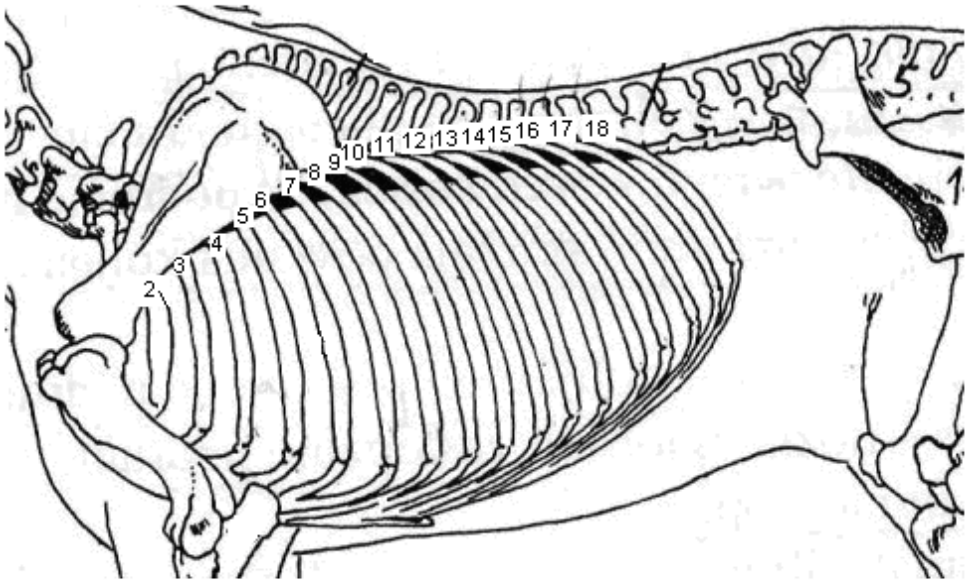

Respiratory Effort score:

1 No abdominal component and little movement of external intercostal muscles

2 Slight abdominal component and/or mildly increased inspiratory thoracic effort

3 Moderate abdominal component and/or moderately increased inspiratory thoracic effort

4 Severe, marked abdominal component/heave and/or severely increased inspiratory thoracic effort

Nostril Flare score:

1 No flaring of nostrils

2 Slight, occasional flaring of nostrils

3 Moderate, continuous flaring of nostrils

4 Severe, continuous flaring of nostrils)

Figure A2: Respiratory effort scoring system. Donkeys were examined and allocated a score for each of the categories detailed above. The sum of these two categories was the final respiratory effort score out of 8.

7.3 Peer reviewed manuscripts

CHEST Original Research
DIFFUSE LUNG DISEASE

Chronic Pleuropulmonary Fibrosis and Elastosis of Aged Donkeys

Similarities to Human Pleuroparenchymal Fibroelastosis

Amy Miele, BVM&S; Kevin Dhaliwal, MBChB, PhD; Nicole Du Toit, BVSc, PhD; John T. Murchison, MBChB, PhD; Catharine Dhaliwal, MBChB, PhD; Harriet Brooks, BVetMed, PhD; Sionagh H. Smith, BVMS, PhD; Nik Hirani, MBChB, PhD; Tobias Schwarz, DrMedVet; Chris Haslett, MBChB; William A. Wallace, MBChB, PhD; and Bruce C. McGorum, BVM&S, PhD

Background: **Donkey pulmonary fibrosis (DPF) is a spontaneous syndrome of aged donkeys with a high prevalence (35%). No previous detailed characterization of DPF has been performed. We sought to determine the similarities between DPF and recognized patterns of human pulmonary fibrosis.**
Methods: **Whole lungs were collected from 32 aged donkeys at routine necropsy. Gross examination revealed pulmonary fibrosis in 19 donkeys (DPF cases), whereas 13 (control cases) had grossly normal lungs. Eighteen whole inflated ex vivo lungs (11 DPF cases, seven control cases) were imaged with high-resolution CT (HRCT) scan, whereas the remainder were sectioned and photographed. Tissue samples were collected from all lungs for histopathologic evaluation using a standardized protocol. HRCT images and histology sections underwent independent blinded review. Lung tissue was analyzed for herpes virus, fungal hyphae, mycobacteria, and dust content.**
Results: **Ten of 19 DPF lungs were categorized as being consistent with pleuroparenchymal fibroelastosis (PPFE) according to previously defined histologic and imaging criteria. All 10 PPFE-like lungs had marked pleural and subpleural fibrosis, predominantly within the upper lung zone, with accompanying intraalveolar fibrosis and elastosis. Asinine herpesvirus was ubiquitously expressed within control and DPF lung tissue. No other etiologic agents were identified.**
Conclusions: **Many cases of DPF share key pathologic and imaging features with human PPFE, a rare interstitial pneumonia. Consequently, further study of DPF may help to elucidate the etiopathogenesis of human PPFE.**
CHEST 2014; 145(6):1325–1332

Abbreviations: AsHV = asinine herpesvirus; DPF = donkey pulmonary fibrosis; EVG = elastic Van Gieson; HRCT = high-resolution CT; PCR = polymerase chain reaction; PPFE = pleuroparenchymal fibroelastosis

Pulmonary fibrosis represents the end point of many diseases and is characterized by excessive and irreversible deposition of extracellular matrix in the lung parenchyma, leading to compromised ventilation and organ dysfunction. Despite considerable research, many fibrotic lung diseases remain elusive in terms of etiology, pathogenesis, and treatment.[1] Progress is hindered by the lack of a translatable animal model with durable and persistent fibrosis.[2]

The term "idiopathic pleuroparenchymal fibroelastosis" was coined by the authors of a case study in 2004 to describe a novel clinicopathologic entity that did not fall within the 2002 American Thoracic Society consensus classification of idiopathic interstitial pneumonias.[3] The authors described a predominantly upper zone distribution of pleural and subpleural fibrosis with elastosis and proposed that previous reports of idiopathic pulmonary fibrosis of upper lung lobes were consistent with pleuroparenchymal fibroelastosis (PPFE).[3] PPFE was subsequently included in the 2013 American Thoracic Society/European Respiratory Society statement "Update of the International Multidisciplinary Classification of the Idiopathic Interstitial Pneumonias" in the category of rare idiopathic interstitial pneumonias.[4] Although PPFE is regarded as usually idiopathic, it has been linked with connective

tissue diseases, genetic predisposition, and autoimmunity following organ transplant.[3-5] Reddy et al[5] suggested that repeated inflammatory damage following recurrent infections in predisposed individuals could lead to PPFE and that airway-centered injury could be key to disease pathogenesis.

Donkey pulmonary fibrosis (DPF) is a syndrome that is also sparsely documented, yet a prevalence of 35% at routine necropsy was reported in a UK cohort.[6] Very little is known about this chronic, potentially debilitating, and currently untreatable idiopathic condition. To test our hypothesis that many cases of DPF share the key pathologic and imaging characteristics of PPFE, we performed the most comprehensive systematic characterization of DPF to date.

Materials and Methods

Tissue Collection and Processing

Whole lungs were collected from 32 aged donkeys during routine necropsy at two UK donkey sanctuaries between June 2009 and January 2013 (e-Appendix 1). Nineteen DPF lungs were selected because of grossly visible fibrosis, whereas 13 grossly unaffected control lungs were selected at random. All lungs were manually inflated, the tracheas clamped, and gross images photographed. Tissue samples were collected from each lung into 10% buffered formalin, essentially as described previously,[7] before undergoing routine processing to paraffin blocks. Sections were stained with hematoxylin and eosin, elastic Van Gieson (EVG), and Masson's trichrome. Tissue samples from eight lungs (four DPF, four control) were collected into RNA*later* (QIAGEN) for DNA extraction and subsequent polymerase chain reaction (PCR). Because this study used only ex vivo tissue collected at routine necropsy, licensing on ethical and humane grounds was not required.

Histology

Histology sections were reviewed independently and blindly by three medical and veterinary pathologists with experience in lung disease. Subsequent to the recognition that the changes observed resembled those of human PPFE, the histologic features were categorized as being consistent with or inconsistent with PPFE according to criteria described by Reddy et al.[5] Cases were categorized as consistent with PPFE on histology if (1) there was pleural thickening with associated subpleural intraalveolar fibrosis and alveolar septal elastosis or (2) intraalveolar fibrosis was present but either not associated with pleural fibrosis, not predominantly subpleural, or not in a dorsal lobe sample. Inconsistent with PPFE was assigned to lungs that lacked these features.

High-Resolution CT Imaging and Digital Photography

Eighteen whole inflated ex vivo lungs (11 DPF, seven control) were imaged with a high-resolution CT (HRCT) scanner (Aquilion One [Toshiba Medical Systems, Toshiba Corp] or Somatom Volume Zoom [Siemens AG]). The remaining lungs (eight DPF, six control) were systematically sectioned transversely and photographed digitally. All images were reviewed independently and blindly by an expert radiologist and were categorized as consistent with or inconsistent with PPFE according to criteria described previously.[5] Cases were categorized as consistent with PPFE if (1) there was pleural thickening with associated subpleural fibrosis predominantly in the dorsal lung or (2) there was dorsal lung pleural thickening and associated subpleural fibrosis, but the distribution of fibrosis was not concentrated in the dorsal lung or coexistent lung disease was evident elsewhere. Inconsistent with PPFE was assigned to lungs that lacked these features. Overall, cases were assigned as PPFE-like only if categorized as consistent with PPFE on both imaging and histology.

PCR for Herpesviral Polymerase

Eight lung samples (four DPF, four control) collected into RNA*later* were processed using an AllPrep DNA/RNA Mini Kit (QIAGEN) according to the manufacturer's instructions. For investigation of the presence of herpesvirus, a region of the herpesvirus DNA polymerase gene was amplified using 100 ng DNA per reaction with two sets of nested degenerate primers as previously described.[8] PCR products were cloned into the TOPO TA vector (Invitrogen by Life Technologies) and sequenced (The GenePool), and BLASTn, version 2.6.2 (National Center for Biotechnology Information) was used to align derived sequences against known herpesvirus sequences.

Special Staining

Lung sections in which there was granulomatous inflammation were stained for acid-fast bacteria using a standard Ziehl-Neelsen stain and for fungal hyphae using Grocott's methenamine silver and periodic acid-Schiff stains.

X-ray Diffraction

Formalin-fixed wet lung tissue samples from four DPF ex vivo lungs were pooled, digested in potassium hydroxide, and prepared for mineral particle analysis under transmission electron microscopy at a magnification of 20,000 and for energy-dispersive x-ray analysis. The mass of dust per gram of dry lung tissue was

Manuscript received June 5, 2013; revision accepted December 28, 2013; originally published Online First March 6, 2014.
Affiliations: From the Medical Research Council Centre for Inflammation Research (Drs Miele, K. Dhaliwal, and Hirani and Prof Haslett), Queen's Medical Research Institute, and Royal (Dick) School of Veterinary Studies and The Roslin Institute (Drs Smith and Schwarz and Prof McGorum), University of Edinburgh, Edinburgh, Scotland; The Donkey Sanctuary (Drs Du Toit and Brooks), Sidmouth, Devon, England; and Department of Radiology (Dr Murchison) and Department of Pathology (Drs C. Dhaliwal and Wallace), New Edinburgh Royal Infirmary, Edinburgh, Scotland.
Drs Miele, K. Dhaliwal, and Wallace and Prof McGorum contributed equally.
Part of this article was presented in abstract form at the British Society of Animal Science Annual Meeting, April 16-17, 2013, Nottingham, England, and at the 7th Joint Meeting of the British Division of the International Academy of Pathology and the Pathological Society of Great Britain & Ireland, June 18-21, 2013, Edinburgh, Scotland.
Funding/Support: This study was funded by the Medical Research Council (MR/J014702/1).
Correspondence to: Bruce C. McGorum, BVM&S, PhD, The Royal (Dick) School of Veterinary Studies and Roslin Institute, University of Edinburgh, Easter Bush, Midlothian, Scotland, EH259RG; e-mail: bruce.mcgorum@ed.ac.uk

DOI: 10.1378/chest.13-1306

Table 1—*Classification of Ex Vivo Donkey Lungs*

Case No.	Imaging Type	Imaging Classification	Histology Classification	Overall Classification
1	HRCT	Inconsistent	Inconsistent	Inconsistent
2	HRCT	Consistent	Inconsistent	Inconsistent
3	HRCT	Consistent	Consistent	Consistent
4	HRCT	Consistent	Consistent	Consistent
5	HRCT	Consistent	Consistent	Consistent
6	HRCT	Consistent	Consistent	Consistent
7	HRCT	Consistent	Consistent	Consistent
8	HRCT	Inconsistent	Inconsistent	Inconsistent
9	HRCT	Consistent	Consistent	Consistent
10	HRCT	Consistent	Consistent	Consistent
11	Digital	Inconsistent	Inconsistent	Inconsistent
12	HRCT	Consistent	Inconsistent	Inconsistent
13	Digital	Consistent	Consistent	Consistent
14	Digital	Consistent	Inconsistent	Inconsistent
15	Digital	Consistent	Inconsistent	Inconsistent
16	Digital	Consistent	Consistent	Consistent
17	Digital	Consistent	Inconsistent	Inconsistent
18	Digital	Consistent	Consistent	Consistent
19	Digital	Inconsistent	Inconsistent	Inconsistent

HRCT = high-resolution CT.

established. Both fibrous and nonfibrous particles were counted and typed.

Results

Ages were not significantly different between DPF (median, 31 years; range, 14-53 years) and control (median, 28 years; range, 4-36 years) donkeys at necropsy (Mann-Whitney $P > .05$). The average donkey lifespan is 30 years. Donkeys comprised 12 neutered males and 20 females (e-Table 1).

Ten of 19 DPF lungs were categorized as being PPFE-like, having features consistent with PPFE on both pathology (Table 1) and imaging (seven on HRCT scan and three on photographed images of sectioned lungs). All 10 PPFE-like lungs had grossly visible visceral pleural fibrosis on the dorsal/costal surface, with no involvement of the parietal pleura. This was characterized by multifocal-to-coalescing vermiform cream/gray lesions that caused visible restriction of pleural expansion on manual lung inflation (Fig 1, e-Fig 1). Because donkeys are quadrupeds, the dorsal lung equates to the human lung upper zone. Histologically, all 10 PPFE-like lungs had dorsal pleural and subpleural fibrosis, with subpleural intraalveolar fibrosis and elastosis evident on EVG-stained sections (Figs 2A-D). Spatial heterogeneity was a consistent feature, often with a sharp interface between fibrotic and adjacent normal tissue (Fig 2E). Other common features (Table 2) included septal and bronchiolocentric fibrosis, lymphoplasmacytic bronchiolitis, granulomatous inflammation, and vascular remodeling within areas of fibrosis (Figs 2F-H). Honeycombing and fibroblastic foci were not detected, although myofibroblasts were demonstrated within fibrotic lesions through α-smooth muscle actin immunohistochemistry (e-Fig 2).

All seven PPFE-like lungs imaged by HRCT scan had pleuroparenchymal thickening (maximum, 5-32 mm) of the dorsal lung lobes, with associated subpleural

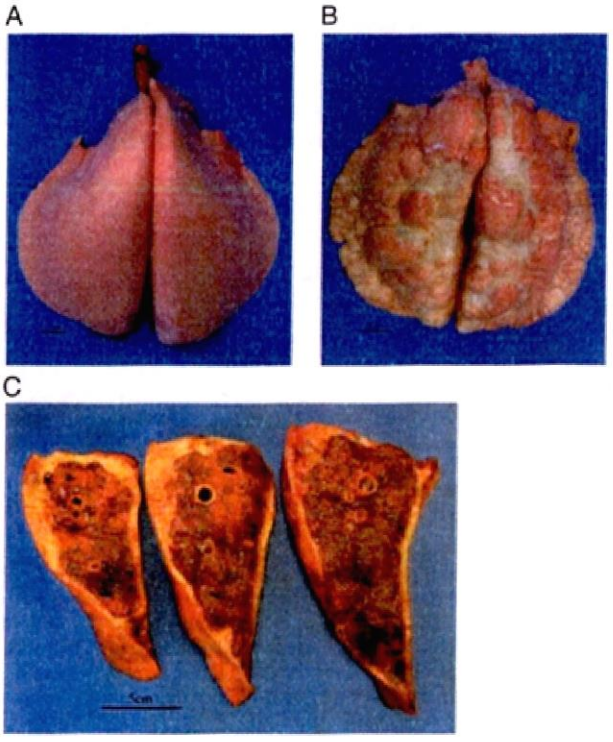

FIGURE 1. A and B, Photographs of the dorsal (uppermost) surface of inflated ex vivo control (A) and pleuroparenchymal fibroelastosis-like (B) lungs. C, Where high-resolution CT scan was not available, lungs were sectioned vertically prior to digital imaging. Note the extensive dorsal pleural fibrosis in B and C.

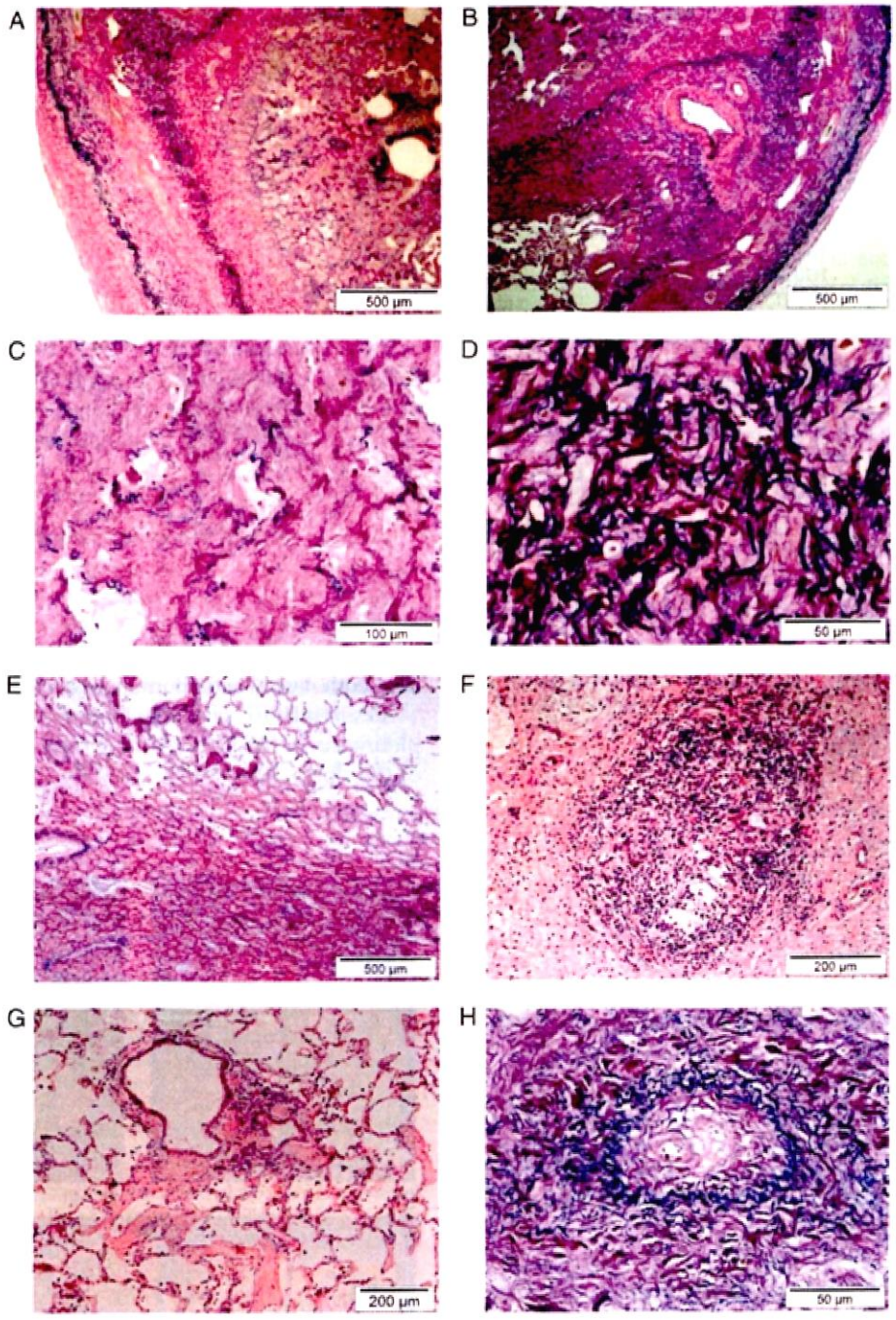

FIGURE 2. Histology images of sections from pleuroparenchymal fibroelastosis (PPFE)-like donkey lungs. A, Pleural and subpleural fibrosis with alveolar septal elastosis and intraalveolar fibrosis (elastic Van Gieson [EVG]). B, Disarray of the pleural elastin with a band of fibrosis extending from the subpleura along an interlobular septum (EVG). C, Higher-powered view of an area of intraalveolar fibrosis (EVG). D, High-power view of an area of diffuse elastosis (EVG). E-H, Other common histologic features of the PPFE-like ex vivo donkey lungs include spatial heterogeneity (EVG) (E), aggregates of mononuclear inflammatory cells (hematoxylin and eosin [H&E]) (F), bronchiolocentric inflammation and fibrosis (H&E) (G), and intimal fibrosis and elastosis of entrapped vessels (EVG) (H). I and J, Sections of donkey pulmonary fibrosis tissue classified as inconsistent with PPFE (H&E), demonstrating intraalveolar inflammation and fibrin deposition (I) and fibrosis of the alveolar walls with conservation of alveolar architecture (J).

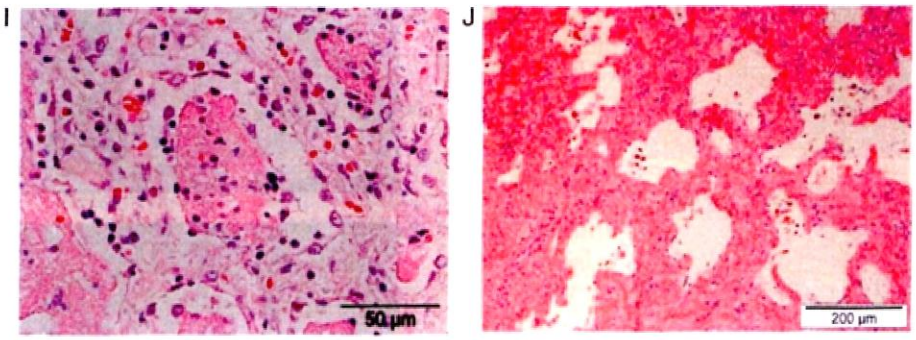

FIGURE 2. Continued.

consolidation consistent with established fibrosis. The consolidation extended from the subpleural region along parenchymal bands (Fig 3). In two of the seven lungs, the fibrosis was relatively superficial and confined solely to the uppermost zones of the dorsal lung surface. The other five cases had consolidation extending along parenchymal bands into mid and ventral zones that often radiated out to surround adjacent bronchi. Features of coexistent disease identified on HRCT scan included primary bronchiectasis and ground glass opacity. Traction bronchiectasis was present to varying degrees in all seven cases (Table 2). Ground glass change was a feature in four of the seven PPFE-like lungs, although some of this was attributed to collapse of dependent parenchyma in the inflated ex vivo tissue, a feature also noted in three of the seven control lungs.

All nine DPF lungs classified as inconsistent with PPFE on histology had pleural, subpleural, or septal fibrosis in at least one section. In four of these lungs, the fibrosis was focused around alveolar walls, with similarities to a nonspecific interstitial pneumonia-type pattern (Fig. 2I, 2J). Importantly, all nine lungs lacked the intraalveolar fibrosis previously reported to be a feature of PPFE,[5] but the majority (seven) had marked intraalveolar mononuclear cell infiltrates with fibrin deposition.

Four of the 19 lungs were classified as inconsistent with PPFE on imaging (two on HRCT scan and two on photographic imaging). Two of these had small amounts of dorsal pleural and subpleural fibrosis that were either asymmetric or considered not to be a predominant feature. One had a predominantly ventral distribution of fibrosis, whereas the other showed diffuse ground glass opacity (Fig 4).

Acid-fast bacteria and fungi were not identified with special staining. Herpesviral sequences were identified in six of eight lung homogenates, with five mapping to asinine herpesvirus (AsHV)-5 and one to AsHV-4. X-ray diffraction analysis revealed a dust burden of 6.98 mg/g dry lung. Small numbers of fibrous particles were identified (talc, 0.28 million fibers/g dry lung; silica, 0.14 million fibers/g dry lung). The percentages of nonfibrous particles were calcium silicate, 95%; potassium silicate, 2%; kaolin, 1%; muscovite, 1%; and silica, 1%. No asbestos fibers were found.

DISCUSSION

To our knowledge, this study is the most comprehensive of a spontaneous large animal model of pulmonary fibrosis to date. Although the donkey may seem an implausible candidate with which to share

Table 2—*Frequency of Imaging and Histologic Features Identified in Ex Vivo PPFE-Like Donkey Lungs*

Imaging		Histology	
Feature	Frequency	Feature	Frequency
Pleuroparenchymal thickening predominant in upper zones	10 of 10	Pleural and subpleural fibrosis with intraalveolar fibrosis and elastosis in dorsal lung sections	10 of 10
Subpleural fibrosis	10 of 10	Interlobular septal fibrosis	10 of 10
Ventral fibrosis	7 of 10	Bronchocentric fibrosis	8 of 10
Parenchymal bands	7 of 7	Lymphoplasmacytic bronchiolitis	10 of 10
Traction bronchiectasis	7 of 7	Venous and arterial intimal fibrosis	9 of 10
Ground glass opacity	4 of 7	PPFE pattern in ventral lobe biopsy specimens	2 of 6
Bronchocentric consolidation	5 of 7	Granulomatous inflammation	3 of 10
		Pleural ossification/calcification	1 of 10

PPFE = pleuroparenchymal fibroelastosis.

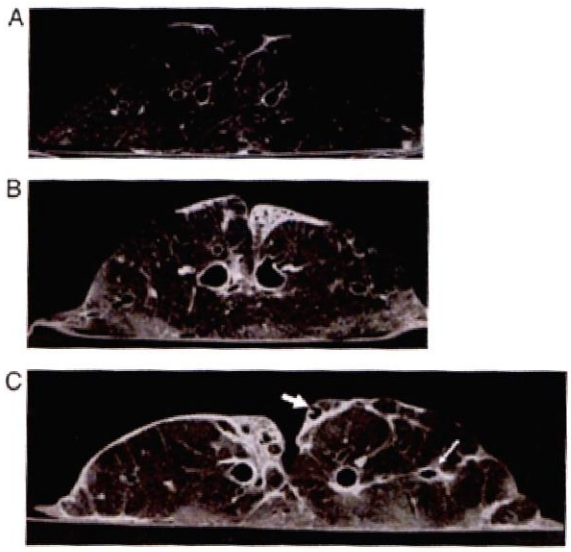

FIGURE 3. Craniocaudal high-resolution CT images of PPFE-like inflated ex vivo donkey lungs. A-C, Pathology ranged from mild dorsal pleural fibrosis extending along parenchymal bands (A) to thick rinds of pleural fibrosis encasing the dorsal surface of the lung (B and C). Also note the traction bronchiectasis (large arrow) and bronchocentric fibrosis (small arrow). See Figure 2 legend for expansion of abbreviation.

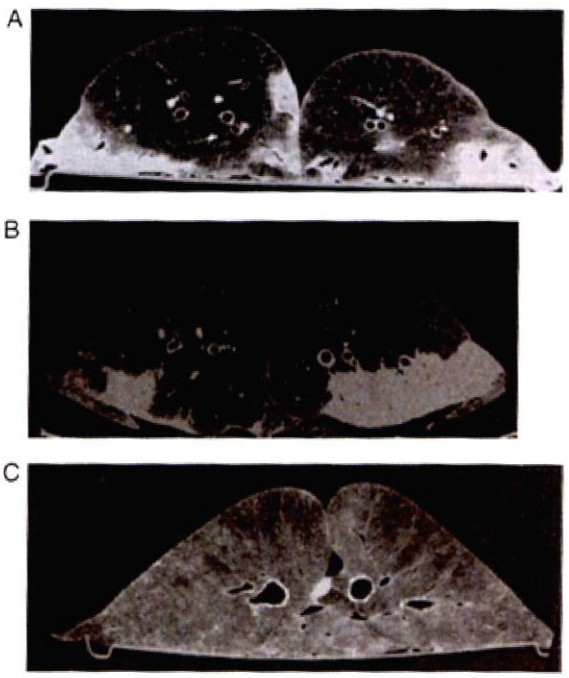

FIGURE 4. High-resolution CT images of fibrotic inflated ex vivo donkey lungs classified as inconsistent with PPFE on both imaging and histology. A and B, These images show a predominantly ventral distribution to the fibrosis. C, Image demonstrates diffuse ground glass change. See Figure 2 legend for expansion of abbreviation.

pathologic features of pulmonary disease, of all the domestic species, the subgross anatomy of the equine lung and visceral pleura most closely resembles that of humans.[9]

DPF was first reported as a common incidental necropsy finding of donkeys resident at a donkey sanctuary in 2001.[10] Reported gross and histopathologic findings were consistent with those for the current study, including a wide spectrum of pleural, subpleural, and septal fibrosis extending into the interstitium of dorsal lung fields, with more diffuse and ventral changes in severely affected cases. Peribronchial cuffing and multifocal aggregates of mononuclear cells were also described.[10] However, the presence of intraalveolar fibrosis and alveolar septal elastosis was not reported, probably because these features are less striking in the absence of EVG staining. It should be noted that fibroblastic foci and honeycombing are not features of DPF.

In the current study, >50% of donkeys with DPF shared key imaging and pathologic characteristics of human PPFE. DPF lungs were classified as PPFE-like only if they had features considered consistent with PPFE[3] on both histology and imaging. In this respect, a greater proportion of DPF lungs were classified as consistent with PPFE on HRCT scan (82%) compared with histology (58%). It is possible that some of the nine lungs classified as inconsistent with PPFE on histology represent an earlier stage of PPFE-like disease. Seven of these had intraalveolar mononuclear inflammatory infiltrates with organizing intraalveolar fibrin, which is a likely prelude to intraalveolar fibrosis (Fig 2I). Furthermore, the marked spatial heterogeneity in extent and pattern of fibrosis means that PPFE-like pathology may have been missed as a result of unrepresentative sampling in some cases.

Imaging of PPFE-like lungs indicated that although all had the characteristic predominantly dorsal distribution of lesions, seven of the 10 lungs also had pleural and subpleural fibrosis in the mid and ventral pulmonary parenchyma. Similarly, Reddy et al[5] reported that six of 12 PPFE lungs had interstitial lung disease in lobes distant from the upper zone on HRCT scan. Furthermore, six of the 12 PPFE lungs had areas of consolidation, and one of the 12 had bronchiectasis. In the present study, HRCT scans showed ground glass opacity in four of seven PPFE-like lungs and traction bronchiectasis in all seven. The presence of bronchocentric consolidation on HRCT images of five of these seven lungs further supports the proposal that chronic airway disease could be key to PPFE pathogenesis.[5] Bronchocentric changes were also evident histologically, with all 10 PPFE-like lungs having variable lymphoplasmacytic bronchiolitis and eight of the 10 having areas of bronchocentric fibrosis. A patchy lymphoplasmacytic infiltrate was a feature in patients with PPFE reported by Frankel et al,[3] whereas Reddy et al[5] found bronchocentric fibrosis in 11 of 12 patients with PPFE, with all 12 having

focal nonspecific chronic inflammation with lymphoid follicle accumulation.

Other features of PPFE shared by donkey PPFE-like lungs included perilobular fibrosis (all 10) and venous and arterial intimal fibrosis (nine of 10).[5,11] Vascular changes in donkey lungs were considered to reflect secondary intimal invasion by the surrounding fibrosis rather than a primary vasculopathy. Although granulomatous inflammation is not a key accepted feature of PPFE, it has been detected in patients with PPFE[5] and was an additional feature of three of the 10 PPFE-like lungs in the current study. However, mycobacteria and fungi were not identified in the granulomatous lesions. Pleural fibrosis is a feature of asbestos-induced pulmonary fibrosis[12] in humans. Inorganic fiber content of the ex vivo donkey lung tissue was minimal, and there was no evidence of asbestos fibers. The presence of nonfibrous dust particles, such as calcium silicate, was unsurprising considering the grazing habits of donkeys and likely reflected local soil composition. Potential toxicity of calcium silicate is believed to be minimal,[13] and the dust burden of ex vivo donkey tissue was not considered to be significant.

The significance of elastosis within fibrotic donkey tissue is unclear. Elastosis and upregulation of elastin gene expression occurs in a murine model of pulmonary fibrosis,[14] and in humans, progressive vascular fibroelastosis occurs in idiopathic interstitial pneumonias and correlates with a poor prognosis in usual interstitial pneumonia.[15] An overall increase in both collagen and elastin with alveolar septal elastosis has been documented during the late phase of ARDS and in usual interstitial pneumonia.[16]

Reddy et al[5] reported that seven of 12 patients with PPFE had a history of recurrent lower respiratory tract infections, leading these authors to postulate the contribution of such infections to the pathogenesis of PPFE. Further investigation is required to determine whether donkeys with PPFE-like disease had preceding recurrent lower respiratory tract infections (e-Table 1, e-Fig 1).

In the horse, a progressive fibrosing interstitial lung disease termed "equine multinodular pulmonary fibrosis" is associated with equine herpesvirus 5 infection.[17] Similarly, AsHV-4 and AsHV-5 were implicated in an acute fibrosing interstitial pneumonia in 11 donkeys in North America and in a pyogranulomatous pneumonia in a mare.[5,18] Kleiboeker et al[8] described multifocal-to-coalescing nodules of fibrosis scattered throughout the lung parenchyma in the most severely affected of the 11 donkeys, a pattern similar to that seen in equine multinodular pulmonary fibrosis and quite different from the pathology described herein for DPF. Kleiboeker et al[8] also detected herpesviral DNA in lung homogenate in all 11 affected donkeys but not in six control animals, which differs from the current findings that lung homogenates from all DPF and control donkeys were positive for AsHV-4 or AsHV-5. The role of AsHV-4 and AsHV-5 in DPF warrants further study.

In conclusion, >50% of donkeys with DPF in this study shared key imaging and pathologic characteristics of human PPFE, a rare and usually idiopathic interstitial pneumonia.[4] Hence, the donkey may provide a unique progressive model in which to study PPFE. The ubiquitous presence of γ-herpesvirus in the study population of donkeys warrants further investigation regarding its potential role in the etiology of DPF.

ACKNOWLEDGMENTS

Author contributions: Drs Miele, K. Dhaliwal, and Wallace and Prof McGorum had full access to all of the data in the study and take responsibility for the integrity of the data and the accuracy of the data analysis.
Dr Miele: contributed to the data collection and writing of the manuscript.
Dr K. Dhaliwal: contributed to the study concept, overall guidance, and writing of the manuscript.
Dr Du Toit: contributed to the tissue collection and review of the manuscript for important intellectual content.
Dr Murchison: contributed to the imaging data description, assessment, and scoring and review of the manuscript for important intellectual content.
Dr C. Dhaliwal: contributed to the scoring of histology data and review of the manuscript for important intellectual content.
Dr Brooks: contributed to the tissue collection and review of the manuscript for important intellectual content.
Dr Smith: contributed to the histology description and review of the manuscript for important intellectual content.
Dr Hirani: contributed to the review of the manuscript for important intellectual content.
Dr Schwarz: contributed to the HRCT scanning and review of the manuscript for important intellectual content.
Prof Haslett: contributed to the review of the manuscript for important intellectual content.
Dr Wallace: contributed to the study concept; histology data description, assessment, and scoring; and review of the manuscript for important intellectual content.
Prof McGorum: contributed to the study concept, overall guidance, and writing of the manuscript.
Financial/nonfinancial disclosures: The authors have reported to *CHEST* that no potential conflicts of interest exist with any companies/organizations whose products or services may be discussed in this article.
Role of sponsors: The sponsor had no role in the design of the study, the collection and analysis of the data, or the preparation of the manuscript.
Other contributions: The authors thank R. Dalziel, BSc, PhD, The Roslin Institute & R(D)SVS, University of Edinburgh, for performing DNA extraction and herpesviral PCR; A. R. Gibbs, MBChB, Environmental Lung Disease Research Group, University Hospital Llandough, Penarth, for performing x-ray diffraction analysis; and the Clinical Research Imaging Centre, University of Edinburgh, for conducting HRCT scans.
Additional information: The e-Appendix, e-Figures, and e-Table can be found in the "Supplemental Materials" area of the online article.

REFERENCES

1. Chua F, Gauldie J, Laurent GJ. Pulmonary fibrosis: searching for model answers. *Am J Respir Cell Mol Biol*. 2005;33(1):9-13.

2. Williams K, Malarkey D, Cohn L, Patrick D, Dye J, Toews G. Identification of spontaneous feline idiopathic pulmonary fibrosis: morphology and ultrastructural evidence for a type II pneumocyte defect. *Chest*. 2004;125(6):2278-2288.
3. Frankel SK, Cool CD, Lynch DA, Brown KK. Idiopathic pleuroparenchymal fibroelastosis: description of a novel clinicopathologic entity. *Chest*. 2004;126(6):2007-2013.
4. Travis WD, Costabel U, Hansell DM, et al; ATS/ERS Committee on Idiopathic Interstitial Pneumonias. An official American Thoracic Society/European Respiratory Society statement: update of the international multidisciplinary classification of the idiopathic interstitial pneumonias. *Am J Respir Crit Care Med*. 2013;188(6):733-748.
5. Reddy TL, Tominaga M, Hansell DM, et al. Pleuroparenchymal fibroelastosis: a spectrum of histopathological and imaging phenotypes. *Eur Respir J*. 2012;40(2):377-385.
6. Morrow LD, Smith KC, Piercy RJ, et al. Retrospective analysis of post-mortem findings in 1,444 aged donkeys. *J Comp Pathol*. 2011;144(2-3):145-156.
7. Williams KJ, Derksen FJ, de Feijter-Rupp H, Pannirselvam RR, Steel CM, Robinson NE. Regional pulmonary veno-occlusion: a newly identified lesion of equine exercise-induced pulmonary hemorrhage. *Vet Pathol*. 2008;45(3):316-326.
8. Kleibocker SB, Schommer SK, Johnson PJ, et al. Association of two newly recognized herpesviruses with interstitial pneumonia in donkeys (*Equus asinus*). *J Vet Diagn Invest*. 2002;14(4):273-280.
9. McLaughlin RF Jr, Tyler WS, Canada RO. Subgross pulmonary anatomy in various mammals and man. *JAMA*. 1961;175(8):694-697.
10. Thiemann A, Bell N. The peculiarities of donkey respiratory disease. In: Lekeux P, ed. *Equine Respiratory Disease* [serial online]. International Veterinary Information Service website. http://www.ivis.org/special_books/Lekeux/bell/ivis.pdf. Accessed January 20, 2011.
11. Piciucchi S, Tomassetti S, Casoni G, et al. High resolution CT and histological findings in idiopathic pleuroparenchymal fibroelastosis: features and differential diagnosis. *Respir Res*. 2011;12:111.
12. Bergin CJ, Castellino RA, Blank N, Moses L. Specificity of high-resolution CT findings in pulmonary asbestosis: do patients scanned for other indications have similar findings? *AJR Am J Roentgenol*. 1994;163(3):551-555.
13. Bolton RE, Addison J, Davis JM, et al. Effects of the inhalation of dusts from calcium silicate insulation materials in laboratory rats. *Environ Res*. 1986;39(1):26-43.
14. Hoff CR, Perkins DR, Davidson JM. Elastin gene expression is upregulated during pulmonary fibrosis. *Connect Tissue Res*. 1999;40(2):145-153.
15. Parra ER, Kairalla RA, de Carvalho CRR, Capelozzi VL. Abnormal deposition of collagen/elastic vascular fibres and prognostic significance in idiopathic interstitial pneumonias. *Thorax*. 2007;62(5):428-437.
16. Negri EM, Montes GS, Saldiva PH, Capelozzi VL. Architectural remodelling in acute and chronic interstitial lung disease: fibrosis or fibroelastosis? *Histopathology*. 2000;37(5):393-401.
17. Williams KJ, Maes R, Del Piero F, et al. Equine multinodular pulmonary fibrosis: a newly recognized herpesvirus-associated fibrotic lung disease. *Vet Pathol*. 2007;44(6):849-862.
18. De Witte FG, Frank N, Wilkes RP, Novak JM. Association of asinine herpesvirus-5 with pyogranulomatous pneumonia in a mare. *J Vet Intern Med*. 2012;26(4):1064-1068.

Optical molecular imaging of lysyl oxidase activity – detection of active fibrogenesis in human lung tissue

Tashfeen Aslam,[a#] Amy Miele,[b#] Sunay V. Chankeshwara,[a#] Alicia Megia-Fernandez,[a] Chesney Michels,[b] Ahsan R Akram,[b] Neil McDonald,[b] Nik Hirani,[b] Chris Haslett,[b] Mark Bradley,[a*] Kevin Dhaliwal.[b*]

Aberrant fibrogenesis is a feature of many diseases in multiple organ systems. The lysyl oxidase family of enzymes are central to tissue homeostasis and elevated lysyl oxidase activity is implicated in fibroproliferation as well as in cancer stroma. We have synthesised a novel fluorogenic reporter for monitoring lysyl oxidase activity that generates a 3-5 fold increase in fluorescence following probe activation in ventilating fibrotic *ex vivo* asinine lung and *ex vivo* human lung tissue. The probe termed "oLOX" can provide real-time measurement of lysyl oxidase activity in a number of biological settings and is tractable from *in vitro* setting to man.

Introduction

Aberrant fibrogenesis is a feature of many diseases in multiple organ systems and is characterised by tissue injury, remodelling and incomplete repair resulting in the excessive deposition of collagen.[1,2] Fibrogenesis is a prominent feature of several lung diseases ranging from adult respiratory distress syndrome in intensive care to chronic obstructive pulmonary disease and interstitial lung diseases.[3] The global impact of these diseases is huge, causing significant financial burden.[4] Despite this, treatment options are very limited and monitoring of disease progression remains a challenge, as there are no rapid bedside biomarkers that can detect active fibroproliferation. Blood biomarkers offer poor molecular specificity for lung pathology, while pulmonary biopsy is invasive and fixed tissue cannot inform on the dynamic enzyme activity that exists *in vivo*.[5]

The Lysyl oxidases are copper dependent amine oxidases that play a central role in fibrogenesis.[6] They facilitate the covalent cross-linking found within elastin and collagen by catalysing the oxidative deamination of peptidyl-lysine and hydoxylysine residues, a step that is crucial to the mature and functional extracellular matrix.[7–9] There are five proteins within the lysyl oxidase family (LOXF): LOX, LOXL1 (Lysyl oxidase like- one), LOXL2, LOXL3 and LOXL4, all of which share the same enzymatically active C-terminus and the cofactor lysine tyrosylquinone.[10,11] A by-product of all of these enzymes is hydrogen peroxide. Lysyl oxidases are important in cancer progression and in many fibrotic diseases including those affecting the lung.[12–15] Of the 5 members of the LOXF, two in particular have been the basis of extensive investigation and therapeutic targeting: LOX and LOXL2. LOX expression correlates with poor survival and is a therapeutic target for patients with certain cancers,[14] while LOXL2 is a focus in the monitoring and treatment of fibrotic lung disease.[15,16]

As the potential for the lysyl oxidases as therapeutic targets becomes clear, there is a discernible need for the development of selective and sensitive oxidase substrates to monitor enzymatic activity in complex biological systems. As a result, fluorescence-based analysis methods have attracted much attention as they can provide simple, effective and powerful tools[17] for real-time monitoring of LOX enzyme activities *in vitro* and *in vivo*.[18–20] Until recently, such reporters have been designed either on a coumarin[21,22] or resorufin[23] scaffold and are based on a single amine oxidation/β-elimination resulting in an amplification of fluorescent signal. However, the excitation wavelength for coumarin (λex 360nm) limits its applicability for cellular-based imaging. Amplex red (*N*-acetyl-3,7-dihydroxyphenoxazine) is a non-fluorescent derivative of dihydroresorufin that is converted to fluorescent resorufin on reaction with hydrogen peroxidase.[24,25] This reagent has been utilised in a number of settings including the quantification of neutrophil NADPH oxidase, monamine oxidase (MAO), glucose oxidase and LOX.[19,24,25] While providing a sensitive method for the detection of hydrogen peroxide[26], Amplex red is non-specific and clearly cannot be used *in vivo* or in cells.[19]

In a recent publication, Li et al reported a probe for the fluorometric detection of monoamine oxidases A and B *in vitro*. The probe was synthesised over 5 steps using the familiar and inexpensive dye, fluorescein **3**. While utilising the amine oxidation/β-elimination mechanism in the presence of MAO-A and B, the fluorescent reporter probe was methyl fluorescein, a dye with a lower quantum yield than **4**.[27] In order to develop a probe for demonstrating the activity of LOXF *in vivo*, a reporter probe with higher quantum yield was required. Herein, we report the synthesis and *ex vivo* biological evaluation of an easily synthesised activity-based fluorescent probe for LOXF that utilises a fluorescein scaffold.

To validate the activation of the optical LOXF probe (oLOX) **1** in the presence of LOX, selective inhibition was desired. β-Aminopropionitrile (BAPN) has been extensively used as the reference LOX inhibitor, with a reported IC_{50} of 10 μM.[28] Though BAPN is widely used as a specific irreversible inhibitor of LOX, it does have affinity for other oxidases,[29,30] indeed its structure suggests non-specificity. Over the last two decades selective inhibitors of LOX, as anti-fibrotic agents, have been developed.[31, 32, 33, 34, 35] Of these the pyridazinone-based class are among the most potent (IC_{50} 0.005-0.07μM)[36]. Compounds **10**

(IC_{50} 3nM)[37] and **11** were thus synthesized for application in inhibition studies.
oLOX was evaluated for LOX activity in freshly isolated human lung tissue, showing for the first time, the ability to measure the dynamic activity of LOXF with optical detection in this model and the potential for *in vivo* utility.

Results and discussion

Synthesis of optical LOXF probes

The chemical "masking" of the phenol groups of fluorescein can suppress fluorescence and facilitate cell permeability.[38,39] In
this investigation, both phenolic groups of **3** were selectively alkylated with aminopropyl moieties, it being hypothesised that upon treatment of oLOX **1** with the appropriate oxidases, the two amino groups would be oxidised to give the bis-aldehyde **2** followed by dual *β*-elimination to release acrolein and fluorescein **4** (Scheme 1a).

The synthesis of oLOX **1** was complicated due to the nature of xanthene dyes such as fluorescein, which exists in either of the two forms, the quinoid **4** and/or lactone **3** form, depending on the pH and solvent environment.[40] The fluorescent, xanthen-3-one tautomer form, is favoured in non-acidic aqueous solutions; whereas a non-fluorescent, lactone tautomer **3**, is favoured at acidic pH's or in non-aqueous solvents. Typically alkylation of fluorescein gives the dual ether/ester (**6**) as the major product, rather than the bis-ether (**5**). To develop the optimal conditions to synthesise the desired bis-ether product **1**, reactions conditions were optimised looking various solvents and bases.[41] It is known that the use of heterogeneous Ag(I) salts favours the desired alkylation reaction over the acylation,[41] and the use of silver oxide in acetonitrile[42] with molecular sieves was effective for the synthesis of **5** in moderate yield (Scheme 1b). The aprotic solvent maintaining fluorescein in its closed form, with the crude reaction mixture affording **5** and **6** in 15% and 65% yields, respectively. **5** was non-fluorescent while quinoid **6** showed emission characteristics (λ_{max} = 520nm) of fluoresein. Treatment of **5** with hydrochloric acid in DCM/ether gave reporter **1** as its HCl salt in quantitative yield. As anticipated, the final probe had good aqueous solubility and was non-fluorescent.

The two specific and potent LOX inhibitors **10** and **11** were synthesised. **11** was designed based on structure activity relationship of similar inhibitors where the introduction of 4-(*p*-fluorophenyl)phenol significantly enhanced the potency of the inhibitor[32]. 2-phenyl-3(2*H*)-pyridazinones, were synthesised in two steps by condensation of mucochloric acid with aryl hydrazine to afford the dichloro pyrazone derivative **7**. In the next step, nucleophilic substitution with *N*-Boc piperazine derivative afforded **8**. Reaction of **8** with 4-phenylphenol or 4-(*p*-fluorophenyl)phenol and Boc deprotection afforded the inhibitors **10** and **11** in good yields (50-55%).

LOX and LOXL2 are expressed in human lung tissue

LOX is important in lung development and is expressed in normal lung tissue.[43,44] Pathological activity of LOXL2 has been shown by Barry-Hamilton *et al* with increased expression of LOXL2 in the lung tissue of patients with idiopathic pulmonary fibrosis (IPF),[15] while Chien *et al* found an association between serum LOXL2 levels and the progression of IPF.[16] Increased expression of LOX has also been well demonstrated in experimental models of pulmonary fibrosis.[45,46] Hence we wished in particular to begin evaluating our probe in the setting of human lung pathology.

The expression of LOX and LOXL2 was firstly confirmed in human lung tissue homogenates using western blot and immunohistochemistry. The 50kDa pro-LOX is secreted from cells then cleaved to the 32kDa mature protein by bone morphogenetic protein-1.[10] In this study we demonstrated the presence of the 50kDa pro-LOX protein and the active 32kDa LOX protein in human lung tissue as well as the enzymatically active 63kDa LOXL2 (Figure 1). Immunohistochemical data supported previous findings whereby LOX and LOXL2 were found to be expressed in lung tissue.[15] Since LOX and LOXL2 were expressed in human lung tissue, homogenised lung tissue was deemed an appropriate model to evaluate the utility of the activity-based sensor oLOX **1**.

*A) Activation of probe oLOXF **1** by LOX*

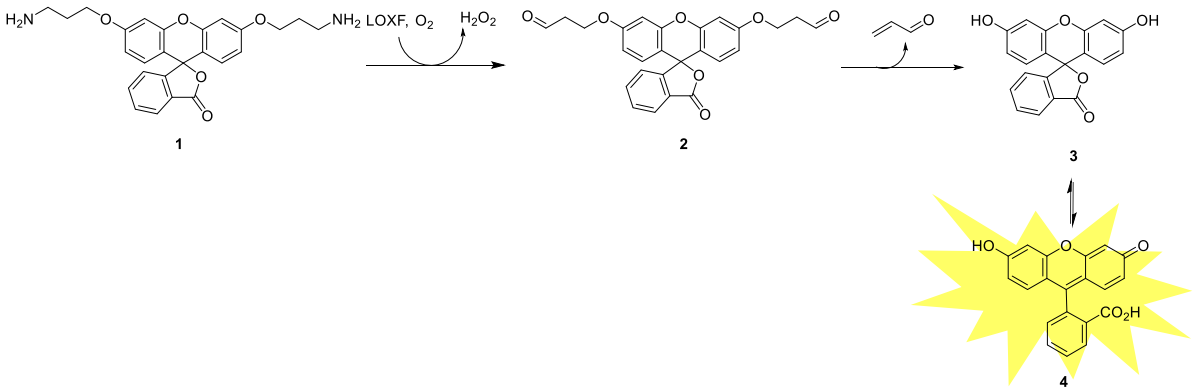

*B) Activity-based probe **1***

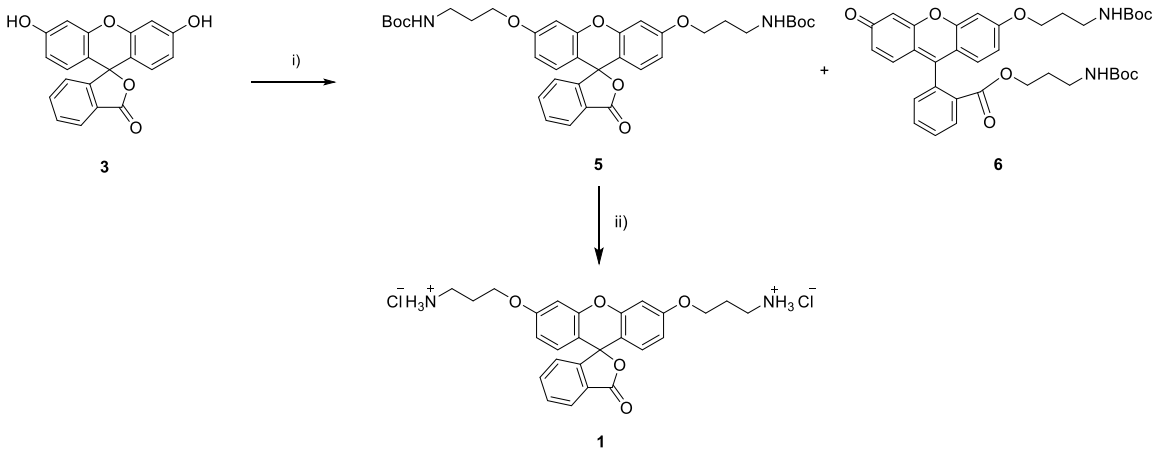

Scheme 1 A: Pathway for the fluorescence activation of probe oLOXF **1** by LOX. **B**: Synthetic route for oLOX, i) $Br(CH_2)_3NHBoc$, Ag_2O, MeCN, py, 4Å MS, 40°C, 48 h, **5** (15%) and **6** (65%); ii) HCl, DCM/ether, 2 h, 93%.

*LOX inhibitors **10** (Inh-1) and **11** (Inh-2)*

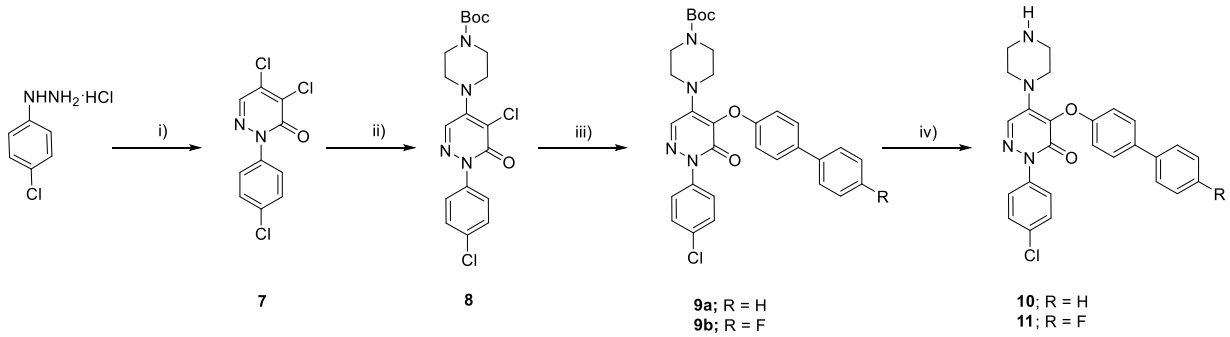

Scheme 2 Synthetic route to the LOX inhibitors. i) Mucochloric acid, 50% aq. MeOH, 3h, 60%; ii) *N*-Boc-piperazine, NaI, dioxane, 100 °C, 20 h, 70%; iii) bisphenol derivative, CuI, Cs_2CO_3, BINOL, dioxane reflux, 12h, 58-73%; iv) 20% TFA in DCM, 1 h, quantitative.

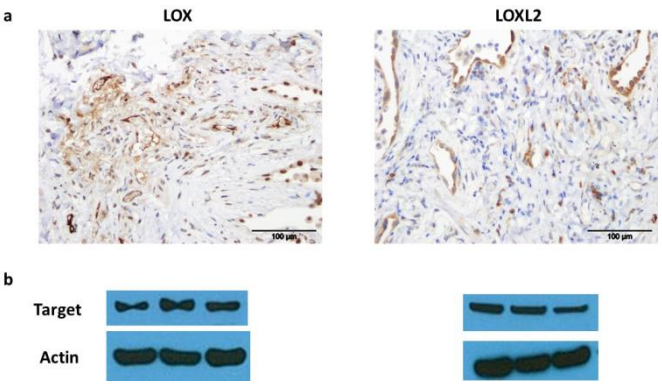

Fig. 1: LOX and LOXL2 are expressed in aged human lung tissue homogenates. (a). Immunohistochemical analysis and (b). western blot of LOX and LOXL2 expression in aged (55-81yr) human lung tissue. Strongest bands for LOX were at 50kDa, consistent with the glycosolated pro-lysyl oxidase, but mature 32kDa LOX was also present in several samples (ESI, Figure S1). Data representative of a minimum of 3 experimental replicates. Scale-bar = 100μm.

oLOXF detects increased LOXF activity in aged human tissue and is inhibited by selective inhibitors

Incubation of oLOX with tissue homogenate resulted in up to a 300% increase in fluorescence (Figure 2a). Importantly, oLOX activation was completely inhibited in a concentration dependent manner by pre-incubation of the homogenate with BAPN (Figure 2b) and the inhibitor **10** and **11** (Figure 2c and 2d). As predicted inhibitor **11** was a more potent inhibitor of probe activation (Figure 2d). Yang *et al* showed that BAPN was a time and temperature dependant irreversible inhibitor of LOX [47,48]. BAPN has been shown to inhibit LOXL1[49], LOXL3[50] and .LOXL4[51], but inhibition of LOXL2 by BAPN is more controversial with mixed reports of success.[26,52] We have shown that both active LOX and LOXL2 are present within the lung tissue homogenates and hypothesise that each of these enzymes contribute to the increase in fluorescent signal observed with our probe. While we have not investigated the expression of other members of the LOXF within the lung tissue, it is certainly possible that they are present at low levels and contribute to the fluorescent signal.

While a probe of related structure has previously been used to report on levels of MAO[27], the potential contribution of MAO to oLOX activation in human lung tissue was negated by the fact that clorgyline (a MAOA inhibitor) and pargyline (a MAOB inhibitor) did not cause any significant reduction in fluorescent signal (Figure 3). Furthermore, BAPN does not inhibit MAO[53], thus confirming that MAO does not cleave **1** in this model.

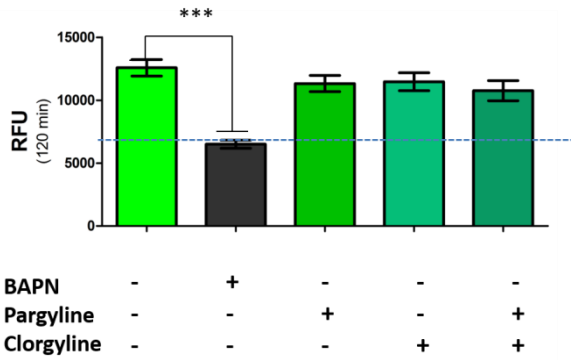

Fig. 3 oLOX is not activated by monoamine oxidases. Human lung homogenate was pre-incubated *(*in triplicate*)* with 500µM of BAPN, clorgyline and/or pargyline at 37°C for 1 hour prior to the addition of 10µM oLOX. The bar show the mean resultant fluorescence intensity after 2 hour incubations (n=3). ***p<0.001, one way ANOVA, dotted line represents background fluorescence of oLOX, error bars depict standard error of the mean.

Optical Molecular Imaging of LOX

Whilst fluorometric determination of LOX in human tissue has been demonstrated (Figure 2), the pivotal advance would be the dynamic imaging of LOX activity in tissue *in situ* without the need for homogenisation. This heralds the capability to perform optical molecular 'biopsies' *in situ* with optical molecular imaging techniques[5455]. Fibre confocal fluorescence microscopy (FCFM) allows a flexible optical fibre bundle to be passed down the working channel of an endoscope while utilising laser excitation at 488nm, allowing visualisation of lung elastin auto-fluorescence. FCFM has been successfully utilised in a number of organ systems including the pulmonary tract[56,57], where the autofluorescence of the elastin allows visualisation of tissue architecture. This approach allows the real-time *in vivo* visualisation of tissue at a cellular level and is a clinically applicable strategy.

Hence we evaluated oLOX **1** in conjunction with FCFM, as an optical molecular imaging strategy by applying oLOX to aged human lung tissue *ex vivo*. To demonstrate that the resultant increase in fluorescence detected by FCFM could be inhibited and prove the specificity of oLOX, we also incubated human lung tissue with BAPN (Figure 4).

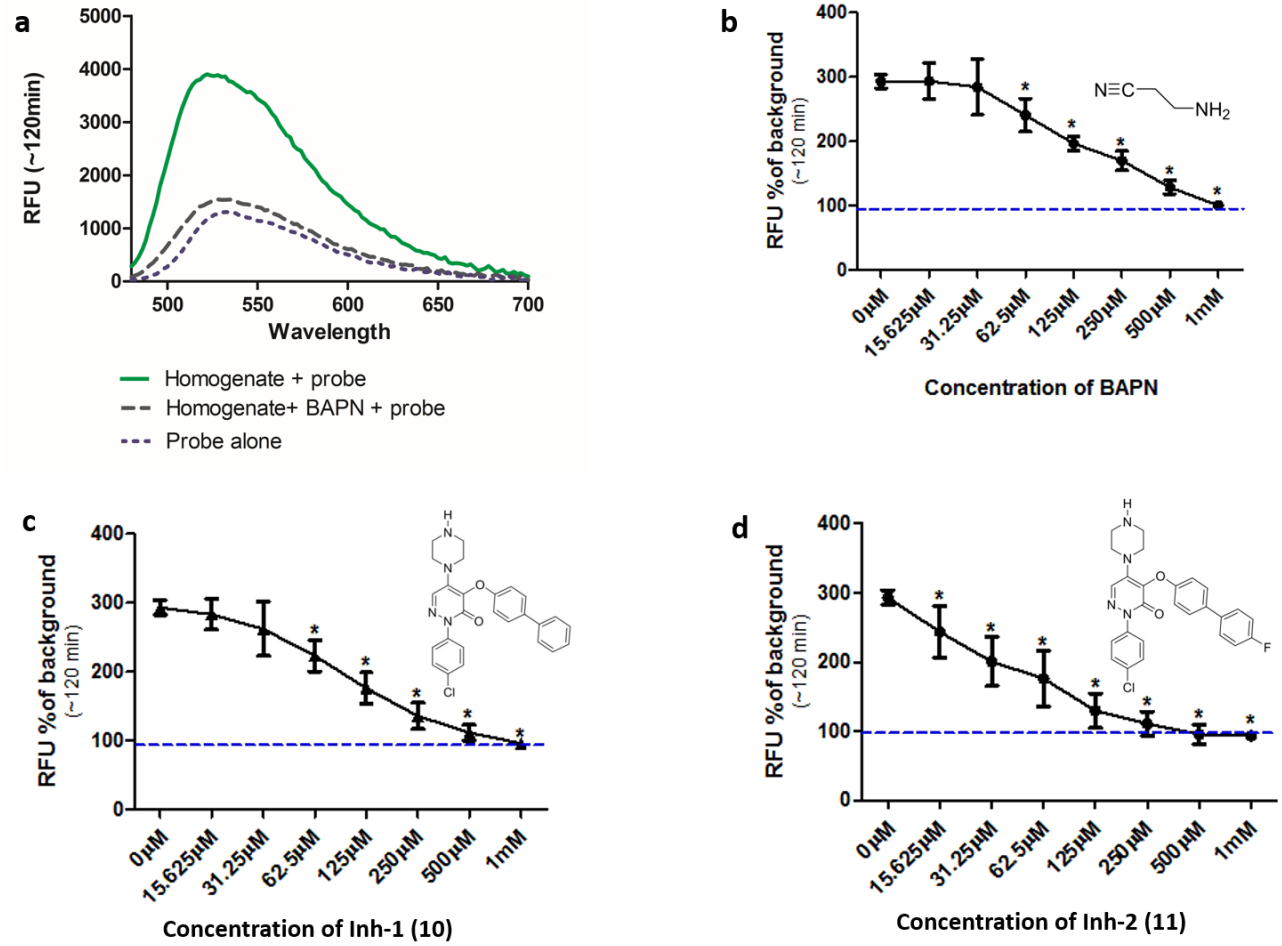

Fig. 2 oLOX is activated in the presence of aged human lung tissue homogenate as shown by an inhibitable increase in fluorescence. (a) Fluorescent intensity of 10μM oLOX after 2h incubation with aged human lung tissue homogenate (solid line). Spectra were recorded with λex =450nm. (b-d) Human lung homogenate was pre-incubated with dilutions of inhibitors at 37°C for 1h prior to the addition of 10μM oLOX. Each graph shows the resultant fluorescence presented as percentage above background after 1h incubation of the reaction (representative of n=3). The minimum concentration of BAPN (b) and Inh-1 (c) found to have a significant inhibitory effect was 62μM ($p<0.01$, one way ANOVA), whereas the minimum concentration of **Inh-2** (d) found to have a significant inhibitory effect was 15 μM ($p<0.01$, one way ANOVA). The dotted line represents background fluorescence of oLOX, error bars depict standard deviation.

Moving from sections of tissue (Figure 4) to whole organ imaging was the next challenge. Hence, in order to assess the utility of oLOX **1** *in situ*, a ventilating *ex vivo* asinine lung model was used (Figure 5 and ESI Figure S2). We have recently reported that aged donkeys suffer from a high prevalence of pulmonary fibrosis (35%), often resulting in euthanasia, which has been likened to a fibrotic interstitial lung disease of humans.[58] A whole donkey lung was thus used to assess the utility of combining FCFM with the local intrapulmonary delivery of oLOX. Utilising this size relevant and spontaneous model negated the need for an experimental model under the 3Rs (Replacement, Reduction and Refinement) ethos. A significant increase in fluorescent signal over background was detected following the installation of oLOX **1** into fibrotic regions of whole ventilating *ex vivo* asinine lung that were subsequently confirmed to express LOX (Figure 5c). The coupling of oLOX **1** with FCFM enables the minimally invasive visualisation of temporal and spatial alterations in the molecular activity of LOXF.

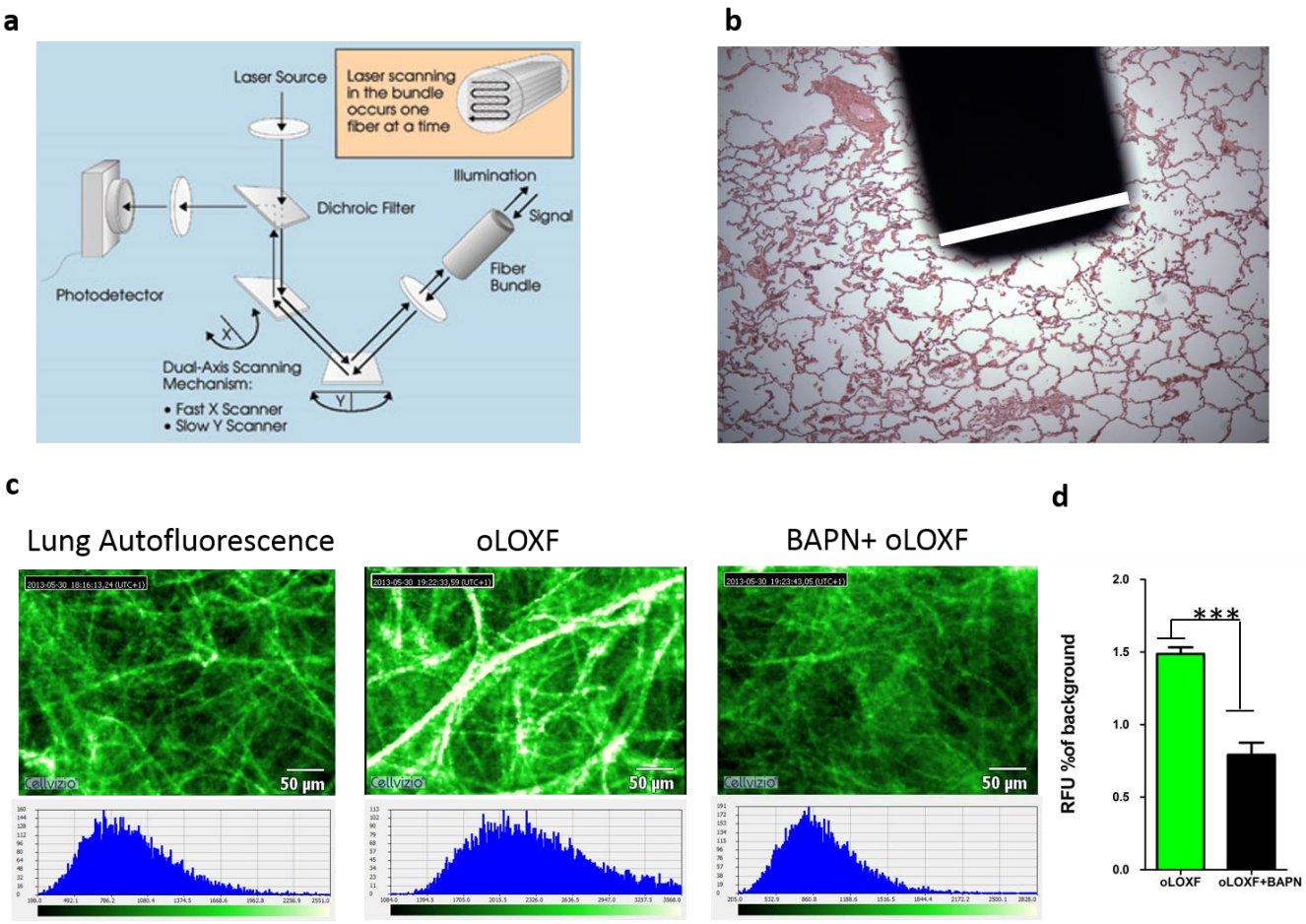

Figure 4: oLOX can be used alongside fibre confocal fluorescence microscopy (FCFM) to demonstrate oLOX activity in whole ex vivo human lung tissue. (a) Architecture of the FCFM (Cellvizio®-Lung System (Mauna Kea Technologies, Paris, France)[†] involving a fibre bundle and scanning confocal microscopy (b) The tip of the fibre optic is superimposed on a fixed lung tissue section with the white bar corresponding to the diameter of the fibre (1.4mm). (c) Representative single frame images generated by FCFM on fresh sections of aged human lung tissue following incubation with 10µM oLOX. The graph (d) represents the mean auto-fluorescence of each 60 second video imaging period adjusted for tissue auto-fluorescence (n=4). Note the significant reduction in fluorescence on incubation with the lysyl oxidase inhibitor, BAPN ($p = 0.0286$, Mann Whitney).

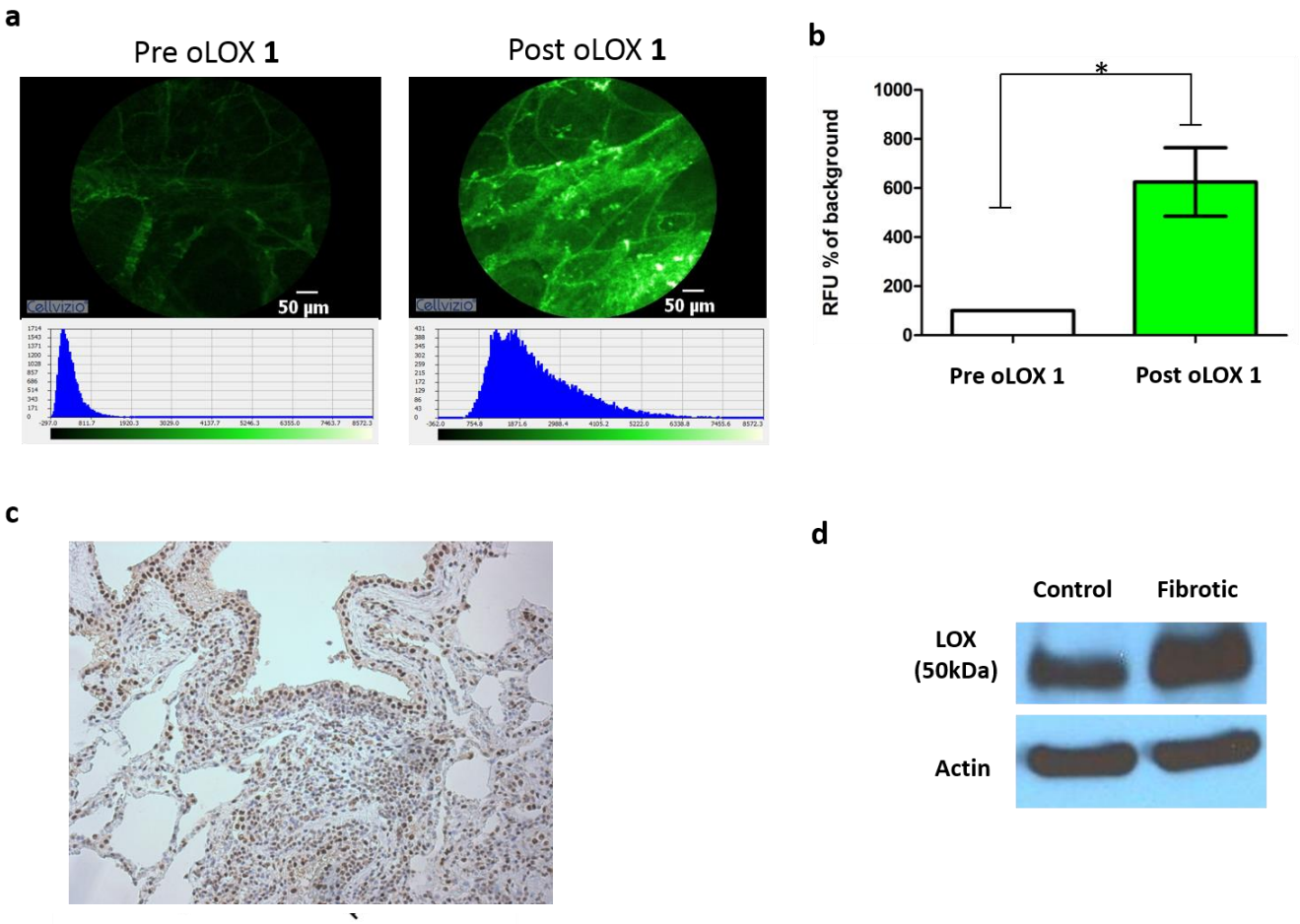

Figure 5: oLOX can be used to image LOXF activity in a fibrotic ventilating ex vivo asinine lung model. Catheter installation of 200µM oLOX instilled in a total volume of 1 mL in PBS into a whole fibrotic ventilating ex vivo asinine lung results in a significant increase in fluorescent signal (a-b, *p= 0.0313, Mann Whitney, n=3); (c). Target tissue was evaluated for LOX expression using immunohistochemistry (20X lens). (d) Western blot confirmed expression of LOX in both fibrotic and grossly unaffected (control) areas of *ex vivo* asinine lung tissue.

Conclusions

We have successfully designed and synthesized an activity-based fluorescent probe capable of the real-time quantification of LOXF activity in fibrogenic conditions. The activation of the probe by LOXF was confirmed in human lung homogenate models. Furthermore, probe activation was inhibited in the presence of a specific LOX inhibitor, thus confirming target specificity. The probe also showed utility in a size-relevant model of lung fibrogenesis. This optical Smartprobe has the potential to image real-time LOXF activity within the lungs of patients at the bedside. Whilst we have not yet assessed the specificity of oLOX to individual members of the LOXF family, targeting individual enzymes is a future goal, exploiting the use of specific inhibitor based imaging agents.

Acknowledgements

The authors would like to thank the MRC, under the Developmental Pathway Funding Scheme (grant number RA2159). A.M-F. acknowledges Fundacion Ramon Areces-Postdoctoral Research Fellowship Program for financial support. The research leading to these results has received funding from the European Union Seventh Framework Programme FP7 2012 under grant agreement no. 326465 (A. M-F.) and EPSRC (EP/K03197X).

Notes and references

[a]School of Chemistry, EaStChem, University of Edinburgh, Joseph Black Building, West Mains Road, Edinburgh, EH9 3FJ, UK. E-mail: mark.bradley@ed.ac.uk

[b]Pulmonary Optical Molecular Imaging Group, MRC/Centre of Inflammation Research, Queen's Medical Research Institute, University of Edinburgh, 47 Little France Crescent, EH16 4TJ, Edinburgh, UK. E-mail: Kev.Dhaliwal@ed.ac.uk.

#These authors contributed equally

†Footnotes should appear here. These might include comments relevant to but not central to the matter under discussion, limited experimental and spectral data, and crystallographic data.

Electronic Supplementary Information (ESI) available: Fig. S1, full experimental details and procedures, characterisation of compounds 1–11. Detail information on human and asinine *ex vivo* tissue models, western blot, immunohistochemistry, fibered confocal fluorescence microscopy (FCFM) . See DOI: 10.1039/b000000x/

1. M. Selman, T. E. King Jr, and A. Pardo, 2001, **134**, 136–151.

2. T. A. Wynn and T. R. Ramalingam, *Nat. Med.*, 2012, **18**, 1028–1040.

3. M. Demedts and U. Costabel, *Eur. Respir. J.*, 2002, **19**, 794–796.

4. C. Mathers, T. Boerma, and D. M. Fat, *The global burden of disease: 2004 Update.*, 2008.

5. C. Z. Chen and M. Raghunath, *Fibrogenesis Tissue Repair*, 2009, **2**, 7.

6. J. Molnar, K. S. K. Fong, Q. P. He, K. Hayashi, Y. Kim, S. F. T. Fong, B. Fogelgren, K. Molnarne Szauter, M. Mink, and K. Csiszar, *Biochim. Biophys. Acta (BBA)-Proteins Proteomics*, 2003, **1647**, 220–224.

7. E. J. Feres-Filho, Y. J. Choi, X. Han, T. E. S. Takala, and P. C. Trackman, *J. Biol. Chem.*, 1995, **270**, 30797–303803.

8. L. I. Smith-Mungo and H. M. Kagan, *Matrix Biol.*, 1998, **16**, 387–398.

9. S. R. Vora, Y. Guo, D. N. Stephens, E. Salih, E. D. Vu, K. H. Kirsch, G. E. Sonenshein, and P. C. Trackman, *Biochemistry*, 2010, **49**, 2962–2972.

10. J. Finney, H.-J. Moon, T. Ronnebaum, M. Lantz, and M. Mure, *Arch. Biochem. Biophys.*, 2014, **546**, 19–32.

11. L. Thomassin, C. C. Werneck, T. J. Broekelmann, C. Gleyzal, I. K. Hornstra, R. P. Mecham, and P. Sommer, *J. Biol. Chem.*, 2005, **280**, 42848–42855.

12. C. Trivedy, K. Warnakulasuriya, V. K. Hazarey, M. Tavassoli, P. Sommer, and N. W. Johnson, *J. Oral Pathol. Med.*, 1999, **28**, 246–251.

13. H. M. Kagan and W. Li, *J. Cell. Biochem.*, 2003, **88**, 660–672.

14. J. T. Erler, K. L. Bennewith, M. Nicolau, N. Dornhöfer, C. Kong, Q.-T. Le, J.-T. A. Chi, S. S. Jeffrey, and A. J. Giaccia, *Nature*, 2006, **440**, 1222–1226.

15. V. Barry-Hamilton, R. Spangler, D. Marshall, S. McCauley, H. M. Rodriguez, M. Oyasu, A. Mikels, M. Vaysberg, H. Ghermazien, C. Wai, C. a Garcia, A. C. Velayo, B. Jorgensen, D. Biermann, D. Tsai, J. Green, S. Zaffryar-Eilot, A. Holzer, S. Ogg, D. Thai, G. Neufeld, P. Van Vlasselaer, and V. Smith, *Nat. Med.*, 2010, **16**, 1009–1017.

16. J. W. Chien, T. J. Richards, K. F. Gibson, Y. Zhang, K. O. Lindell, L. Shao, S. K. Lyman, J. I. Adamkewicz, V. Smith, N. Kaminski, and T. O'Riordan, *Eur. Respir. J.*, 2014, **43**, 1430–1438.

17. J. Zhang, R. E. Campbell, A. Y. Ting, and R. Y. Tsien, *Nat. Rev. Mol. Cell Biol.*, 2002, **3**, 906–918.

18. G. Chen, D. J. Yee, N. G. Gubernator, and D. Sames, *J. Am. Chem. Soc.*, 2005, **127**, 4544–4555.

19. A. H. Palamakumbura and P. C. Trackman, *Anal. Biochem.*, 2002, **300**, 245–251.

20. M. H. Lim, D. Xu, and S. J. Lippard, *Nat. Chem. Biol.*, 2006, **2**, 375–380.

21. J. Aw, Q. Shao, Y. Yang, T. Jiang, C. Ang, and B. Xing, *Chem. – An Asian J.*, 2010, **5**, 1317–1321.

22. S. Long, L. Chen, Y. Xiang, M. Song, Y. Zheng, and Q. Zhu, *Chem. Commun. (Camb).*, 2012, **48**, 7164–7166.

23. A. E. Albers, K. A. Rawls, and C. J. Chang, *Chem. Commun. (Camb).*, 2007, **1**, 4647–4649.

24. J. G. Mohanty, J. S. Jaffe, E. S. Schulman, and D. G. Raible, *J. Immunol. Methods*, 1997, **202**, 133–141.

25. M. Zhou, Z. Diwu, N. Panchuk-Voloshina, and R. P. Haugland, *Anal. Biochem.*, 1997, **253**, 162–168.

26. H. M. Rodriguez, M. Vaysberg, A. Mikels, S. McCauley, A. C. Velayo, C. Garcia, and V. Smith, *J. Biol. Chem.*, 2010, **285**, 20964–20974.

27. X. Li, H. Zhang, Y. Xie, Y. Hu, H. Sun, and Q. Zhu, *Org. Biomol. Chem.*, 2014, **12**, 2033–2036.

28. A. Sampath Narayanan, R. C. Siegel, and G. R. Martin, *Biochem. Biophys. Res. Commun.*, 1972, **46**, 745–751.

29. S. S. Tang, P. C. Trackman, and H. M. Kagan, *J. Biol. Chem.*, 1983, **258**, 4331–4338.

30. N. Mercier, A. Kakou, P. Challande, P. Lacolley, and M. Osborne-Pellegrin, *Toxicol. Appl. Pharmacol.*, 2009, **239**, 258–267.

31. M. Nesbit, 2006, WO 2006128740 A2.

32. E. Burchardt, C. Faeste, C. Hirth-Dietrich, J. Keldenich, A. Knorr, T. Lampe, P. Naab, G. Schmidt, D. Schmidt, and R. Schohe-Loop, 2008, US 7320977 B2.

33. H. M. Kagan and S. N. Gacheru, 1991, US 4997854 A.

34. M. Nesbit, 2007, WO 2006128740 A3.

35. K. Apstein, Bernstine, Kagan, Nellaiappan, 1996, WO 1996040746 A1.

36. M. E. Helge Tolleshaug, Ben Newton, Anna Rydbeck, Salah Chettibi, 2007, WO2007066119 A2.

37. D. S. Rudolf Schohe-Loop, Elmar Burchardt, Christiane Faeste, Claudia Hirth-Dietrich, Jorg Keldenich, Andreas Knorr, Thomas Lampe, Paul Naab, 2006, US 20060004015 A1.

38. B. C. Dickinson, C. Huynh, and C. J. Chang, *J. Am. Chem. Soc.*, 2010, **132**, 5906–5915.

39. J. E. T. Carrie and D. R. Trentham, *J. Chem. Soc. Perkin Trans. 1*, 1995, 1993–200.

40. R. Sjoback, J. Nygren, and M. Kubista, *Spectrochim. Acta Part A*, 1995, **51**, L2–L21.

41. L. D. Lavis, T. Chao, and R. T. Raines, 2011, 521–530.

42. H. Abe, Y. Ito, and K. Furukawa, 2010, EP 2204371 A1.

43. J. M. Mäki, R. Sormunen, S. Lippo, R. Kaarteenaho-Wiik, R. Soininen, and J. Myllyharju, *Am. J. Pathol.*, 2005, **167**, 927–936.

44. A. R. Woznick, A. L. Braddock, M. Dulai, M. L. Seymour, R. E. Callahan, R. J. Welsh, G. W. Chmielewski, G. B. Zelenock, and C. J. Shanley, *Am. J. Surg.*, 2005, **189**, 297–301.

45. D. F. Counts, J. N. Evans, T. A. Dipetrillo, K. M. Sterling, and J. Kelley, *J. Pharmacol. Exp. Ther.*, 1981, **219**, 675–678.

46. A. Poole, R. Myllyla, J. C. Wagner, and R. C. Brown, *Br. J. Exp. Pathol.*, 1985, **66**, 567–575.

47. X. Yang, S. Li, W. Li, J. Chen, X. Xiao, Y. Wang, G. Yan, and L. Chen, *Oncol Rep*, 2013, **29**, 541–548.

48. C. Machon, B. Le Calve, S. Coste, M. Riviere, L. Payen, D. Bernard, and J. Guitton, *Biomed. Chromatogr.*, 2014, **28**, 1017–1023.

49. A. Borel, D. Eichenberger, J. Farjanel, E. Kessler, C. Gleyzal, D. J. Hulmes, P. Sommer, and B. Font, *J. Biol. Chem.*, 2001, **276**, 48944–48949.

50. J.-E. Lee and Y. Kim, *J. Biol. Chem.*, 2006, **281**, 37282–37290.

51. H. Ito, H. Akiyama, H. Iguchi, K. Iyama, M. Miyamoto, K. Ohsawa, and T. Nakamura, *J. Biol. Chem.*, 2001, **276**, 24023–24029.

52. Y.-M. Kim, E.-C. Kim, and Y. Kim, *Mol. Biol. Rep.*, 2011, **38**, 145–149.

53. K. R. Wilmarth and J. R. Froines, *J. Toxicol. Environ. Heal. Part A Curr. Issues*, 1991, **32**, 415–427.

54. D. a. Dorward, C. D. Lucas, a. G. Rossi, C. Haslett, and K. Dhaliwal, *Pharmacol. Ther.*, 2012, **135**, 182–199.

55. V. Ntziachristos, *Nat. Methods*, 2010, **7**, 603–614.

56. L. Thiberville, M. Salaun, S. Lachkar, S. Dominique, S. Moreno-Swirc, C. Vever-Bizet, and G. Bourg-Heckly, Am Thoracic Soc, 2009, vol. 6, p. 444.

57. F. S. Fuchs, S. Zirlik, K. Hildner, M. Frieser, M. Ganslmayer, S. Schwarz, M. Uder, and M. F. Neurath, *Respiration*, 2011, **81**, 32–38.

58. A. Miele, K. Dhaliwal, N. Du Toit, J. T. Murchison, C. Dhaliwal, H. Brooks, S. H. Smith, N. Hirani, T. Schwarz, C. Haslett, W. A. Wallace, and B. C. McGorum, *Chest*, 2014, **145**, 1325–1332.

7.4 Oral and poster presentations

Miele, Dhaliwal, Du Toit, Nicole, Murchison, Dhaliwal, Brooks, Smith, Hirani, Schwarz, Haslett, Wallace, and McGorum. Clinical, Histopathological and Molecular Characterisation of Asinine Pulmonary Fibrosis- A Unique Multidisciplinary Approach to Deliver Cutting Edge Diagnostics and Therapeutics for Animal and Human Health (2012). Keystones Symposium on Fibrosis, Big Sky, Montana, [Poster].

Miele, Dhaliwal, Du Toit, Nicole, Murchison, Dhaliwal, Brooks, Smith, Hirani, Schwarz, Haslett, Wallace, and McGorum. Clinical, Histopathological and Molecular Characterisation of Asinine Pulmonary Fibrosis (2012). WMIC, Dublin, [Poster].

Miele and Hirani. Pulmonary Fibrosis: A frustrating challenge to medical and veterinary scientists (2012). Clinical Club, RDSVS, Edinburgh, [Oral].

Miele, Dhaliwal, Du Toit, Nicole, Murchison, Dhaliwal, Brooks, Smith, Hirani, Schwarz, Haslett, Wallace, and McGorum. Clinical, Histopathological and Molecular Characterisation of Asinine Pulmonary Fibrosis (2013). Edinburgh Infectious Disease Respiratory Virus Workshop, Moredun Research Institute, Edinburgh, [Poster].

Miele, Dhaliwal, Du Toit, Nicole, Murchison, Dhaliwal, Brooks, Smith, Hirani, Schwarz, Haslett, Wallace, and McGorum. Characterisation of Asinine Pulmonary Fibrosis and similarities to an emerging human interstitial lung disease (2013). British Society of Animal Science Annual Meeting, Nottingham, [Oral].

Miele, Dhaliwal, Du Toit, Nicole, Murchison, Dhaliwal, Brooks, Smith, Hirani, Schwarz, Haslett, Wallace, and McGorum. Characterisation of Asinine Pulmonary Fibrosis and similarities to an emerging human interstitial lung disease (2013). 7th Joint Meeting of the British Division of the IAP and the Pathological Society, Edinburgh, [Poster]

7.5 Prizes

Winner of British Society of Animal Science President's Prize for the best theatre presentation, Nottingham, November 2013.

7.6 References

ABE, R., DONNELLY, S. C., PENG, T., BUCALA, R. & METZ, C. N. 2001. Peripheral blood fibrocytes: Differentiation pathway and migration to wound sites. *Journal of Immunology,* 166**,** 7556-7562.

ANDERSSON-SJÖLAND, A., DE ALBA, C. G., NIHLBERG, K., BECERRIL, C., RAMÍREZ, R., PARDO, A., WESTERGREN-THORSSON, G. & SELMAN, M. 2008. Fibrocytes are a potential source of lung fibroblasts in idiopathic pulmonary fibrosis. *The international journal of biochemistry & cell biology,* 40**,** 2129-2140.

APSTEIN, B., KAGAN, NELLAIAPPAN, KALIAPPANADAR 1996. Lysyl oxidase inhibitors. WO 1996040746 A1.

ARDI, V. C., KUPRIYANOVA, T. A., DERYUGINA, E. I. & QUIGLEY, J. P. 2007. Human neutrophils uniquely release TIMP-free MMP-9 to provide a potent catalytic stimulator of angiogenesis. *Proc Natl Acad Sci U S A,* 104**,** 20262-7.

ARMANIOS, M. 2012. Telomerase and idiopathic pulmonary fibrosis. *Mutation Research/Fundamental and Molecular Mechanisms of Mutagenesis,* 730**,** 52-58.

ATKINSON, J. J. & SENIOR, R. M. 2003. Matrix Metalloproteinase-9 in Lung Remodeling. *American journal of respiratory cell and molecular biology,* 28**,** 12-24.

AVLONITIS, N., DEBUNNE, M., ASLAM, T., MCDONALD, N., HASLETT, C., DHALIWAL, K. & BRADLEY, M. 2013. Highly specific, multi-branched fluorescent reporters for analysis of human neutrophil elastase. *Org Biomol Chem,* 11**,** 4414-8.

AZOULAY, E., PAUGAM, B., HEYMANN, M., KAMBOUCHNER, M., HALOUN, A., VALEYRE, D., BATTESTI, J. & TAZI, A. 1999. Familial extensive idiopathic bilateral pleural fibrosis. *European Respiratory Journal,* 14**,** 971-973.

BAGGIOLINI, M., DEWALD, B. & MOSER, B. 1997. Human chemokines: an update. *Annu Rev Immunol,* 15**,** 675-705.

BARROW, M. V., SIMPSON, C. F. & MILLER, E. J. 1974. Lathyrism: A Review. *The Quarterly Review of Biology,* 49**,** 101-128.

BARRY-HAMILTON, V., SPANGLER, R., MARSHALL, D., MCCAULEY, S., RODRIGUEZ, H. M., OYASU, M., MIKELS, A., VAYSBERG, M., GHERMAZIEN, H., WAI, C., GARCIA, C. A., VELAYO, A. C., JORGENSEN, B., BIERMANN, D., TSAI, D., GREEN, J., ZAFFRYAR-EILOT, S., HOLZER, A., OGG, S., THAI, D., NEUFELD, G., VAN VLASSELAER, P. & SMITH, V. 2010. Allosteric inhibition of lysyl

oxidase-like-2 impedes the development of a pathologic microenvironment. *Nat Med,* 16**,** 1009-1017.

BEDELL-HOGAN, D., TRACKMAN, P., ABRAMS, W., ROSENBLOOM, J. & KAGAN, H. 1993. Oxidation, cross-linking, and insolubilization of recombinant tropoelastin by purified lysyl oxidase. *J Biol Chem,* 268**,** 10345-50.

BENTWOOD, B. J. & HENSON, P. 1980. The sequential release of granule constitutents from human neutrophils. *The Journal of Immunology,* 124**,** 855-862.

BERGERS, G. & SONG, S. 2005. The role of pericytes in blood-vessel formation and maintenance. *Neuro-Oncology,* 7**,** 452-464.

BERGIN, C., CASTELLINO, R., BLANK, N. & MOSES, L. 1994. Specificity of high-resolution CT findings in pulmonary asbestosis: do patients scanned for other indications have similar findings? *American Journal of Roentgenology,* 163**,** 551-555.

BETSUYAKU, T., FUKUDA, Y., PARKS, W. C., SHIPLEY, J. M. & SENIOR, R. M. Gelatinase B Is Required for Alveolar Bronchiolization after Intratracheal Bleomycin. *The American journal of pathology,* 157**,** 525-535.

BOLTON, R., ADDISON, J., DAVIS, J., DONALDSON, K., JONES, A., MILLER, B. & WRIGHT, A. 1986. Effects of the inhalation of dusts from calcium silicate insulation materials in laboratory rats. *Environmental research,* 39**,** 26.

BOREL, A., EICHENBERGER, D., FARJANEL, J., KESSLER, E., GLEYZAL, C., HULMES, D. J., SOMMER, P. & FONT, B. 2001. Lysyl Oxidase-like Protein from Bovine Aorta Isolation and maturation to an active form by bone morphogenetic protein-1. *Journal of Biological Chemistry,* 276**,** 48944-48949.

BRAMBILLA, C., ABRAHAM, J., BRAMBILLA, E., BENIRSCHKE, K. & BLOOR, C. 1979. Comparative pathology of silicate pneumoconiosis. *The American journal of pathology,* 96**,** 149.

BREMER, C., TUNG, C.-H. & WEISSLEDER, R. 2001. In vivo molecular target assessment of matrix metalloproteinase inhibition. *Nat Med,* 7**,** 743-748.

BROWN, P. D. 1999. Clinical studies with matrix metalloproteinase inhibitors. *Apmis,* 107**,** 174-180.

BUCALA, R., SPIEGEL, L. A., CHESNEY, J., HOGAN, M. & CERAMI, A. 1994. Circulating fibrocytes define a new leukocyte subpopulation that mediates tissue repair. *Mol Med,* 1**,** 71-81.

BUERGELT, C., HINES, S., CANTOR, G., STIRK, A. & WILSON, J. 1986. A retrospective study of proliferative interstitial lung disease of horses in Florida. *Veterinary Pathology Online,* 23**,** 750.

BURCHARDT, E., FAESTE, C., HIRTH-DIETRICH, C., KELDENICH, J., KNORR, A., LAMPE, T., NAAB, P., SCHMIDT, G., SCHMIDT, D. & SCHOHE-LOOP, R. 2008. Substituted 2-phenyl-3 (2h)-pyridazinones. US 7320977 B2.

CABRERA, S., GAXIOLA, M., ARREOLA, J. L., RAMÍREZ, R., JARA, P., D'ARMIENTO, J., RICHARDS, T., SELMAN, M. & PARDO, A. 2007. Overexpression of MMP9 in macrophages attenuates pulmonary fibrosis

induced by bleomycin. *The international journal of biochemistry & cell biology,* 39**,** 2324-2338.

CAMUS, P., VON DER THÜSEN, J., HANSELL, D. M. & COLBY, T. V. 2014. Pleuroparenchymal fibroelastosis: one more walk on the wild side of drugs? *European Respiratory Journal,* 44**,** 289-296.

CANFIELD, P., ROTHWELL, T., PAPADIMITRIOU, J. & MOORE, J. 1989. Siliceous pneumoconiosis in two dogs. *Journal of Comparative Pathology,* 100**,** 199-202.

CASSIDY, P. J. & RADDA, G. K. 2005. Molecular imaging perspectives. *Journal of the royal society interface,* 2**,** 133-144.

CASSOL, E., ALFANO, M., BISWAS, P. & POLI, G. 2006. Monocyte-derived macrophages and myeloid cell lines as targets of HIV-1 replication and persistence. *Journal of leukocyte biology,* 80**,** 1018-1030.

CHANG, H. J., YANG, M. J., YANG, Y. H., HOU, M. F., HSUEH, E. J. & LIN, S. R. 2009. MMP13 is potentially a new tumor marker for breast cancer diagnosis. *Oncol Rep,* 22**,** 1119-27.

CHEN, C. Z. & RAGHUNATH, M. 2009. Focus on collagen: in vitro systems to study fibrogenesis and antifibrosis state of the art. *Fibrogenesis Tissue Repair,* 2**,** 7.

CHESNEY, J., METZ, C., STAVITSKY, A. B., BACHER, M. & BUCALA, R. 1998. Regulated production of type I collagen and inflammatory cytokines by peripheral blood fibrocytes. *The Journal of Immunology,* 160**,** 419.

CHIEN, J. W., RICHARDS, T. J., GIBSON, K. F., ZHANG, Y., LINDELL, K. O., SHAO, L., LYMAN, S. K., ADAMKEWICZ, J. I., SMITH, V., KAMINSKI, N. & O'RIORDAN, T. 2014. Serum lysyl oxidase-like 2 levels and idiopathic pulmonary fibrosis disease progression. *Eur Respir J,* 43**,** 1430-8.

CHOI, Y. H., BURDICK, M. D. & STRIETER, R. M. 2010. Human Circulating Fibrocytes Have The Capacity To Differentiate Osteoblasts And Chondrocytes. *The international journal of biochemistry & cell biology,* 42**,** 662-671.

CHUA, F., GAULDIE, J. & LAURENT, G. J. 2005. Pulmonary fibrosis: searching for model answers. *American journal of respiratory cell and molecular biology,* 33**,** 5.

COOL, C. D., GROSHONG, S. D., RAI, P. R., HENSON, P. M., STEWART, J. S. & BROWN, K. K. 2006. Fibroblast foci are not discrete sites of lung injury or repair: the fibroblast reticulum. *American journal of respiratory and critical care medicine,* 174**,** 654-658.

CORCORAN, B., COBB, M., MARTIN, M., DUKES-MCEWAN, J., FRENCH, A., LUIS FUENTES, V., BOSWOOD, A. & RHIND, S. 1999. Chronic pulmonary disease in West Highland white terriers. *Veterinary Record,* 144**,** 611.

COSTA, L. R. R., SEAHORN, T. L., MOORE, R. M., TAYLOR, H. W., GAUNT, S. D. & BEADLE, R. E. 2000. Correlation of clinical score, intrapleural pressure, cytologic findings of bronchoalveolar fluid, and histopathologic lesions of pulmonary tissue in horses with summer pasture-associated obstructive pulmonary disease. *American journal of veterinary research,* 61**,** 167-173.

COUNTS, D., EVANS, J., DIPETRILLO, T., STERLING, K. & KELLEY, J. 1981. Collagen lysyl oxidase activity in the lung increases during bleomycin-induced lung fibrosis. *Journal of Pharmacology and Experimental Therapeutics,* 219**,** 675.

COUSSENS, L. M., FINGLETON, B. & MATRISIAN, L. M. 2002. Matrix Metalloproteinase Inhibitors and Cancer—Trials and Tribulations. *Science,* 295**,** 2387-2392.

CRISP, J. L., SAVARIAR, E. N., GLASGOW, H. L., ELLIES, L. G., WHITNEY, M. A. & TSIEN, R. Y. 2014. Dual targeting of integrin alphavbeta3 and matrix metalloproteinase-2 for optical imaging of tumors and chemotherapeutic delivery. *Mol Cancer Ther,* 13**,** 1514-25.

DAHL, R., TITLESTAD, I., LINDQVIST, A., WIELDERS, P., WRAY, H., WANG, M., SAMUELSSON, V., MO, J. & HOLT, A. 2012. Effects of an oral MMP-9 and -12 inhibitor, AZD1236, on biomarkers in moderate/severe COPD: A randomised controlled trial. *Pulmonary pharmacology & therapeutics,* 25**,** 169-177.

DANCER, R. C., WOOD, A. M. & THICKETT, D. R. 2011. Metalloproteinases in idiopathic pulmonary fibrosis. *Eur Respir J,* 38**,** 1461-7.

DEGRYSE, A. L., TANJORE, H., XU, X. C., POLOSUKHIN, V. V., JONES, B. R., MCMAHON, F. B., GLEAVES, L. A., BLACKWELL, T. S. & LAWSON, W. E. 2010. Repetitive intratracheal bleomycin models several features of idiopathic pulmonary fibrosis. *American Journal of Physiology-Lung Cellular and Molecular Physiology,* 299**,** L442.

DEMEDTS, I. K., BRUSSELLE, G. G., BRACKE, K. R., VERMAELEN, K. Y. & PAUWELS, R. A. 2005. Matrix metalloproteinases in asthma and COPD. *Curr Opin Pharmacol,* 5**,** 257-63.

DEMEDTS, M. & COSTABEL, U. 2002. ATS/ERS international multidisciplinary consensus classification of the idiopathic interstitial pneumonias. *European Respiratory Journal,* 19**,** 794-796.

DENYS, H., DERYCKE, L., HENDRIX, A., WESTBROEK, W., GHELDOF, A., NARINE, K., PAUWELS, P., GESPACH, C., BRACKE, M. & DE WEVER, O. 2008. Differential impact of TGF-beta and EGF on fibroblast differentiation and invasion reciprocally promotes colon cancer cell invasion. *Cancer Lett,* 266**,** 263-74.

DESMOULIÈRE, A., GEINOZ, A., GABBIANI, F. & GABBIANI, G. 1993. Transforming growth factor-beta 1 induces alpha-smooth muscle actin expression in granulation tissue myofibroblasts and in quiescent and growing cultured fibroblasts. *The Journal of cell biology,* 122**,** 103-111.

DEVY, L. & DRANSFIELD, D. T. 2011. New Strategies for the Next Generation of Matrix-Metalloproteinase Inhibitors: Selectively Targeting Membrane-Anchored MMPs with Therapeutic Antibodies. *Biochemistry Research International,* 2011.

DICKINSON, B. C., HUYNH, C. & CHANG, C. J. 2010. A palette of fluorescent probes with varying emission colors for imaging hydrogen peroxide signaling in living cells. *J Am Chem Soc,* 132**,** 5906-15.

DORWARD, D. A., LUCAS, C. D., ROSSI, A. G., HASLETT, C. & DHALIWAL, K. 2012. Imaging inflammation: molecular strategies to visualize key

components of the inflammatory cascade, from initiation to resolution. *Pharmacol Ther,* 135**,** 182-99.

EISENTHAL, R., DANSON, M. J. & HOUGH, D. W. 2007. Catalytic efficiency and k cat/K M: a useful comparator? *Trends in biotechnology,* 25**,** 247-249.

ELLARD, J. M., ZOLLITSCH, T., CUMMINS, W. J., HAMILTON, A. L. & BRADLEY, M. 2002. Fluorescence enhancement through enzymatic cleavage of internally quenched dendritic peptides: a sensitive assay for the AspN endoproteinase. *Angew Chem Int Ed Engl,* 41**,** 3233-6.

ERLER, J. T., BENNEWITH, K. L., NICOLAU, M., DORNHOFER, N., KONG, C., LE, Q. T., CHI, J. T., JEFFREY, S. S. & GIACCIA, A. J. 2006. Lysyl oxidase is essential for hypoxia-induced metastasis. *Nature,* 440**,** 1222-6.

FANJUL-FERNÁNDEZ, M., FOLGUERAS, A. R., CABRERA, S. & LÓPEZ-OTÍN, C. 2010. Matrix metalloproteinases: Evolution, gene regulation and functional analysis in mouse models. *Biochimica et Biophysica Acta (BBA) - Molecular Cell Research,* 1803**,** 3-19.

FARINA, A. R. & MACKAY, A. R. 2014. Gelatinase B/MMP-9 in Tumour Pathogenesis and Progression. *Cancers (Basel),* 6**,** 240-96.

FEGHALI-BOSTWICK, C. A., GADGIL, A. S., OTTERBEIN, L. E., PILEWSKI, J. M., STONER, M. W., CSIZMADIA, E., ZHANG, Y., SCIURBA, F. C. & DUNCAN, S. R. 2008. Autoantibodies in patients with chronic obstructive pulmonary disease. *American journal of respiratory and critical care medicine,* 177**,** 156-163.

FERES-FILHO, E. J., CHOI, Y. J., HAN, X., TAKALA, T. E. S. & TRACKMAN, P. C. 1995. Pre-and Post-translational Regulation of Lysyl Oxidase by Transforming Growth Factor-1 in Osteoblastic MC3T3-E1 Cells. *Journal of Biological Chemistry,* 270**,** 30797.

FINNEY, J., MOON, H.-J., RONNEBAUM, T., LANTZ, M. & MURE, M. 2014. Human Copper-Dependent Amine Oxidases. *Archives of biochemistry and biophysics*.

FRANKEL, S. K., COOL, C. D., LYNCH, D. A. & BROWN, K. K. 2004. Idiopathic Pleuroparenchymal FibroelastosisDescription of a Novel Clinicopathologic Entity. *CHEST Journal,* 126**,** 2007-2013.

FRANKOWSKI, H., GU, Y.-H., HEO, J. H., MILNER, R. & DEL ZOPPO, G. J. 2012. Use of Gel Zymography to Examine Matrix Metalloproteinase (Gelatinase) Expression in Brain Tissue or in Primary Glial Cultures. *Methods in molecular biology (Clifton, N.J.),* 814**,** 221-233.

FUCHS, F. S., ZIRLIK, S., HILDNER, K., FRIESER, M., GANSLMAYER, M., SCHWARZ, S., UDER, M. & NEURATH, M. F. 2011. Fluorescein-aided confocal laser endomicroscopy of the lung. *Respiration,* 81**,** 32-38.

FUKUDA, Y., ISHIZAKI, M., KUDOH, S., KITAICHI, M. & YAMANAKA, N. 1998. Localization of matrix metalloproteinases-1, -2, and -9 and tissue inhibitor of metalloproteinase-2 in interstitial lung diseases. *Lab Invest,* 78**,** 687-98.

GIANNANDREA, M. & PARKS, W. C. 2014. Diverse functions of matrix metalloproteinases during fibrosis. *Dis Model Mech,* 7**,** 193-203.

GIBBS, A., POOLEY, F., GRIFFITHS, D. & MITHA, R. 1994. Silica and silicate pneumoconioses—a pathological and mineralogical study. *Annals of Occupational Hygiene,* 38**,** 851-856.

GIBBS, A. R. & POOLEY, F. D. 1996. Analysis and interpretation of inorganic mineral particles in "lung" tissues. *Thorax,* 51**,** 327-34.

GOETZ, M. & WANG, T. D. 2010. Molecular imaging in gastrointestinal endoscopy. *Gastroenterology,* 138**,** 828-833. e1.

GOLDSMITH, S. J. Receptor imaging: competitive or complementary to antibody imaging? Seminars in nuclear medicine, 1997. Elsevier, 85-93.

GRAVES, D. T., JIANG, Y., WILLIAMSON, M. J. & VALENTE, A. J. 1989. Identification of monocyte chemotactic activity produced by malignant cells. *Science,* 245**,** 1490-1493.

HANSEN, H. J., JAMA, F. M., NILSSON, C., NORRGREN, L. & ABDURAHMAN, O. S. 1989. Silicate pneumoconiosis in camels (Camelus dromedarius L.). *Journal of Veterinary Medicine Series A,* 36**,** 789-796.

HARARI, S. & CAMINATI, A. 2010. IPF: new insight on pathogenesis and treatment. *Allergy,* 65**,** 537-553.

HARRIS JR, E. D. & KRANE, S. M. 1972. An endopeptidase from rheumatoid synovial tissue culture. *Biochimica et Biophysica Acta (BBA) - Enzymology,* 258**,** 566-576.

HAYASHI, K., FONG, K. S., MERCIER, F., BOYD, C. D., CSISZAR, K. & HAYASHI, M. 2004. Comparative immunocytochemical localization of lysyl oxidase (LOX) and the lysyl oxidase-like (LOXL) proteins: changes in the expression of LOXL during development and growth of mouse tissues. *Journal of molecular histology,* 35**,** 845-855.

HELLEBUST, A. & RICHARDS-KORTUM, R. 2012. Advances in molecular imaging: targeted optical contrast agents for cancer diagnostics. *Nanomedicine (London, England),* 7**,** 429-445.

HENRY, M., MCMAHON, K., MACKAREL, A., PRIKK, K., SORSA, T., MAISI, P., SEPPER, R., FITZGERALD, M. & O'CONNOR, C. 2002. Matrix metalloproteinases and tissue inhibitor of metalloproteinase-1 in sarcoidosis and IPF. *European Respiratory Journal,* 20**,** 1220-1227.

HERRERA, D. R., SILVA, E. J., SANTOS, C. C., ZAIA, A. A., FERRAZ, C. C., ALMEIDA, J. F. & GOMES, B. P. 2014. Root canal content from primary endodontic infection and upregulation of gelatinases in fibroblast cells. *Int Endod J.*

HOFF, C. R., PERKINS, D. R. & DAVIDSON, J. M. 1999. Elastin gene expression is upregulated during pulmonary fibrosis. *Connective tissue research,* 40**,** 145.

HONG, K. M., BELPERIO, J. A., KEANE, M. P., BURDICK, M. D. & STRIETER, R. M. 2007. Differentiation of Human Circulating Fibrocytes as Mediated by Transforming Growth Factor-β and Peroxisome Proliferator-activated Receptor γ. *Journal of Biological Chemistry,* 282**,** 22910-22920.

HONG, K. M., BURDICK, M. D., PHILLIPS, R. J., HEBER, D. & STRIETER, R. M. 2005. Characterization of human fibrocytes as circulating adipocyte progenitors and the formation of human adipose tissue in SCID mice. *The FASEB Journal,* 19**,** 2029-2031.

HOROWITZ, J. C. & THANNICKAL, V. J. 2006. Idiopathic pulmonary fibrosis: new concepts in pathogenesis and implications for drug therapy. *Treatments in respiratory medicine,* 5**,** 325.

HUNG, C., LINN, G., CHOW, Y.-H., KOBAYASHI, A., MITTELSTEADT, K., ALTEMEIER, W. A., GHARIB, S. A., SCHNAPP, L. M. & DUFFIELD, J. S. 2013. Role of Lung Pericytes and Resident Fibroblasts in the Pathogenesis of Pulmonary Fibrosis. *American journal of respiratory and critical care medicine,* 188**,** 820-830.

ITO, H., AKIYAMA, H., IGUCHI, H., IYAMA, K.-I., MIYAMOTO, M., OHSAWA, K. & NAKAMURA, T. 2001. Molecular cloning and biological activity of a novel lysyl oxidase-related gene expressed in cartilage. *Journal of Biological Chemistry,* 276**,** 24023-24029.

ITOH, Y. 2015. Membrane-type matrix metalloproteinases: Their functions and regulations. *Matrix Biol*.

IYER, V. R., EISEN, M. B., ROSS, D. T., SCHULER, G., MOORE, T., LEE, J. C., TRENT, J. M., STAUDT, L. M., HUDSON, J. & BOGUSKI, M. S. 1999. The transcriptional program in the response of human fibroblasts to serum. *Science,* 283**,** 83-87.

IYONAGA, K., TAKEYA, M., SAITA, N., SAKAMOTO, O., YOSHIMURA, T., ANDO, M. & TAKAHASHI, K. 1994. Monocyte chemoattractant protein-1 in idiopathic pulmonary fibrosis and other interstitial lung diseases. *Human pathology,* 25**,** 455-463.

JACKSON, P. L., XU, X., WILSON, L., WEATHINGTON, N. M., CLANCY, J. P., BLALOCK, J. E. & GAGGAR, A. 2010. Human neutrophil elastase-mediated cleavage sites of MMP-9 and TIMP-1: implications to cystic fibrosis proteolytic dysfunction. *Molecular medicine,* 16**,** 159.

JARES-ERIJMAN, E. A. & JOVIN, T. M. 2003. FRET imaging. *Nat Biotech,* 21**,** 1387-1395.

JIANG, T., OLSON, E. S., NGUYEN, Q. T., ROY, M., JENNINGS, P. A. & TSIEN, R. Y. 2004. Tumor imaging by means of proteolytic activation of cell-penetrating peptides. *Proc Natl Acad Sci U S A,* 101**,** 17867-72.

JONES, H. A., CLARK, R. J., RHODES, C. G., SCHOFIELD, J. B., KRAUSZ, T. & HASLETT, C. 1994. In vivo measurement of neutrophil activity in experimental lung inflammation. *American journal of respiratory and critical care medicine,* 149**,** 1635.

KAGAN, H. M. & GACHERU, S. N. 1991. Enzyme inhibitors. US 4997854 A.

KAGAN, H. M., SULLIVAN, K. A., OLSSON, T. A. & CRONLUND, A. L. 1979. Purification and properties of four species of lysyl oxidase from bovine aorta. *Biochem. J,* 177**,** 203-214.

KANG, M. J., THOLEY, A. & HEINZLE, E. 2000. Quantitation of low molecular mass substrates and products of enzyme catalyzed reactions using matrix-assisted laser desorption/ionization time-of-flight mass spectrometry. *Rapid Communications in Mass Spectrometry,* 14**,** 1972-1978.

KANG, M. J., THOLEY, A. & HEINZLE, E. 2001. Application of automated matrix-assisted laser desorption/ionization time-of-flight mass spectrometry for the measurement of enzyme activities. *Rapid Communications in Mass Spectrometry,* 15**,** 1327-1333.

KEELEY, E. C., MEHRAD, B. & STRIETER, R. M. 2010. Fibrocytes: Bringing new insights into mechanisms of inflammation and fibrosis. *The international journal of biochemistry & cell biology,* 42**,** 535-542.

KHALIL, N., BEREZNAY, O., SPORN, M. & GREENBERG, A. 1989. Macrophage production of transforming growth factor beta and fibroblast collagen synthesis in chronic pulmonary inflammation. *The Journal of Experimental Medicine,* 170**,** 727.

KHALIL, N., O'CONNOR, R., UNRUH, H., WARREN, P., FLANDERS, K., KEMP, A., BEREZNAY, O. & GREENBERG, A. 1991. Increased production and immunohistochemical localization of transforming growth factor-beta in idiopathic pulmonary fibrosis. *American journal of respiratory cell and molecular biology,* 5**,** 155.

KIM, G. E., LEE, J. S., CHOI, Y. D., LEE, K. H., LEE, J. H., NAM, J. H., CHOI, C., KIM, S. S., PARK, M. H., YOON, J. H. & KWEON, S. S. 2014. Expression of matrix metalloproteinases and their inhibitors in different immunohistochemical-based molecular subtypes of breast cancer. *BMC Cancer,* 14**,** 959.

KIM, K. K., KUGLER, M. C., WOLTERS, P. J., ROBILLARD, L., GALVEZ, M. G., BRUMWELL, A. N., SHEPPARD, D. & CHAPMAN, H. A. 2006. Alveolar epithelial cell mesenchymal transition develops in vivo during pulmonary fibrosis and is regulated by the extracellular matrix. *Proceedings of the National Academy of Sciences,* 103**,** 13180.

KIM, Y., REMACLE, A. G., CHERNOV, A. V., LIU, H., SHUBAYEV, I., LAI, C., DOLKAS, J., SHIRYAEV, S. A., GOLUBKOV, V. S., MIZISIN, A. P., STRONGIN, A. Y. & SHUBAYEV, V. I. 2012. The MMP-9/TIMP-1 axis controls the status of differentiation and function of myelin-forming Schwann cells in nerve regeneration. *PLoS One,* 7**,** e33664.

KIM, Y. M., KIM, E. C. & KIM, Y. 2011. The human lysyl oxidase-like 2 protein functions as an amine oxidase toward collagen and elastin. *Mol Biol Rep,* 38**,** 145-9.

KING, T. E., BRADFORD, W. Z., CASTRO-BERNARDINI, S., FAGAN, E. A., GLASPOLE, I., GLASSBERG, M. K., GORINA, E., HOPKINS, P. M., KARDATZKE, D., LANCASTER, L., LEDERER, D. J., NATHAN, S. D., PEREIRA, C. A., SAHN, S. A., SUSSMAN, R., SWIGRIS, J. J. & NOBLE, P. W. 2014. A Phase 3 Trial of Pirfenidone in Patients with Idiopathic Pulmonary Fibrosis. *New England Journal of Medicine,* 370**,** 2083-2092.

KJELDSEN, L., SENGELOV, H., LOLLIKE, K., NIELSEN, M. H. & BORREGAARD, N. 1994. Isolation and characterization of gelatinase granules from human neutrophils. *Blood,* 83**,** 1640-9.

KLEIBOEKER, S. B., SCHOMMER, S. K., JOHNSON, P. J., EHLERS, B., TURNQUIST, S. E., BOUCHER, M. & KREEGER, J. M. 2002. Association of two newly recognized herpesviruses with interstitial pneumonia in donkeys (Equus asinus). *Journal of Veterinary Diagnostic Investigation,* 14**,** 273.

KNIGHT, C. G., WILLENBROCK, F. & MURPHY, G. 1992. A novel coumarin-labelled peptide for sensitive continuous assays of the matrix metalloproteinases. *FEBS Lett,* 296**,** 263-6.

KUDO, Y., IIZUKA, S., YOSHIDA, M., TSUNEMATSU, T., KONDO, T., SUBARNBHESAJ, A., DERAZ, E. M., SIRIWARDENA, S. B., TAHARA, H., ISHIMARU, N., OGAWA, I. & TAKATA, T. 2012. Matrix metalloproteinase-13 (MMP-13) directly and indirectly promotes tumor angiogenesis. *J Biol Chem,* 287**,** 38716-28.

LANONE, S., ZHENG, T., ZHU, Z., LIU, W., LEE, C. G., MA, B., CHEN, Q., HOMER, R. J., WANG, J., RABACH, L. A., RABACH, M. E., SHIPLEY, J. M., SHAPIRO, S. D., SENIOR, R. M. & ELIAS, J. A. 2002. Overlapping and enzyme-specific contributions of matrix metalloproteinases-9 and -12 in IL-13–induced inflammation and remodeling. *The Journal of Clinical Investigation,* 110**,** 463-474.

LAWSON, W. E., CROSSNO, P. F., POLOSUKHIN, V. V., ROLDAN, J., CHENG, D. S., LANE, K. B., BLACKWELL, T. R., XU, C., MARKIN, C. & WARE, L. B. 2008. Endoplasmic reticulum stress in alveolar epithelial cells is prominent in IPF: association with altered surfactant protein processing and herpesvirus infection. *American Journal of Physiology- Lung Cellular and Molecular Physiology,* 294**,** L1119.

LAYMAN, D. L., NARAYANAN, A. S. & MARTIN, G. R. 1972. The production of lysyl oxidase by human fibroblasts in culture. *Archives of biochemistry and biophysics,* 149**,** 97-101.

LEE, C. G., HOMER, R. J., ZHU, Z., LANONE, S., WANG, X., KOTELIANSKY, V., SHIPLEY, J. M., GOTWALS, P., NOBLE, P., CHEN, Q., SENIOR, R. M. & ELIAS, J. A. 2001. Interleukin-13 Induces Tissue Fibrosis by Selectively Stimulating and Activating Transforming Growth Factor β1. *The Journal of Experimental Medicine,* 194**,** 809-822.

LEE, J. E. & KIM, Y. 2006. A tissue-specific variant of the human lysyl oxidase-like protein 3 (LOXL3) functions as an amine oxidase with substrate specificity. *J Biol Chem,* 281**,** 37282-90.

LEE, S., RYU, J. H., PARK, K., LEE, A., LEE, S.-Y., YOUN, I.-C., AHN, C.-H., YOON, S. M., MYUNG, S.-J. & MOON, D. H. 2009. Polymeric nanoparticle-based activatable near-infrared nanosensor for protease determination in vivo. *Nano letters,* 9**,** 4412-4416.

LEE, S., XIE, J. & CHEN, X. 2010. Activatable Molecular Probes for Cancer Imaging. *Current topics in medicinal chemistry,* 10**,** 1135-1144.

LEMJABBAR, H., GOSSET, P., LECHAPT-ZALCMAN, E., FRANCO-MONTOYA, M.-L., WALLAERT, B., HARF, A. & LAFUMA, C. 1999. Overexpression of Alveolar Macrophage Gelatinase B (MMP-9) in Patients with Idiopathic Pulmonary Fibrosis. *American journal of respiratory cell and molecular biology,* 20**,** 903-913.

LEPIDI, S., KENAGY, R. D., RAINES, E. W., CHIU, E. S., CHAIT, A., ROSS, R. & CLOWES, A. W. 2001. MMP9 production by human monocyte-derived macrophages is decreased on polymerized type I collagen. *J Vasc Surg,* 34**,** 1111-8.

LEVIN, J. I., CHEN, J., DU, M., HOGAN, M., KINCAID, S., NELSON, F. C., VENKATESAN, A. M., WEHR, T., ZASK, A., DIJOSEPH, J., KILLAR, L. M., SKALA, S., SUNG, A., SHARR, M., ROTH, C., JIN, G., COWLING, R., MOHLER, K. M., BLACK, R. A., MARCH, C. J. & SKOTNICKI, J. S.

2001. The discovery of anthranilic acid-based MMP inhibitors. Part 2: SAR of the 5-position and P1(1) groups. *Bioorg Med Chem Lett,* 11**,** 2189-92.

LI, W., CHOU, I., BOAK, A. & KAGAN, H. M. 1995. Downregulation of lysyl oxidase in cadmium-resistant fibroblasts. *American journal of respiratory cell and molecular biology,* 13**,** 418-425.

LI, W., NELLAIAPPAN, K., STRASSMAIER, T., GRAHAM, L., THOMAS, K. M. & KAGAN, H. M. 1997. Localization and activity of lysyl oxidase within nuclei of fibrogenic cells. *Proceedings of the National Academy of Sciences,* 94**,** 12817-12822.

LI, X., ZHANG, H., XIE, Y., HU, Y., SUN, H. & ZHU, Q. 2014. Fluorescent probes for detecting monoamine oxidase activity and cell imaging. *Org Biomol Chem,* 12**,** 2033-6.

LOK, S., STEWART, J., KELLY, B., HASLETON, P. & EGAN, J. 2001. Epstein-Barr virus and wild p53 in idiopathic pulmonary fibrosis. *Respiratory medicine,* 95**,** 787-791.

LONE, B. A. 2014. MMP-9, MMP-2 Profile in Different Mice Tissues and LPS Induced MMP-9 and MMP-2 Expression in RAW 264.7 Cells, Down Regulated by Emodin Treatment. *International Journal of Interdisciplinary and Multidisciplinary Studies,* 1**,** 1-7.

LONG, S., CHEN, L., XIANG, Y., SONG, M., ZHENG, Y. & ZHU, Q. 2012. An activity-based fluorogenic probe for sensitive and selective monoamine oxidase-B detection. *Chemical Communications,* 48**,** 7164-7166.

LOZANO, R., NAGHAVI, M., FOREMAN, K., LIM, S., SHIBUYA, K., ABOYANS, V., ABRAHAM, J., ADAIR, T., AGGARWAL, R. & AHN, S. Y. 2013. Global and regional mortality from 235 causes of death for 20 age groups in 1990 and 2010: a systematic analysis for the Global Burden of Disease Study 2010. *The Lancet,* 380**,** 2095-2128.

LU, Y., CAI, Z., GALSON, D. L., XIAO, G., LIU, Y., GEORGE, D. E., MELHEM, M. F., YAO, Z. & ZHANG, J. 2006. Monocyte chemotactic protein-1 (MCP-1) acts as a paracrine and autocrine factor for prostate cancer growth and invasion. *The prostate,* 66**,** 1311-1318.

MACHON, C., LE CALVE, B., COSTE, S., RIVIERE, M., PAYEN, L., BERNARD, D. & GUITTON, J. 2014. Quantification of beta-aminopropionitrile, an inhibitor of lysyl oxidase activity, in plasma and tumor of mice by liquid chromatography tandem mass spectrometry. *Biomed Chromatogr*.

MAGNUSSEN, H., WATZ, H., KIRSTEN, A., WANG, M., WRAY, H., SAMUELSSON, V., MO, J. & KAY, R. 2011. Safety and tolerability of an oral MMP-9 and -12 inhibitor, AZD1236, in patients with moderate-to-severe COPD: A randomised controlled 6-week trial. *Pulmonary pharmacology & therapeutics,* 24**,** 563-570.

MAHARAJ, S., SHIMBORI, C. & KOLB, M. 2013. Fibrocytes in pulmonary fibrosis: a brief synopsis. *Eur Respir Rev,* 22**,** 552-7.

MARTÍNEZ-RIZO, A., BUENO-TOPETE, M., GONZÁLEZ-CUEVAS, J. & ARMENDÁRIZ-BORUNDA, J. 2010. Plasmin plays a key role in the regulation of profibrogenic molecules in hepatic stellate cells. *Liver International,* 30**,** 298-310.

MASON, D. P., BRIZZIO, M. E., ALSTER, J. M., MCNEILL, A. M., MURTHY, S. C., BUDEV, M. M., MEHTA, A. C., MINAI, O. A., PETTERSSON, G. B. & BLACKSTONE, E. H. 2007. Lung transplantation for idiopathic pulmonary fibrosis. *The Annals of thoracic surgery,* 84**,** 1121-1128.

MASSOVA, I., KOTRA, L. P., FRIDMAN, R. & MOBASHERY, S. 1998. Matrix metalloproteinases: structures, evolution, and diversification. *The FASEB Journal,* 12**,** 1075-1095.

MCANULTY, R. J. 2007. Fibroblasts and myofibroblasts: their source, function and role in disease. *The international journal of biochemistry & cell biology,* 39**,** 666-671.

MCKEOWN, S., RICHTER, A. G., O'KANE, C., MCAULEY, D. F. & THICKETT, D. 2009. MMP expression and abnormal lung permeability are important determinants of outcome in IPF. *European Respiratory Journal,* 33**,** 77-84.

MCLAUGHLIN JR, R. F. & TYLER, W. S. 1961. Subgross pulmonary anatomy in various mammals and man. *JAMA: The Journal of the American Medical Association,* 175**,** 694-697.

MERCIER, N., KAKOU, A., CHALLANDE, P., LACOLLEY, P. & OSBORNE-PELLEGRIN, M. 2009. Comparison of the effects of semicarbazide and beta-aminopropionitrile on the arterial extracellular matrix in the Brown Norway rat. *Toxicol Appl Pharmacol,* 239**,** 258-67.

MIELE, A., DHALIWAL, K., DU TOIT, N., MURCHISON, J. T., DHALIWAL, C., BROOKS, H., SMITH, S. H., HIRANI, N., SCHWARZ, T., HASLETT, C., WALLACE, W. A. & MCGORUM, B. 2014. Chronic pleuropulmonary fibrosis and elastosis of aged donkeys - similarities to human pleuroparenchymal fibroelastosis (ppfe). *CHEST Journal*.

MINCHIN, R. F. & MARTIN, D. J. 2010. Minireview: Nanoparticles for Molecular Imaging—An Overview. *Endocrinology,* 151**,** 474-481.

MOELLER, A., GILPIN, S. E., ASK, K., COX, G., COOK, D., GAULDIE, J., MARGETTS, P. J., FARKAS, L., DOBRANOWSKI, J., BOYLAN, C., O'BYRNE, P. M., STRIETER, R. M. & KOLB, M. 2009. Circulating Fibrocytes Are an Indicator of Poor Prognosis in Idiopathic Pulmonary Fibrosis. *American journal of respiratory and critical care medicine,* 179**,** 588-594.

MOHANTY, J. G., JAFFE, J. S., SCHULMAN, E. S. & RAIBLE, D. G. 1997. A highly sensitive fluorescent micro-assay of H2O2 release from activated human leukocytes using a dihydroxyphenoxazine derivative. *J Immunol Methods,* 202**,** 133-41.

MOLNAR, J., FONG, K., HE, Q., HAYASHI, K., KIM, Y., FONG, S., FOGELGREN, B., MOLNARNE SZAUTER, K., MINK, M. & CSISZAR, K. 2003. Structural and functional diversity of lysyl oxidase and the LOX-like proteins. *Biochimica et Biophysica Acta (BBA)-Proteins and Proteomics,* 1647**,** 220-224.

MON, N. N., HASEGAWA, H., THANT, A. A., HUANG, P., TANIMURA, Y., SENGA, T. & HAMAGUCHI, M. 2006. A Role for Focal Adhesion Kinase Signaling in Tumor Necrosis Factor-α–Dependent Matrix Metalloproteinase-9 Production in a Cholangiocarcinoma Cell Line, CCKS1. *Cancer research,* 66**,** 6778-6784.

MORBINI, P., INGHILLERI, S., CAMPO, I., OGGIONNI, T., ZORZETTO, M. & LUISETTI, M. 2011. Incomplete expression of epithelial-mesenchymal transition markers in idiopathic pulmonary fibrosis. *Pathol Res Pract,* 207**,** 559-67.

MORROW, L., SMITH, K., PIERCY, R., DU TOIT, N., BURDEN, F., OLMOS, G., GREGORY, N. & VERHEYEN, K. 2010. Retrospective Analysis of Post-Mortem Findings in 1,444 Aged Donkeys. *Journal of Comparative Pathology*.

MOUSTAKAS, A. & STOURNARAS, C. 1999. Regulation of actin organisation by TGF-beta in H-ras-transformed fibroblasts. *J Cell Sci,* 112 (Pt 8)**,** 1169-79.

MUKHOPADHYAY, S. & GAL, A. A. 2010. Granulomatous lung disease: an approach to the differential diagnosis. *Archives of pathology & laboratory medicine,* 134**,** 667-690.

NAGAOKA, I., TRAPNELL, B. & CRYSTAL, R. 1990. Upregulation of platelet-derived growth factor-A and-B gene expression in alveolar macrophages of individuals with idiopathic pulmonary fibrosis. *Journal of Clinical Investigation,* 85**,** 2023.

NAGASE, H. & FIELDS, G. B. 1996. Human matrix metalloproteinase specificity studies using collagen sequence-based synthetic peptides. *Biopolymers,* 40**,** 399-416.

NARAYANAN, A. S., SIEGEL, R. C. & MARTIN, G. R. 1972. On the inhibition of lysyl oxidase by -aminopropionitrile. *Biochem Biophys Res Commun,* 46**,** 745-51.

NAVARATNAM, V., FLEMING, K., WEST, J., SMITH, C., JENKINS, R., FOGARTY, A. & HUBBARD, R. 2011. The rising incidence of idiopathic pulmonary fibrosis in the UK. *Thorax,* 66**,** 462-467.

NEGRI, E., MONTES, G., SALDIVA, P. & CAPELOZZI, V. 2000. Architectural remodelling in acute and chronic interstitial lung disease: fibrosis or fibroelastosis? *Histopathology,* 37**,** 393-401.

NEGUS, R., STAMP, G., RELF, M., BURKE, F., MALIK, S., BERNASCONI, S., ALLAVENA, P., SOZZANI, S., MANTOVANI, A. & BALKWILL, F. R. 1995. The detection and localization of monocyte chemoattractant protein-1 (MCP-1) in human ovarian cancer. *Journal of Clinical Investigation,* 95**,** 2391.

NESBIT, M. 2006. Anti-vascular methods and therapies employing lysyl oxidase inhibitors. WO 2006128740 A2.

NESBIT, M. 2007. Anti-vascular methods and therapies employing lysyl oxidase inhibitors. WO 2006128740 A3.

NETZEL-ARNETT, S., MALLYA, S. K., NAGASE, H., BIRKEDAL-HANSEN, H. & VAN WART, H. E. 1991. Continuously recording fluorescent assays optimized for five human matrix metalloproteinases. *Anal Biochem,* 195**,** 86-92.

NOTH, I., ZHANG, Y., MA, S.-F., FLORES, C., BARBER, M., HUANG, Y., BRODERICK, S. M., WADE, M. S., HYSI, P. & SCUIRBA, J. 2013. Genetic variants associated with idiopathic pulmonary fibrosis susceptibility and mortality: a genome-wide association study. *The Lancet Respiratory Medicine,* 1**,** 309-317.

NTZIACHRISTOS, V. 2006. Fluorescence molecular imaging. *Annu Rev Biomed Eng,* 8**,** 1-33.

OGATA, Y., ENGHILD, J. J. & NAGASE, H. 1992. Matrix metalloproteinase 3 (stromelysin) activates the precursor for the human matrix metalloproteinase 9. *J Biol Chem,* 267**,** 3581-4.

OGAWA, M., LARUE, A. C. & DRAKE, C. J. 2006. Hematopoietic origin of fibroblasts/myofibroblasts: its pathophysiologic implications. *Blood,* 108**,** 2893.

OHNISHI, K., TAKAGI, M., KUROKAWA, Y., SATOMI, S. & KONTTINEN, Y. T. 1998. Matrix metalloproteinase-mediated extracellular matrix protein degradation in human pulmonary emphysema. *Laboratory investigation; a journal of technical methods and pathology,* 78**,** 1077-1087.

OHTANI, Y., SAIKI, S., KITAICHI, M., USUI, Y., INASE, N., COSTABEL, U. & YOSHIZAWA, Y. 2005. Chronic bird fancier's lung: histopathological and clinical correlation. An application of the 2002 ATS/ERS consensus classification of the idiopathic interstitial pneumonias. *Thorax,* 60**,** 665-671.

OLSON, E. S., AGUILERA, T. A., JIANG, T., ELLIES, L. G., NGUYEN, Q. T., WONG, E. H., GROSS, L. A. & TSIEN, R. Y. 2009. In vivo characterization of activatable cell penetrating peptides for targeting protease activity in cancer. *Integr Biol (Camb),* 1**,** 382-93.

ONG, S. L., GRAVANTE, G., METCALFE, M. S. & DENNISON, A. R. 2013. History, ethics, advantages and limitations of experimental models for hepatic ablation. *World Journal of Gastroenterology : WJG,* 19**,** 147-154.

OVERALL, C. M. & LOPEZ-OTIN, C. 2002. Strategies for MMP inhibition in cancer: innovations for the post-trial era. *Nat Rev Cancer,* 2**,** 657-672.

PALAMAKUMBURA, A. H. & TRACKMAN, P. C. 2002. A fluorometric assay for detection of lysyl oxidase enzyme activity in biological samples. *Analytical biochemistry,* 300**,** 245-251.

PALMARINI, M. & FAN, H. 2001. Retrovirus-Induced Ovine Pulmonary Adenocarcinoma, an Animal Model for Lung Cancer. *Journal of the National Cancer Institute,* 93**,** 1603-1614.

PARRA, E. R., KAIRALLA, R. A., DE CARVALHO, C. R. R. & CAPELOZZI, V. L. 2007. Abnormal deposition of collagen/elastic vascular fibres and prognostic significance in idiopathic interstitial pneumonias. *Thorax,* 62**,** 428-437.

PHAN, S. H. Biology of fibroblasts and myofibroblasts. 2008. Am Thoracic Soc, 334.

PODLUTSKY, A., BALLABH, P. & CSISZAR, A. 2010. Oxidative stress and endothelial dysfunction in pulmonary arteries of aged rats. *American Journal of Physiology-Heart and Circulatory Physiology,* 298**,** H346-H351.

POOLE, A., MYLLYLA, R., WAGNER, J. C. & BROWN, R. C. 1985. Collagen biosynthesis enzymes in lung tissue and serum of rats with experimental silicosis. *Br J Exp Pathol,* 66**,** 567-75.

PRIEDITIS, H. & ADAMSON, I. 1996. Alveolar macrophage kinetics and multinucleated giant cell formation after lung injury. *Journal of leukocyte biology,* 59**,** 534-538.

PROTEUS. 2014. Edinburgh: University of Edinburgh. Available: http://proteus.ac.uk/ [Accessed 27.4.2015.

PRUDOVA, A., AUF DEM KELLER, U., BUTLER, G. S. & OVERALL, C. M. 2010. Multiplex N-terminome analysis of MMP-2 and MMP-9 substrate degradomes by iTRAQ-TAILS quantitative proteomics. *Molecular & Cellular Proteomics,* 9**,** 894-911.

RAMIREZ, G., HAGOOD, J. S., SANDERS, Y., RAMIREZ, R., BECERRIL, C., SEGURA, L., BARRERA, L., SELMAN, M. & PARDO, A. 2011. Absence of Thy-1 results in TGF-[beta] induced MMP-9 expression and confers a profibrotic phenotype to human lung fibroblasts. *Lab Invest,* 91**,** 1206-1218.

RAMOS, C., MONTANO, M., GARCIA-ALVAREZ, J., RUIZ, V., UHAL, B. D., SELMAN, M. & PARDO, A. 2001. Fibroblasts from idiopathic pulmonary fibrosis and normal lungs differ in growth rate, apoptosis, and tissue inhibitor of metalloproteinases expression. *American journal of respiratory cell and molecular biology,* 24**,** 591.

RAULO, S. M., SORSA, T., TERVAHARTIALA, T., PIRILÄ, E. & MAISI, P. 2001. MMP-9 as a marker of inflammation in tracheal epithelial lining fluid (TELF) and in bronchoalveolar fluid (BALF) of COPD horses. *Equine Veterinary Journal,* 33**,** 128-136.

RAVANTI, L., HEINO, J., LÓPEZ-OTíN, C. & KÄHÄRI, V.-M. 1999. Induction of Collagenase-3 (MMP-13) Expression in Human Skin Fibroblasts by Three-dimensional Collagen Is Mediated by p38 Mitogen-activated Protein Kinase. *Journal of Biological Chemistry,* 274**,** 2446-2455.

RAZZAQUE, M. S. & TAGUCHI, T. 2003. Pulmonary fibrosis: Cellular and molecular events. *Pathology international,* 53**,** 133-145.

REDDY, T. L., TOMINAGA, M., HANSELL, D. M., VON DER THUSEN, J., RASSL, D., PARFREY, H., GUY, S., TWENTYMAN, O., RICE, A. & MAHER, T. M. 2012. Pleuroparenchymal fibroelastosis: a spectrum of histopathological and imaging phenotypes. *European Respiratory Journal,* 40**,** 377-385.

RICHELDI, L., DU BOIS, R. M., RAGHU, G., AZUMA, A., BROWN, K. K., COSTABEL, U., COTTIN, V., FLAHERTY, K. R., HANSELL, D. M., INOUE, Y., KIM, D. S., KOLB, M., NICHOLSON, A. G., NOBLE, P. W., SELMAN, M., TANIGUCHI, H., BRUN, M., LE MAULF, F., GIRARD, M., STOWASSER, S., SCHLENKER-HERCEG, R., DISSE, B. & COLLARD, H. R. 2014. Efficacy and Safety of Nintedanib in Idiopathic Pulmonary Fibrosis. *New England Journal of Medicine,* 370**,** 2071-2082.

RINKEVICH, Y., WALMSLEY, G. G., HU, M. S., MAAN, Z. N., NEWMAN, A. M., DRUKKER, M., JANUSZYK, M., KRAMPITZ, G. W., GURTNER, G. C., LORENZ, H. P., WEISSMAN, I. L. & LONGAKER, M. T. 2015. Identification and isolation of a dermal lineage with intrinsic fibrogenic potential. *Science,* 348.

ROBERTS, C. J., BIRKENMEIER, T., MCQUILLAN, J., AKIYAMA, S., YAMADA, S., CHEN, W., YAMADA, K. & MCDONALD, J. 1988. Transforming growth factor beta stimulates the expression of fibronectin and of both subunits of the human fibronectin receptor by cultured human lung fibroblasts. *Journal of Biological Chemistry,* 263**,** 4586-4592.

ROBINSON, N. E. 2001. International Workshop on Equine Chronic Airway Disease Michigan State University 16–18 June 2000. *Equine Veterinary Journal,* 33**,** 5-19.

ROCK, J. R., BARKAUSKAS, C. E., CRONCE, M. J., XUE, Y., HARRIS, J. R., LIANG, J., NOBLE, P. W. & HOGAN, B. L. M. 2011. Multiple stromal populations contribute to pulmonary fibrosis without evidence for epithelial to mesenchymal transition. *Proc Natl Acad Sci U S A,* 108**,** E1475-E1483.

RODRIGUEZ, H. M., VAYSBERG, M., MIKELS, A., MCCAULEY, S., VELAYO, A. C., GARCIA, C. & SMITH, V. 2010. Modulation of lysyl oxidase-like 2 enzymatic activity by an allosteric antibody inhibitor. *Journal of Biological Chemistry,* 285**,** 20964-20974.

ROOMI, M. W., MONTERREY, J. C., KALINOVSKY, T., RATH, M. & NIEDZWIECKI, A. 2009. Patterns of MMP-2 and MMP-9 expression in human cancer cell lines. *Oncol Rep,* 21**,** 1323-33.

RUDOLF SCHOHE-LOOP, E. B., CHRISTIANE FAESTE, CLAUDIA HIRTH-DIETRICH, JORG KELDENICH, ANDREAS KNORR, THOMAS LAMPE, PAUL NAAB, DELF SCHMIDT 2006. Fibrotic disorders; disorders characterized by harmful buildup of collagen and/or by excessive lysyl oxidase enzymatic activity. US 20060004015 A1.

RUSH, B., RAUB, E., RHOADS, W., FLAMINIO, M., MATSON, C., HAKALA, J. & GILLESPIE, J. 1998. Pulmonary function in horses with recurrent airway obstruction after aerosol and parenteral administration of beclomethasone dipropionate and dexamethasone, respectively. *American journal of veterinary research,* 59**,** 1039-1043.

RYU, J. H., LEE, A., NA, J. H., LEE, S., AHN, H. J., PARK, J. W., AHN, C. H., KIM, B. S., KWON, I. C., CHOI, K., YOUN, I. & KIM, K. 2011. Optimization of matrix metalloproteinase fluorogenic probes for osteoarthritis imaging. *Amino Acids,* 41**,** 1113-22.

SAITO, H., PAPACONSTANTINOU, J., SATO, H. & GOLDSTEIN, S. 1997. Regulation of a novel gene encoding a lysyl oxidase-related protein in cellular adhesion and senescence. *Journal of Biological Chemistry,* 272**,** 8157-8160.

SAPSFORD, K. E., BERTI, L. & MEDINTZ, I. L. 2006. Materials for Fluorescence Resonance Energy Transfer Analysis: Beyond Traditional Donor–Acceptor Combinations. *Angewandte Chemie International Edition,* 45**,** 4562-4589.

SAREN, P., WELGUS, H. G. & KOVANEN, P. T. 1996. TNF-alpha and IL-1beta selectively induce expression of 92-kDa gelatinase by human macrophages. *J Immunol,* 157**,** 4159-65.

SCHNUTE, M. E., O'BRIEN, P. M., NAHRA, J., MORRIS, M., HOWARD ROARK, W., HANAU, C. E., RUMINSKI, P. G., SCHOLTEN, J. A., FLETCHER, T. R., HAMPER, B. C., CARROLL, J. N., PATT, W. C., SHIEH, H. S., COLLINS, B., PAVLOVSKY, A. G., PALMQUIST, K. E., ASTON, K. W., HITCHCOCK, J., ROGERS, M. D., MCDONALD, J., JOHNSON, A. R., MUNIE, G. E., WITTWER, A. J., MAN, C.-F., SETTLE, S. L., NEMIROVSKIY, O., VICKERY, L. E., AGAWAL, A., DYER, R. D. & SUNYER, T. 2010. Discovery of (pyridin-4-yl)-2H-tetrazole as a novel

scaffold to identify highly selective matrix metalloproteinase-13 inhibitors for the treatment of osteoarthritis. *Bioorg Med Chem Lett,* 20**,** 576-580.

SCHWARTZ, L., KNIGHT, H., WHITTIG, L., MALLOY, R., ABRAHAM, J. & TYLER, N. 1981. Silicate pneumoconiosis and pulmonary fibrosis in horses from the Monterey-Carmel peninsula. *Chest,* 80**,** 82S.

SCOTT, P., GRIFFITHS, D. & COUSENS, C. 2013. Diagnosis and control of ovine pulmonary adenocarcinoma (Jaagsiekte). *In Practice,* 35**,** 382-397.

SELMAN, M., RUIZ, V., CABRERA, S., SEGURA, L., RAMIREZ, R., BARRIOS, R. & PARDO, A. 2000. TIMP-1, -2, -3, and -4 in idiopathic pulmonary fibrosis. A prevailing nondegradative lung microenvironment? *Am J Physiol Lung Cell Mol Physiol,* 279**,** L562-74.

SENDON-LAGO, J., SEOANE, S., EIRO, N., BERMUDEZ, M. A., MACIA, M., GARCIA-CABALLERO, T., VIZOSO, F. J. & PEREZ-FERNANDEZ, R. 2014. Cancer progression by breast tumors with Pit-1-overexpression is blocked by inhibition of Metalloproteinase (MMP)-13. *Breast Cancer Res,* 16**,** 505.

SHEPHERD, F. A., GIACCONE, G., SEYMOUR, L., DEBRUYNE, C., BEZJAK, A., HIRSH, V., SMYLIE, M., RUBIN, S., MARTINS, H., LAMONT, A., KRZAKOWSKI, M., SADURA, A. & ZEE, B. 2002. Prospective, Randomized, Double-Blind, Placebo-Controlled Trial of Marimastat After Response to First-Line Chemotherapy in Patients With Small-Cell Lung Cancer: A Trial of the National Cancer Institute of Canada-Clinical Trials Group and the European Organization for Research and Treatment of Cancer. *Journal of clinical oncology,* 20**,** 4434-4439.

SHIMIZU, Y., TEMMA, T., SANO, K., ONO, M. & SAJI, H. 2011. Development of membrane type-1 matrix metalloproteinase-specific activatable fluorescent probe for malignant tumor detection. *Cancer Sci,* 102**,** 1897-903.

SMITH-MUNGO, L. I. & KAGAN, H. M. 1998. Lysyl oxidase: properties, regulation and multiple functions in biology. *Matrix Biology,* 16**,** 387-398.

SNOEK-VAN BEURDEN, P. A. & VON DEN HOFF, J. W. 2005. Zymographic techniques for the analysis of matrix metalloproteinases and their inhibitors. *Biotechniques,* 38**,** 73-83.

STACK, M. S. & GRAY, R. D. 1989. Comparison of vertebrate collagenase and gelatinase using a new fluorogenic substrate peptide. *J Biol Chem,* 264**,** 4277-81.

SUGA, M., IYONAGA, KAZUHIRO, OKAMOTO, TATSUYA, GUSHIMA, YASUHIRO, & IGUCHI, H. 2000. Characteristic elevation of matrix metalloproteinase activity in idiopathic interstitial pneumonias. *American journal of respiratory and critical care medicine,* 162**,** 1949-1956.

SWEENEY, C. Equine Restrictive Lung Disease. Part 3: Interstitial Diseases (12-Nov-2002).

SZÁJLI, E., FEHÉR, T. & MEDZIHRADSZKY, K. F. 2008. Investigating the Quantitative Nature of MALDI-TOF MS. *Molecular & Cellular Proteomics,* 7**,** 2410-2418.

TALLANT, C., MARRERO, A. & GOMIS-RUTH, F. X. 2010. Matrix metalloproteinases: fold and function of their catalytic domains. *Biochim Biophys Acta,* 1803**,** 20-8.

TANG, S. S., TRACKMAN, P. C. & KAGAN, H. M. 1983. Reaction of aortic lysyl oxidase with beta-aminopropionitrile. *J Biol Chem,* 258**,** 4331-8.

TANJORE, H., CHENG, D. S., DEGRYSE, A. L., ZOZ, D. F., ABDOLRASULNIA, R., LAWSON, W. E. & BLACKWELL, T. S. 2011. Alveolar epithelial cells undergo epithelial-to-mesenchymal transition in response to endoplasmic reticulum stress. *J Biol Chem,* 286**,** 30972-80.

TERNON, M., DíAZ-MOCHÓN, J. J., BELSOM, A. & BRADLEY, M. 2004. Dendrimers and combinatorial chemistry—tools for fluorescent enhancement in protease assays. *Tetrahedron,* 60**,** 8721-8728.

THIBERVILLE, L., SALAUN, M., LACHKAR, S., DOMINIQUE, S., MORENO-SWIRC, S., VEVER-BIZET, C. & BOURG-HECKLY, G. 2009a. Confocal fluorescence endomicroscopy of the human airways. *Proc Am Thorac Soc,* 6**,** 444-9.

THIBERVILLE, L., SALAUN, M., LACHKAR, S., DOMINIQUE, S., MORENO-SWIRC, S., VEVER-BIZET, C. & BOURG-HECKLY, G. Confocal fluorescence endomicroscopy of the human airways. 2009b. Am Thoracic Soc, 444.

THIEMANN, A. 2012. Respiratory disease in the donkey. *Equine Veterinary Education,* 24**,** 469-478.

THIEMANN, A. & BELL, N. 2001. The peculiarities of donkey respiratory disease. *LEKEUX, P. Equine respiratory disease. International Veterinary Information Service*.

THOMASSIN, L., WERNECK, C. C., BROEKELMANN, T. J., GLEYZAL, C., HORNSTRA, I. K., MECHAM, R. P. & SOMMER, P. 2005. The Pro-regions of lysyl oxidase and lysyl oxidase-like 1 are required for deposition onto elastic fibers. *Journal of Biological Chemistry,* 280**,** 42848-42855.

TOLLESHAUG, H., NEWTON, B., RYDBECK, A., CHETTIBI, S. & ERIKSEN, M. 2007. Novel imaging agents for fibrosis. Google Patents.

TRACKMAN, P. C., ZOSKI, C. G. & KAGAN, H. M. 1981. Development of a peroxidase-coupled fluorometric assay for lysyl oxidase. *Analytical biochemistry,* 113**,** 336-342.

TRAVIS, W. D., COSTABEL, U., HANSELL, D. M., KING JR, T. E., LYNCH, D. A., NICHOLSON, A. G., RYERSON, C. J., RYU, J. H., SELMAN, M. & WELLS, A. U. 2013. An official American Thoracic Society/European Respiratory Society statement: Update of the international multidisciplinary classification of the idiopathic interstitial pneumonias. *American journal of respiratory and critical care medicine,* 188**,** 733-748.

TRIVEDY, C., WARNAKULASURIYA, K., HAZAREY, V., TAVASSOLI, M., SOMMER, P. & JOHNSON, N. 1999. The upregulation of lysyl oxidase in oral submucous fibrosis and squamous cell carcinoma. *Journal of Oral Pathology & Medicine,* 28**,** 246-251.

TUNG, C.-H. 2004. Fluorescent peptide probes for in vivo diagnostic imaging. *Peptide Science,* 76**,** 391-403.

VAN DER STRATE, B. W., POSTMA, D. S., BRANDSMA, C.-A., MELGERT, B. N., LUINGE, M. A., GEERLINGS, M., HYLKEMA, M. N., VAN DEN BERG, A., TIMENS, W. & KERSTJENS, H. A. 2006. Cigarette Smoke–

induced Emphysema: A Role for the B Cell? *American journal of respiratory and critical care medicine,* 173**,** 751-758.

VANCHERI, C. 2012. Idiopathic pulmonary fibrosis: an altered fibroblast proliferation linked to cancer biology. *Proc Am Thorac Soc,* 9**,** 153-7.

VANDENBROUCKE, R. E. & LIBERT, C. 2014. Is there new hope for therapeutic matrix metalloproteinase inhibition? *Nat Rev Drug Discov,* 13**,** 904-927.

VINCENT-CHONG, V. K., SALAHSHOURIFAR, I., KAREN-NG, L. P., SIOW, M. Y., KALLARAKKAL, T. G., RAMANATHAN, A., YANG, Y. H., KHOR, G. H., RAHMAN, Z. A., ISMAIL, S. M., PREPAGERAN, N., MUSTAFA, W. M., ABRAHAM, M. T., TAY, K. K., CHEONG, S. C. & ZAIN, R. B. 2014. Overexpression of MMP13 is associated with clinical outcomes and poor prognosis in oral squamous cell carcinoma. *ScientificWorldJournal,* 2014**,** 897523.

VOLOSHENYUK, T. G., LANDESMAN, E. S., KHOUTOROVA, E., HART, A. D. & GARDNER, J. D. 2011. Induction of cardiac fibroblast lysyl oxidase by TGF-beta1 requires PI3K/Akt, Smad3, and MAPK signaling. *Cytokine,* 55**,** 90-7.

VORA, S. R., GUO, Y., STEPHENS, D. N., SALIH, E., VU, E. D., KIRSCH, K. H., SONENSHEIN, G. E. & TRACKMAN, P. C. 2010. Characterization of Recombinant Lysyl Oxidase Propeptide. *Biochemistry,* 49**,** 2962-2972.

WAKASAKI, H. & OOSHIMA, A. 1990. Immunohistochemical localization of lysyl oxidase with monoclonal antibodies. *Laboratory investigation; a journal of technical methods and pathology,* 63**,** 377-384.

WALLACE, W. E., GUPTA, N. C., HUBBS, A. F., MAZZA, S. M., BISHOP, H. A., KEANE, M. J., BATTELLI, L. A., MA, J. & SCHLEIFF, P. 2002. Cis-4-[18F] fluoro-L-proline PET imaging of pulmonary fibrosis in a rabbit model. *Journal of Nuclear Medicine,* 43**,** 413-420.

WANG, J. F., JIAO, H., STEWART, T. L., SHANKOWSKY, H. A., SCOTT, P. G. & TREDGET, E. E. 2007. Fibrocytes from burn patients regulate the activities of fibroblasts. *Wound Repair and Regeneration,* 15**,** 113-121.

WATERS, J. C. 2009. Accuracy and precision in quantitative fluorescence microscopy. *The Journal of cell biology,* 185**,** 1135-1148.

WEISSLEDER, R. 1999. Molecular imaging: exploring the next frontier 1. *Radiology,* 212**,** 609-614.

WHITTAKER, M., FLOYD, C. D., BROWN, P. & GEARING, A. J. 1999. Design and therapeutic application of matrix metalloproteinase inhibitors. *Chem Rev,* 99**,** 2735-76.

WILLIAMS, K., MAES, R., DEL PIERO, F., LIM, A., WISE, A., BOLIN, D., CASWELL, J., JACKSON, C., ROBINSON, N. & DERKSEN, F. 2007. Equine multinodular pulmonary fibrosis: a newly recognized herpesvirus-associated fibrotic lung disease. *Veterinary Pathology Online,* 44**,** 849.

WILLIAMS, K., MALARKEY, D., COHN, L., PATRICK, D., DYE, J. & TOEWS, G. 2004. Identification of Spontaneous Feline Idiopathic Pulmonary Fibrosis*. *Chest,* 125**,** 2278-2288.

WILLIS, B. C. & BOROK, Z. 2007. TGF-beta-induced EMT: mechanisms and implications for fibrotic lung disease. *American Journal of Physiology- Lung Cellular and Molecular Physiology,* 293**,** L525.

WILMARTH, K. R. & FROINES, J. R. 1991. Role of monoamine oxidase in aminopropionitrile-induced neurotoxicity. *J Toxicol Environ Health,* 32**,** 415-27.

WINKLER, M. K. & FOWLKES, J. L. 2002. Metalloproteinase and growth factor interactions: do they play a role in pulmonary fibrosis? *American Journal of Physiology- Lung Cellular and Molecular Physiology,* 283**,** 1.

WITTE, F. G., FRANK, N., WILKES, R. & NOVAK, J. 2012. Association of Asinine Herpesvirus-5 with Pyogranulomatous Pneumonia in a Mare. *Journal of Veterinary Internal Medicine*.

WOESSNER, R. D., MATTERN, M. R., MIRABELLI, C., JOHNSON, R. & DRAKE, F. 1991. Proliferation-and cell cycle-dependent differences in expression of the 170 kilodalton and 180 kilodalton forms of topoisomerase II in NIH-3T3 cells. *Cell growth & differentiation: the molecular biology journal of the American Association for Cancer Research,* 2**,** 209-214.

WONG, D. M., BELGRAVE, R. L., WILLIAMS, K. J., DEL PIERO, F., ALCOTT, C. J., BOLIN, S. R., MARR, C. M., NOLEN-WALSTON, R., MYERS, R. K. & WILKINS, P. A. 2008. Multinodular pulmonary fibrosis in five horses. *Journal of the American Veterinary Medical Association,* 232**,** 898-905.

WOO, C. H., LIM, J. H. & KIM, J. H. 2004. Lipopolysaccharide induces matrix metalloproteinase-9 expression via a mitochondrial reactive oxygen species-p38 kinase-activator protein-1 pathway in Raw 264.7 cells. *J Immunol,* 173**,** 6973-80.

WYNN, T. A. 2008. Cellular and molecular mechanisms of fibrosis. *The Journal of pathology,* 214**,** 199-210.

WYNN, T. A. & RAMALINGAM, T. R. 2012. Mechanisms of fibrosis: therapeutic translation for fibrotic disease. *Nat Med,* 18**,** 1028-40.

XIE, J., WANG, C., HUANG, D.-Y., ZHANG, Y., XU, J., KOLESNIKOV, S. S., SUNG, K. L. P. & ZHAO, H. 2013. TGF-beta1 induces the different expressions of lysyl oxidases and matrix metalloproteinases in anterior cruciate ligament and medial collateral ligament fibroblasts after mechanical injury. *Journal of Biomechanics,* 46**,** 890-898.

YU, Q. & STAMENKOVIC, I. 2000. Cell surface-localized matrix metalloproteinase-9 proteolytically activates TGF-beta and promotes tumor invasion and angiogenesis. *Genes Dev,* 14**,** 163-76.

ZHANG, X., BLOCH, S., AKERS, W. & ACHILEFU, S. 2012. Near-infrared molecular probes for in vivo imaging. *Curr Protoc Cytom,* Chapter 12**,** Unit12 27.

ZHAO, J., SHI, W., WANG, Y. L., CHEN, H., BRINGAS JR, P., DATTO, M. B., FREDERICK, J. P., WANG, X. F. & WARBURTON, D. 2002. Smad3 deficiency attenuates bleomycin-induced pulmonary fibrosis in mice. *American Journal of Physiology- Lung Cellular and Molecular Physiology,* 282**,** 585.

ZHOU, M., DIWU, Z., PANCHUK-VOLOSHINA, N. & HAUGLAND, R. P. 1997. A stable nonfluorescent derivative of resorufin for the fluorometric determination of trace hydrogen peroxide: applications in detecting the activity of phagocyte NADPH oxidase and other oxidases. *Analytical biochemistry,* 253**,** 162-168.